National Library of Canada
Acquisitions and Bibliographic Services Branch
395 Wellington Street
Ottawa, Ontario
K1A 0N4

Bibliothèque nationale du Canada
Direction des acquisitions et des services bibliographiques
395, rue Wellington
Ottawa (Ontario)
K1A 0N4

Your file Votre référence

Our file Notre référence

NOTICE

The quality of this microform is heavily dependent upon the quality of the original thesis submitted for microfilming. Every effort has been made to ensure the highest quality of reproduction possible.

If pages are missing, contact the university which granted the degree.

Some pages may have indistinct print especially if the original pages were typed with a poor typewriter ribbon or if the university sent us an inferior photocopy.

AVIS

La qualité de cette microforme dépend grandement de la qualité de la thèse soumise au microfilmage. Nous avons tout fait pour assurer une qualité supérieure de reproduction.

S'il manque des pages, veuillez communiquer avec l'université qui a conféré le grade.

La qualité d'impression de certaines pages peut laisser à désirer, surtout si les pages originales ont été dactylographiées à l'aide d'un ruban usé ou si l'université nous a fait parvenir une photocopie de qualité inférieure.

Canada

Laser Shadowgraph Study of Early Flame Propagation in Swirling Flows Near the Lean Misfire Limit

by

Abdolreza Sheikhi

A thesis submitted to the School of Graduate Studies

in partial fulfilment of the requirement for the degree of

Master of Applied Science

in

Mechanical Engineering

Ottawa-Carleton Institute for Mechanical and Aerospace Engineering

Department of Mechanical Engineering

University of Ottawa

ISBN 0-612-07806-X

Canada

UNIVERSITÉ D'OTTAWA
UNIVERSITY OF OTTAWA

ABSTRACT

The effects of swirling flow and spark locations on the specific rate of growth of flame area, the flame speed and the convection velocity are investigated experimentally in a constant volume vessel near the lean misfire limit for an equivalence ratio of 0.645 using the shadowgraph technique.

The circular and the elliptical models are used as flame contours to calculate the flame speed and the convection velocity. The circular model indicates that the flame speed decreases as the swirl flow decays and as the spark location is moved towards the center of the combustion chamber. The modified elliptical model shows the same result for the average flame speed S_{ws}. Both models show an overlap in convection velocity when comparison is made at a given spark location for different swirl levels because of cyclic variation; even though the average is higher for higher swirl level.

The specific rate of growth of flame area $(\frac{1}{A}\frac{dA}{dt})$ is obtained using three models for flame area A : (i) 2-D flame area A_f measured from the photographs, (ii) spherical flame geometry model, and (iii) ellipsoidal geometry model.

The stretch factor $K=(\frac{\delta_l}{u_l})(\frac{1}{A}\frac{dA}{dt})$ at 0.5 ms from ignition time for the 2-D and the spherical models at $\frac{r}{R}=0.68$ was within the range 0.63-0.97 and at $\frac{r}{R}=0.55$ was within the

range 0.5-0.59. The stretch factor for the ellipsoidal model at $\frac{r}{R}$ =0.68 was within the range 0.53-1.05 and at $\frac{r}{R}$ =0.55 was within the range 0.46-0.53.

All three models for flame area indicate that the specific rate of growth of flame area and the stretch factor at 0.5 ms from ignition time decrease as the swirl flow decays and as the spark location approaches the center of the combustion chamber.

ACKNOWLEDGEMENTS

I would like to express my appreciation to my supervisor Dr. R. Milane for his guidance, interest and encouragement throughout my research. Thanks are due to Dr. D.G.E. Robertson for his help and for providing access to the analyzing projector in the Biomechanics Lab of the School of Human Kinetics at the University of Ottawa. I also wish to thank Dr. S. Tavoularis and Dr. M.I. Yaras for reading and commenting on this thesis.

Sincere appreciation is also expressed to the government of the Islamic Republic of Iran especially the Ministry of Petroleum, for providing financial support for this graduate study.

Finally I would like to thank my wife, my parents and my brothers for their encouragement and support throughout my work.

Table of Contents

List of Tables

List of Figures

NOMENCLATURE

A	3-D area of flame surface
A_f	2-D flame area measured by the planimeter
A_c	contact area
a	semi-major axis of the ellipse
b	semi-minor axis of the ellipse
C_{pm}	specific heat at constant pressure for the mixture
D	diffusion coefficient of the deficient reactant
f	focal length
f_c	contact area fraction
K	stretch factor
L	integral length scale

Le	Lewis number
M	molecular weight
M_p	molecular weight of propane
M_a	molecular weight of air
N	refractive index
P	pressure
P_p	partial pressure of propane
P_a	partial pressure of air
p	perimeter of the flame area
R_A	specific gas constant of air
R_c	distance between the flame centroid and the center of vessel
R_e	equivalent flame radius
R_L	turbulent Reynolds number based upon integral length scale
R_m	gas constant of a mixture
R_p	specific gas constant of propane
r	distance between the ignition position and the center of the vessel
r/R	dimensionless radial distance
S_k	flame speed based on Keck's analysis
S_w	flame speed based on elliptical model
S_{ws}	modified flame speed based on elliptical model
t	time
T	temperature

U	local velocity of flow
U_t	tangential velocity of swirl flow
u'	rms turbulent fluctuation
u_l	laminar burning velocity
V_k	convection velocity based on Keck's analysis
V_{rk}	radial velocity based on Keck's analysis
V_w	convection velocity based on elliptical model
V_{wt}	modified convection velocity based on elliptical model
X	mole fraction
$\bar{x}, \bar{y}$	flame centroid coordinates

Greek Symbols

δ_l	laminar flame thickness
ε_{12} / k	molecular potential energy characteristics of 1-2
λ	Taylor microscale of turbulence
λ_m	thermal conductivity of the mixture
μ_m	viscosity of the mixture
ν_m	kinematic viscosity of the mixture
ρ_m	density of the mixture
σ_{12}	molecular potential energy characteristics of 1-2
ϕ	equivalence ratio

ψ	deflection angle
$\Omega_{12}^{(l,1)^*}$	dimensionless collision integral

Chapter 1

INTRODUCTION

1.1 General Overview

The internal combustion engine has been used since 1885. From that time till the mid-60's oil was a cheap commodity, therefore fuel economy was not considered as an important factor. In the mid-60's exhaust emissions and fuel economy became two major design factors in

designing internal combustion engines and during the last two decades great emphasis has been placed on improving the engine efficiency.

From the thermodynamic Otto Cycle, it can be shown that :

1-The higher the value of the compression ratio, the more efficient is the engine, but there is a limit to this value which is set by the onset of knock.

2-The thermal efficiency will be greater when using leaner mixtures, however there is a limit to the leaning off of mixtures which is set by the onset of misfire.

The most practical approach in improving fuel economy is using a lean mixture. However lean mixtures burn much more slowly than richer mixtures and the flame propagation may continue further during the expansion stroke resulting in poor efficiency, power loss and increase in hydrocarbon emissions. By increasing the burning rate, the heat release from lean mixtures occurs at a more effective time during the cycle and the combustion performance can be improved.

One way of increasing the burning rate is to induce motion in the mixture instead of using a quiescent mixture and one of the common methods of producing mixture motion in an engine is the generation of swirl. The objective of this study is to investigate the characteristics of a swirling combusting flow near the lean misfire limit.

1.2 Literature Review

Studies on lean mixtures in gasoline engines have shown that the dominant factors in lean-engine operation which affect the initial flame kernel development are the properties of the

mixture, the local flow field at the spark plug, the degree of mixture homogeneity, the spark plug location and the mixture temperature.

There is a strong relation between lean mixture operation and mixture motion. In ultra-lean mixtures, excessive mixture motion reduces the mean flame kernel growth (Ho and Santavicca, 1987), draws the heat away from the reaction zone and extinguishes the flame. In moderately lean mixtures, mixture motion increases the burning rate but, if the motion is too strong, the flame is extinguished. Therefore a kind of mixture motion is required which does not extinguish the flame but increases the rate of combustion.

1.2.1 Swirl Flows

Inducing swirl in the unburned gas mixture is one of the most practical ways of increasing the rate of burning in engines. Vichnievsky and Sale (1958) reported that inducing swirl using a shrouded intake valve had an important steadying effect on cylinder pressure development. Jones and Mackworth (1975) showed that by using swirl there would be a consistent combustion at very lean mixture strengths with low carbon monoxide emission. Pischinger and Adams (1980) checked various methods to produce swirl in their engine and found that the use of shrouded valves produced the fastest ignition and shortest burning times. Young (1981) found that swirl motion decreases the effect of cyclic variation in pressure and combustion development and causes a remarkable improvement in burning rate.

Witze and Vilchis (1981) studied the effect of swirl on homogeneous combustion and reported that for engine cycles where the flame detachment from electrodes occurred early, the burn was slow; when the flame stayed attached to the spark plug, the burn was fast. In the latter case the spark plug electrode acted as a flame holder, and the very rapid burn was due mainly to the convection of unburned mixture into the reaction zone by the high swirl velocity. Witze (1982) investigated the effect of spark location on burn duration and found that ignition at the center of the chamber was preferable for low swirl numbers. For higher swirl numbers the mid-radius spark location was favourable and for very high swirl numbers the side-wall spark location was found to be best.

Hanson and Thomas (1984) investigated the effects of swirl on flame development and found the presence of two combustion phenomena:

1- A centrifugal force driving the flame to the center of the vessel away from the walls for off-center and near-wall ignitions, and

2- The pencilling of the flame shape in the axial direction, which was enhanced by increasing the rotational speed for central ignition and for greater leanness of the mixture.

They found that for off-center ignition, swirl enhances combustion performance because the flame is centered by the centrifugal force which reduces quenching by the walls and results in shorter combustion duration. They also found that high swirl adversely affects centrally ignited explosions. In this case the combustion time increases remarkably because the pencilling effect results in faster flame quenching by the end plates. The effect of shear was also examined and it was found that a higher shear rate resulted in higher rate of growth of the flame area and

therefore shorter burn duration.

Wakisaka et al (1979) repoted that a considerable amount of turbulence was associated with swirl in motored engines. Swirl supplies energy to the turbulence and higher turbulence in the combustion chamber increases the burning rate, particularly during the main stage of combustion (Ozdor et al, 1994). Herweg et al (1988) observed that the influence of turbulence on the burning velocity during flame kernel formation is less than during the main combustion period. In a recent work, Herweg and Maly (1990) reported that increasing the turbulence intensity has led to a steady increase of the flame speed of the early flame kernel due to wrinkling of the flame surface.

Bianco et al (1991) used the fiber-optic spark plug and compared three types of flow pattern, namely quiescent , swirl and tumble. It was found that in every stage of combustion the burning rate of the quiescent case was slower than that in the swirl and tumble flows. In tumble case the best improvement to the burning rate was in the early stage of combustion, when the burnt mass fraction was between 5 and 10 percent. In the swirl case, the best improvement to the burning rate was observed in the middle of the combustion process, when the burnt mass fraction was between 30 and 50 percent.

Arcoumanis and Bae (1993) showed that, for higher mean flow velocity and turbulence intensity, the combustion duration was shorter. The correlation between flow velocity and combustion duration was almost linear.

Lord et al (1993) analyzed early flame kernel growth dynamics and reported that high swirl levels resulted in the highest values of flame kernel growth rate.

1.2.2 Misfire

Misfire which is related to the flammability limits was first recognized by Humbolt and Gay Tussac (1804) and then determined by Dovy (1816). Peters and Quader (1978) compared the lean limit for both a shrouded and an unshrouded valve. They found that by using a shrouded valve the lean limit was lowered from an equivalence ratio of 0.76 to 0.55. In a constant pressure flow reactor, Chomiak and Jarosinski (1982) found that, if the stretch factor (ratio of chemical time to turbulent break-up time) is larger than a critical number (0.5-3.0), quenching by turbulence occurs. Arici et al (1983) showed that higher temperature and higher RPM would extend the lean misfire limit. Anderson and Lim (1985) found experimentally that increasing the spark gap and retarding the spark advance would also extend the lean limit. Pischinger and Heywood (1990) suggested that a large contact area between flame kernel and electrodes may result in a likelihood of misfire because excessive heat loss to the spark plugs results in a slower flame growth. This effect is smaller when using smaller size electrodes. It was also found that the contact area is largely controlled by the local flow field in the spark plug vicinity. A large flow velocity convects the flame kernel away from the electrodes, reducing the contact area and heat loss to the electrodes. They defined a contact area fraction f_c as the ratio of contact area to flame surface area. It was found that for the very early stages of ignition, misfire is likely to occur if $f_c \geq 0.67$. Bondok (1992) investigated the lean misfire limit for a swirling flow in a closed vessel. By testing eleven equivalence ratios for three off-center radially located ignition points, they found that the lean misfire limit was richer with the ignition point farthest from the center.

1.2.3 Flame Development

The important factors affecting the flame kernel development are the flow characteristics, spark plug geometry and ignition energy.

Ho and Santavicca (1987) investigated the turbulence effects on flame kernel growth. They found that the ignition energy strongly affected the initial flame kernel size and the growth rate. High ignition energy leads to a large initial expansion velocity which can delay the onset of turbulence effects on flame kernel growth and this can reduce the probability of misfire. The authors reported that, in a very lean mixture (ϕ=0.58), increased turbulence reduced the mean flame kernel growth rate, but at higher equivalence ratios (greater than ϕ=0.8), increased turbulence resulted in increased mean flame kernel growth rate.

Anderson and Lim (1987) used a high speed schlieren system to record spark kernel development in a quiescent propane-air mixture of 0.7 equivalence ratio. They reported that the effects of power input and spark energy on the kernel development create a difference in the kernel size within the first 100 microseconds. For the same spark energy, the kernel size develops faster with increasing power input, and larger initial flame kernels result in a shorter combustion duration.

Thomas (1983) derived an expression for a two-dimensional flame on a steady laminar burner showing that the specific rate of growth of flame area, also called the flame stretching factor, at any point was proportional to the velocity gradient at that point. For combustion in engines, the specific rate of growth of flame area was obtained from a spherically expanding flame assumption. In this case, it was found that the specific rate of growth of flame area was

the principal governing influence on the time of combustion and large values of this factor were necessary for flame development in an engine. The analysis of flame development also showed that the time of combustion was inversely proportional to the specific rate of growth of flame area.

Pischinger and Heywood (1990) reported that under lean operating conditions the heat loss to the spark plug electrodes has a significant impact on the flame development process. The results showed that the flame growth rate was reduced significantly when the rate of heat loss to the electrodes was comparable to the rate of energy gained from the flame kernel in combustion.

Mantel (1992) investigated the effect of spark plug orientation on flame kernel growth by using a three-dimensional computational simulations of flame kernel formation. Orienting the spark plug gap towards the flow produced the shortest combustion duration and the lowest lean limit.

Arcoumanis and Bae (1993) investigated the relationship between the flame development and the spark plug orientation relative to the mean flow. The initial flame development was quantified in terms of two-dimensional images obtained from single shot shadowgraphs. The two-dimensional flame images were considered representative of the enflamed area rather than the actual three-dimensional flame surface area. It was found that for high mean velocities and high turbulence intensities the case where the spark plug gap faced the flow offered advantages in terms of flame kernel formation and development. However at lower mean velocities and turbulence intensities, the flame kernel development and propagation were less dependent on the orientation of the spark plug relative to the mean flow.

1.2.4 Quenching due to Stretching

Karlovitz et al (1953) introduced a flame stretch factor in a two-dimensional laminar flame to characterize misfire as:

$$K=(\frac{\delta_l}{U})(\frac{dU}{dy}) \tag{1.1}$$

Where δ_l is the thickness of the laminar flame, U is the local velocity of flow and $\frac{dU}{dy}$ is the velocity gradient. For a very small angle between the flame front and the approaching flow, K is also expressed as:

$$K=(\frac{\delta_l}{U})(\frac{1}{A}\frac{dA}{dt}) \tag{1.2}$$

Where $(\frac{1}{A}\frac{dA}{dt})$ is the specific rate of growth of flame area. For large values of the stretch factor ($K \geq 1$), quenching occurs.

Kilmov and Williams (1975) introduced the stretch factor to characterize different combustion regimes as:

$$K=(\frac{\delta_l}{u_l})(\frac{1}{A}\frac{dA}{dt}) \tag{1.3}$$

Where u_l is the laminar burning velocity. For $K \geq 1$ quenching occurs.

Abdel-Gayed and Bradley (1985) introduced a stretch factor as the ratio of chemical lifetime to eddy lifetime as:

$$K=(\frac{u'}{L})(\frac{\delta_l}{u_l}) \qquad \text{for } R_L < 300 \tag{1.4}$$

Where L is the integral scale of turbulence, u' is the rms turbulent fluctuation, $\frac{u'}{L}$ is reciprocal eddy lifetime, $\frac{\delta_l}{u_l}$ is chemical lifetime, and R_L is the turbulent Reynolds number based upon L. For high Reynolds numbers, the stretch factor was introduced as :

$$K=(\frac{u'}{\lambda})(\frac{\delta_l}{u_l}) \qquad \text{for } R_L>300 \tag{1.5}$$

Where λ is the Taylor microscale of turbulence, and $\frac{u'}{\lambda}$ is a strain rate or a reciprocal eddy lifetime based on λ. For high values of $\frac{u'}{L}$ or $\frac{u'}{\lambda}$ quenching occurs.

Later on, Abdel-Gayed and Bradley (1989) correlated flame quenching conditions with the product K.Le for $R_L>300$, where Le is the Lewis number based on the diffusion coefficient D of the deficient reactant. In explosions with a low strain rate, K.Le $\leq$ 0.15, a continuous wrinkled laminar flame sheet was observed. The flame sheet started to break up at higher strain with K.Le $\geq$ 0.15. This process continued up to a value of K.Le= 0.3. At higher values partial quenching was observed in a fragmented reaction zone. For K.Le$\approx$1.5, 20% of the events misfired and 100% misfire occurred when K.Le >6. For $R_L<300$ the Lewis number had no effect, and complete flame quenching occurred when:

$$K.(R_L)^{-0.5}>0.079 \qquad \text{for } R_L<300 \tag{1.6}$$

1.2.5 Flame Kernel Geometry Models

Many studies have been performed on the flame kernel development. Visual techniques like fiber-optics and schlieren or shadowgraph photography have been employed to investigate parameters such as the flame kernel convection velocity and the rate of flame kernel radius

growth. To analyze the behaviour of kernel volume and surface, different flame kernel geometry models have been used. The assumption of spherically expanding flame kernel has been extensively used for a quiescent combustion. Anderson et al (1987) reported that a spark kernel can be treated as a sphere during the ignition phase, but as time progresses it expands more in the direction transverse to the electrodes axis and less in the axial direction. The spherical model is even used in the presence of swirl, tumble, or squish motion in the combustion chamber [Witze (1982), Thomas (1983), Milane and Hill (1988)].

Keck et al (1987) investigated the effects of swirl and squish on flame development. They reported that errors associated with the assumption of spherical symmetry are somewhat smaller than those associated with synchronization of the photographic and pressure records. Witze et al (1988) found that the spherical model was adequate when there was little or no bulk motion in the combustion chamber, but it did not adequately characterize the data when there was high swirl. Milane and Hill (1988) investigated turbulent characteristics of flame propagation in a swirling flow of a stoichiometric mixture of propane-air centrally ignited in a closed cylindrical vessel. Two different models, spherical and cylindrical, were used. It was found that, in a swirling flow, the shape of a spark kernel is between a sphere and a cylinder. Ozdor et al (1994) reported that the presence of either swirl, tumble, or squish motion in the combustion chamber distorts the spherical propagation of the flame and convects it farther along the chamber. However, the higher is the burning rate, the less is the deviation of the flame shape from a sphere, and the less is the distance to which its center is convected during the flame propagation.

Pischinger and Heywood (1990) proposed a flame kernel geometry model based on experimental evidence from their schlieren movies. According to this model, the flame centroid

moves with the flame displacement velocity. The flame can be assumed to be spherical as long as the origin (spark gap center) is within the flame kernel, otherwise the flame is stretched into an ellipsoid.

Kerstein and Witze (1990) presented a flame-kernel model for the analysis of data obtained from fiber-optic flame detectors. In this model it is assumed that the flame kernel shape is elliptical. The growth of the semi-minor axis of the ellipse is interpreted to be due to the flame speed. The growth of the major axis between the spark gap and the farthest point of the flame is taken to be due to the convection velocity and the flame speed. The definitions of convection velocity and flame speed are based on assumptions concerning the influence of combustion, expansion and convection on the shape of the kernel. This model is different from Keck's analysis (1987) which assumes that the increase in flame-kernel area is due to combustion and expansion, whereas convection is an area preserving process.

Herweg and Maly (1992) presented a detailed, time dependent, one-dimensional model for flame kernel formation. In this model the flame kernel is started as a sphere and is convected by the mean flow velocity. In case of a flame holder effect, new flame kernels are generated by continuous ignition at the electrodes while the previously generated kernels are convected away from the spark location. The envelope of these kernels forms a "horn of plenty" which shapes the overall flame kernel. In the model this "horn of plenty" was modelled. In order to compare the results with experiment, kernel formation was measured by simultaneous high speed schlieren filming from two orthogonal views. The results showed a very good agreement between model prediction and experiment for all parameter changes except for the case where the flame detached from the electrodes.

1.3 Objectives

The development of the early flame is very critical under lean operating conditions and visualization is the best way to investigate minor changes in the initial stages of flame development. In this research, laser shadowgraph study of early flame kernel is conducted using a high speed camera. The objective of this investigation is to analyze the behaviour of the flame movement. The circular and the elliptical models are used to calculate the flame speed and the convection velocity. The specific rate of growth of flame area ($\frac{1}{A}\frac{dA}{dt}$) is obtained using three models for flame area A : (i) 2-D flame area A_f measured from the photographs, (ii) spherical flame geometry model, and (iii) ellipsoidal geometry model. The effects of different swirl levels and radial spark locations on the flame speed, the convection velocity, the specific rate of growth of flame area, and the stretch factor at 0.5 ms from ignition time are investigated.

Chapter 2

EXPERIMENTAL TECHNIQUE AND MEASURING PROCEDURES

2.1 Flow Visualization Techniques

The methods which will be described in this chapter are based on the information

obtained from a light beam transmitted through the flow field. This information depends on the variation of the refractive index of the flowing fluid. The deviation of the light beam by the flow field is due to the inhomogeneous distribution of the refractive index in the fluid.

The shadowgraph method, the schlieren (German for streaks or striae) method, and the interferometry method all depend on the optical effects resulting from local variations of refractive index associated with density changes in a fluid. Though they are all dependent on refractive index changes, the methods give different information and supplement each other.

In combustion the shadowgraph method is used in studying how fuels burn, and investigations of heat transfer are aided by the ability of shadowgraph photography to show the paths taken by air passing over a hot surface. In general, the shadowgraph technique can be used to advantage whenever it is desirable to visualize the flow of gases. Movements of the surface of a liquid and convection current within liquids during heating and cooling can also be recorded by using variations of this technique. Being optical, shadowgraph methods do not interfere with the subject being observed.

Other optical methods are also commonly used for visualizing gas flow. Most important of these are the interferometric method and schlieren photography. The interferometric method requires the use of high quality and expensive optical components. This method has the characteristic of producing an image in which the differences in density are proportional to the differences in refractive index in the field. Thus, it is adaptable to quantitative measurements. With shadow photography, the differences in density of the image are proportional to the derivative of the gradient in refractive index. It is most useful in cases where the gradients are numerous and changing rapidly. Schlieren photography, an intermediate between these two cases,

indicates the gradient in refractive index. Its capabilities are adequate for the majority of cases where flow patterns are of interest. Combinations of the three methods sometimes are used.

A major disadvantage of the interferometer for investigating gas flow is its great cost to assemble. Also, much care must be taken in adjusting the instrument, and the results are usually difficult to interpret.

The relationship between the methods can be illustrated by figure 1. A ray of light incident from the left would ordinarily strike the screen at point Q. If a model is placed in the working area near the origin of the coordinates, the airflow will be disturbed, and as a result there will be local changes in density and therefore in refractive index. The incident ray is deviated through a very small angle ψ, and will then strike the screen at the point Q^*, a distance ΔQ from Q. The direct shadow technique gives a measure of ΔQ; the schlieren method gives a measure of ψ; and the interferometric method a measure (in fringe shift) of the change in optical path, $\Delta(Nl)$. In the last expression, N is the refractive index, and l the geometric distance between an arbitrary point ahead of working section and the screen; both quantities change, and it is the difference in the product which is measured in the interferometric method.

These different methods show another behaviour: the shadowgraph responds to changes in the second derivative of the gas density, the schlieren system is sensitive to changes in the first derivative of the gas density, and the interferometric method measures the absolute gas density changes. The schlieren and shadowgraph methods are described briefly in what follows.

2.1.1 The Schlieren Method

Early schlieren systems were used to determine variations in the refractive index of glass.

Other applications were first discovered in 1866 by A.Toepler. Many possible combination of elements can be assembled to form schlieren systems. Figure 2 illustrates a schlieren system based on the use of two Schlieren Heads which is the most popular of all schlieren systems. Although mirrors are shown, good-quality lenses could be used. This system has the unique advantage that parallel rays of light pass through the Schlieren Field, thus producing an image of superior resolution. Another advantage is that the Schlieren Field is located away from the mirrors. The knife edge close to the light source intercepts part of the beam so that the resultant beam has a sharply defined edge. With this technique, after the parallel beam has traversed the test area, it is reconverted at the second knife edge, close to the camera, set to cut off about half of the rays otherwise transmitted to the screen. Rays deviated upward, pass over the knife edge and add to the illumination of the screen, whereas rays deviated downwards are blocked by the knife edge. Changes in refractive index near the object, deviate the rays and cause changes in illumination at the corresponding point in the image. The image is thus surrounded by a shaded pattern indicating air density changes [Holder and North (1963), Palmer (1982), Merzkirch (1987)].

2.1.2 The Shadowgraph Method

The arrangement of this technique is very similar to schlieren method except that the knife edge close to the camera is not used. Although, in some cases the schlieren method gives greater contrast than the shadowgraph method, for engine application there are definite advantages to the

shadowgraph method. Foremost of these is the fact that the density gradients are sufficiently high to give good contrast, so that use of the second schlieren knife edge is unnecessary and merely results in a loss of light intensity. The other advantage is that the shadowgraph is far less sensitive to the quality of the optical components in the system and considerable cost saving can be realized [Witze and Vilchis (1981)]. Due to these reasons the shadowgraph technique is used in this study. Two different types of shadowgraph, using the laser beam as a light source, are described briefly in what follows.

2.1.2.1 Direct Shadowgraph Method

As shown in figure 3, lens L_1 which is usually a microscope objective, focuses the laser beam onto aperture A. The aperture serves as a spatial filter. The expanding beam is recollimated by lens L_2 and is passed through the test section, and the shadowgraph is imaged on a screen.

2.1.2.2 Focused Shadowgraph Method

The previous method has two disadvantages: (1) the location of image may be very close to or far from the test section, and (2) the image size is equal to the test section while it is often desirable to be larger or smaller.

By adding another lens L_3 between the image plane and the test section, both of these problems can be overcome (figure 4). Because lenses of adequate quality generally are not available in sizes more than a few inches in diameter, it is more convenient to use concave

spherical mirrors. This method adopted in this study is called Focused Shadowgraph Technique and is the most popular of all shadowgraph methods.

2.2 Experimental Apparatus

The schematic of the experimental set up is illustrated in figure 5. The complete device consists of a cylindrical combustion chamber, an intake valve, a solenoid valve, a control box with a capacitor discharge ignition system, a high pressure air tank supplying air to activate the air cylinder of the intake valve, a tank containing the mixture of propane and air, a charging tank (small tank) connected to the vessel and a vacuum pump.

2.2.1 Combustion Chamber

The combustion chamber (figures 6 and 7) is a constant volume vessel of disk shape with a diameter of 89 mm and a diameter to width ratio of 0.5, simulating the combustion process near the top-dead-center in an internal combustion engine. The vessel is fitted with one inch thick quartz glass window on each end to permit an optical access. The pressure transducer and the intake valve are flush fitted along the wall of the chamber. A shroud on the intake vale is used to produce the swirling flow in the vessel by directing the flow tangentially to the wall. Because of the valve inertia, the intake valve opens 40 ms after triggering the control box. The intake valve closing occurs 80 ms afterwards.

2.2.2 Control Box

The control box controls both the ignition time and the duration of mixture injection to the combustion chamber. One signal activates the solenoid valve to open and close the intake valve while the second signal triggers the ignition system by discharging the capacitors connected to the primary of the coil. The spark energy can be changed by changing the capacitors. In the control box two capacitors, each with a capacitance of $47\mu f$ and a voltage rating of 100 volts, are connected in series to provide the spark energy of 320 mJ while the voltage across the capacitors was always maintained at 165 volts for all experiments.

2.2.3 Mixture Preparation

Propane and air were premixed into a mixture tank where their equivalence ratio was determined based on their partial pressures. The mixture global chemical reaction describing the combustion of propane and air is :

$$C_3H_8 + \frac{5}{\phi}O_2 + \frac{5\times 3.76}{\phi}N_2 \rightarrow (\frac{5}{\phi} - 5)O_2 + 3CO_2 + 4H_2O + \frac{5\times 3.76}{\phi}N_2 \qquad (2.1)$$

where ϕ is the equivalence ratio. Since the partial pressure method is used, the equivalence ratio can be defined as :

$$\phi = A\frac{P_p}{P_a} \qquad (2.2)$$

where

$$A = \frac{(\frac{M_p}{M_a})}{(\frac{m_p}{m_a})_s} \qquad (2.3)$$

P_p and P_a are the partial pressures of propane and air respectively, $(m_p/m_a)_s$ is the stoichiometric propane-air ratio, and M_p and M_a are the molecular weights of propane and air, respectively.

The pressure regulator of the propane tank and the air tank was adjusted according to the calculated partial pressure of propane and air. When filling up the mixture in the evacuated large tank, propane was injected first, followed by air. It is recommended to fill up the tank slowly to avoid the heating effect from compression, and allow it to reach ambient temperature before any re-adjustment of pressure. After preparation the mixture is allowed three days to mix and reach homogeneity.

2.2.4 Pressure Measurement

The pressure within the combustion chamber was measured using a Kistler Model 601B1 piezoelectric pressure transducer coated with a high temperature silicone rubber compound. The transducer is connected to a Kistler charge amplifier Model No. 5004. The amplifier was set for a long duration time, the transducer sensitivity range was 10-110 and the scale was 5 bar/volts. During the combustion the signals from pressure transducer were digitized and stored on a Nicolet model 3019 digital oscilloscope. For each experiment, 4000 digitized data were transferred and stored on a floppy disk of a micro computer using the program STRM-91 previously developed by Milane and Hill (1988).

2.2.5 Experimental procedure

For each experiment, the combustion chamber was evacuated and then the mixture of propane-air was injected through the intake valve to the chamber from a charging tank with the initial pressure of 320 kPa. All experiments were undertaken for an intake valve lift of 7 mm and an equivalence ratio of 0.645. The ignition was produced by a spark between the electrodes with a gap of 2 mm. The electrodes were taped to a diameter of 0.05 mm from a base diameter of 3 mm to minimize heat transfer from the initial kernel to the electrodes. In this study two different ignition locations at the dimensionless radial distances of 0.55 and 0.68 were investigated.

To investigate the effect of swirl, two different swirl levels were obtained by igniting at two different times, 51ms and 74 ms, after the closure of the intake valve which defines the start of the decaying process of the swirling flow in the combustion chamber.

Focused Shadowgraph Method has been used in this study and the arrangement is illustrated in figure 8. A 10 mW Helium-Neon laser is used as a light source. A microscope objective lens, 40/0.85, with a very short focal length is used to make the parallel laser beam divergent. The spatial filter after the microscope objective lens is used to clear the laser beam of diffraction noise. Two parallel mirrors of 0.15 m diameter with a focal length of 1.1 m are placed 3 m away from each other which is more than twice their focal length to provide space for the test section between the entrance and exit cones of light. The first mirror is placed exactly one focal length away from the spatial filter so that the reflected beam from the first mirror has parallel rays. After the parallel beam has traversed the test area, it is received by the second mirror. The angle α (figure 8) was minimized as much as possible (about 9°) in order to

minimize aberration. The high speed camera is focused at the focal point of the second mirror so that the shadowgraph was imaged directly onto the film. For each event, a high speed tungsten 16 mm × 30.5 m roll of film, Eastman Kodak catalogue No: 1218684, was used. Since the desired camera speed was considered to be 4000 frames per second, the camera was adjusted so that after reaching the desired speed, it triggered the control system.

2.3 Measurements and Calculation Procedures

Photographs of the growing flame kernels were obtained by developing the movies taken by the high speed camera (see Appendix A). The movies were analyzed by enlarging each frame six times and tracing the outer flame boundary using an analyzing projector in the Biomechanics Lab in the School of Human Kinetics at the University of Ottawa.

It was observed that in most cases, a small portion of the flame area, called the contact area A_c, covers some parts of the electrodes. All calculations in this thesis were performed for two cases, with and without considering the contact area.

For each picture the two-dimensional projection of the burned zone area A_f was measured by a Planimeter six times to obtain an average value.

The analysis consists of calculating the flame centroid coordinates, the contact area fraction, the convection velocity, the flame speed, the specific rate of growth of flame area and the stretch factor.

2.3.1 The Flame Centroid

To calculate the flame centroid, each flame area was divided into several parts of rectangular shape. The area A_p of each shape is multiplied by its coordinates x and y to obtain the moments of that area. The sum of the moments for all shapes divided by the total area gives the corresponding coordinates of the flame centroid as:

$$\bar{x}=\frac{\Sigma A_p x}{\Sigma A_p} \qquad \bar{y}=\frac{\Sigma A_p y}{\Sigma A_p} \tag{2.4}$$

The distance between the centroid of the flame and the center of the vessel is:

$$R_c=\sqrt{\bar{x}^2+\bar{y}^2} \tag{2.5}$$

2.3.2 Contact Area Fraction

Pischinger and Heywood (1992) defined a contact area fraction f_c as the ratio of contact area with spark electrodes A_c to total flame area A_f as:

$$f_c=\frac{A_c}{A_f} \tag{2.6}$$

For the very early stages of ignition, misfire due to heat transfer to electrodes is avoided if $f_c<0.67$.

2.3.3 The Circular Model

In this model the two-dimensional flame-kernel shape is assumed to be circular, and in many cases this is a good assumption. The equivalent flame radius R_e is obtained using the flame area A_f, measured by the planimeter as:

$$R_e = \sqrt{\frac{A_f}{\pi}} \tag{2.7}$$

The convection velocity and the flame speed are calculated using Keck's analysis (1987). According to this analysis, the definitions of the flame speed and the convection velocity are based on the assumption that the increase in flame kernel area is attributed to combustion and expansion, whereas convection is an area preserving process. The role of convection is only to distort the shape of the flame kernel and to displace the centroid of the flame kernel.

2.3.3.1 Convection Velocity

The convection velocity was calculated from the displacement of the flame centroid (see figure 9) as:

$$V_k(t) = \frac{((\bar{x}(t+\Delta t) - \bar{x}(t))^2 + (\bar{y}(t+\Delta t) - \bar{y}(t))^2)^{0.5}}{\Delta t} \tag{2.8}$$

where $\bar{x}$, $\bar{y}$ are the flame centroid coordinates.

The radial component V_{rk} of the convection velocity (figure 9) is defined as:

$$V_{rk}(t) = V_k(t)\cos\beta(t) \tag{2.9}$$

The angle β can be calculated from the triangle Δ OAB (figure 9), where the points A and B are the flame centroid in consecutive frames and the point O represents the center of the vessel. Therefore cos β (t) is defined as:

$$\cos\beta(t) = \frac{AB^2 + R_c^2(t) - R_c^2(t+\Delta t)}{2 * R_c(t) * R_c(t+\Delta t)} \tag{2.10}$$

where R_c is the distance between the flame centroid and the center of the vessel.

2.3.3.2 Flame Speed

The flame speed S_k in Keck's analysis is defined as:

$$S_k = \left(\frac{dA_f}{dt}\right)\left(\frac{1}{p}\right) \tag{2.11}$$

Using the central difference method for the derivative, this expression is approximated as:

$$S_k(t) = \left(\frac{A_f(t+\Delta t) - A_f(t-\Delta t)}{2\Delta t}\right)\left(\frac{1}{p(t)}\right) \tag{2.12}$$

where A_f is the two-dimensional area measured by the planimeter, Δt is the time between consecutive frames and p the perimeter of the flame using the circular model is defined as:

$$p = 2\pi R_e \tag{2.13}$$

2.3.4 The Elliptical Model

For swirling flows in which the flame is stretched by the swirl motion, while it is attached to the electrodes, the elliptical flame-kernel shape proposed by Kerstein and Witze (1990) can be used (figure 10).

In this model, the growth of the semi-minor axis is interpreted to be due to the flame speed, S_w. The growth of the major axis, from the spark gap to the farthest point of the flame (figure 10), is taken to be due to the sum of the convection velocity V_w and the flame speed S_w. The minor axis of the ellipse b for each frame is calculated as:

$$b=\frac{A_f}{\pi a} \tag{2.14}$$

where a is the major axis of the ellipse which is measured directly for each frame.

2.3.4.1 Flame Speed

The definitions of the flame speed and the convection velocity in this model are based on the assumption that the increase in flame kernel area is due to the combustion, the expansion and the convection processes. The flame speed S_w which is the sum of the combustion and expansion velocities is defined as:

$$S_w=\frac{b}{t} \tag{2.15}$$

where t is the time from ignition.

2.3.4.2 Convection Velocity

The convection velocity V_w (figure 10) is defined as:

$$V_w = \frac{(2a-b)}{t} \tag{2.16}$$

The expansion of the initial flame kernel due to the spark energy leads to an initial value for the ellipse axes a and b at the ignition time. In order to omit the effect of these initial values on the flame speed S_w and convection velocity V_w in subsequent times, the following expressions are also proposed:

$$S_{ws} = \frac{db}{dt} \tag{2.17}$$

$$V_{ws} = \frac{d(2a)}{dt} - \frac{db}{dt} \tag{2.18}$$

The derivatives in (2.17) and (2.18) have been obtained using central difference approximation. Since the frames were taken at discrete times with a frequency of 4000 frames/sec, the first frame in which the flame appears is taken 0.25 ms after the last frame in which no flame appears. The moment of ignition occurred somewhere between two frames, resulting in an uncertainty of up to 0.25 ms in an estimate of the precise moment of ignition. This can be avoided using 2.17 and 2.18 which are not directly dependent on the time of ignition.

2.3.5 Specific Rate of Growth of Flame Area

The specific rate of growth of flame area is approximated using the central difference method for the derivative as :

$$\frac{1}{A}\frac{dA}{dt}=\left(\frac{1}{A(t)}\right)\left(\frac{A(t+\Delta t)-A(t-\Delta t)}{2\Delta t}\right) \tag{2.19}$$

These calculations were performed for flame area A using three different models:

1- A is assumed to be the measured two-dimensional flame area. In this case the values of the 2-D flame area A_f was used in the expression 2.19.

2- A is assumed to be a three-dimensional flame area using the spherical geometry model. In this model the 2-D flame area A_f is assumed to be circular and the three-dimensional flame area A used in expression 2.19 is:

$$A=4A_f \tag{2.20}$$

3- A is assumed to be a three-dimensional flame area using the ellipsoidal geometry model. The surface of the flame kernel, assumed to be an ellipsoid, is formed by the rotation of the ellipse about its major axis (2a) and was calculated using the formula from Hodgman (1963) as:

$$A=2\pi b^2+2\pi a b\,\frac{\arcsin(\varepsilon)}{\varepsilon} \tag{2.21}$$

where

$$\varepsilon=\frac{(a^2-b^2)^{0.5}}{a} \tag{2.22}$$

2.3.6 Flame Stretching calculations

The effect of flame straining is quantified using the stretch factor expressed by Kilmov and Williams (1975) as:

$$K=(\frac{\delta_l}{u_l})(\frac{1}{A}\frac{dA}{dt}) \tag{2.23}$$

where $(\frac{1}{A}\frac{dA}{dt})$ is the specific rate of growth of flame area, δ_l is the laminar flame thickness and u_l is the laminar burning velocity so that $\frac{\delta_l}{u_l}$ is a chemical lifetime or a reciprocal of the chemical flame strain rate. Ignition will be successful for K < 1. In other words, for successful ignition the specific rate of growth of flame area should be smaller than the reciprocal of the chemical lifetime.

One of the objectives of this study was the calculation of the stretch factor K and the product K.Le at ignition time, and it was done for all experiments performed in this research.

Since the measurement of the chemical lifetime and Lewis number was necessary for future investigation in this vessel, these parameters were evaluated for three radial ignition positions, three swirling levels and the nine equivalence ratios (ϕ) used in Bondok's investigation (1992).

2.3.6.1 Lewis Number Calculations

The Lewis number is defined as:

$$Le = \frac{\lambda_m}{D\rho_m Cp_m} \tag{2.24}$$

where D is the diffusion coefficient of the deficient reactant, λ_m , ρ_m and Cp_m are the thermal conductivity, the density and the specific heat for the mixture, respectively.

The expression of the coefficient of diffusion for a binary mixture was taken from Hirschfelder et al (1964) as:

$$[D_{12}]_1 = 0.0026280 \frac{\sqrt{\frac{T^3(M_1+M_2)}{2M_1M_2}}}{P\sigma_{12}^2\Omega_{12}^{(1,1)*}(T_{12}^*)} \tag{2.25}$$

where D_{12} is the diffusion coefficient in $\frac{cm^2}{\sec}$, P is the pressure in atmospheres, T is the temperature in K, M_1 and M_2 are the molecular weights of fuel and air respectively, $\Omega_{12}^{(1,1)*}$ is the dimensionless collision integral, σ_{12} and $\frac{\epsilon_{12}}{k}$ are molecular potential energy parameters characteristic of 1-2 interaction in Å and K, respectively and T_{12}^* is equal to $\frac{kT}{\epsilon_{12}}$.

The expression of the thermal conductivity for a binary gas mixture (air and fuel) λ_m, was taken from Mason and Saxena (1958) :

$$\lambda_m = \frac{\lambda_1}{1+G_{12}\frac{x_2}{x_1}} + \frac{\lambda_2}{1+G_{21}\frac{x_1}{x_2}} \tag{2.26}$$

where

$$G_{12}=\frac{1.065}{2\sqrt{2}}\left(1+\frac{M_1}{M_2}\right)^{-\frac{1}{2}}\left[1+\left(\frac{M_2\mu_1}{M_1\mu_2}\right)^{\frac{1}{2}}\left(\frac{M_1}{M_2}\right)^{\frac{1}{4}}\right]^2 \tag{2.27}$$

In expression 2.26 x_1 and x_2 are the mole fraction of fuel and air, respectively.

The density of the mixture is:

$$\rho_m=\frac{P}{R_mT} \tag{2.28}$$

where P and T are pressure and temperature respectively and R_m is the gas constant of the mixture which for a binary mixture of propane and air is:

$$R_m=\frac{A\phi R_p+R_A}{A\phi+1} \tag{2.29}$$

where A is fuel fraction at stoichiometry, ϕ is equivalence ratio, R_p and R_A are specific gas constants of propane and air, respectively.

2.3.6.2 Chemical Lifetime Calculations

The laminar flame thickness (δ_l) is defined as:

$$\delta_l=\frac{\nu_m}{u_l} \tag{2.30}$$

where $\nu_m\left(=\frac{\mu_m}{\rho_m}\right)$ is the kinematic viscosity.

The expression for the viscosity of a binary mixture (μ_m) was taken from Wilke (1949):

$$\mu_m = \frac{\mu_1}{1+(\frac{x_2}{x_1})\Gamma_{12}} + \frac{\mu_2}{1+(\frac{x_1}{x_2})\Gamma_{21}} \tag{2.31}$$

where

$$\Gamma_{12} = \frac{[\,1+(\frac{\mu_1}{\mu_2})^{\frac{1}{2}}+(\frac{M_2}{M_1})^{\frac{1}{4}}\,]^2}{(\frac{4}{\sqrt{2}})[\,1+(\frac{M_1}{M_2})\,]^{\frac{1}{2}}} \tag{2.32}$$

The following correlation has been chosen from Gülder (1984) to calculate the burning velocity:

$$u_l(\phi, T, P) = S_{u_o}(\phi)[\,\frac{T_u}{T_{u_o}}\,]^{\alpha}[\,\frac{P}{P_o}\,]^{\beta} \tag{2.33}$$

where

$$S_{u_o}(\phi) = Z.\ W.\ \phi^{\eta}\exp[\,-\xi(\phi-1.075)^2\,] \tag{2.34}$$

ϕ is the equivalence ratio, P_o=100 KPa and T_{u_o}=300 K . For propane, the constant values are:

Z=1

W=0.446 $\frac{m}{s}$

η=0.12

ξ=4.95

β=-0.2

α=1.77

Chapter 3

ANALYSIS OF THE RESULTS AND DISCUSSION

The effects of the different electrode positions and different swirl levels on the stretch factor, on the specific rate of growth of flame area, on the convection velocity and on the flame speed were investigated near the lean misfire limit for an equivalence ratio of 0.645. The ignition point was positioned at two radial locations, $\frac{r}{R}$ =0.55 and $\frac{r}{R}$ =0.68. The swirl levels at ignition time (I.T.) were obtained by igniting the mixture at two different times, 51 ms and 74 ms, after

closing the intake valve.

3.1 The Error Sources

The errors in this study can be attributed to the following sources:

1- The experimental set-up:

Figure 8 shows that the parallel rays passing through the combustion chamber are reflected by the second mirror. The angle α in this set-up produces larger images of the test section when reflected from the second mirror. Figure 11.a shows the front view of the combustion chamber. Because of the angle α, the image of the x-component of the vessel diameter along the electrodes, L sin β, (figure 11.a) is increased to (L sin β)/cos α (figure 11.b), while the y-component of the vessel diameter along the electrodes, L cos β, (figure 11.a) remains unchanged. As a result the image of the length L is increased to L' (figure 11.c) as :

$$L' = (L^2 \cos^2\beta + \frac{L^2 \sin^2\beta}{\cos^2\alpha})^{0.5} \qquad (4.1)$$

In this study, $\beta \approx 30°$ and $\alpha \approx 9°$, therefore $L' = 1.003$ L.

2- The measurements:

The errors which are associated with the measurements are due to the measurements of the flame area A_f and the flame centroid coordinates $(\bar{x}, \bar{y})$. There was up to 6% relative

difference in values obtained from several flame area measurements by the planimeter. There was also about 6% error in calculating the flame centroid coordinates when using different sizes of rectangulars forming the flame area.

3.2 The Pressure Traces

Figure 12 shows the pressure traces versus time. Figure 13 shows the pressure traces when the ignition times of all the experiments start from the origin. Unfortunately due to a flaw in the floppy disk, the pressure traces of the experiments 4 and 5 could not be obtained. The values of the peak pressure and the combustion duration in table 1 are obtained from the stored pressure measurement data on the floppy disk.

For experiment 1, the peak pressure (table 1) is 19.67 bars which is higher than that of experiment 2 (19.53 bars). However the combustion duration of experiment 1, 60.50 ms, is lower than that of experiment 2, 68.50 ms. Therefore a higher peak pressure corresponds to a shorter combustion duration. A similar conclusion is obtained for each pair of experiments with the same operating conditions.

The times of flame detachment from the upper electrode for the different experiments are shown in table 1, and no relation between these values and the peak pressure or combustion duration was identified.

3.3 Contact Area Fraction

The contact area fraction for each frame was calculated from equation 2.6. The results are given in table 2. As can be seen these values are much less than 0.67. Therefore misfire due to heat transfer to the electrodes is not an important mechanism in the present configuration.

3.4 The Circular Model

In this model the flame shape is assumed to be a circle. Appendix A shows the flame traces of all experiments with the circles that have the same center and area as the flame. The following analyses are based on this model and Keck's analysis.

3.4.1 Convection Velocity

According to Keck's analysis, the convection velocity V_k is obtained from the displacement of the centroid of the flame kernel (equation 2.8). Figures 14-17 show the convection velocity using Keck's analysis versus time. The average value for each experiment is given in table 3 which can be compared with the results obtained from Laser Doppler Velocimetry performed by another study on the present vessel. There is an overlap in convection velocity V_k when comparison is made at a given $\frac{r}{R}$ for different swirl levels and also when comparison is made at a given swirl level for different spark locations because of cyclic

variation; even though the average is higher for higher swirl level and for ignition location closer to the wall.

3.4.2 Radial Velocity

The radial velocity values calculated from equation 2.9 are given in table 4. Figures 18-21 show the radial velocity using Keck's analysis versus time. No specific trend in these values was observed.

3.4.3 Flame Speed

Figures 22-25 compare the flame speed, obtained from equation 2.12, for different cases and the average value of S_t for each experiment is given in table 5. Figure 22 compares the flame speed values at $\frac{r}{R}$ =0.55 and $\frac{r}{R}$ =0.68 for I.T.=74 ms. The results indicate greater values of flame speed when ignition location is closer to the wall (experiments 1 and 2). A similar result is obtained at I.T.=51 ms (figure 23). This result correlates with the higher specific rate of growth of flame area near the wall which will be shown later. Figure 24 compares the flame speed at I.T.=51 ms and I.T.=74 ms for $\frac{r}{R}$ = 0.55. The results indicate greater flame speed values for a higher swirl level (experiments 5 and 6). The reason can be due to the greater turbulence intensity in higher swirl levels resulting in faster flame speed. A similar conclusion was not obtained for $\frac{r}{R}$ = 0.68 due to cyclic variations (figure 25).

Table 5 confirms these results for average values of S_t; even though there is an overlap of flame speed values in experiments 1 with 3 due to cyclic variations.

3.5 The Elliptical Model

In this model the flame shape is assumed to be an ellipse. Appendix A shows two sets of flame traces for all experiments with the ellipses that have the same area as the flame. The two cases are :

1- One axis of the ellipse (2a) is taken from the spark gap to the farthest point of the flame.

2- One axis of the ellipse (2a) is taken from the flame edge near the spark gap to the farthest point of the flame.

The following analyses are based on the first case.

3.5.1 Axes of Ellipse

Figures 26-29 show the values of the major axis of the ellipse a measured directly from each frame, and figures 30-33 show the values of the minor axis of the ellipse b obtained from equation 2.14. As can be seen, these values increase almost linearly with time and are used for calculation of the convection velocity and the flame speed in the elliptical model.

3.5.2 Convection Velocity

Figures 34-41 show the convection velocities V_w and V_{ws} obtained from equations 2.16 and 2.18, respectively. The average values of V_w and V_{ws} for each experiment are given in table 3. Generally V_{ws} is lower than V_w by a maximum of 25%. There is an overlap in V_{ws} when comparison is made at a given $\frac{r}{R}$ for different swirl levels because of cyclic variation; even though the average is higher for higher swirl level.

3.5.3 Flame Speed

Figures 42-49 show the flame speeds S_w and S_{ws} obtained from equations 2.15 and 2.17, respectively. S_w decreases at the beginning and after 0.5 ms, it is almost independent of time. The average values of S_w and S_{ws} for each experiment are given in table 5. S_w is higher than S_{ws} by a maximum of 46%. S_w is also generally higher than S_k by a maximum of 36%. The values of S_k are higher than that of S_{ws} by a maximum of 32%. As can be seen, the average flame speed magnitude S_{ws} becomes smaller as the flow decays and as the ignition position approaches the center of the vessel, except the overlap of experiment 1 with 3 and 4 due to cyclic variation.

3.6 Specific Rate of Growth of Flame Area

The values of $(\frac{1}{A}\frac{dA}{dt})$ for the two-dimensional flame area are calculated from equation

2.19. Figures 50-53 show the values of the specific rate of growth of flame area versus flame area. These values decrease as the flame kernel grows. The flame stretching is higher at the beginning of the ignition. The specific rate of growth of flame area values are lower than the values of the reciprocal of the chemical lifetime, which have already been calculated for different situations (table 14), and this is the reason for the successful flame propagation in all experiments.

A comparison of $(\frac{1}{A}\frac{dA}{dt})$ at $\frac{r}{R}$ =0.55 and $\frac{r}{R}$ =0.68 for I.T.=74 ms is shown in figure 54 for the 2-D model, in figure 55 for the spherical model and in figure 56 for the elliptical model. The results indicate greater values of the specific rate of growth of flame area at $\frac{r}{R}$ =0.68 (experiments 1 and 2). A similar conclusion is obtained for I.T.=51 ms (figures 57-59). The reason is due to the highest mean shear rate near the wall in a swirling flow which results in a higher growth rate of the flame area. In a previous work, Borgnakke et al. (1981) introduced an expression for the profile of the mean swirling flow in a constant volume vessel as:

$$U_t = \alpha r + \beta r^2 \tag{4.2}$$

Where α and β are the constant parameters. Therefore the mean shear stress at any location r would be:

$$\frac{\partial U_t}{\partial r} - \frac{U_t}{r} = \beta r \tag{4.3}$$

As can be seen the mean shear stress value is greater as the wall is approached.

Hanson and Thomas (1984) correlated the specific rate of growth of flame area with the shear rate :

$$(\frac{1}{A}\frac{dA}{dt})_{shear} = (\frac{1}{A}\frac{dA}{dt})_{quiescent} + k(\frac{\partial U_t}{\partial r} - \frac{U_t}{r}) \tag{4.4}$$

Where k is a constant. The higher shear rate leads to higher specific rate of growth of flame area, and since the mean shear stress is higher near the wall (equation 4.3), the specific rate of growth of flame area would be higher near the wall. The variation of $(\frac{1}{A}\frac{dA}{dt})$ with spark location explains well the behaviour of the probability of misfire which is higher for the mixture ignited closer to the wall (Bondok, 1993).

A comparison of $(\frac{1}{A}\frac{dA}{dt})$ at I.T.=51 ms and I.T.=74 ms for $\frac{r}{R}$ =0.55 is shown in figure 60 for the 2-D model, in figure 61 for the spherical model and in figure 62 for the elliptical model. The results indicate greater values of the specific rate of growth of flame area for a higher swirl level (experiments 5 and 6). This result is consistent with the fact that the probability of misfire decreases as the flow decays. The reason is due to the fact that in ultra-lean mixtures, excessive mixture motion draws the heat away from the reaction zone and increases the probability of misfire. This is in agreement with the results of previous works (Ho and Santavicca, 1967 & Abdel-Gayed et al., 1986) which indicate that the misfire is more likely as the turbulence intensity is increased beyond a certain level.

Such a conclusion was not obtained for $\frac{r}{R}$ =0.68 (figures 63-65) comparing experiment 1 with 3 & 4. The overlap of $(\frac{1}{A}\frac{dA}{dt})$ values in experiment 1 with 3 & 4 is due to the cyclic variations. This is confirmed by the pressure measurements which indicate identical pressure traces for experiments 1 and 3 even though they are for different swirl levels (figure 13 and table 1).

3.7 Stretch Factor

The calculation of Lewis number and chemical lifetime in different flow conditions is

very important for future investigations in this vessel to check various correlations for the misfire limit. Therefore the values of Lewis number and chemical lifetime are calculated, from equations 2.24 to 2.34, for nine equivalence ratios in three different spark locations and three swirl levels. The results are shown in tables 6 to 14. These values decrease as the ignition position moves toward the center of the vessel, as the swirl level is increased and as the equivalence ratio is richer. The trends in Lewis number and chemical lifetime are due to the fact that they are inversely proportional to the temperature and equivalence ratio.

The stretch factor K and the product K.Le at 500 μs from ignition time were calculated from equations 2.23 and 2.24 and are shown in table 15 for the 2-D and the spherical models and in table 16 for the elliptical model. Tables 15 and 16 indicate that the stretch factor K and the product K.Le have greater values for mixture ignited closer to the wall. The reason is due to the highest mean shear rate near the wall in a swirling flow which results in a higher stretch factor. Tables 15 and 16 also show that K and K.Le values become greater as the swirl level increases. The reason is due to the fact that as the turbulence intensity is increased beyond a certain level, the misfire is more likely.

Chapter 4

CONCLUSIONS & RECOMMENDATIONS

4.1 Conclusions

The flame kernel development of lean propane-air mixture at an equivalence ratio of ϕ=0.645 were visualized by the shadowgraph technique. The parameters which varied during the investigation were the swirl level and the ignition location. The main conclusions of this

investigation about the flame speed and the convection velocity using the circular model and Keck's analysis are summarized below:

1- The flame speed increases as the ignition position approaches the wall.

2- The flame speed decreases as the flow decays.

3- No relation between the time of flame detachment from the upper electrode and the peak pressure or combustion duration was identified.

The main conclusion about the elliptical model are summarized as below:

1- The average flame speed from modified elliptical model S_{wr}, becomes smaller as the flow decays and as the ignition position approaches the center of the vessel.

2- Both the circular and the elliptical models show an overlap in convection velocity when comparison is made at a given spark location for different swirl levels because of cyclic variation; even though the average is higher for higher swirl level.

The main findings of this investigation about the specific rate of growth of flame area and the stretch factor using the 2-D, the spherical and the ellipsoidal models for flame area are summarized as below:

1- The specific rate of growth of flame area increases as the ignition position approaches the wall.

2- The specific rate of growth of flame area decreases as the flow decays.

3- The values of the stretch factor and the product K.Le at 0.5 ms from ignition time increase as the ignition position approaches the wall.

4- The values of the stretch factor and the product K.Le at 0.5 ms from ignition time decrease as the flow decays.

4.2 Recommendations

It is recommended that the behaviour of combustion in swirling conditions, especially in off-center ignition, be modelled numerically to predict the flame position and three-dimensional flame development with time.

It is also recommended that various correlations for the misfire limit be investigated using the values of the chemical lifetime and the Lewis number from this study and the flow characteristics from Laser Doppler Velocimetry.

BIBLIOGRAPHY

[1] Abdel-Gayed, R.G. and Bradley, D. (1985), "Criteria for Turbulent Propagation Limits of Premixed Flames", Combustion and Flame, 62 : 61-68.

[2] Abdel-Gayed, R.G. and Bradley, D. (1989), "Short Communication: Combustion Regimes and the Straining of Turbulent Premixed Flames", Combustion and Flame Vol. 76 : 213-218.

[3] Anderson, R.W. and Lim, M.T. (1985), "Investigation of Misfire in a Fast Burn Spark Ignition Engine", Combustion Science and Technology Vol. 43, pp. 183-196.

[4] Anderson, R.W. and Lim, M.T. (1987), " Experimental Study of a Developing Spark Kernel", Combustion Science and Technology Vol. 44.

[5] Arici, O., Tabaczynski, R.J. and Arpaci, V.S. (1983), "A Model for the Lean misfire Limit in Spark-Ignition Engine", Combustion Science and Technology Vol. 30, pp. 31-45.

[6] Arcoumanis, C. and Bae, C-S. (1993), "Visualization of Flow/Flame Interaction in a Constant-Volume Combustion Chamber", SAE paper 930868.

[7] Bianco, Y., Cheng, W.C. and Heywood, J.B. (1991), "The Effect of Initial Flame Kernel Conditions on Flame Development in SI Engines", SAE paper 912402.

[8] Bondok, A. (1992), "Misfire of Spark Ignited Lean Mixture of Propane-Air in a Constant Volume Vessel", M.Sc. Thesis, University of Ottawa.

[9] Borgnakke, C., Davis, G.C. and Tabaczynski R. J. (1981), "prediction of in-Cylinder Swirl Velocity and Turbulence Intensity for an Open Chamber Cup in Piston Engine", SAE paper 810224.

[10] Chomiak, J. and Jarosinski, J. (1982), "Flame Quenching by Turbulence", Combustion and Flame Vol. 48 pp. 241-249.

[11] Dovy, J. (1816), Phil. Trans. Roy. Soc., 106, 1.

[12] Gülder, O.L. (1984), "Correlation of Laminar Combustion Data for Alternative S.I. Engine Fuels", SAE paper 841000.

[13] Hanson, R.J. and Thomas, A. (1984), "Flame Development in Swirling Flows in Closed

Vessels", Combustion and Flame Vol. 55.

[14] Herweg, R., Begleris, Ph., Zettlitz, A. and Ziegler, G. F. W. (1988), "Flow Field Effects on Flame Kernel Formation in a Spark-Ignition Engine", SAE paper 881639.

[15] Herweg, R. and Maly, R. R. (1992), "A Fundamental Model for Flame Kernel Formation in S. I. Engines", SAE paper 922243.

[16] Heywood, J.B. And Pischinger, S. (1990), "How Heat Losses To The Spark Plug Electrodes Affect Flame Kernel Development in an SI-Engine", SAE Paper 900021.

[17] Hirschfelder, J.O., Curtiss, C.F. and Bird, R.B. (1964), "Molecular Theory of Gases and Liquids", Wiley, New York, p. 539.

[18] Ho, C.M. and Santavicca, D.A. (1987), " Turbulence Effects on Early Flame Kernel Growth", SAE Paper 872100.

[19] Hodgman, C.D. (1963), "Standard Mathematical Tables", Chemical Rubber Publishing Company, New York.

[20] Holder, D.W. and North, R.J. (1963), "Schlieren Methods," Notes on Applied Science No. 31., National Physical Laboratory, London.

[21] Humbolt, A. and Gay Tussac, J.F. (1804), De Physique, 60, 129-168.

[22] Jones, B.E. and Mackworth, J.D. (1975), "Induction Swirl in Spark Ignition Engines", I. Mech. E. Conf. Publ.

[23] Karlovitz, B., Denniston, D.W., Knapschaefer, D.H. and Wells, F.E. (1953), Fourth Symposium (Int.) on Combustion , Williams and Wilkins, Baltlimore, pp. 613-620.

[24] Keck, J.C., Heywood, J. B. and Noske, G. (1987), "Early Flame Development and Burning Rates in Spark Ignition Engines and Their Cyclic Variability", SAE paper 870164.

[25] Kerstein, A.R. and Witze, P.O. (1990), "Flame-Kernel Model for Analysis of Fiber-Optic Instrumented Spark Plug Data", SAE paper 900022.

[26] Kilmov, A.M. and Williams, F.A. (1975), AGARD Conference Proceedings (164), pp. II:1-1-II:1-25.

[27] Lord, D.L., Anderson, R.W., Brehob, D.D. and Kim, Y. (1993),"The Effect of Charge Motion on Early Flame Kernel Development", SAE paper 930463.

[28] Mantel, T. (1992),"Three Dimensional Study of Flame Kernel Formation Around a Spark Plug", SAE paper 920587.

[29] Mason, E.A. and Saxena, W.H. (1958), "Approximate Formula for the Thermal Conductivity of Gas Mixtures", Physics Fluids, 1: 361-369.

[30] Merzkirch, W. (1987), "Flow Visualization", Academic Press, London.

[31] Milane, R.E. and Hill, P.G. (1988), "Turbulent Characteristics of Flame Propagation in a Swirling Flow of Premixed Fuel and Air", Combust. Sci. and Tech. Vol 59.

[32] Ozdor, N., Dulger, M. and Sher, E. (1994), "Cyclic Variability in Spark Ignition Engines - A Literature Survey", SAE paper 940987.

[33] Palmer, C.H. (1982), "Optics Experiments and Demonstrations", The John Hopkins University.

[34] Peters, B.D. and Quader, A. (1978), "Wetting the Appetite of Spark Ignition Engines for Lean Combustion", SAE paper 780234, SAE Trans. Vol. 87.

[35] Pischinger, F. and Adams, W. (1980), "Influence of Intake Swirl on the Characteristics of a Stratified Charged Engine with Prechamber Injection", I. Mech. E. Conf. Publ.

[36] Pischinger, S. and Heywood, J.B. (1990), " How Heat Losses To The Spark Plug Electrodes Affect Flame Kernel Development in an SI-Engine", SAE Paper 900021.

[37] Thomas, A. (1983), " Flame Development in Spark - Ignition Engine", Combustion & Flame, 50 pp. 305- 322.

[38] Vichnievsky, R. and Sale, B. (1958), "Study of Combustion in a Monocylinder Engine" J. Soc. Ing. Auto., Vol. 31.

[39] Wakisaka. T., Hamamoto, Y., Ohigashl, S. and Hashimoto, M. (1979), "Measurements of Air Swirl and its Turbulence Characteristics in the Cylinder of an Internal Combustion Engine.", I. Mech. E. Conf. Publ., Paper No. C91/79.

[40] Wilke, C.R. (1950), "A Viscosity Equation for Gas Mixtures", The Journal of Chemical Physics, 18: 517-519.

[41] Witze, P.O. and Vilchis F.R. (1981), " Stroboscopic Laser Shadowgraph Study of the Effect of Swirl on Homogeneous Combustion in a Spark Ignition Engine ", SAE Paper 810226.

[42] Witze, P.O. (1982), " The Effect of Spark Location on Combustion in a Variable - Swirl Engine", SAE Paper 820044.

[43] Witze, P.O., Hall, M.J. and Wallace, J.S. (1988), "Fiber Optic Instrumented Spark Plug for Measuring Early Flame Development in Spark Ignition Engines", SAE paper 881638.

[44] Witze, P.O. and Matthew J.H. (1990), "Cycle-Resolved Measurements of Flame Kernel Growth and Motion Correlated with Combustion Duration", SAE Paper 900023.

[45] Young, M.B. (1981), "Cyclic Dispersion in the Homogeneous-Charge Spark-Ignition - A Literature Survey", SAE paper 810020.

TABLES

Table 1 : The values of peak pressure, combustion duration and flame detachment time from the upper electrode.

Experiment Number	Location (r /R)	Time from closing intake valve (ms)	Peak pressure (bar)	Combustion duration (ms)	Detachment Time (ms)
1	0.68	74	19.67	60.50	5.50
2	0.68	74	19.53	68.50	3.50
3	0.68	51	19.57	61.00	2.75
4	0.68	51	18.82	-----	6.00
5	0.55	51	18.97	-----	2.50
6	0.55	51	19.03	68.70	3.00
7	0.55	74	19.40	70.00	5.25
8	0.55	74	19.82	67.50	2.50

Table 2 : Contact area fraction f_c

Exp. No \ Frame No	1	2	3	4	5	6
1	0	0.003	0.010	0.025	0.034	0.031
2	0	0.108	0.068	0.073	0.055	0.072
3	0	0.017	0.048	0.059	0.053	0.047
4	0	0.023	0.050	0.101	0.070	0.062
5	0	0.075	0.034	0.067	0.079	0.061
6	0	0.083	0.033	0.058	0.044	0.050
7	0	0.017	0.014	0.044	0.056	0.054
8	0	0.039	0.050	0.053	0.059	0.061

Table 3 : The average values of the convection velocities.

Experiment Number	Location (r/R)	Time from closing intake valve (ms)	V_w	V_{ws}	V_k
1	0.68	74	3.01	3.40	3.10
2	0.68	74	3.97	3.72	3.76
3	0.68	51	3.75	3.67	5.11
4	0.68	51	4.96	4.30	3.59
5	0.55	51	4.17	3.10	2.95
6	0.55	51	4.06	4.64	4.10
7	0.55	74	5.00	4.04	3.73
8	0.55	74	3.13	2.78	3.02

Table 4 : The average values of the radial velocity.

Experiment Number	Location (r/R)	Time from closing intake valve (ms)	V_{rk} (m/s)
1	0.68	74	1.42
2	0.68	74	1.11
3	0.68	51	0.45
4	0.68	51	1.3
5	0.55	51	0.73
6	0.55	51	2.43
7	0.55	74	1.94
8	0.55	74	1.86

Table 5 : The average values of the flame speeds.

Experiment Number	Location (r/R)	Time from closing intake valve (ms)	S_w	S_{ws}	S_k
1	0.68	74	4.09	2.49	2.71
2	0.68	74	3.18	2.15	2.54
3	0.68	51	3.45	2.33	2.65
4	0.68	51	2.67	2.41	2.84
5	0.55	51	2.41	1.86	2.16
6	0.55	51	3.38	1.81	2.47
7	0.55	74	1.76	1.21	1.79
8	0.55	74	2.51	1.24	1.60

Table 6 : Chemical lifetime and Lewis number values for equivalence ratio ϕ=0.57.

Parameters	Time from closing intake valve (ms)	r/R=0.68	r/R=0.55	r/R=0.25
T (K)	28	331	341	357
	51	329	336	351
	74	326	333	345
$\nu \times 10^6$ $(\frac{m^2}{s})$	28	5.66	5.96	6.45
	51	5.60	5.81	6.26
	74	5.52	5.72	6.08
$U_l(\frac{m}{s})$	28	0.110	0.116	0.126
	51	0.108	0.113	0.122
	74	0.107	0.111	0.118
$\delta_l \times 10^6$ (m)	28	51.45	51.38	51.19
	51	51.47	51.41	51.31
	74	51.58	51.53	51.52
$\frac{\delta_l}{U_l} \times 10^6$ (s)	28	467.72	442.93	406.27
	51	473.00	454.95	420.57
	74	482.05	464.23	436.61
Le	28	2.341	2.335	2.324
	51	2.343	2.338	2.328
	74	2.345	2.340	2.332

Table 7 : Chemical lifetime and Lewis number values for equivalence ratio ϕ=0.58.

Parameters	Time from closing intake valve (ms)	r/R=0.68	r/R=0.55	r/R=0.25
T (K)	28	331	341	357
	51	329	336	351
	74	326	333	345
$\nu \times 10^6$ $(\frac{m^2}{s})$	28	5.66	5.95	6.44
	51	5.60	5.80	6.25
	74	5.51	5.71	6.07
$U_l(\frac{m}{s})$	28	0.116	0.123	0.133
	51	0.115	0.120	0.129
	74	0.113	0.118	0.125
$\delta_l \times 10^6$ (m)	28	48.79	48.37	48.42
	51	48.69	48.33	48.45
	74	48.76	48.39	48.56
$\frac{\delta_l}{U_l} \times 10^6$ (s)	28	420.60	393.25	364.06
	51	423.39	402.75	375.58
	74	431.50	410.08	388.48
Le	28	2.339	2.331	2.320
	51	2.340	2.335	2.324
	74	2.343	2.338	2.328

Table 8 : Chemical lifetime and Lewis number values for equivalence ratio ϕ=0.59.

Parameters	Time from closing intake valve (ms)	r/R=0.68	r/R=0.55	r/R=0.25
T (K)	28	331	341	357
	51	329	336	351
	74	326	333	345
$\nu \times 10^6$ $(\frac{m^2}{s})$	28	5.65	5.95	6.43
	51	5.59	5.80	6.25
	74	5.50	5.71	6.07
$U_l(\frac{m}{s})$	28	0.122	0.129	0.140
	51	0.121	0.125	0.136
	74	0.119	0.123	0.131
$\delta_l \times 10^6$ (m)	28	46.31	46.12	45.92
	51	46.19	46.40	45.95
	74	46.20	46.42	46.33
$\frac{\delta_l}{U_l} \times 10^6$ (s)	28	379.59	357.52	328.00
	51	381.73	371.20	337.86
	74	388.23	377.39	353.66
Le	28	2.336	2.328	2.317
	51	2.337	2.332	2.321
	74	2.340	2.335	2.326

Table 9 : Chemical lifetime and Lewis number values for equivalence ratio ϕ=0.60.

Parameters	Time from closing intake valve (ms)	r/R=0.68	r/R=0.55	r/R=0.25
T (K)	28	331	341	357
	51	329	336	351
	74	326	333	345
$\nu \times 10^6$ $(\frac{m^2}{s})$	28	5.65	5.94	6.43
	51	5.59	5.79	6.24
	74	5.50	5.70	6.06
$U_l(\frac{m}{s})$	28	0.129	0.136	0.147
	51	0.127	0.132	0.143
	74	0.125	0.130	0.138
$\delta_l \times 10^6$ (m)	28	43.79	43.67	43.74
	51	44.01	43.86	43.63
	74	44.00	43.84	43.91
$\frac{\delta_l}{U_l} \times 10^6$ (s)	28	339.45	321.10	297.55
	51	346.53	332.27	305.10
	74	352.00	337.23	318.18
Le	28	2.333	2.326	2.313
	51	2.335	2.329	2.317
	74	2.338	2.332	2.322

Table 10 : Chemical lifetime and Lewis number values for equivalence ratio ϕ=0.61.

Parameters	Time from closing intake valve (ms)	r/R=0.68	r/R=0.55	r/R=0.25
T (K)	28	331	341	357
	51	329	336	351
	74	326	333	345
$\nu \times 10^6$ $(\frac{m^2}{s})$	28	5.64	5.94	6.43
	51	5.58	5.79	6.24
	74	5.50	5.70	6.06
$U_l(\frac{m}{s})$	28	0.135	0.143	0.155
	51	0.134	0.139	0.150
	74	0.132	0.137	0.146
$\delta_l \times 10^6$ (m)	28	41.77	41.53	41.48
	51	41.64	41.65	41.60
	74	41.66	41.60	41.50
$\frac{\delta_l}{U_l} \times 10^6$ (s)	28	309.40	290.42	267.61
	51	310.74	299.64	277.33
	74	315.60	303.65	284.24
Le	28	2.329	2.318	2.310
	51	2.331	2.323	2.314
	74	2.335	2.327	2.319

Table 11 : Chemical lifetime and Lewis number values for equivalence ratio ϕ=0.62.

Parameters	Time from closing intake valve (ms)	r/R=0.68	r/R=0.55	r/R=0.25
T (K)	28	331	341	357
	51	329	336	351
	74	326	333	345
$\nu \times 10^6$ $(\frac{m^2}{s})$	28	5.64	5.93	6.42
	51	5.60	5.79	6.24
	74	5.49	5.70	6.05
$U_l(\frac{m}{s})$	28	0.141	0.149	0.161
	51	0.140	0.145	0.157
	74	0.137	0.143	0.152
$\delta_l \times 10^6$ (m)	28	40.00	39.79	39.87
	51	40.00	39.93	39.74
	74	40.07	39.86	39.80
$\frac{\delta_l}{U_l} \times 10^6$ (s)	28	283.68	267.04	247.64
	51	285.71	275.38	253.12
	74	292.48	278.74	261.84
Le	28	2.326	2.318	2.306
	51	2.327	2.322	2.310
	74	2.330	2.324	2.315

Table 12 : Chemical lifetime and Lewis number values for equivalence ratio ϕ=0.63.

Parameters	Time from closing intake valve (ms)	r/R=0.68	r/R=0.55	r/R=0.25
T (K)	28	331	341	357
	51	329	336	351
	74	326	333	345
$\nu \times 10^6$ $(\frac{m^2}{s})$	28	5.64	5.93	6.42
	51	5.58	5.78	6.23
	74	5.49	5.69	6.05
$U_l(\frac{m}{s})$	28	0.148	0.156	0.170
	51	0.147	0.152	0.165
	74	0.144	0.150	0.160
$\delta_l \times 10^6$ (m)	28	38.10	38.01	37.76
	51	37.96	38.02	37.75
	74	38.12	37.93	37.81
$\frac{\delta_l}{U_l} \times 10^6$ (s)	28	257.43	243.65	222.11
	51	258.23	250.13	228.78
	74	264.75	252.86	236.31
Le	28	2.326	2.317	2.303
	51	2.328	2.321	2.308
	74	2.331	2.324	2.313

Table 13 : Chemical lifetime and Lewis number values for equivalence ratio ϕ=0.64.

Parameters	Time from closing intake valve (ms)	r/R=0.68	r/R=0.55	r/R=0.25
T (K)	28	331	341	357
	51	329	336	351
	74	326	333	345
$\nu \times 10^6$ $(\frac{m^2}{s})$	28	5.63	5.93	6.41
	51	5.57	5.78	6.23
	74	5.49	5.69	6.05
$U_l(\frac{m}{s})$	28	0.156	0.164	0.178
	51	0.154	0.160	0.173
	74	0.152	0.158	0.168
$\delta_l \times 10^6$ (m)	28	36.08	36.16	36.01
	51	36.16	36.12	36.01
	74	36.11	36.01	36.01
$\frac{\delta_l}{U_l} \times 10^6$ (s)	28	231.28	220.48	202.30
	51	234.85	225.75	208.15
	74	237.56	227.91	214.34
Le	28	2.324	2.315	2.300
	51	2.326	2.319	2.308
	74	2.329	2.322	2.311

Table 14 : Chemical lifetime and Lewis number values for equivalence ratio ϕ=0.645.

Parameters	Time from closing intake valve (ms)	r/R=0.68	r/R=0.55	r/R=0.25
T (K)	28	331	341	357
	51	329	336	351
	74	326	333	345
$\nu \times 10^6$ $(\frac{m^2}{s})$	28	5.63	5.93	6.41
	51	5.56	5.78	6.23
	74	5.49	5.68	6.05
$U_l(\frac{m}{s})$	28	0.160	0.168	0.182
	51	0.157	0.164	0.177
	74	0.156	0.162	0.172
$\delta_l \times 10^6$ (m)	28	35.07	35.23	35.13
	51	35.27	35.17	35.13
	74	35.10	35.05	35.11
$\frac{\delta_l}{U_l} \times 10^6$ (s)	28	218.21	208.89	192.39
	51	223.16	213.56	197.83
	74	223.96	215.43	203.35
Le	28	2.323	2.314	2.298
	51	2.325	2.318	2.308
	74	2.328	2.321	2.310

Table 15 : Stretch factor and the product K.Le at 0.5 ms from ignition time for the 2-D and the spherical models.

Experiment Number	Location (r/R)	Time from closing intake valve (ms)	K	K . Le
1	0.68	74	0.66	1.53
2	0.68	74	0.63	1.46
3	0.68	51	0.76	1.76
4	0.68	51	0.97	2.25
5	0.55	51	0.54	1.25
6	0.55	51	0.59	1.36
7	0.55	74	0.54	1.25
8	0.55	74	0.50	1.16

Table 16 : Stretch factor and the product K.Le at 0.5 ms from ignition time for the ellipsoidal model.

Experiment Number	Location (r/R)	Time from closing intake valve (ms)	K	K . Le
1	0.68	74	0.67	1.55
2	0.68	74	0.53	1.23
3	0.68	51	0.77	1.79
4	0.68	51	1.05	2.44
5	0.55	51	0.53	1.23
6	0.55	51	0.52	1.20
7	0.55	74	0.53	1.23
8	0.55	74	0.46	1.06

Figures

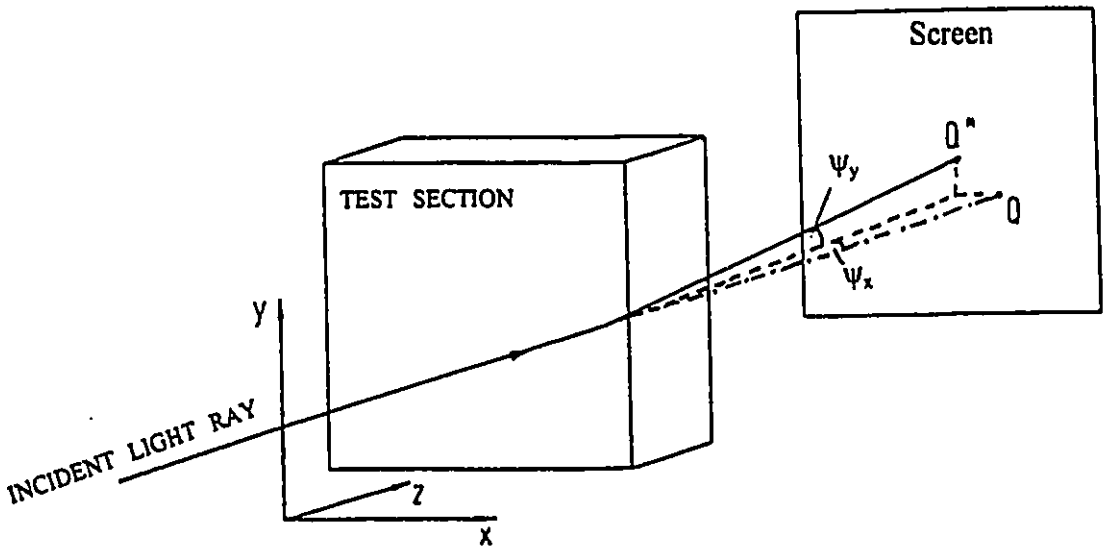

Figure 1 : Deflection of a light ray in an inhomogeneous test section.

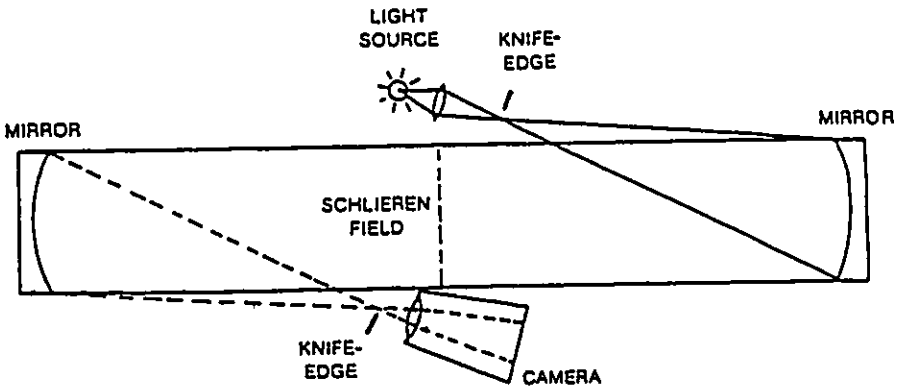

Figure 2 : Two-element schlieren system.

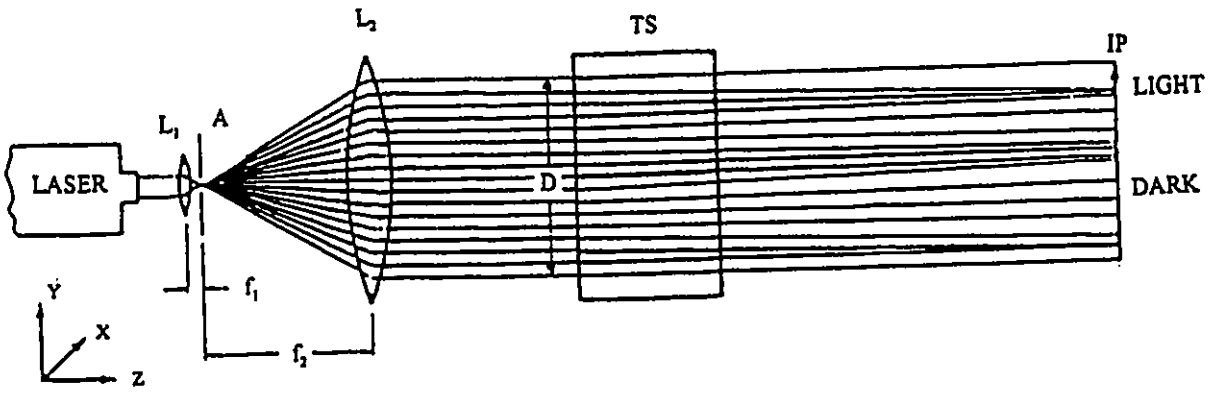

Figure 3 : Direct shadowgraph method.

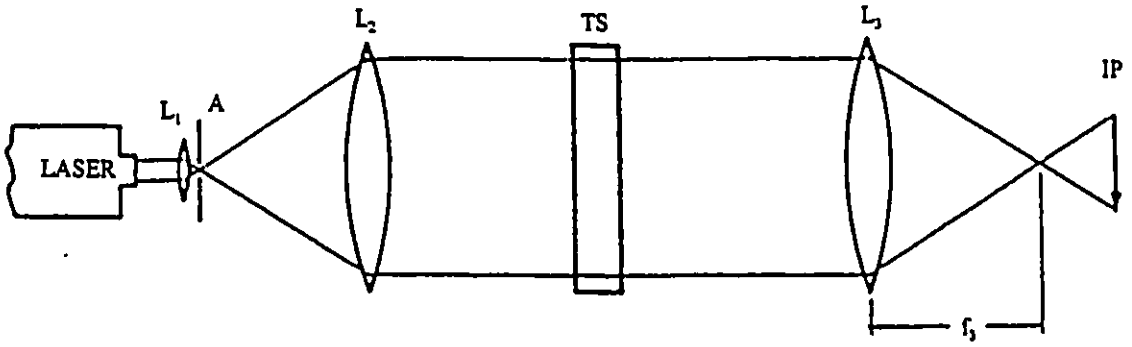

Figure 4 : Focused shadowgraph method.

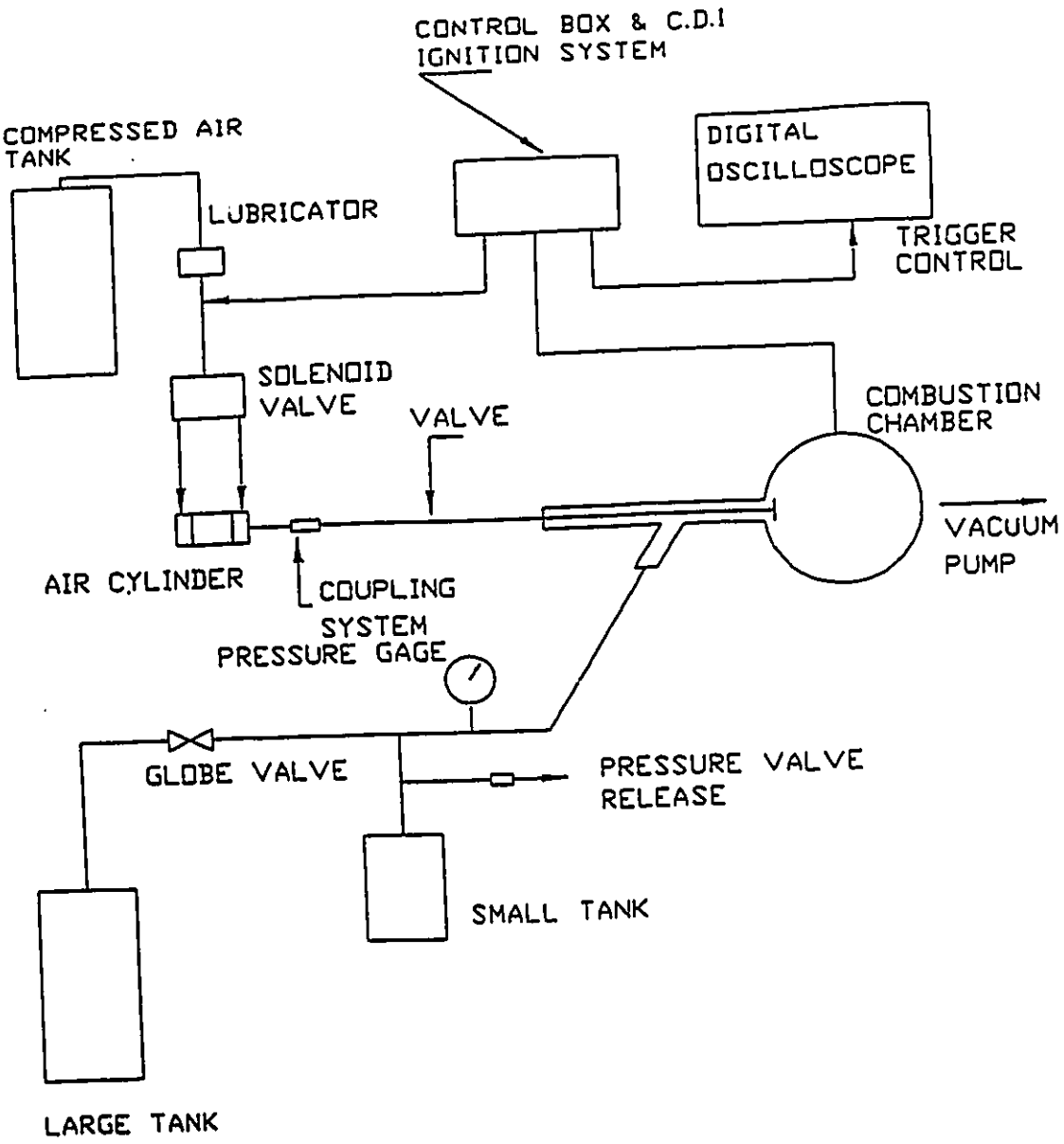

Figure 5 : Schematic of experimental set-up.

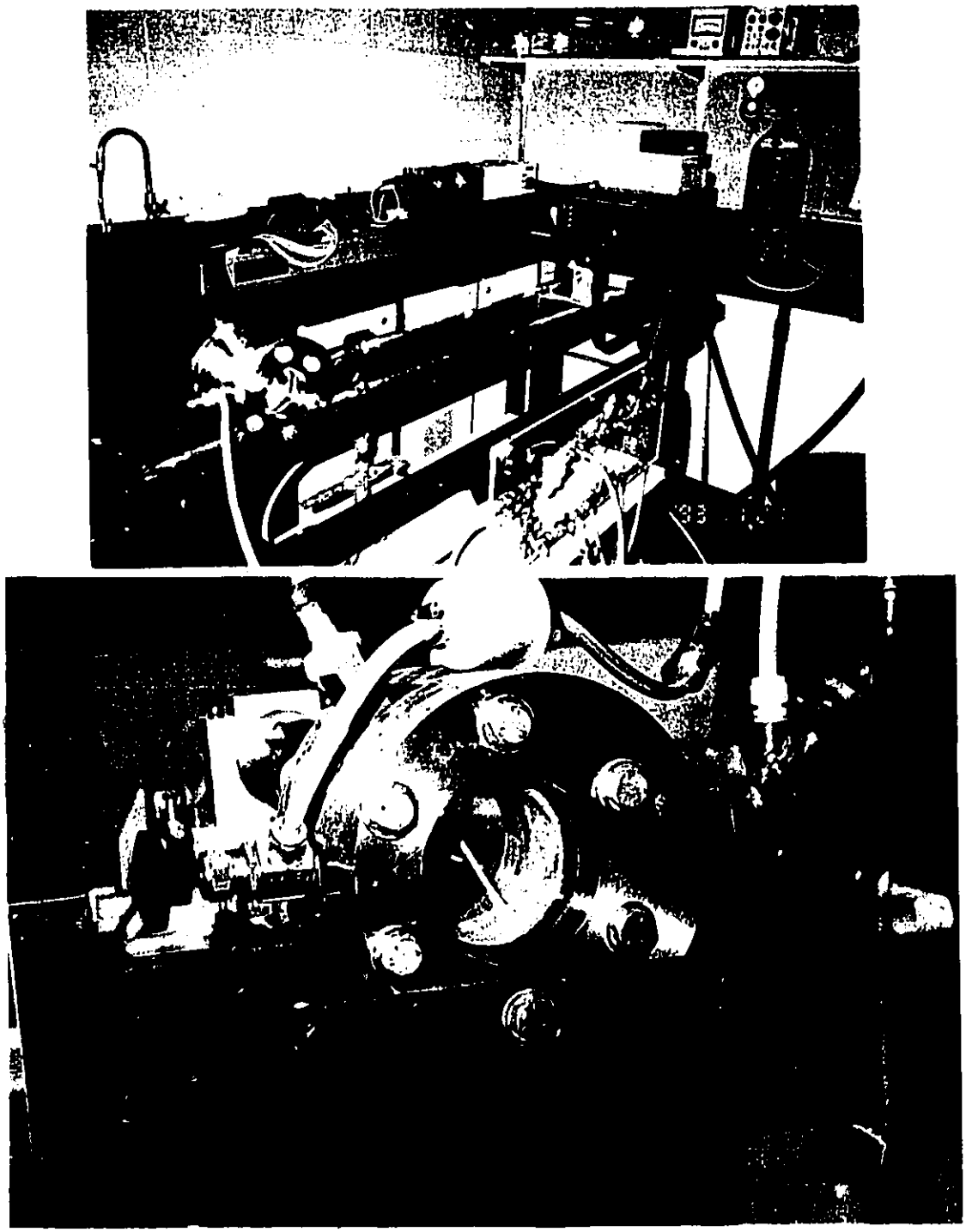

Figure 6 Top : Photograph of the apparatus. Bottom : Photograph of the vessel.

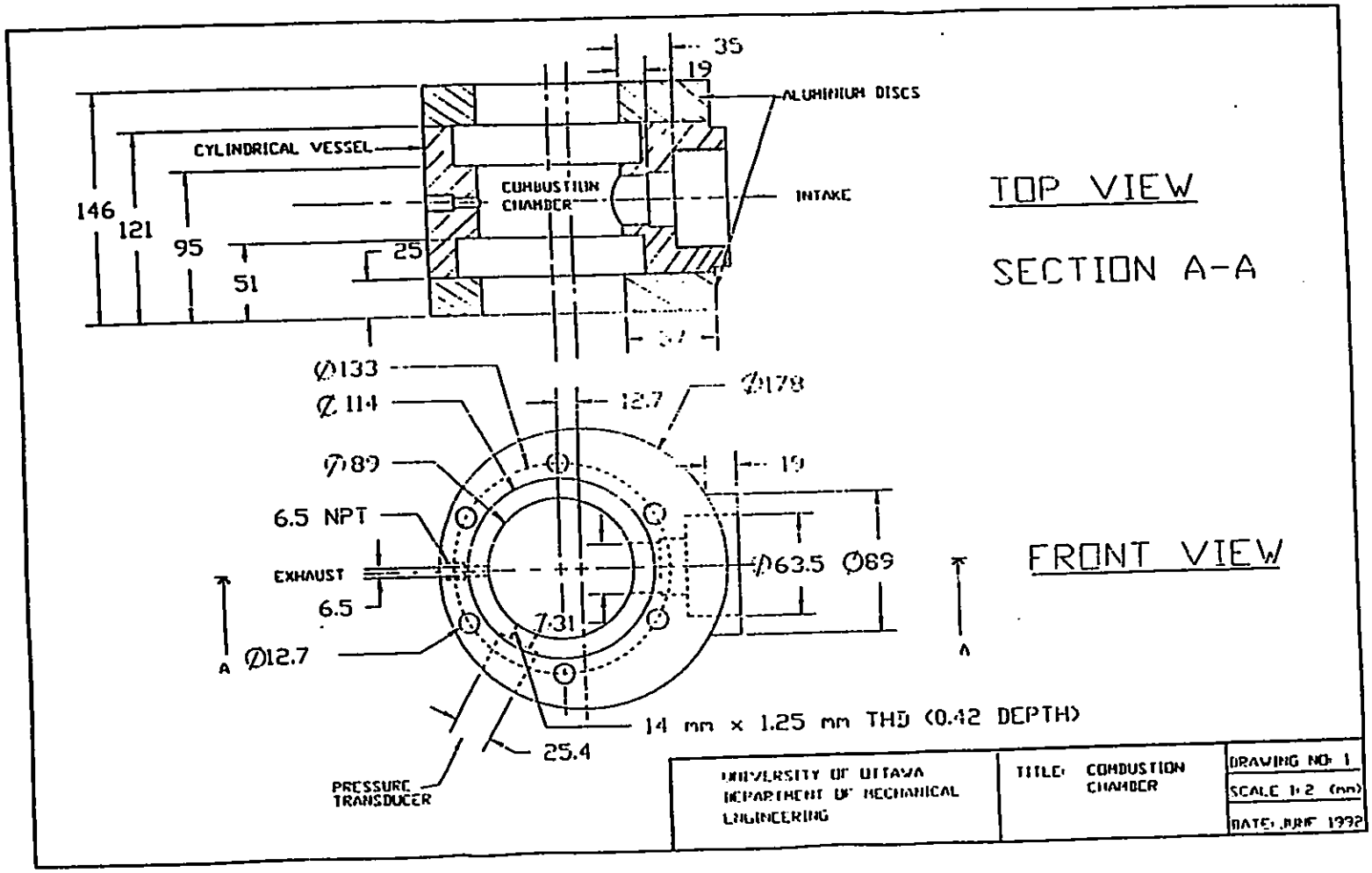

Figure 7 : Top and front view of the vessel.

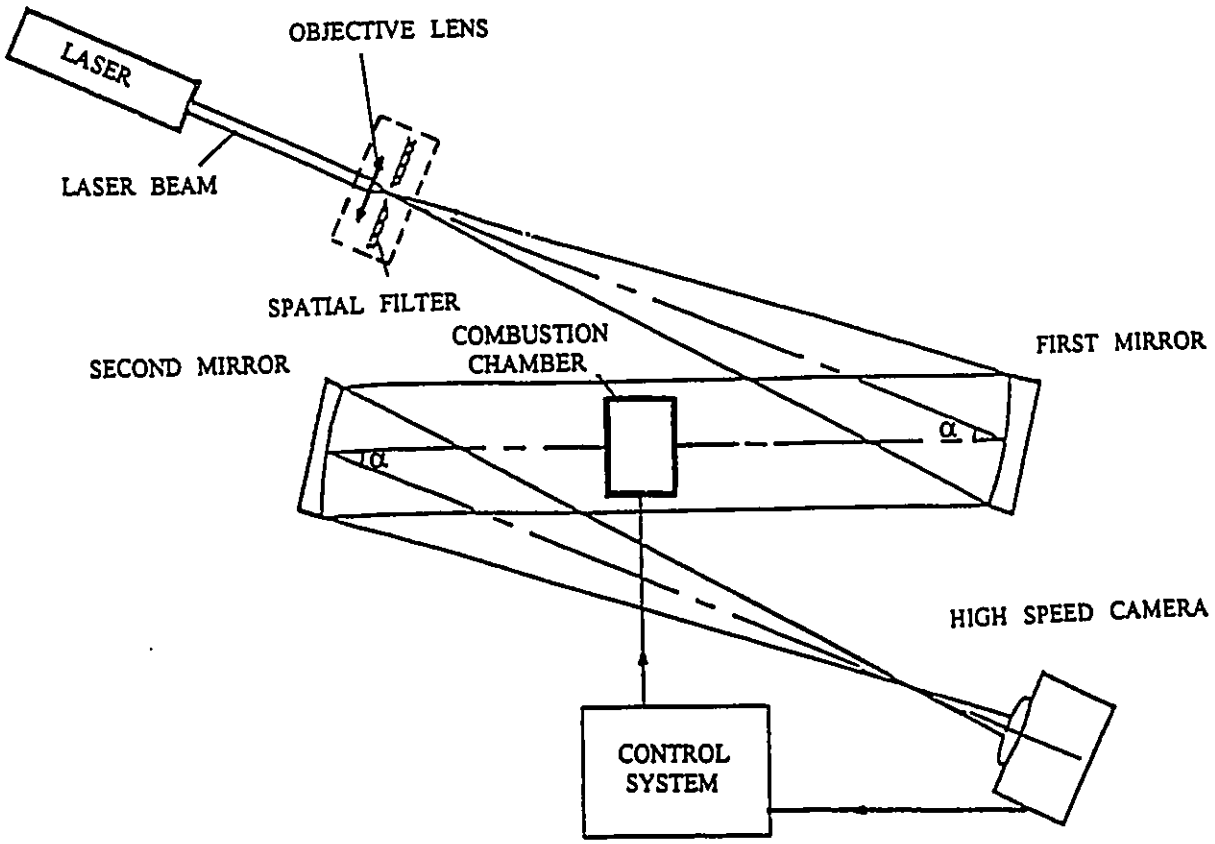

Figure 8 : Schematic of laser shadowgraph set-up.

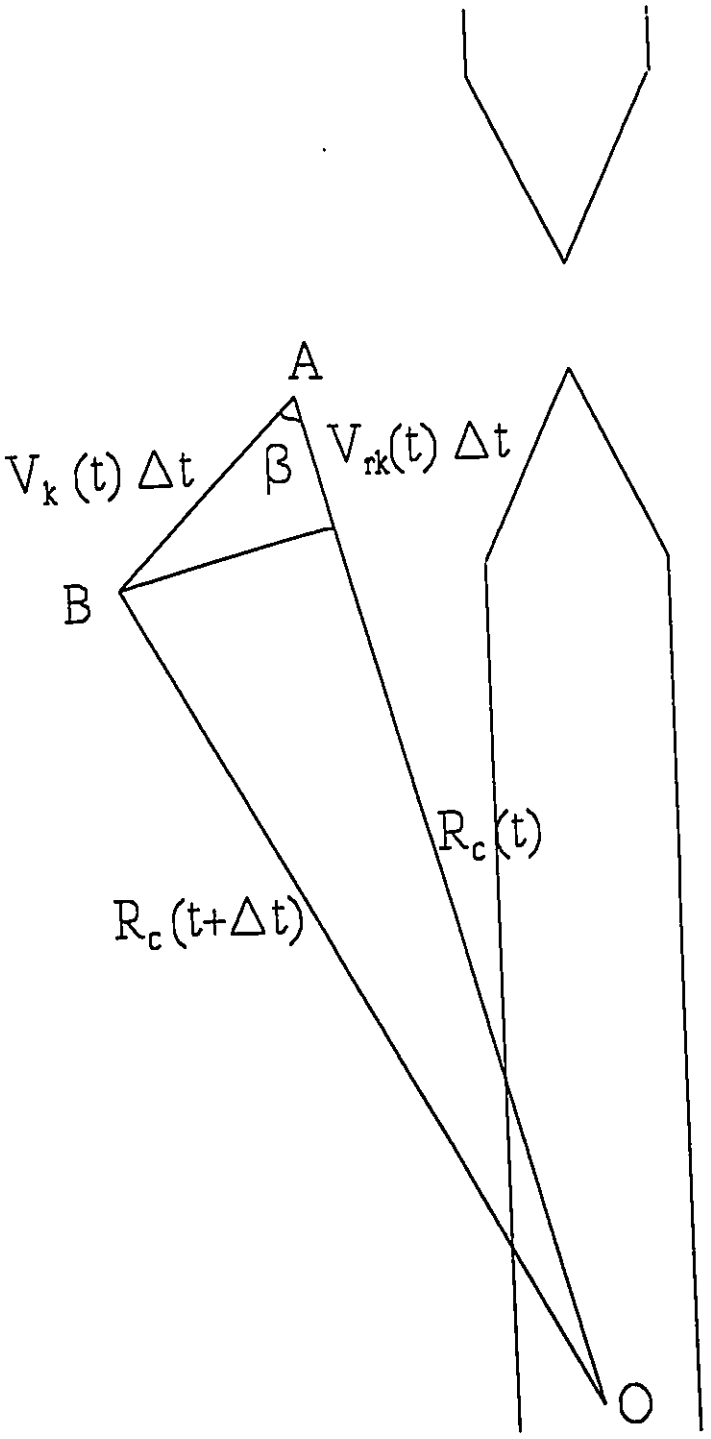

Figure 9 : Convection and radial velocities (Keck's analysis).

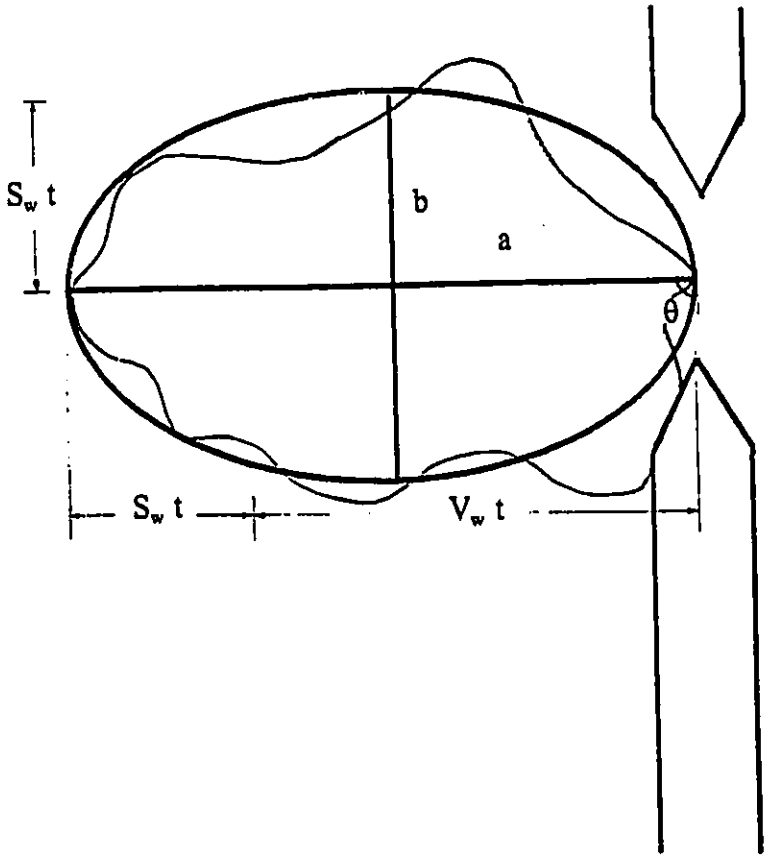

Figure 10 : Convection velocity and flame speed (Elliptical model).

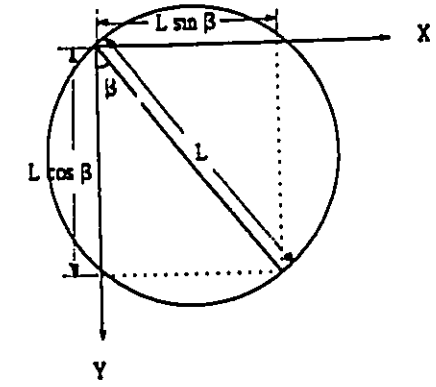

Front view of combustion chamber

11.a

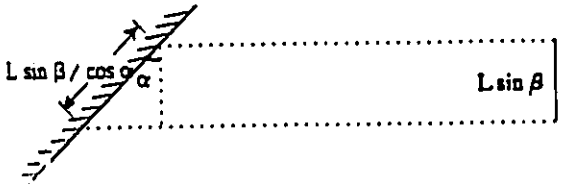

Second mirror

Top view

11.b

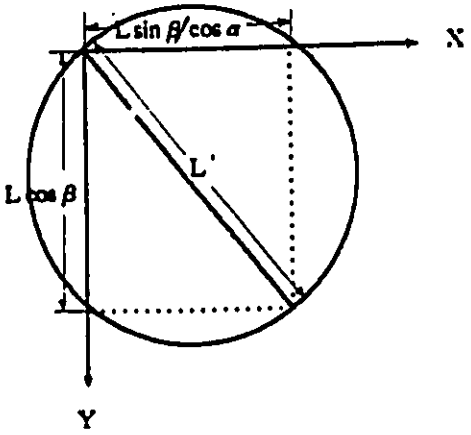

11.c

Figure 11 : The error due to the shadowgraph set-up.

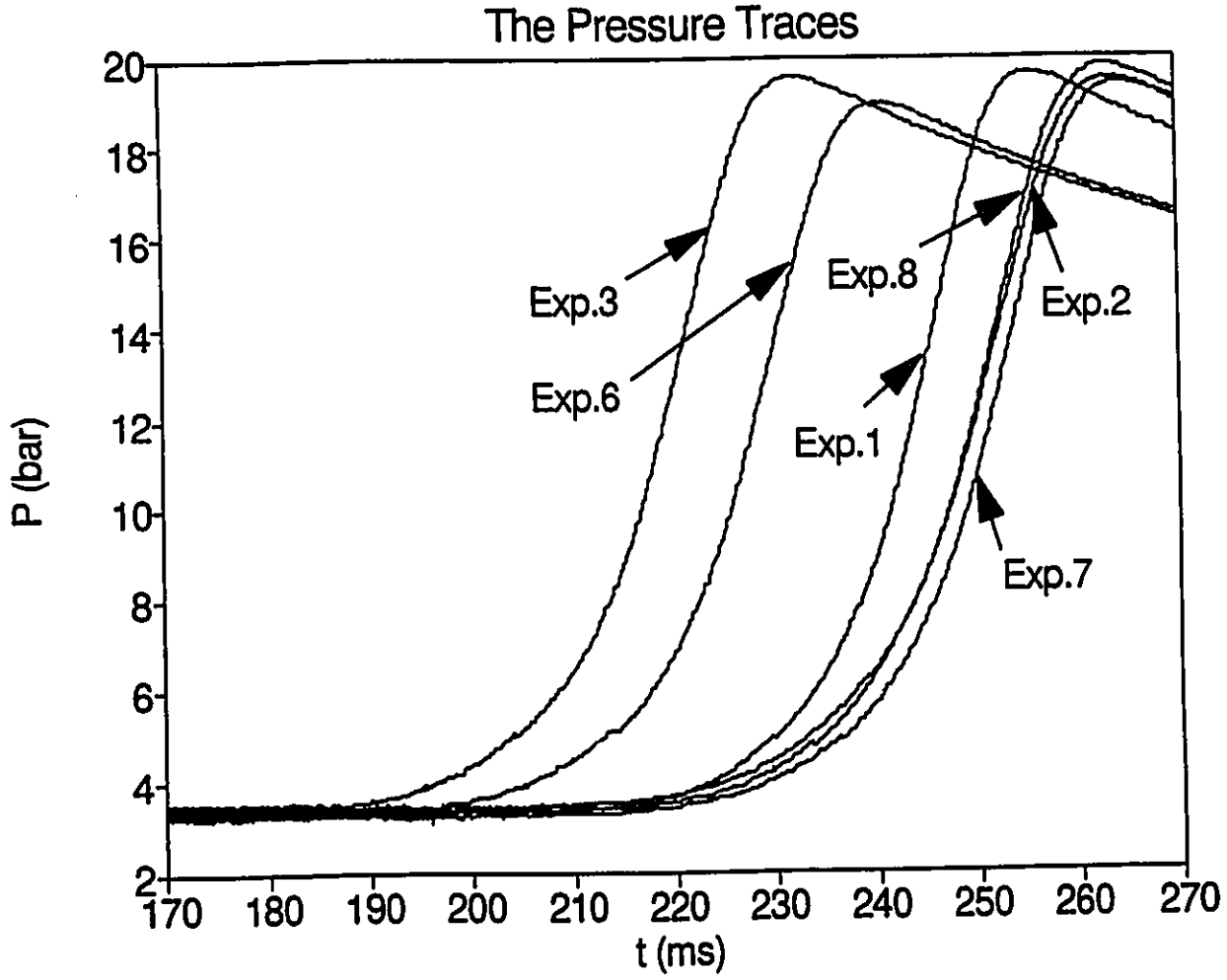

Figure 12 : Pressure versus time for different experiments.

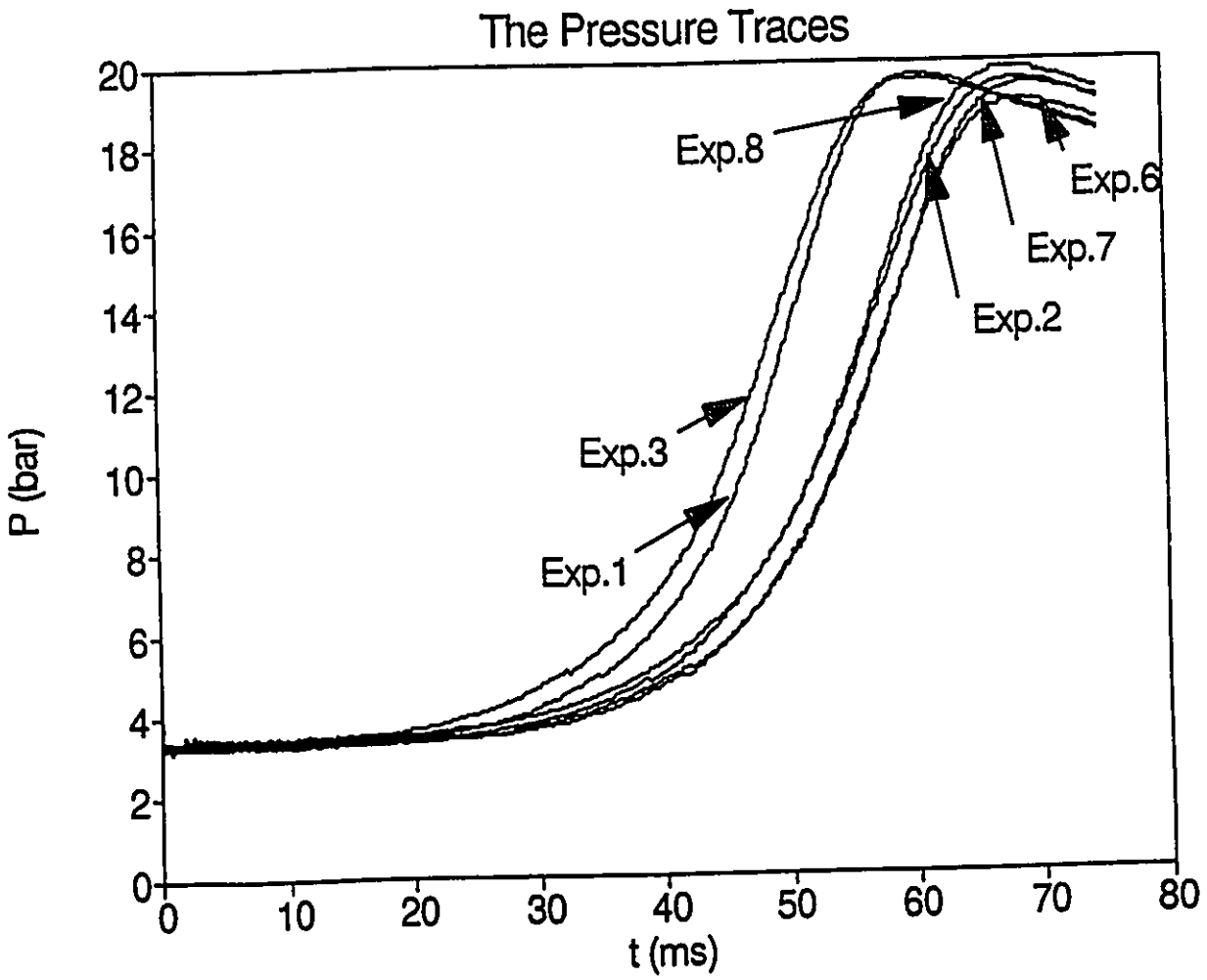

Figure 13 : Pressure traces showing the ignition times start from the origin.

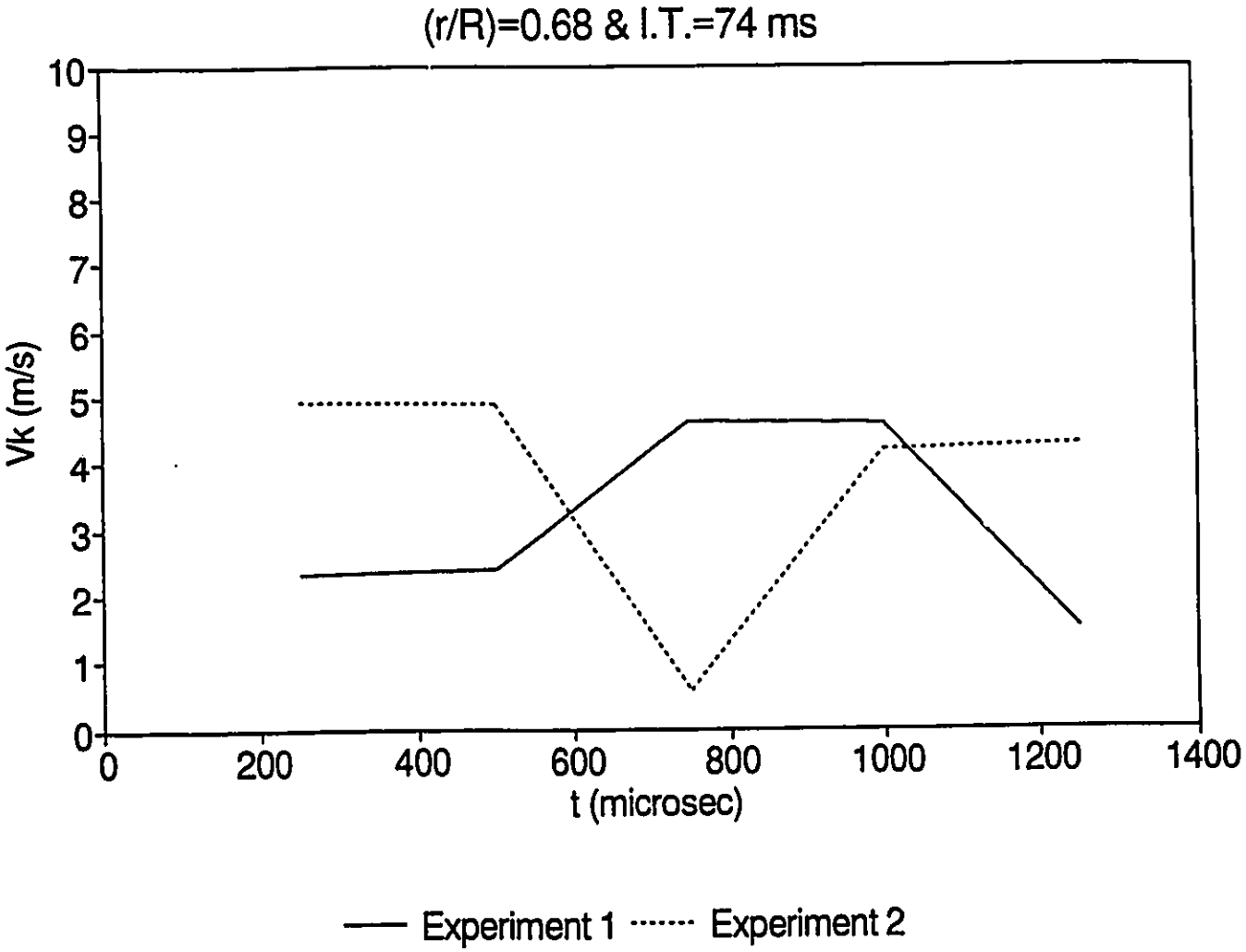

Figure 14 : Convection velocity using Keck's analysis for (r/R)=0.68 and I.T.=74 ms.

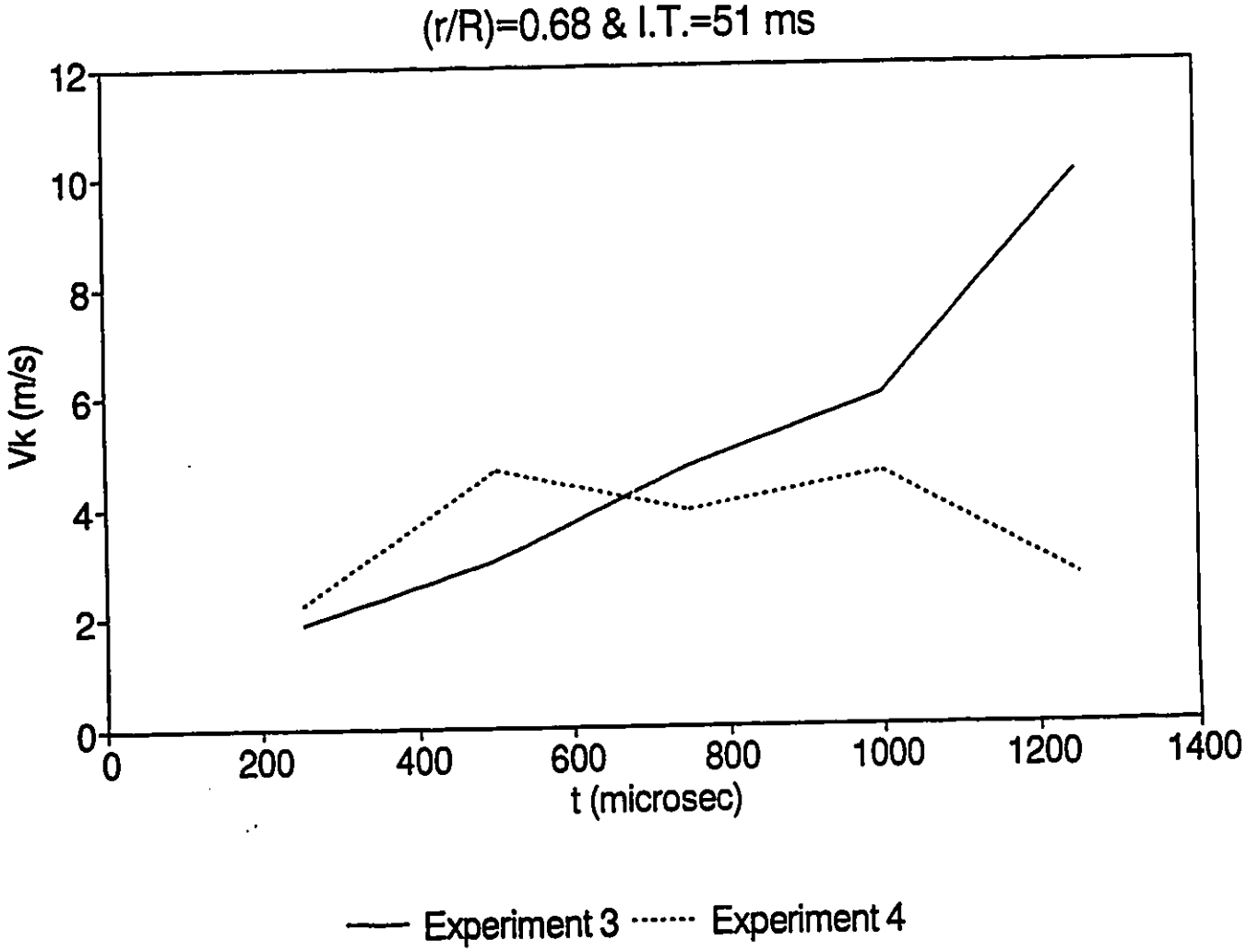

Figure 15 : Convection velocity using Keck's analysis for (r/R)=0.68 and I.T.=51 ms.

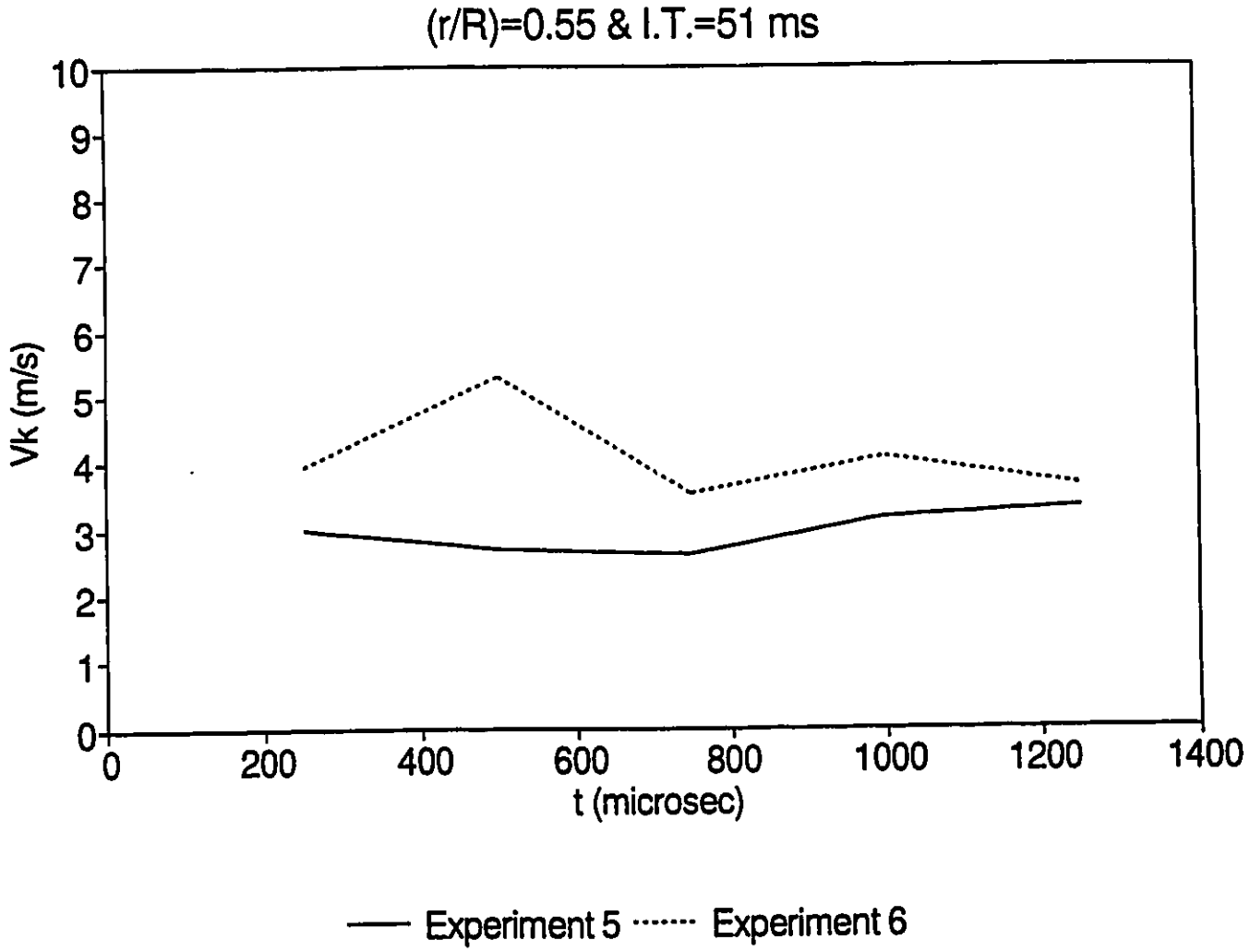

Figure 16 : Convection velocity using Keck's analysis for (r/R)=0.55 and I.T.=51 ms.

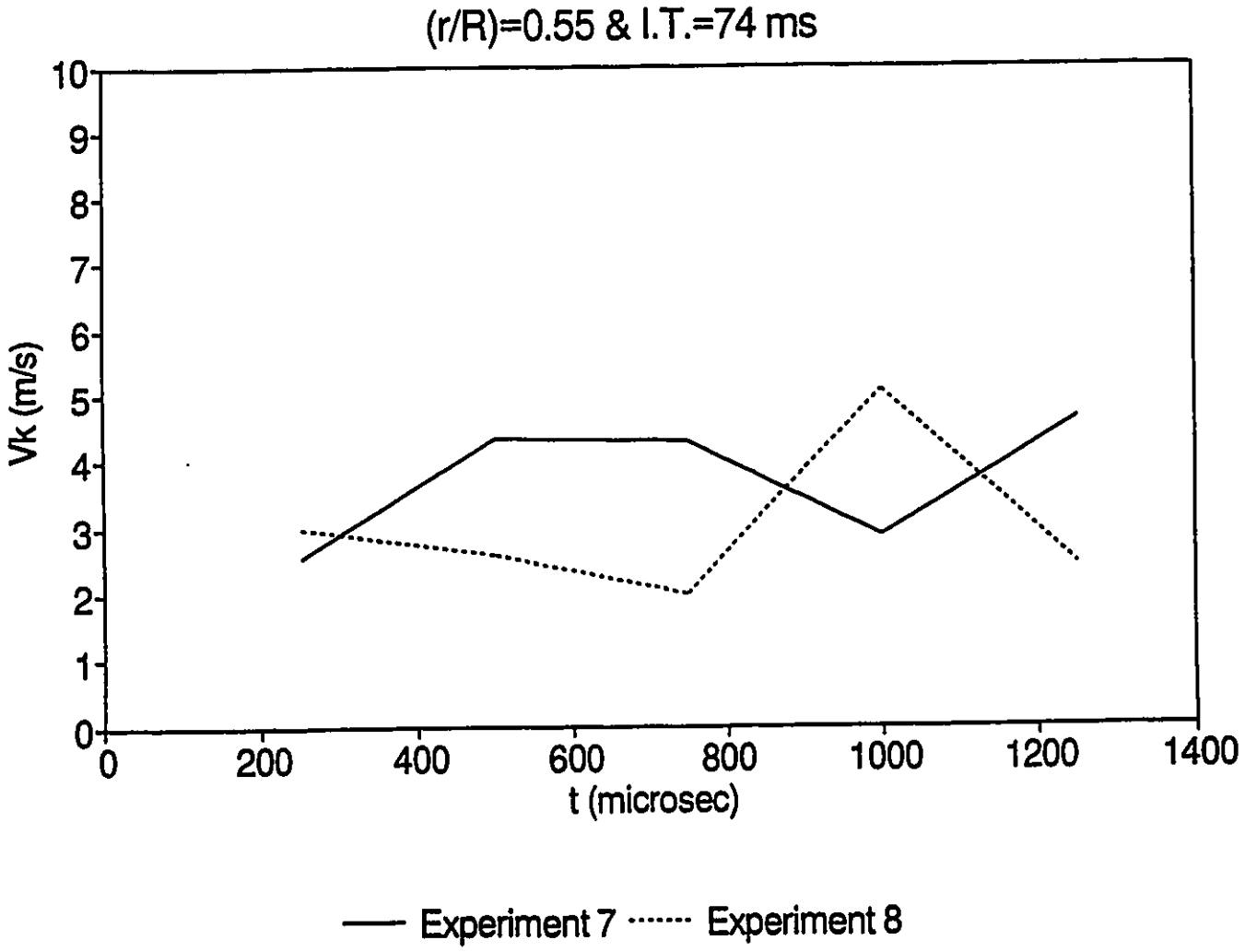

Figure 17 : Convection velocity using Keck's analysis for (r/R)=0.55 and I.T.=74 ms.

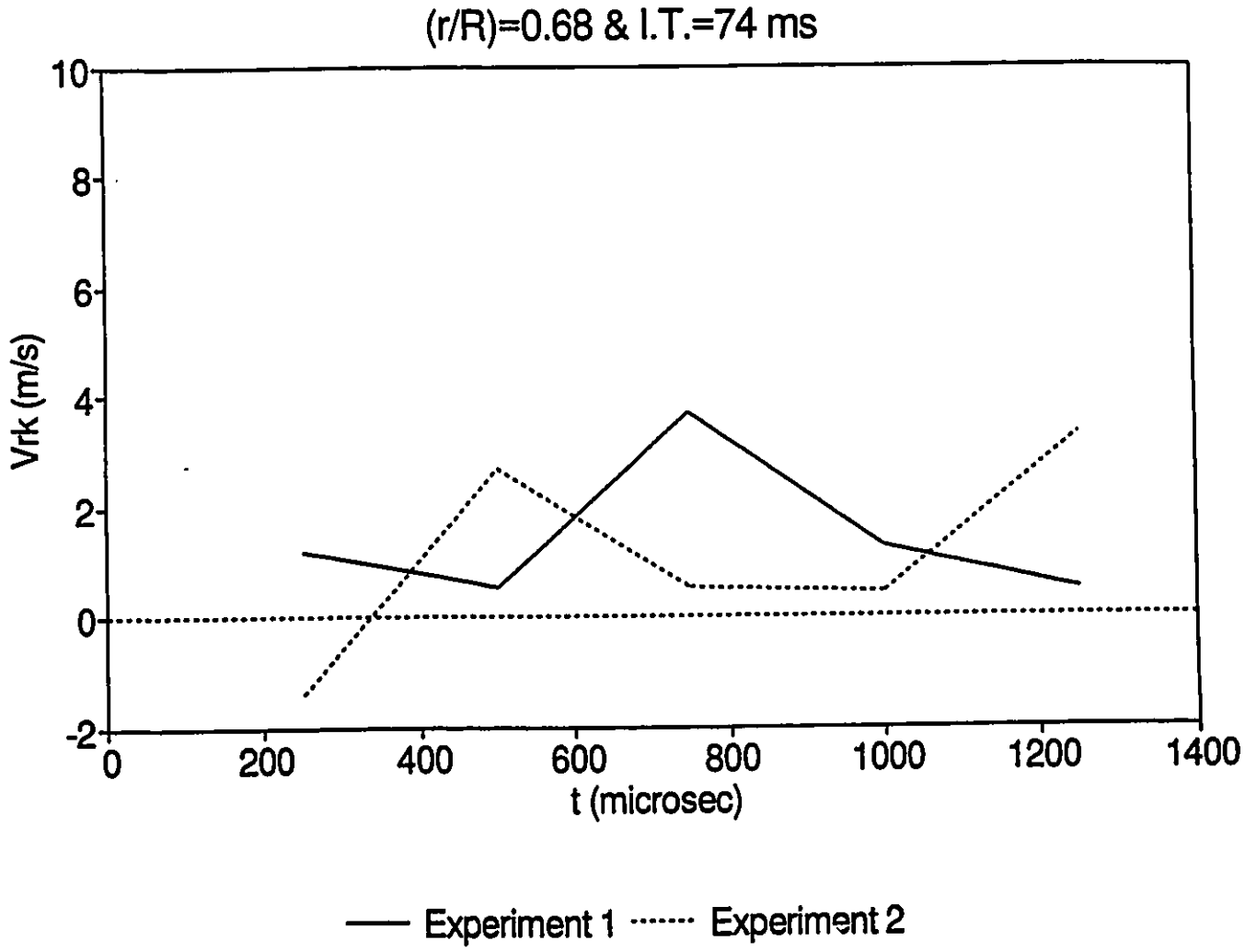

Figure 18 : Radial velocity using Keck's analysis for (r/R)=0.68 and I.T.=74 ms.

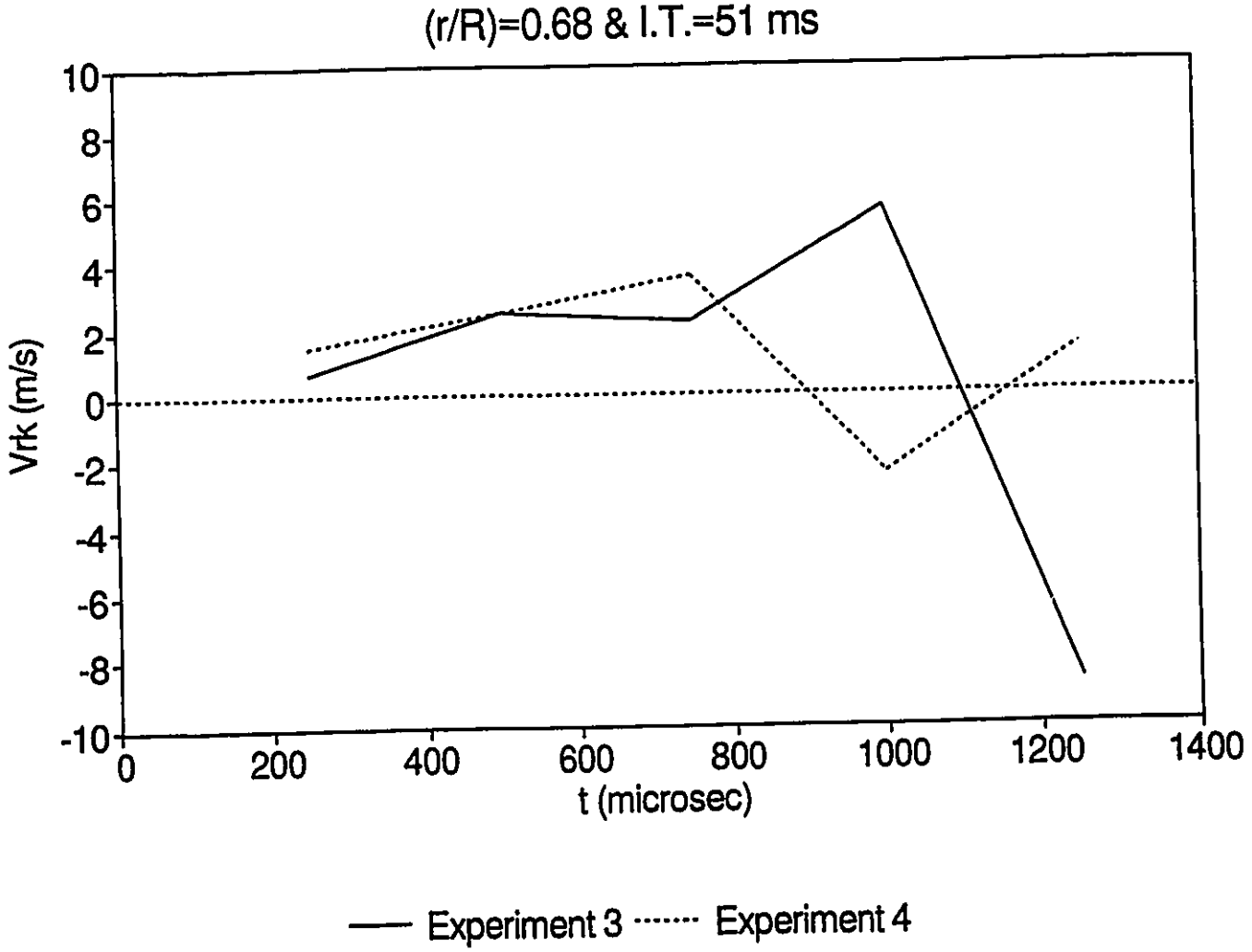

Figure 19 : Radial velocity using Keck's analysis for (r/R)=0.68 and I.T.=51 ms.

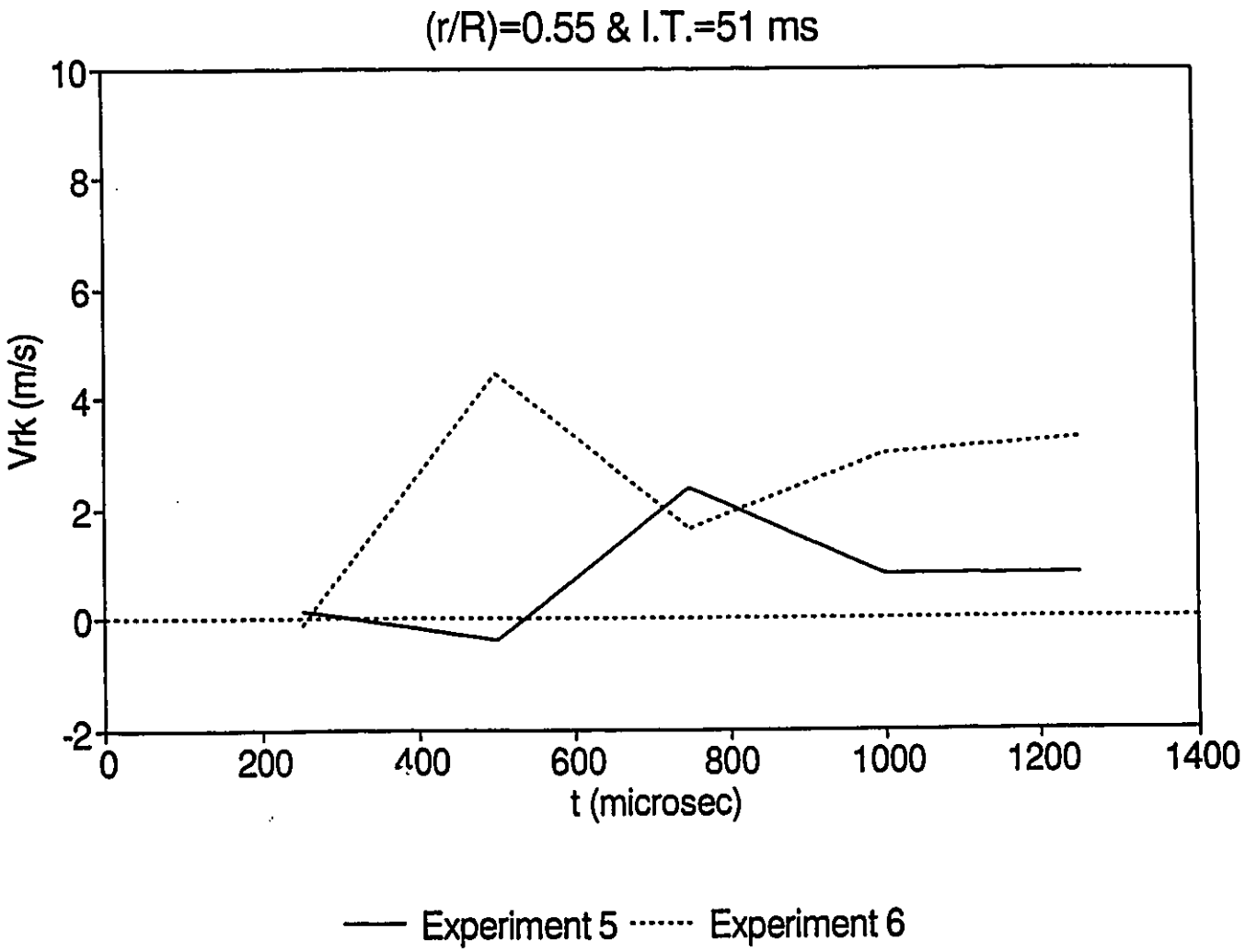

Figure 20 : Radial velocity using Keck's analysis for (r/R)=0.55 and I.T.=51 ms.

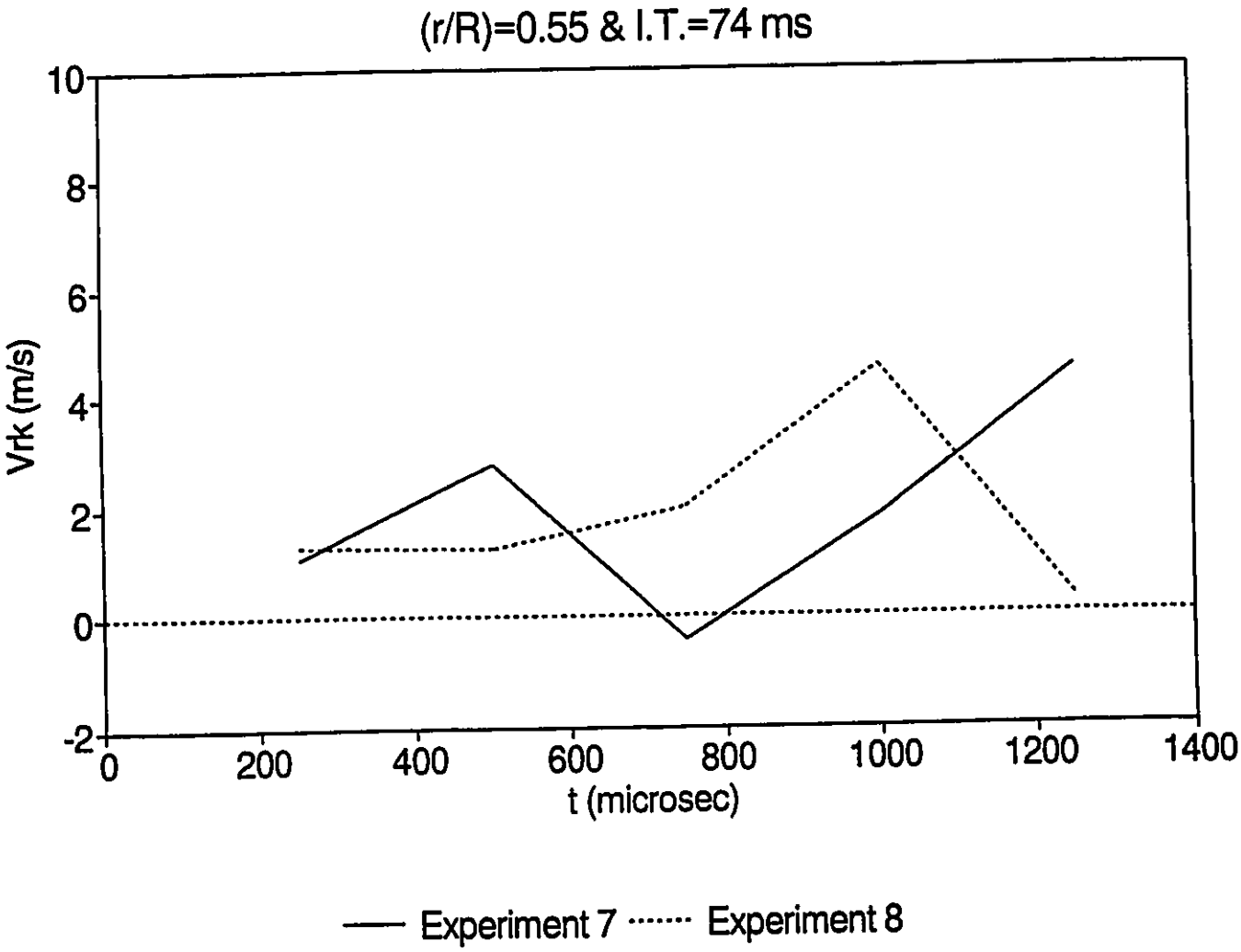

Figure 21 : Radial velocity using Keck's analysis for (r/R)=0.55 and I.T.=74 ms.

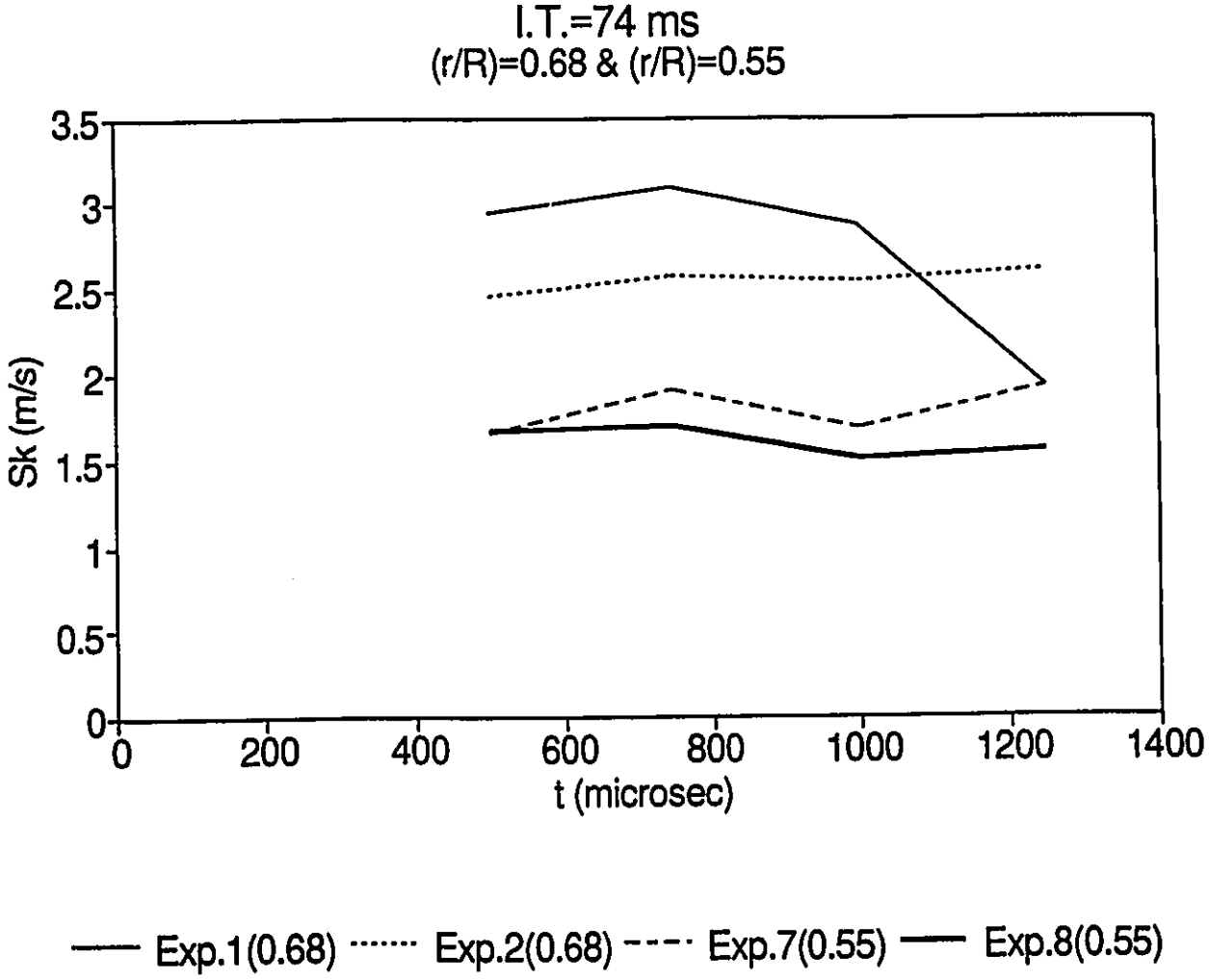

Figure 22 : Comparing the values of flame speed using Keck's analysis at different spark locations for I.T.=74 ms.

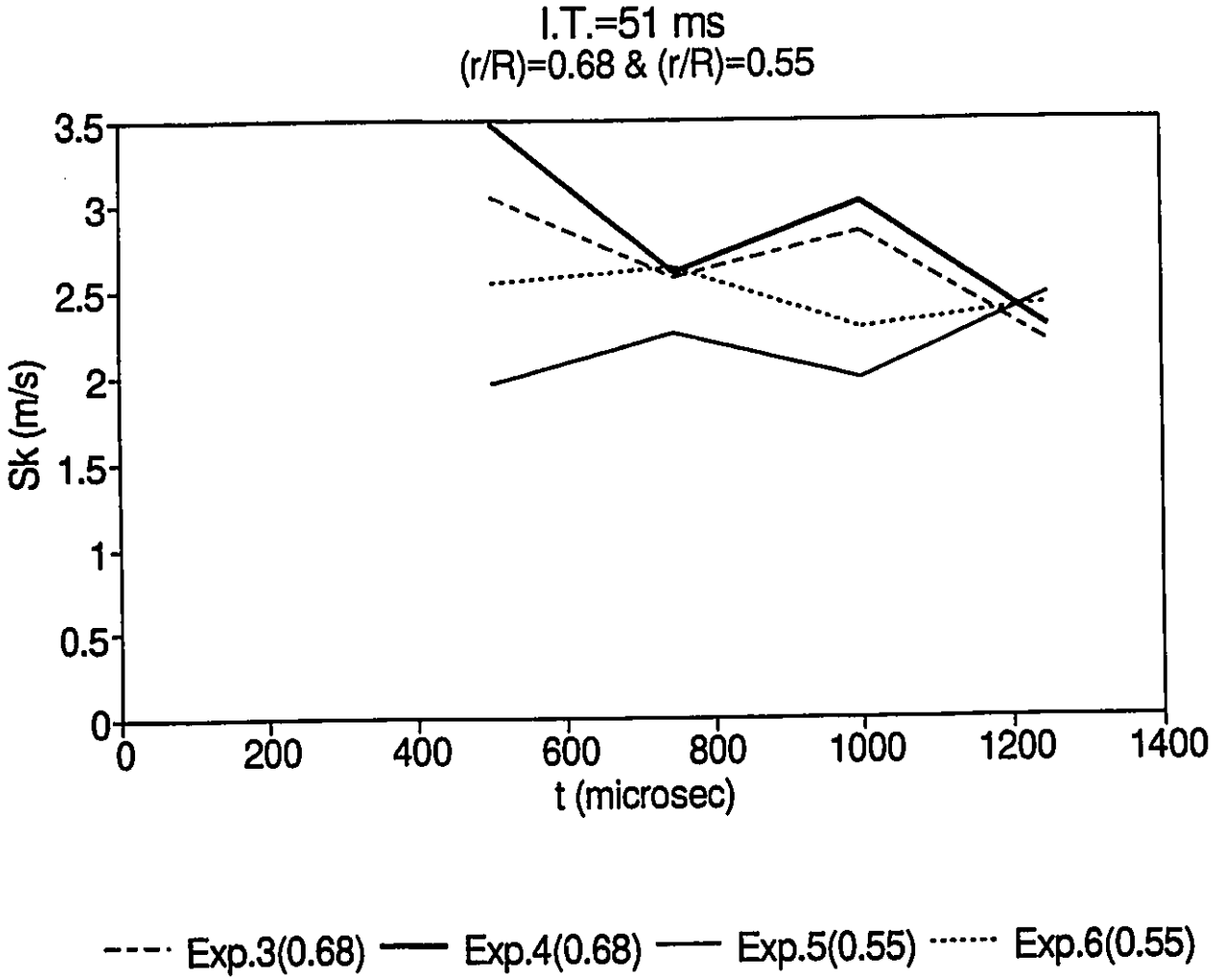

Figure 23 : Comparing the values of flame speed using Keck's analysis at different spark locations for I.T.=51 ms.

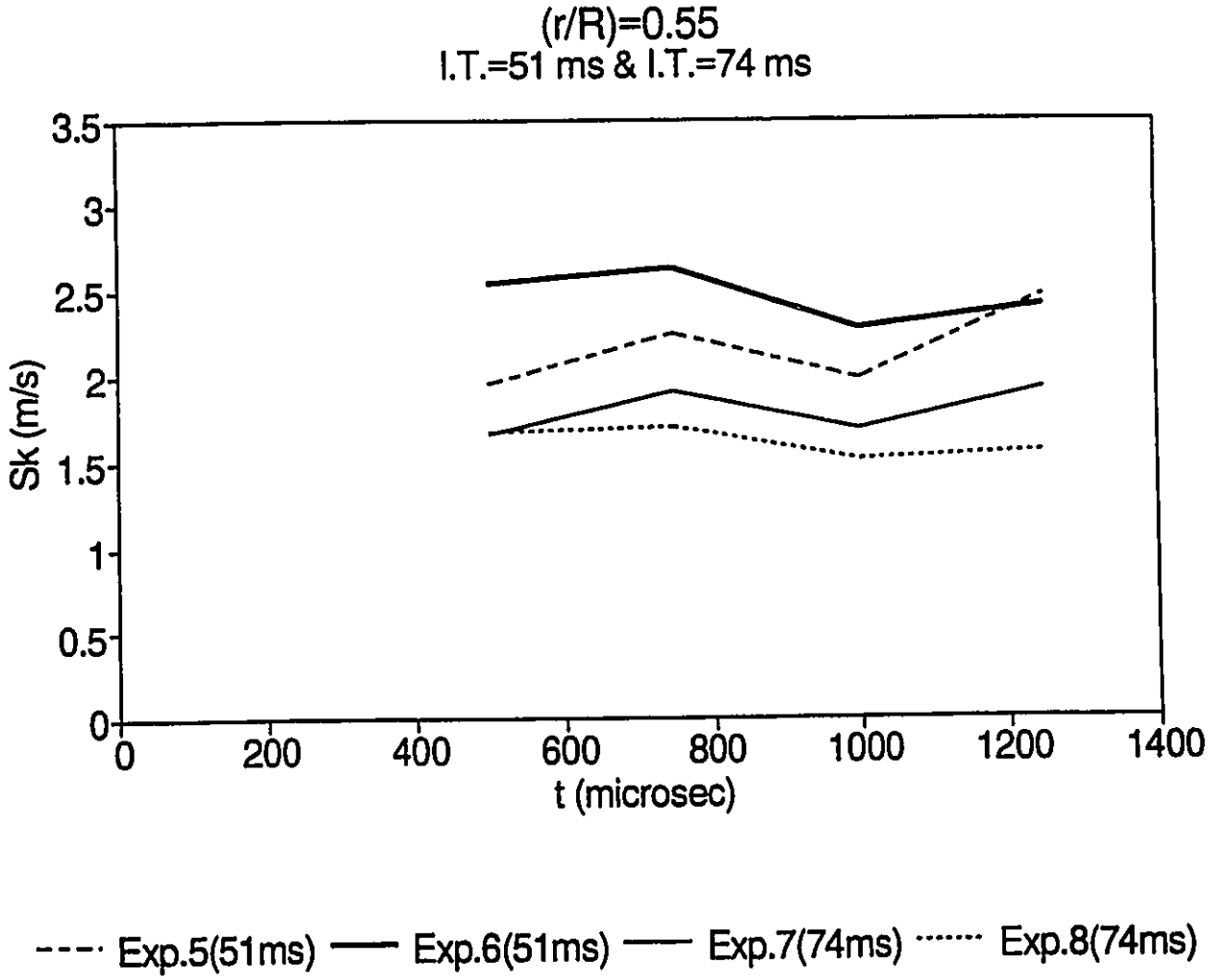

Figure 24 : Comparing the values of flame speed using Keck's analysis at different swirling levels for (r/R)=0.55.

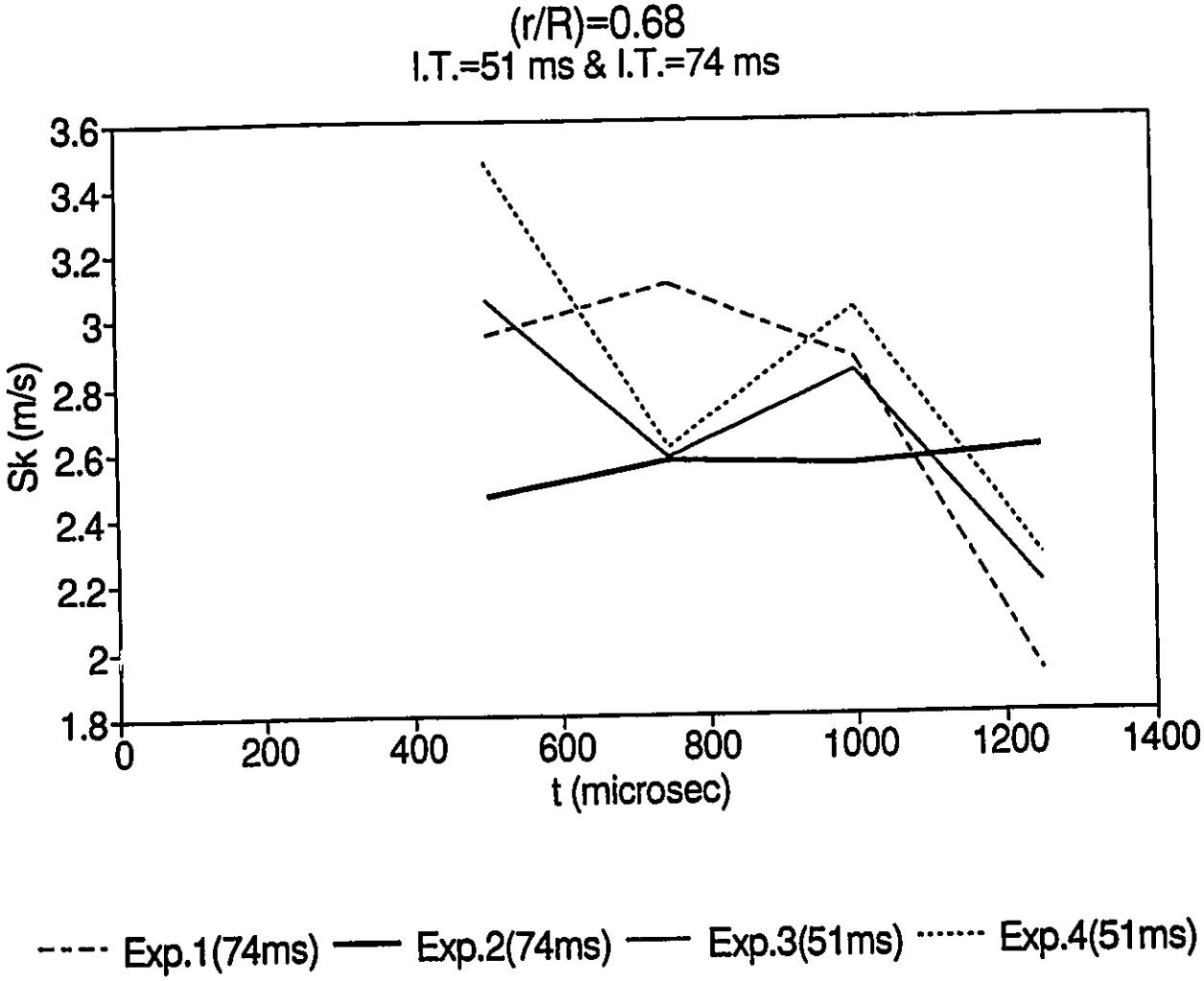

Figure 25 : Comparing the values of flame speed using Keck's analysis at different swirling levels for (r/R)=0.68.

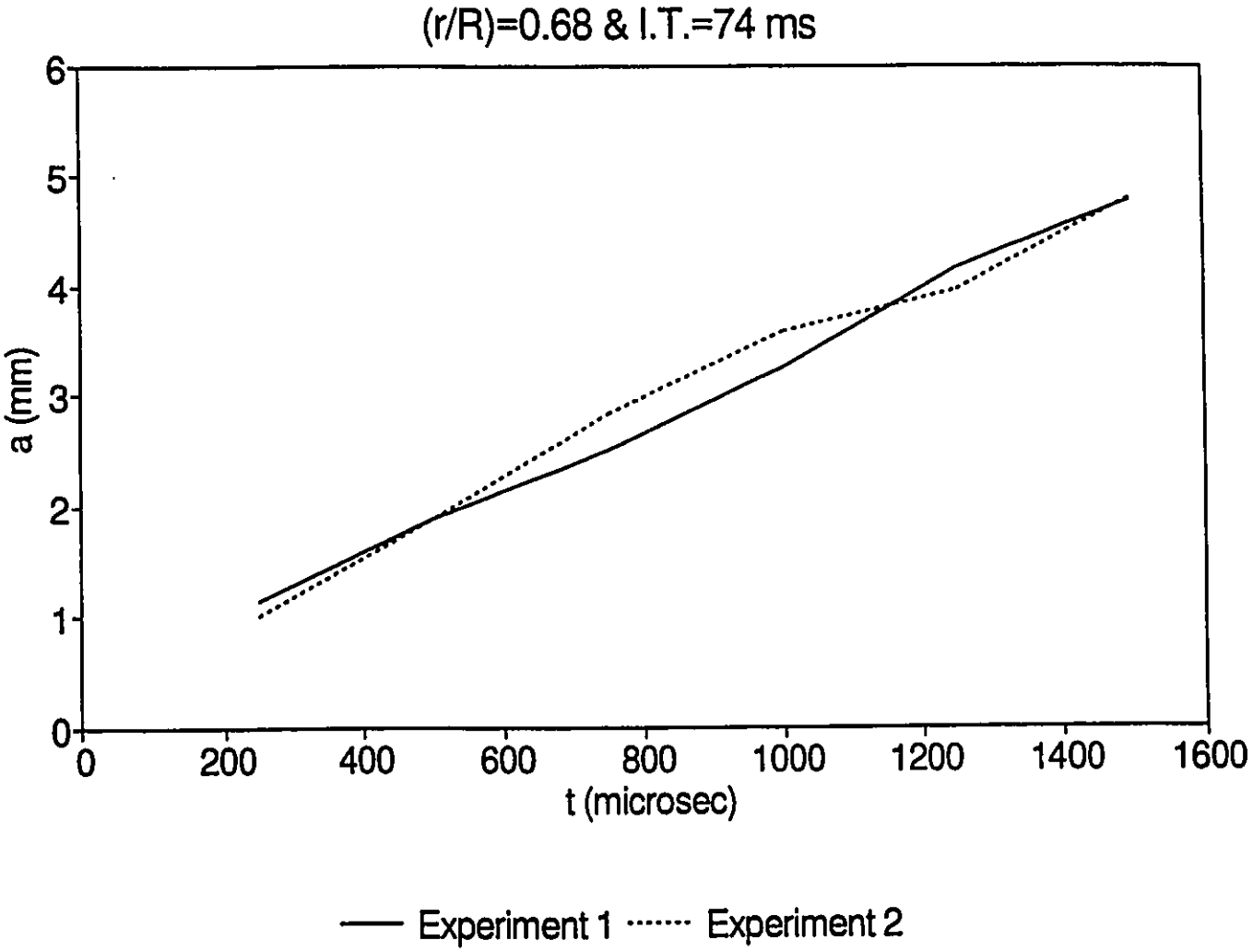

Figure 26 : Semi-major axis of the ellipse versus time for (r/R)=0.68 and I.T.=74 ms.

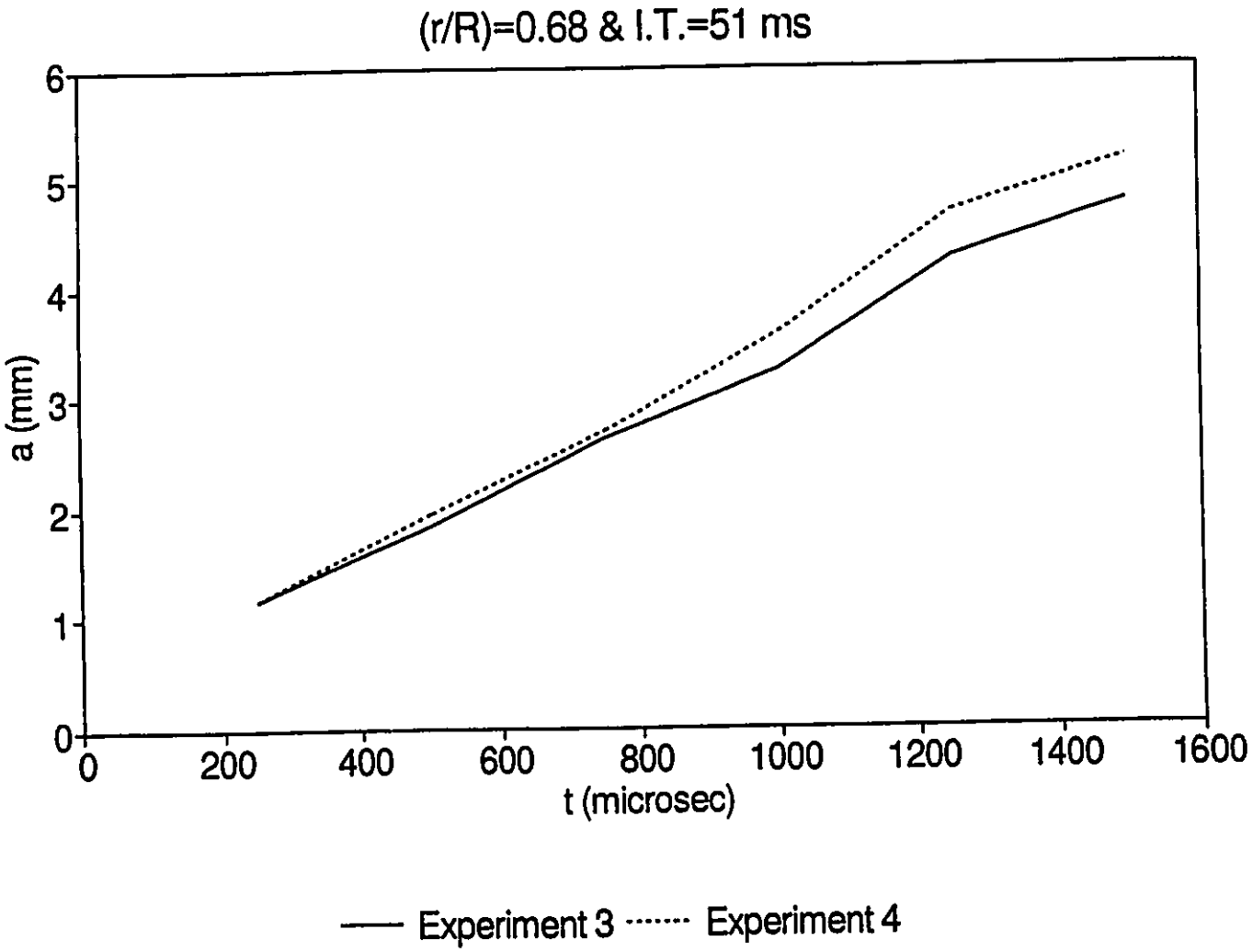

Figure 27 : Semi-major axis of the ellipse versus time for (r/R)=0.68 and I.T.=51 ms.

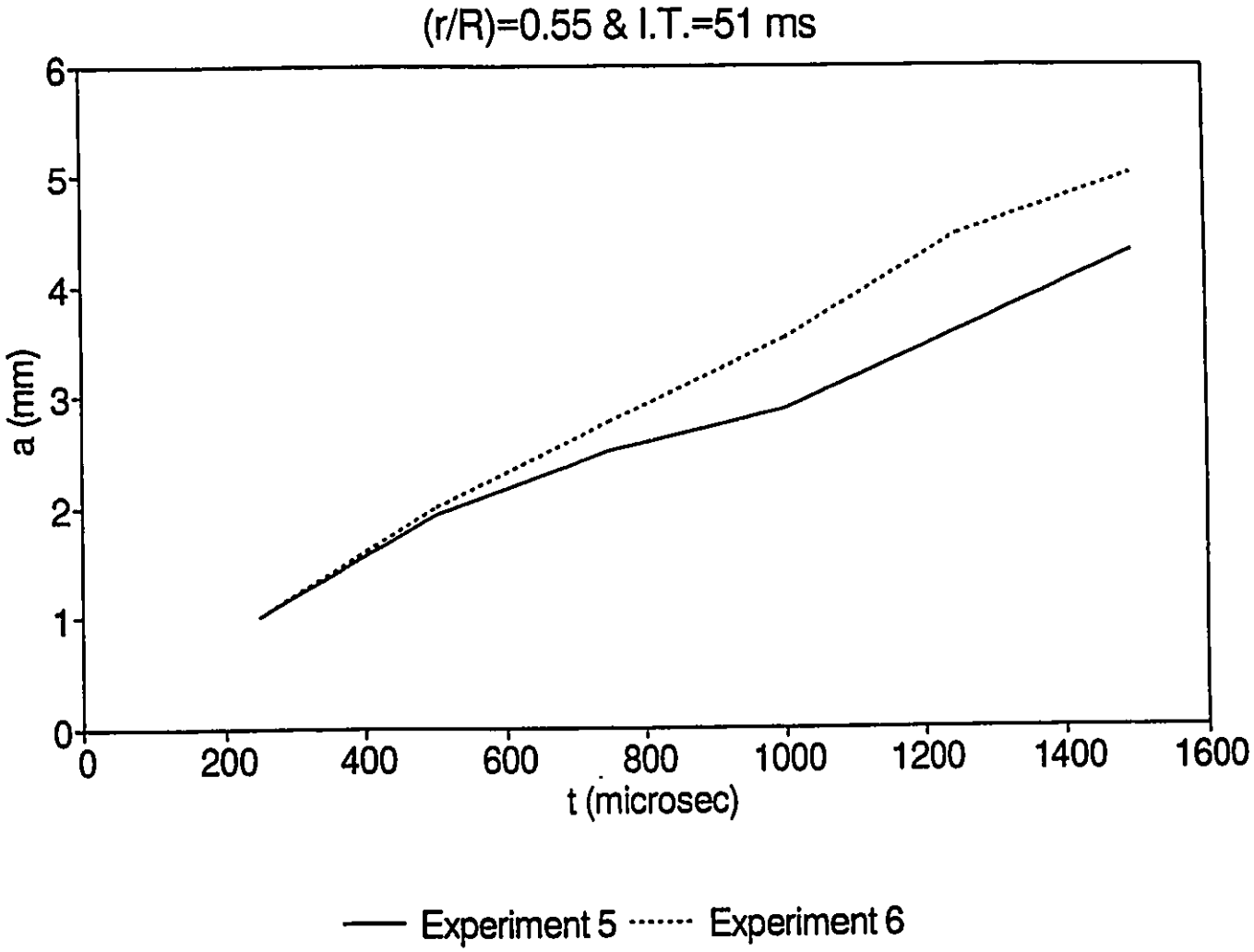

Figure 28 : Semi-major axis of the ellipse versus time for (r/R)=0.55 and I.T.=51 ms.

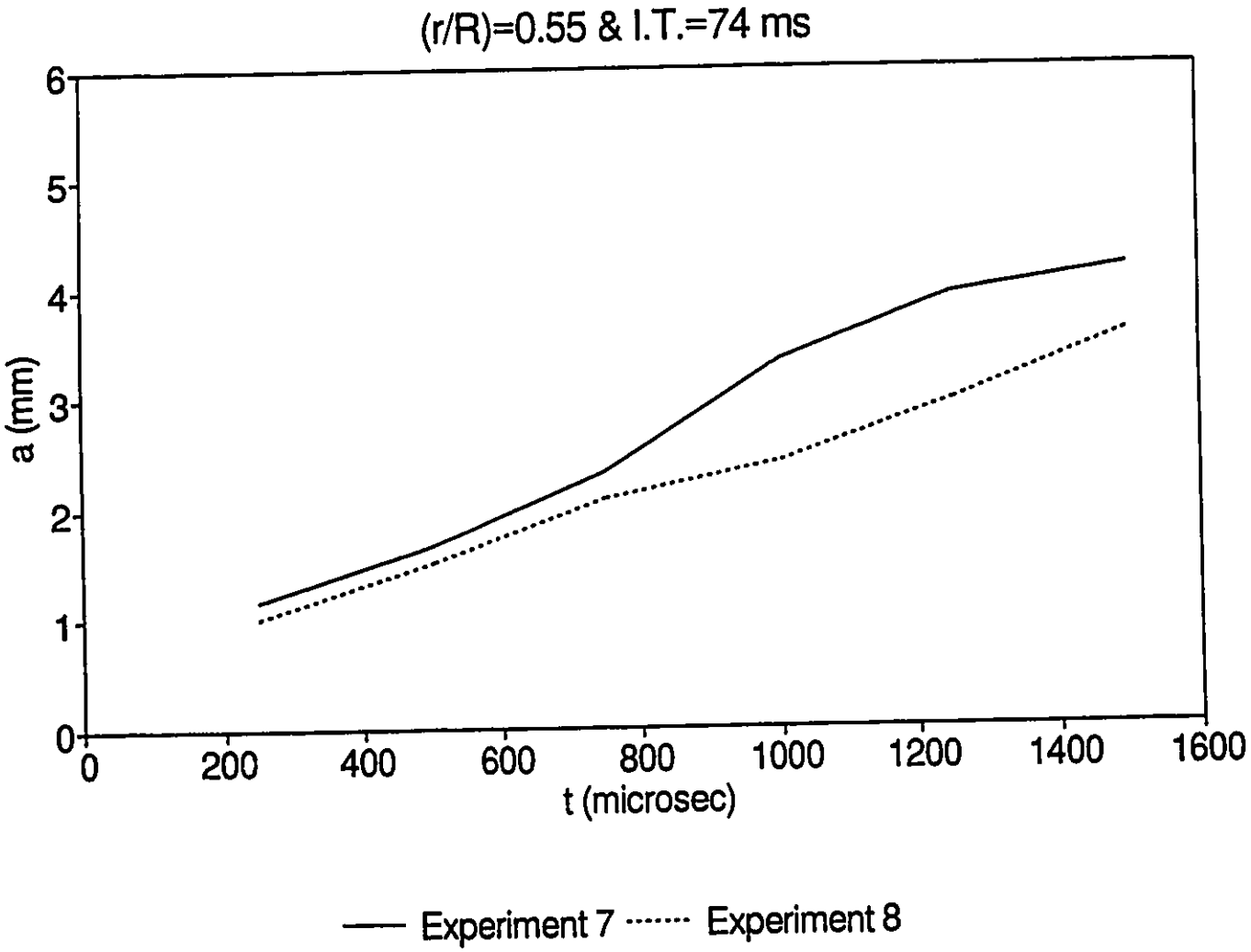

Figure 29 : Semi-major axis of the ellipse versus time for (r/R)=0.55 and I.T.=74 ms.

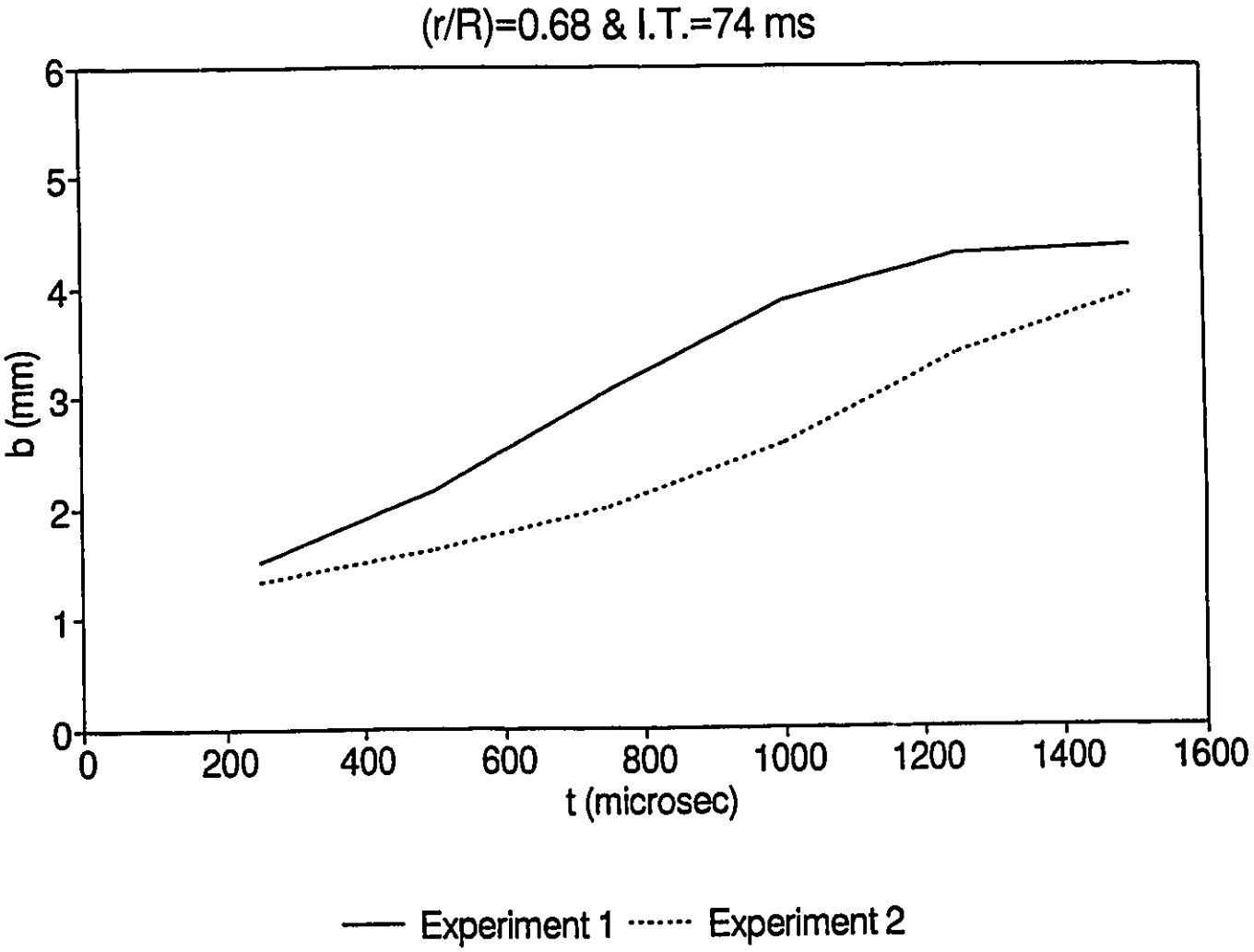

Figure 30 : Semi-minor axis of the ellipse versus time for (r/R)=0.68 and I.T.=74 ms.

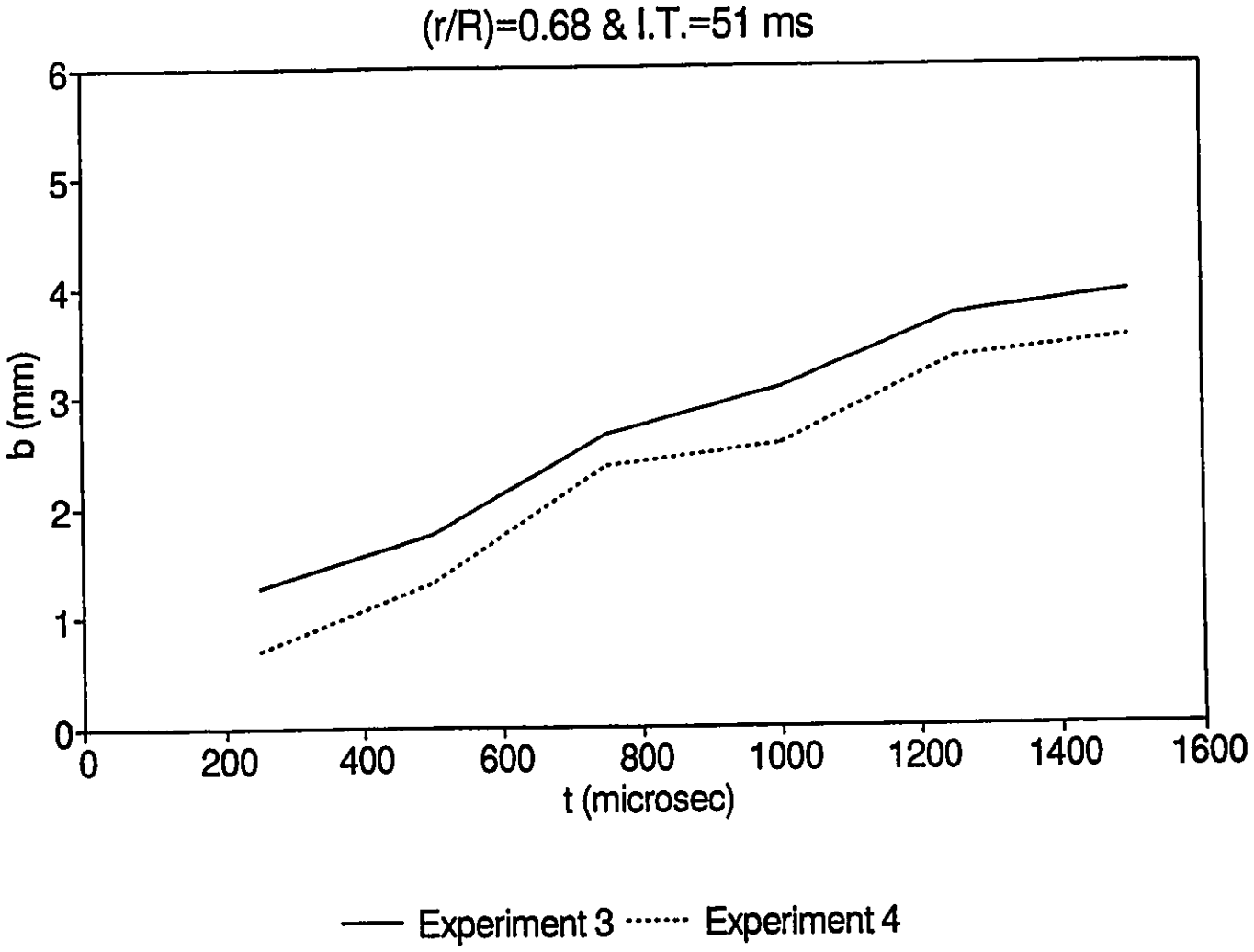

Figure 31 : Semi-minor axis of the ellipse versus time for (r/R)=0.68 and I.T.=51 ms.

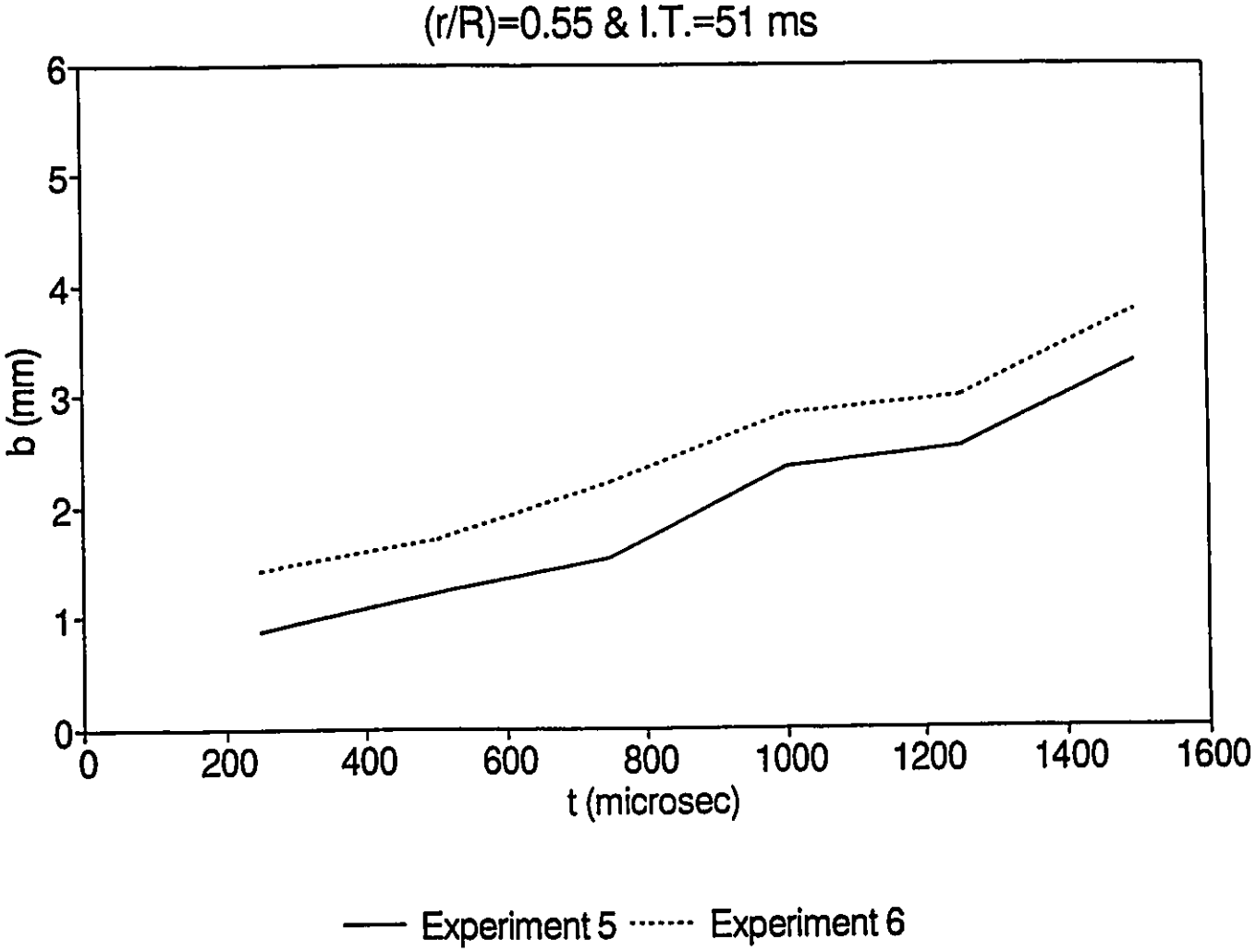

Figure 32 : Semi-minor axis of the ellipse versus time for (r/R)=0.55 and I.T.=51 ms.

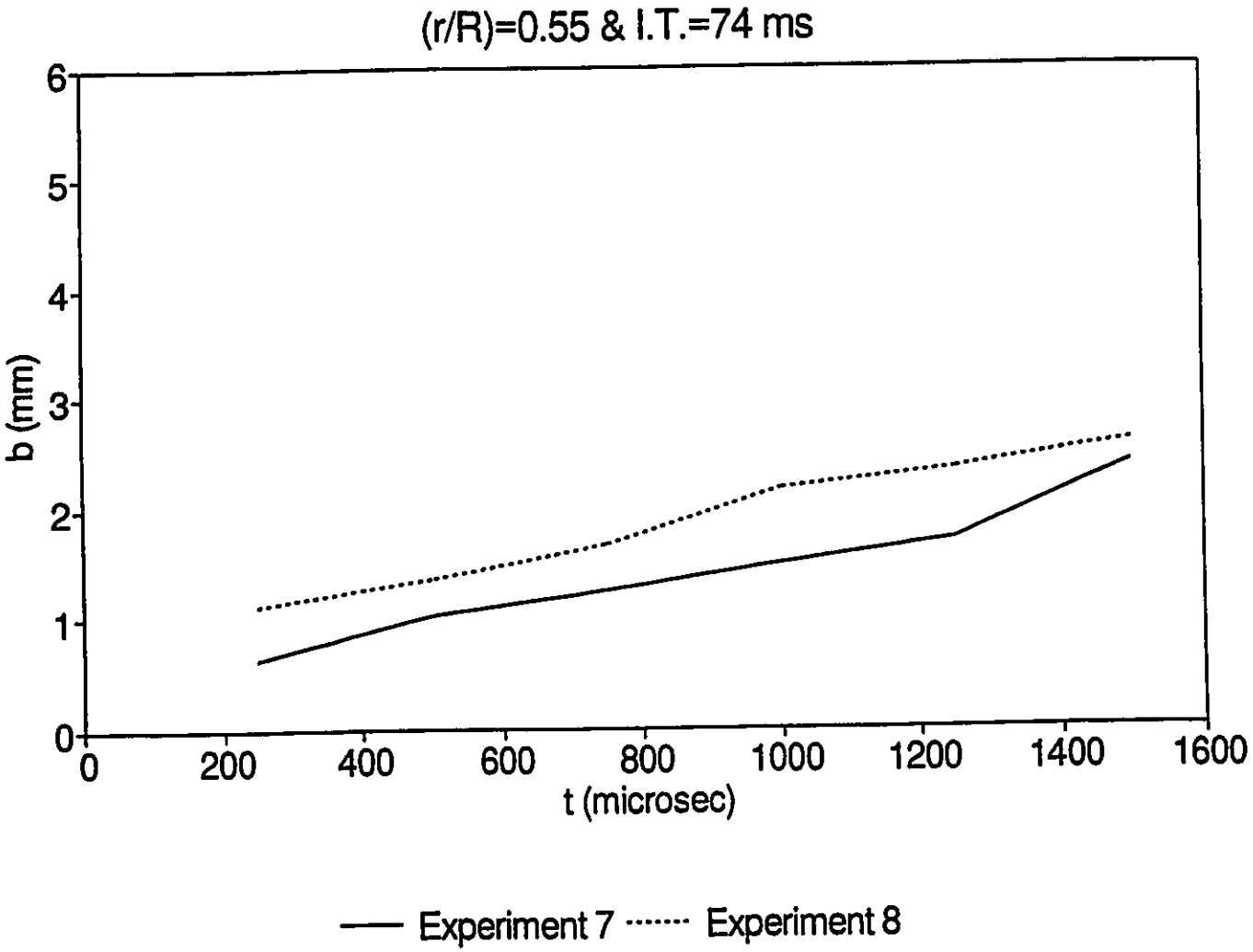

Figure 33 : Semi-minor axis of the ellipse versus time for (r/R)=0.55 and I.T.=74 ms.

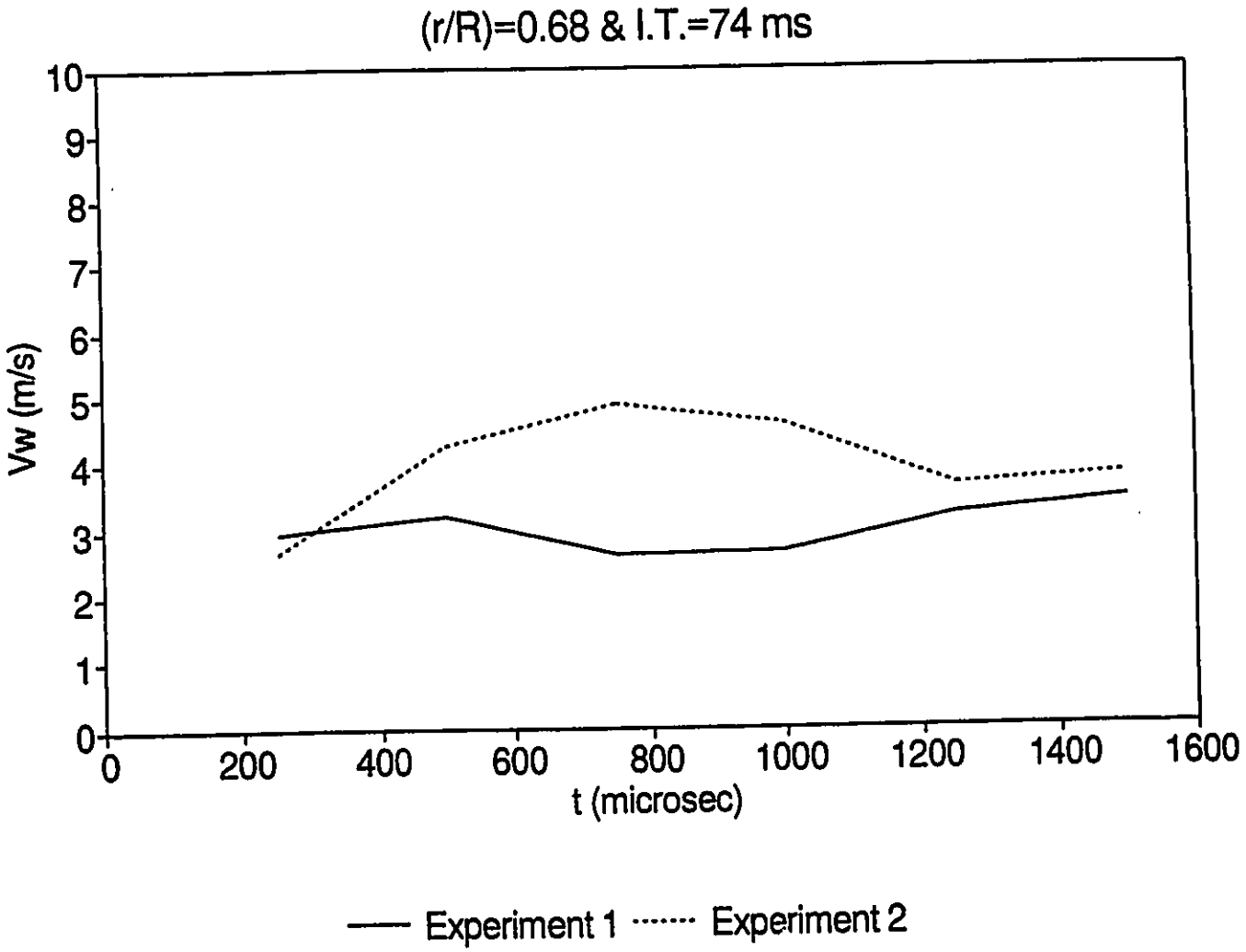

Figure 34 : Convection velocity using elliptical model for (r/R)=0.68 and I.T.=74 ms.

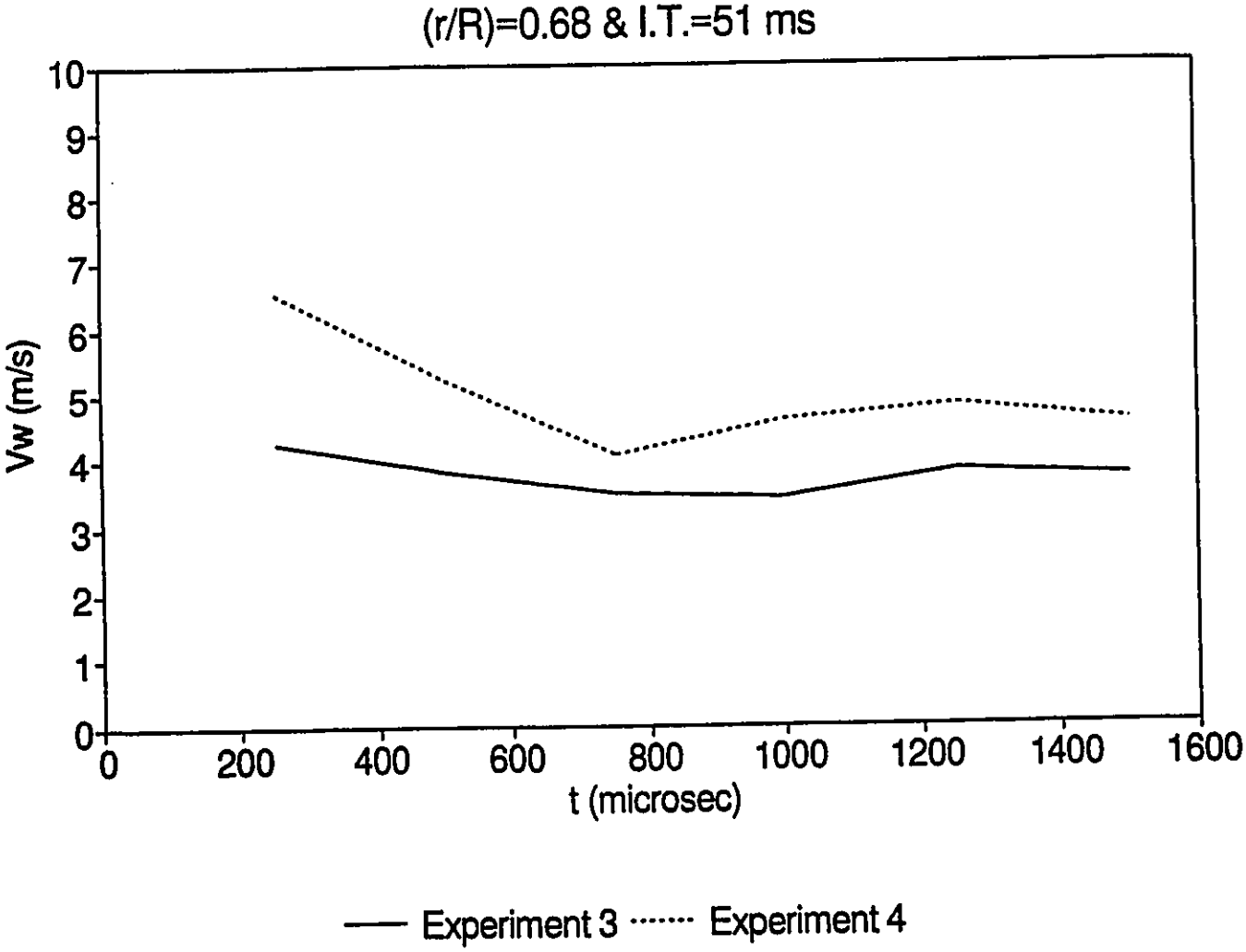

Figure 35 : Convection velocity using elliptical model for (r/R)=0.68 and I.T.=51 ms.

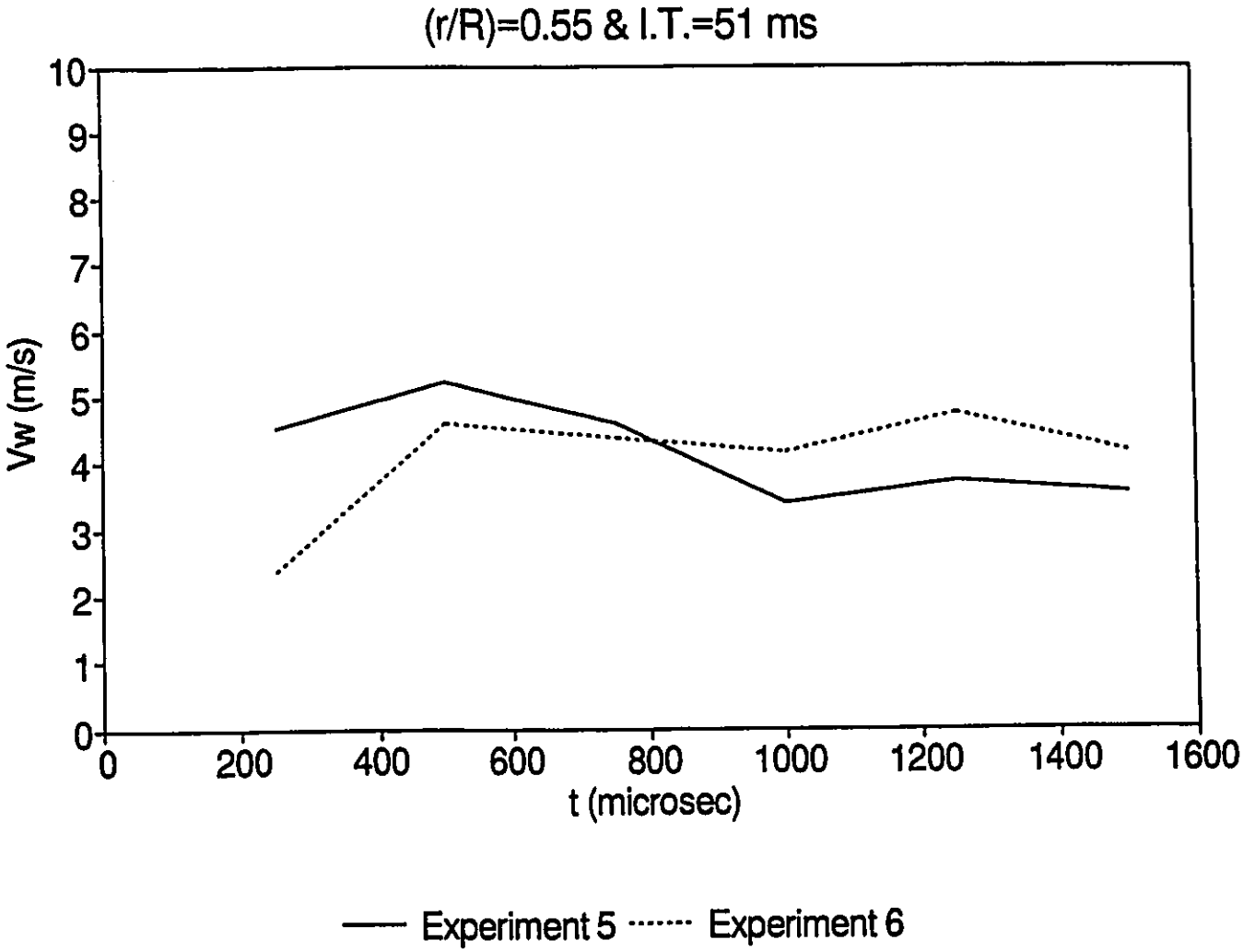

Figure 36 : Convection velocity using elliptical model for (r/R)=0.55 and I.T.=51 ms.

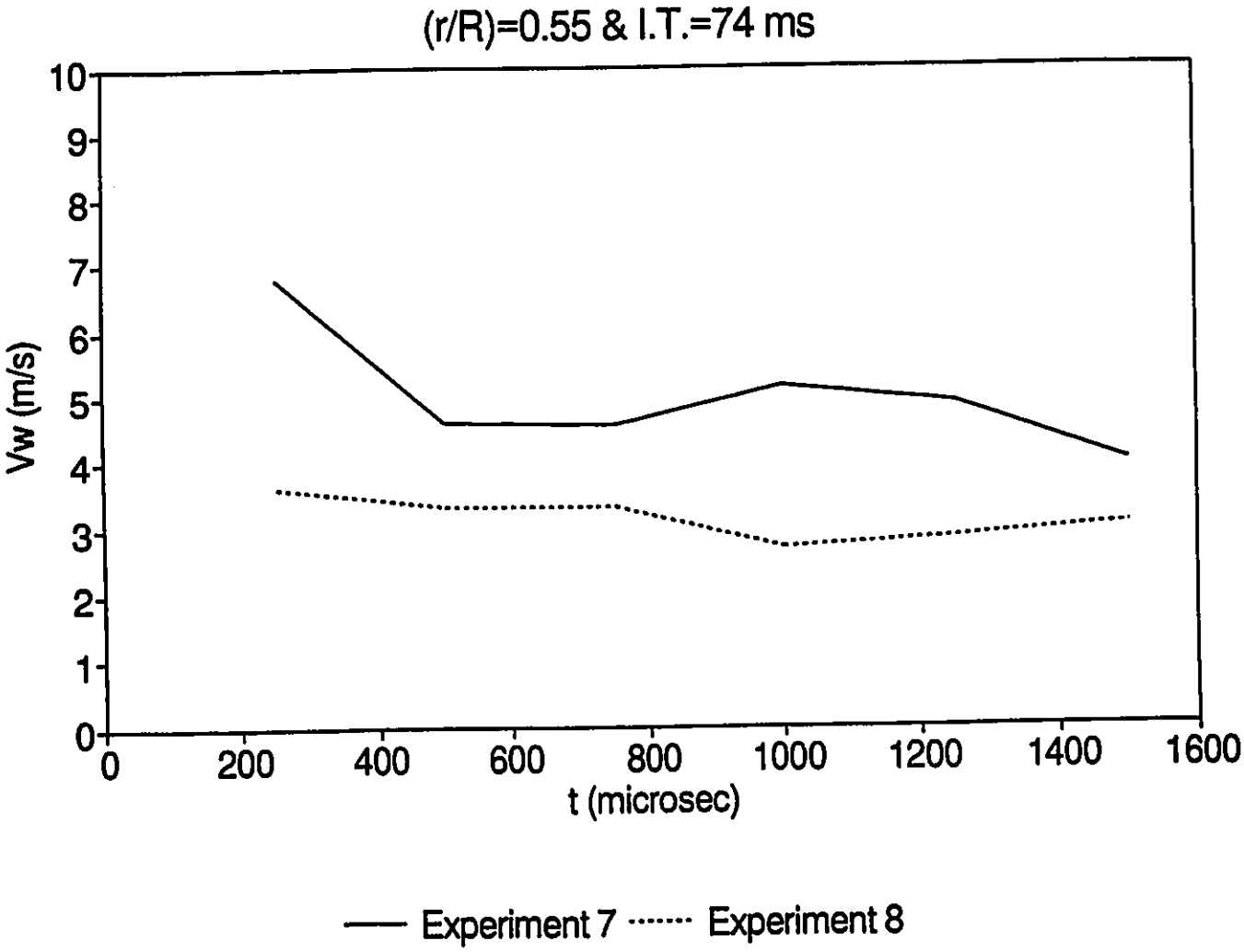

Figure 37 : Convection velocity using elliptical model for (r/R)=0.55 and I.T.=74 ms.

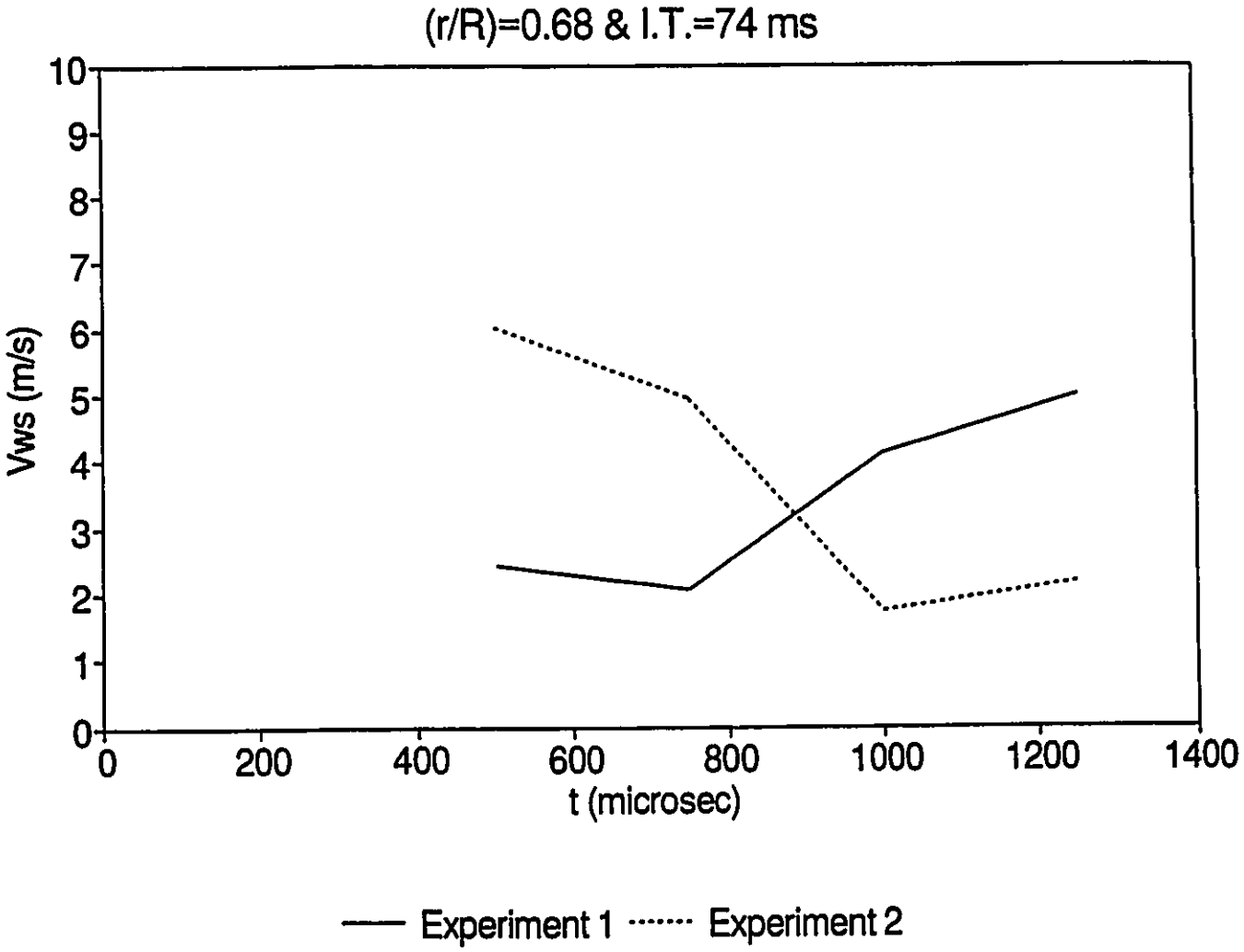

Figure 38 : Convection velocity using modified elliptical model for (r/R)=0.68 and I.T.=74 ms.

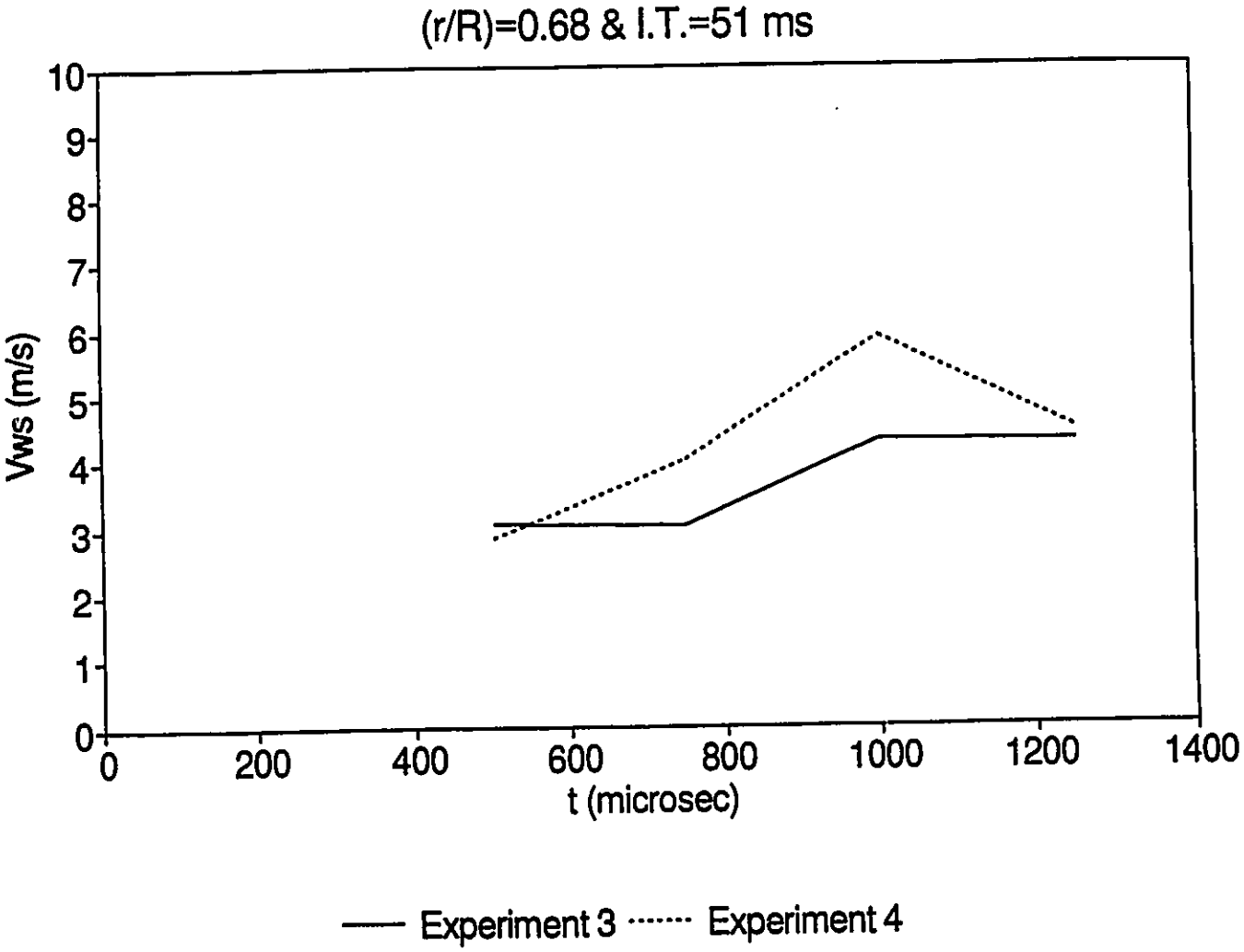

Figure 39 : Convection velocity using modified elliptical model for (r/R)=0.68 and I.T.=51 ms.

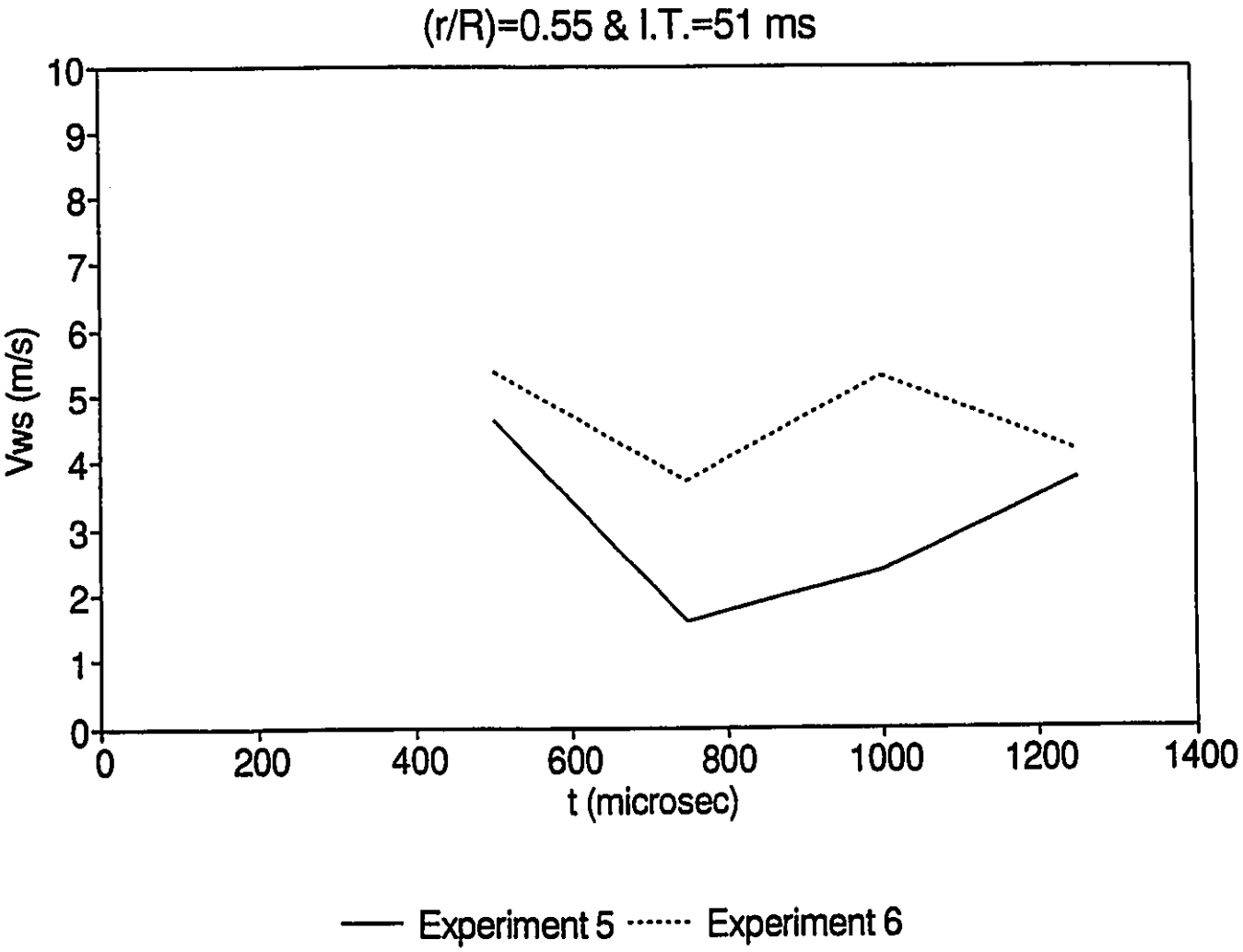

Figure 40 : Convection velocity using modified elliptical model for (r/R)=0.55 and I.T.=51 ms.

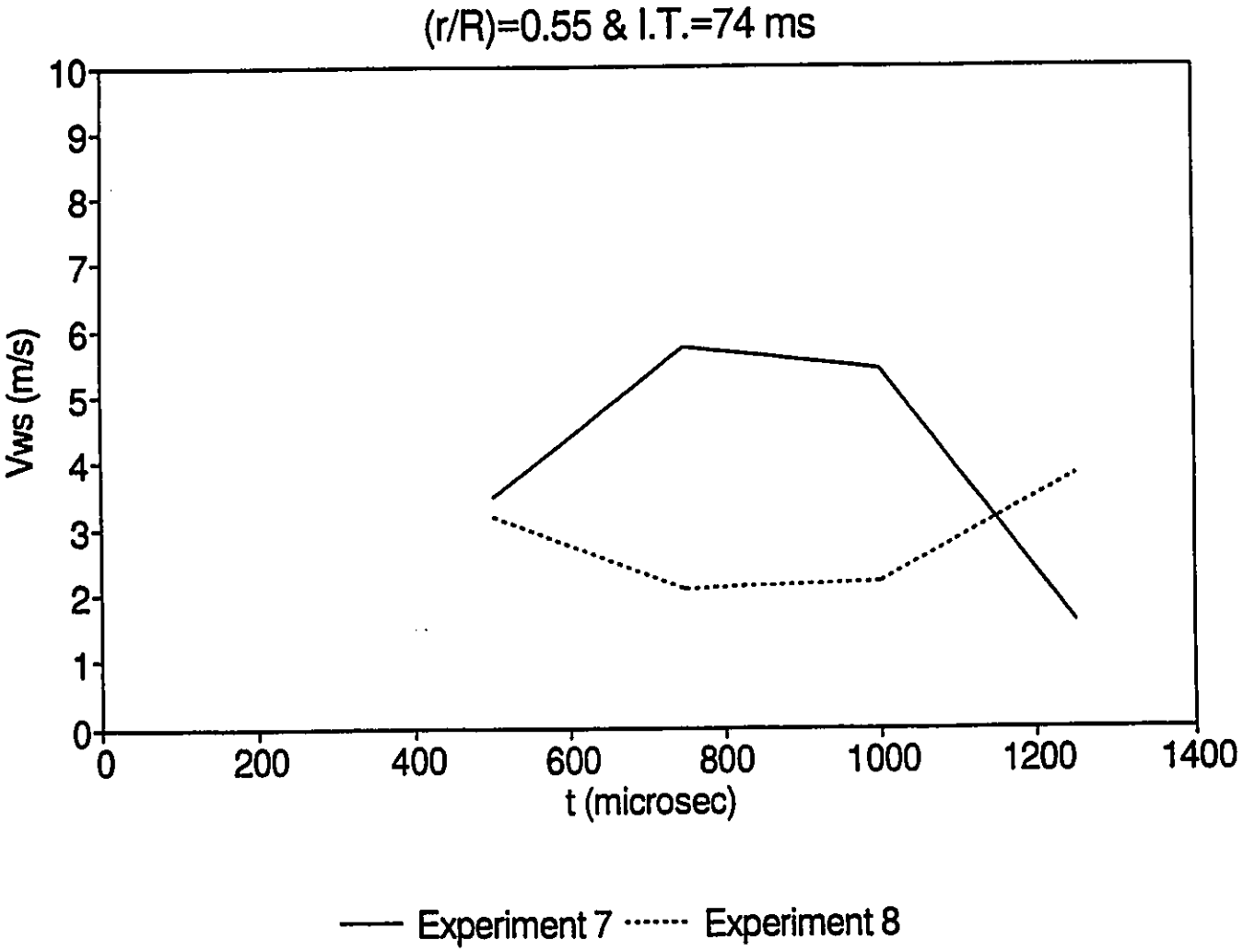

Figure 41 : Convection velocity using modified elliptical model for (r/R)=0.55 and I.T.=74 ms.

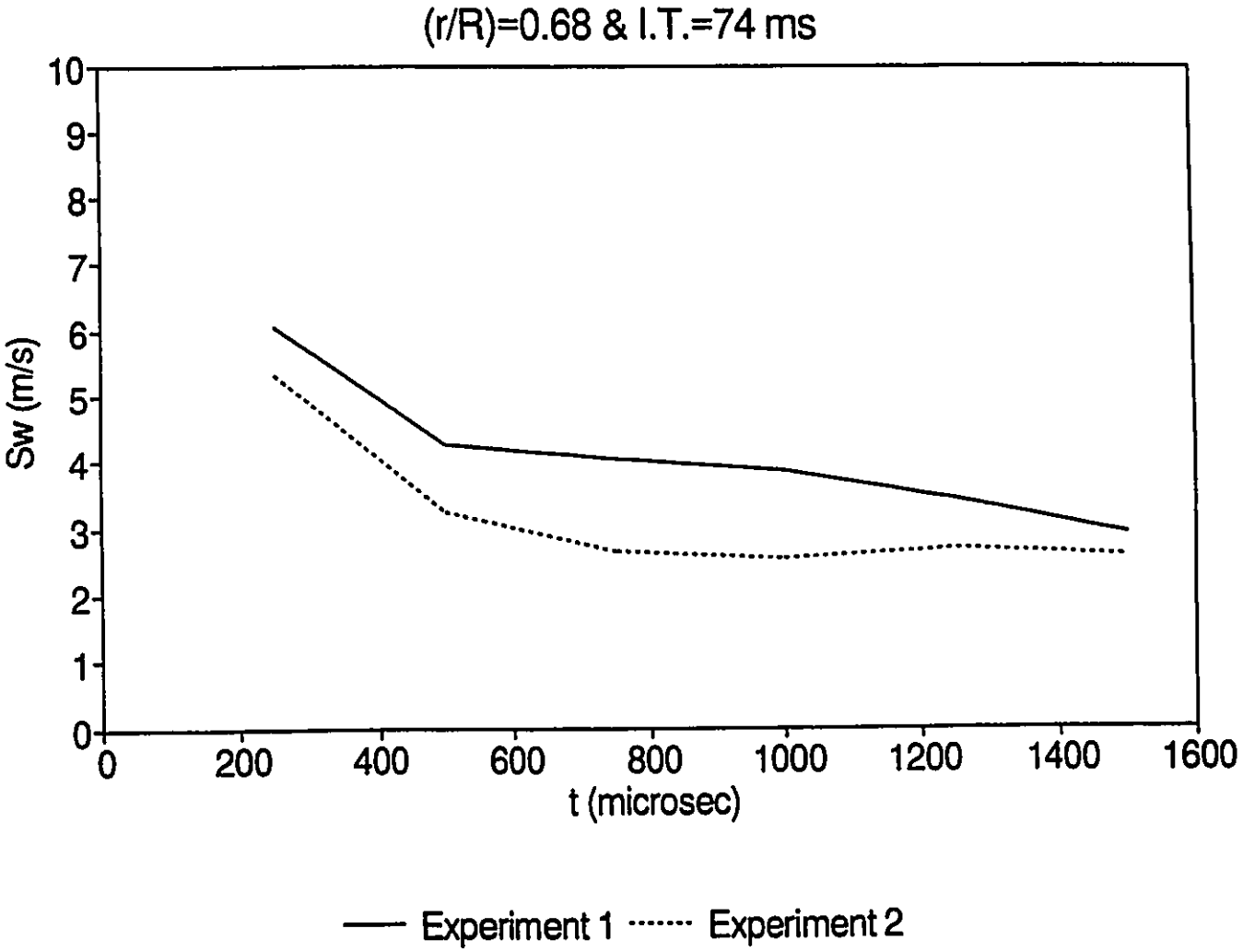

Figure 42 : Flame speed using elliptical model for (r/R)=0.68 and I.T.=74 ms.

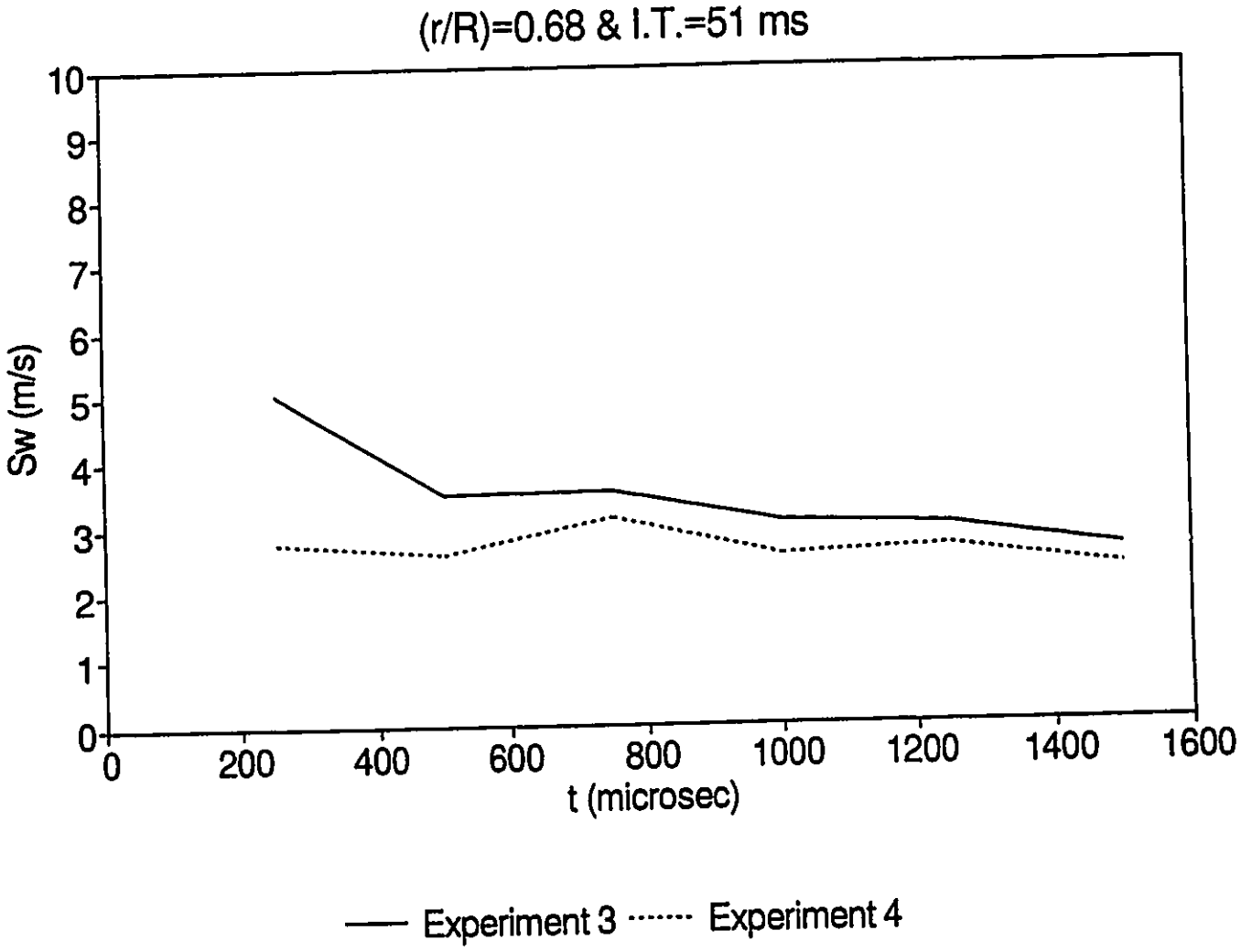

Figure 43 : Flame speed using elliptical model for (r/R)=0.68 and I.T.=51 ms.

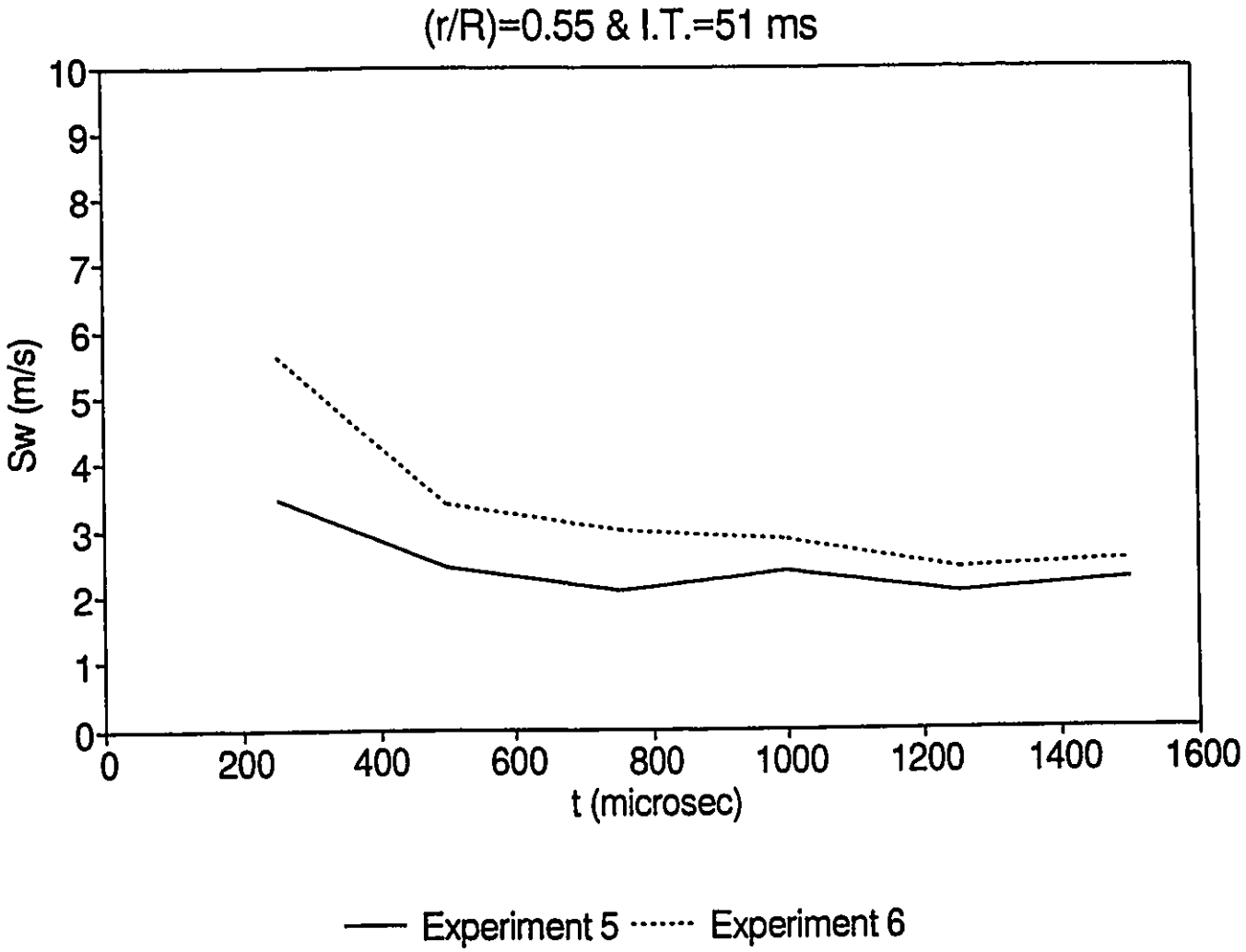

Figure 44 : Flame speed using elliptical model for (r/R)=0.55 and I.T.=51 ms.

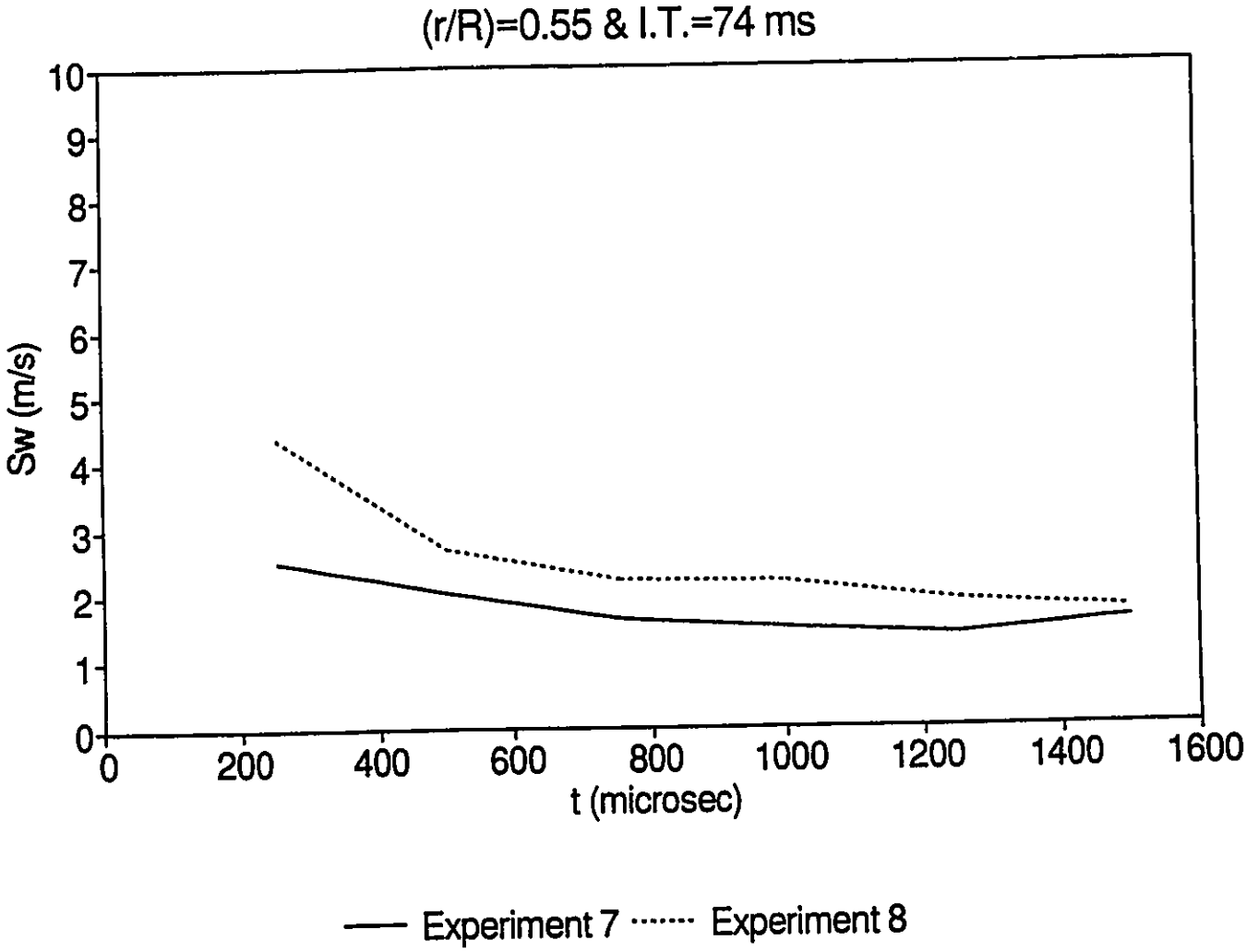

Figure 45 : Flame speed using elliptical model for (r/R)=0.55 and I.T.=74 ms.

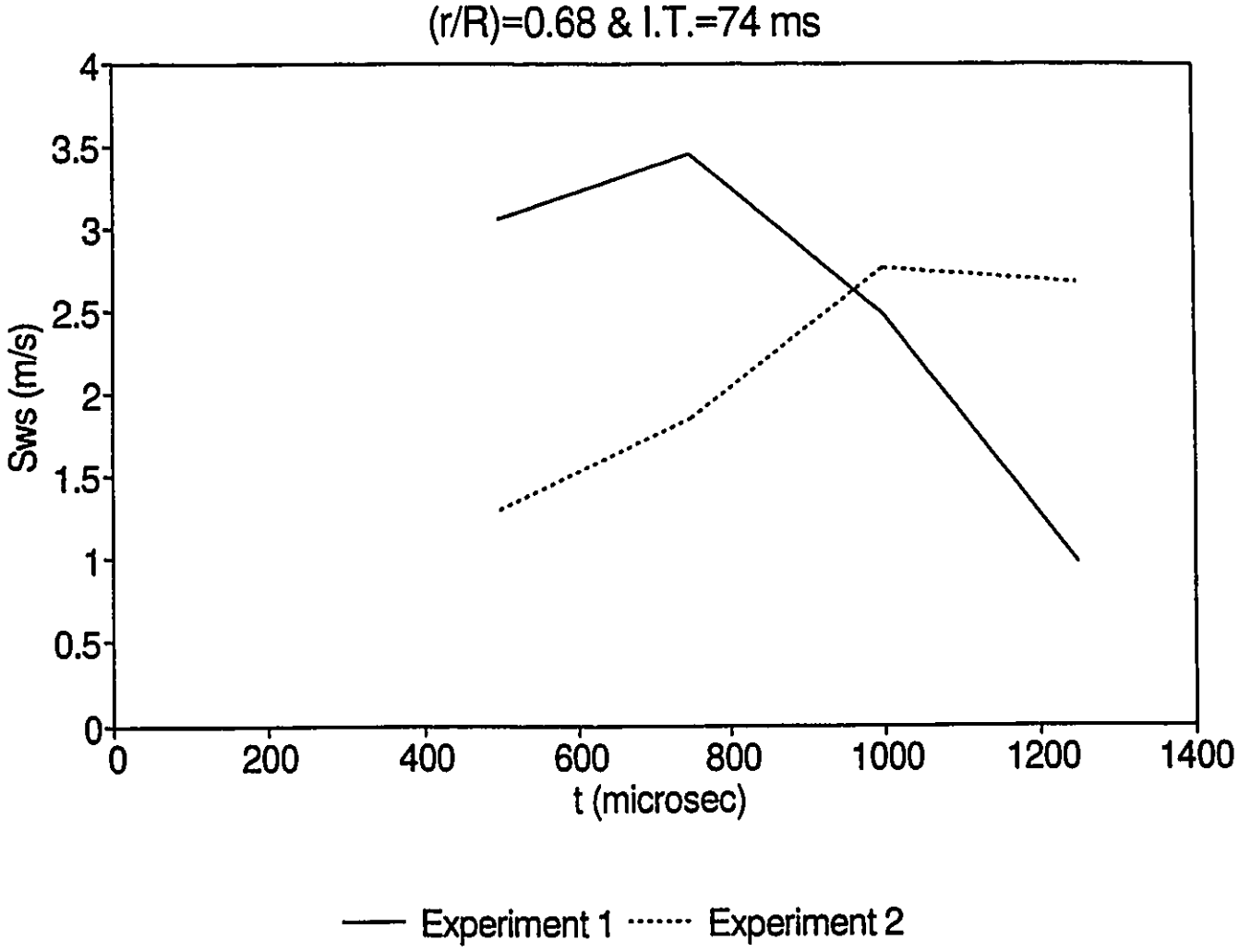

Figure 46 : Flame speed using modified elliptical model for (r/R)=0.68 and I.T.=74 ms.

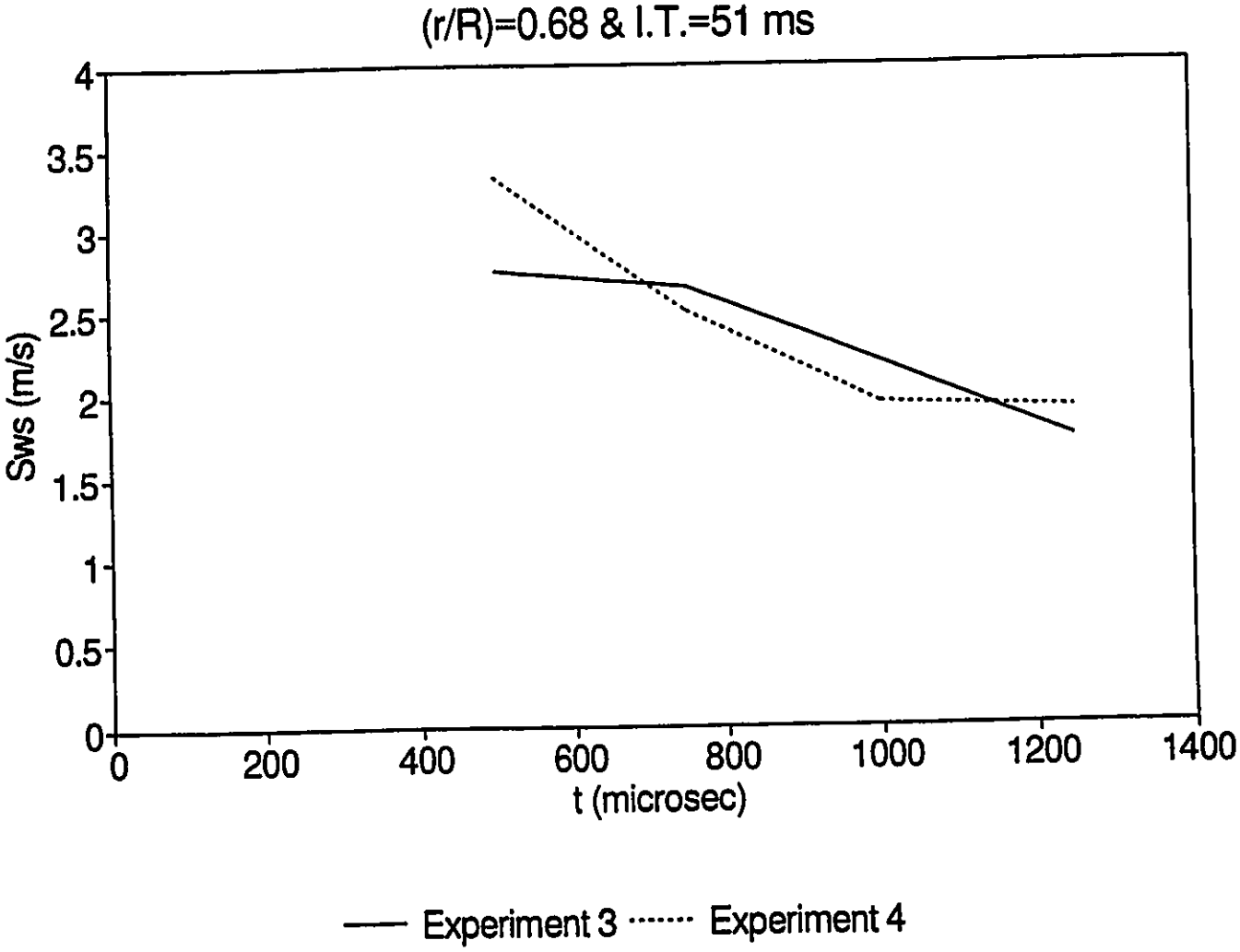

Figure 47 : Flame speed using modified elliptical model for (r/R)=0.68 and I.T.=51 ms.

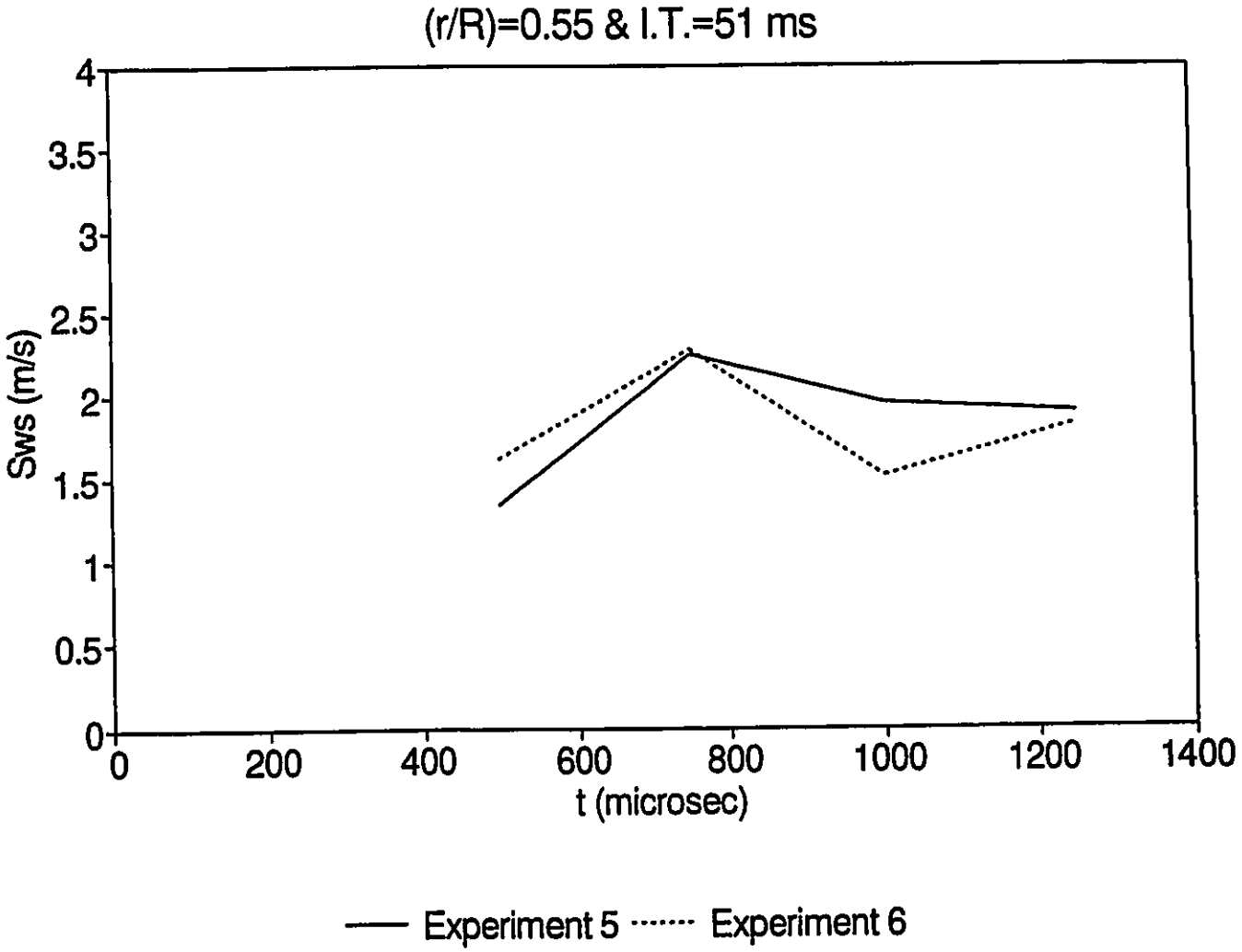

Figure 48 : Flame speed using modified elliptical model for (r/R)=0.55 and I.T.=51 ms.

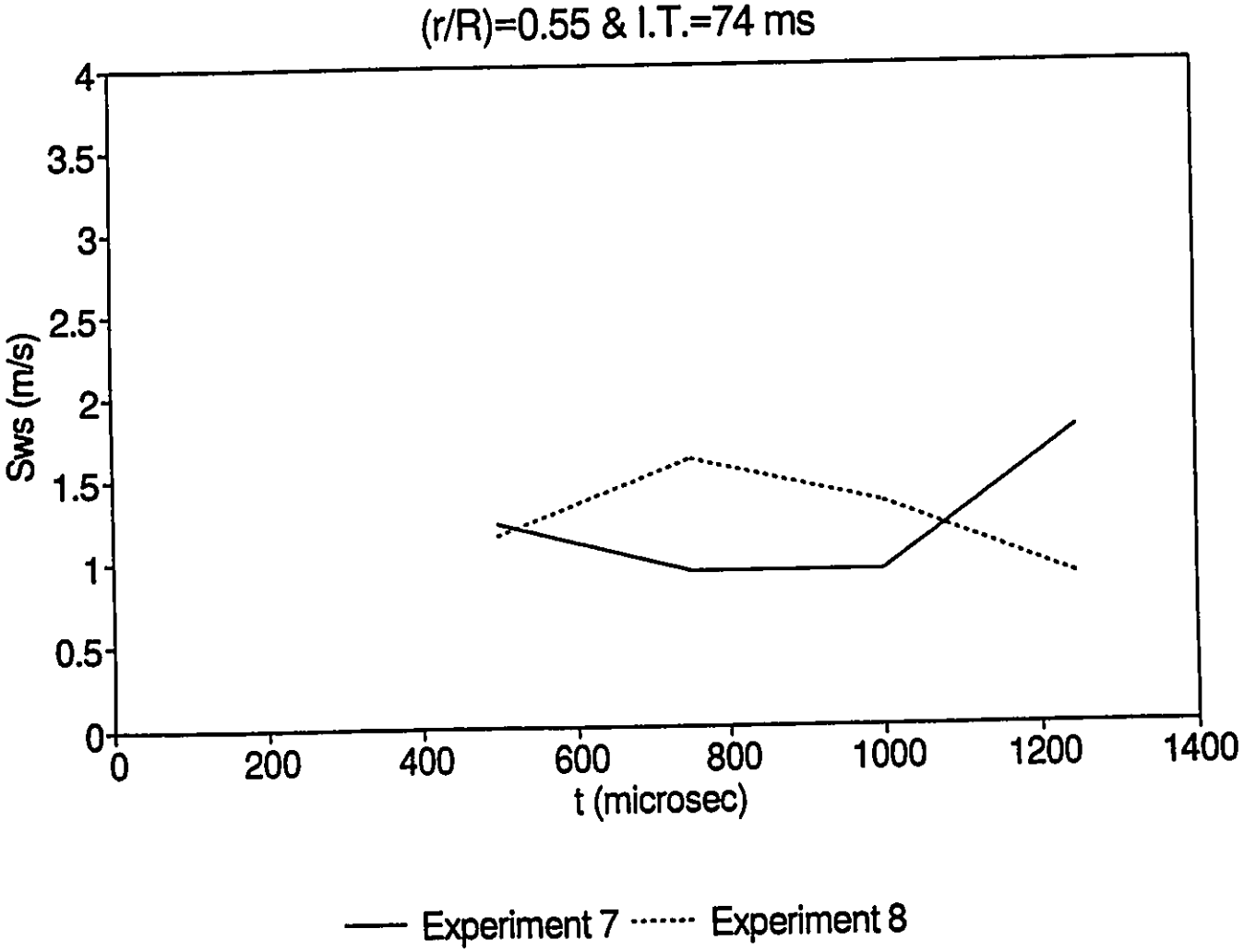

Figure 49 : Flame speed using modified elliptical model for (r/R)=0.55 and I.T.=74 ms.

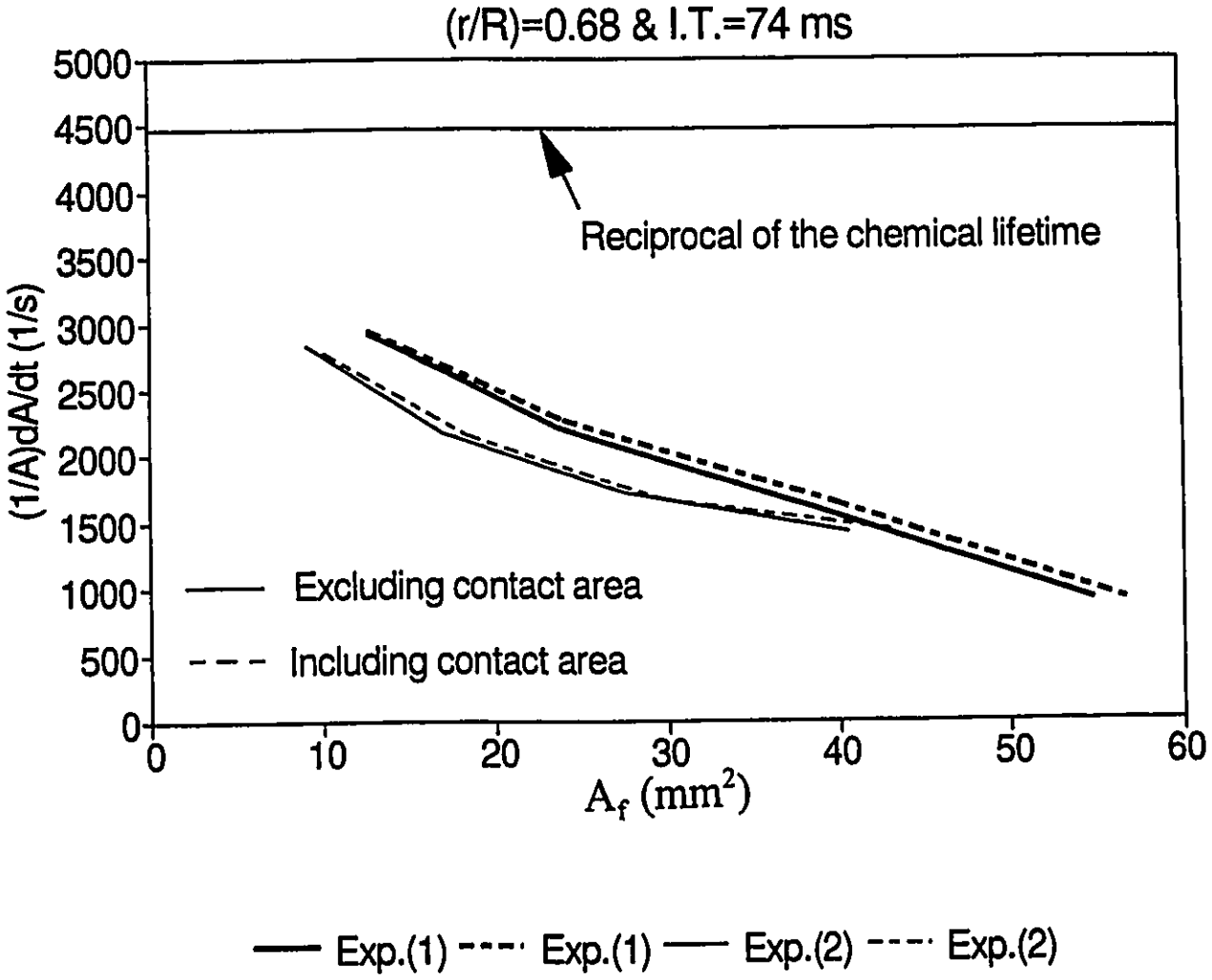

Figure 50 : Specific rate of growth of flame area versus flame area using the 2-D model for (r/R)=0.68 and I.T.=74 ms.

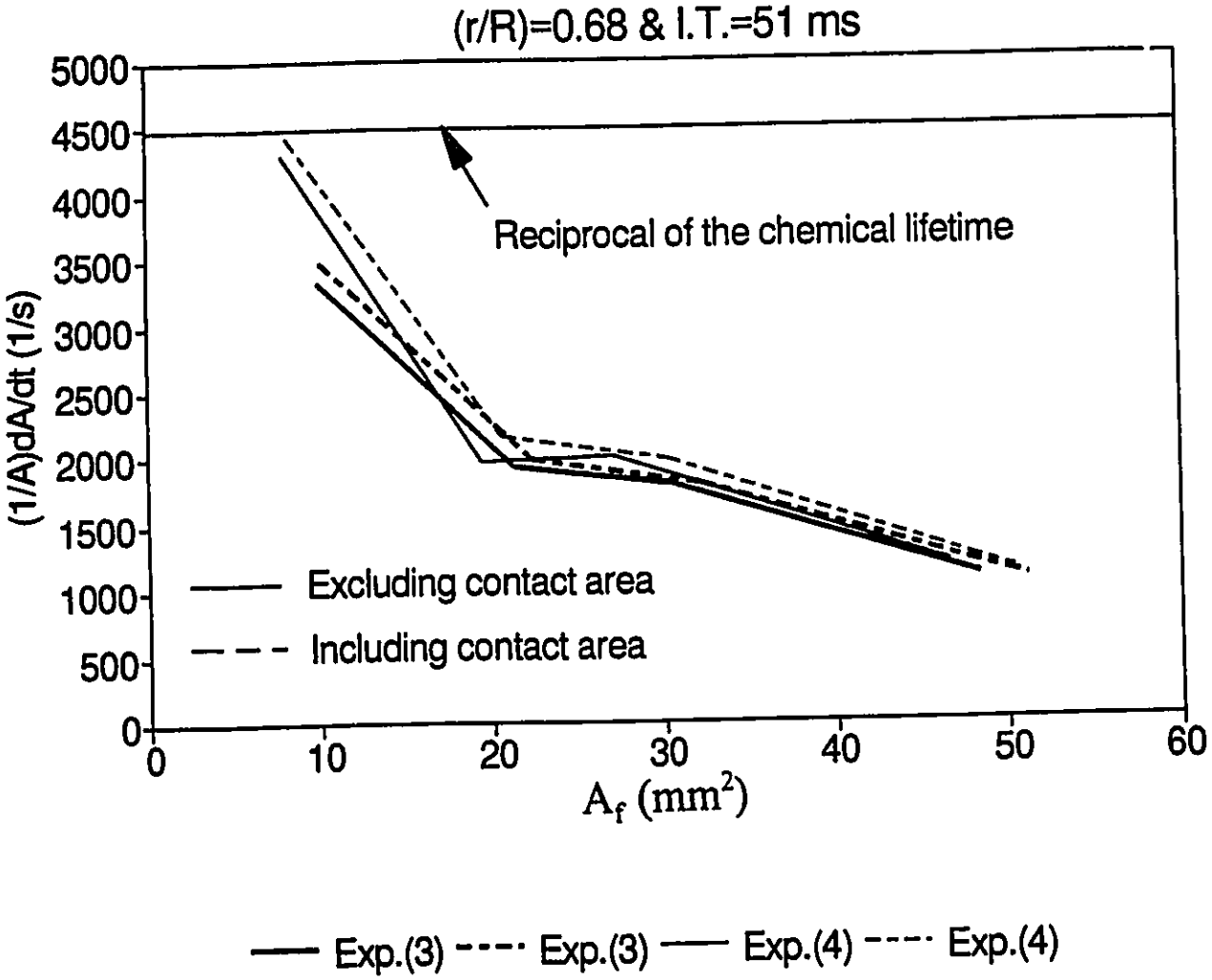

Figure 51 : Specific rate of growth of flame area versus flame area using the 2-D model for (r/R)=0.68 and I.T.=51 ms.

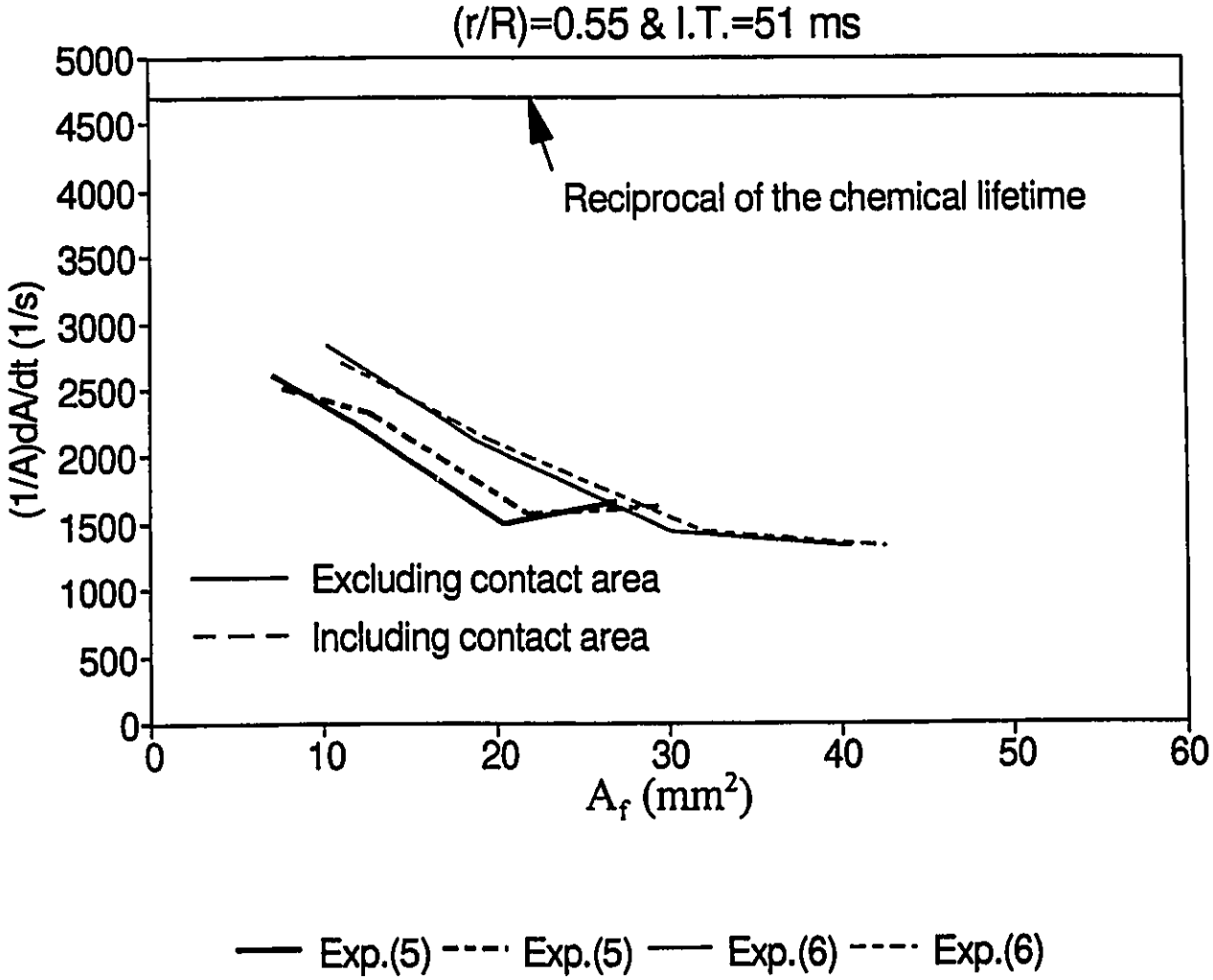

Figure 52 : Specific rate of growth of flame area versus flame area using the 2-D model for (r/R)=0.55 and I.T.=51 ms.

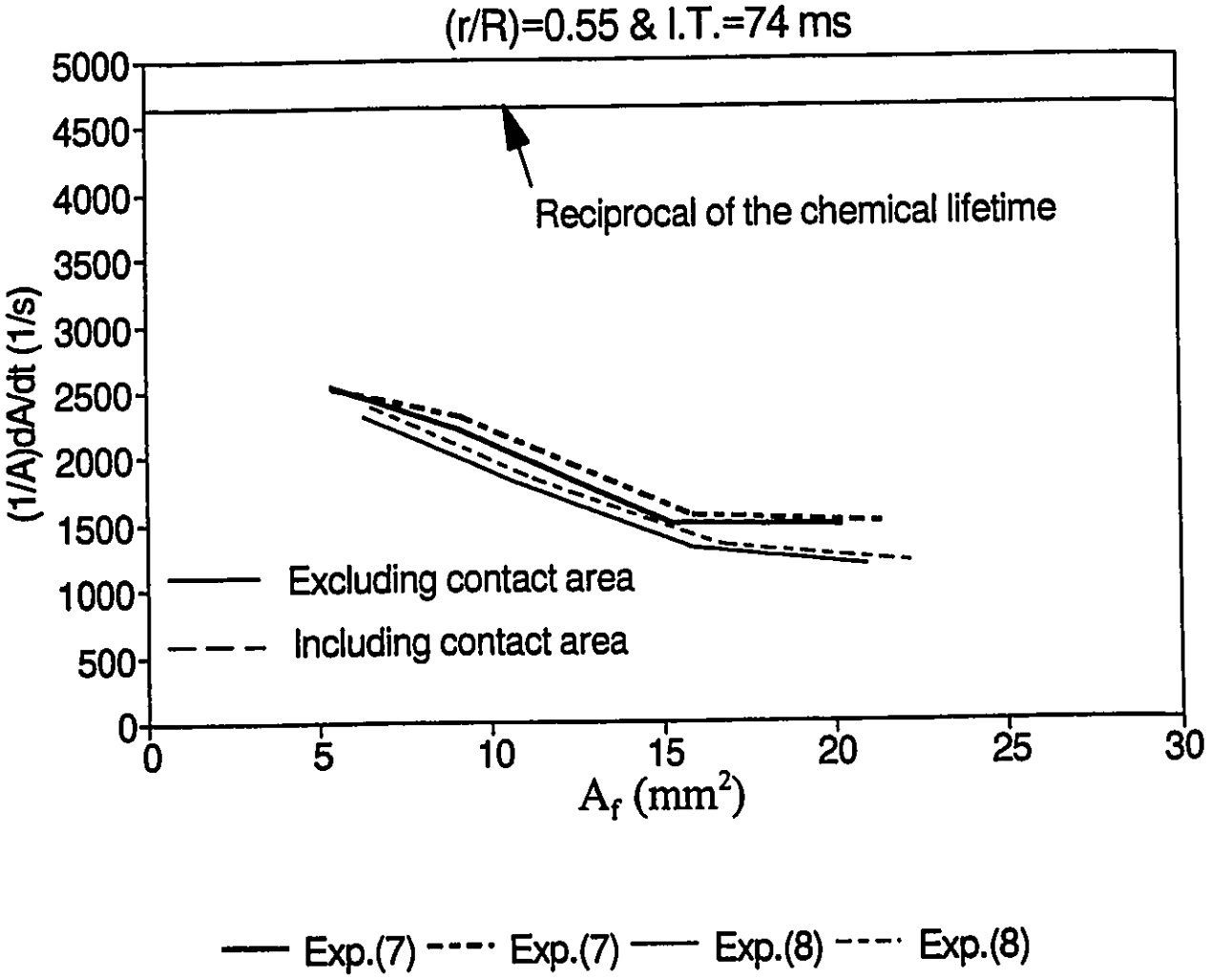

Figure 53 : Specific rate of growth of flame area versus flame area using 2-D model for (r/R)=0.55 and I.T.=74 ms.

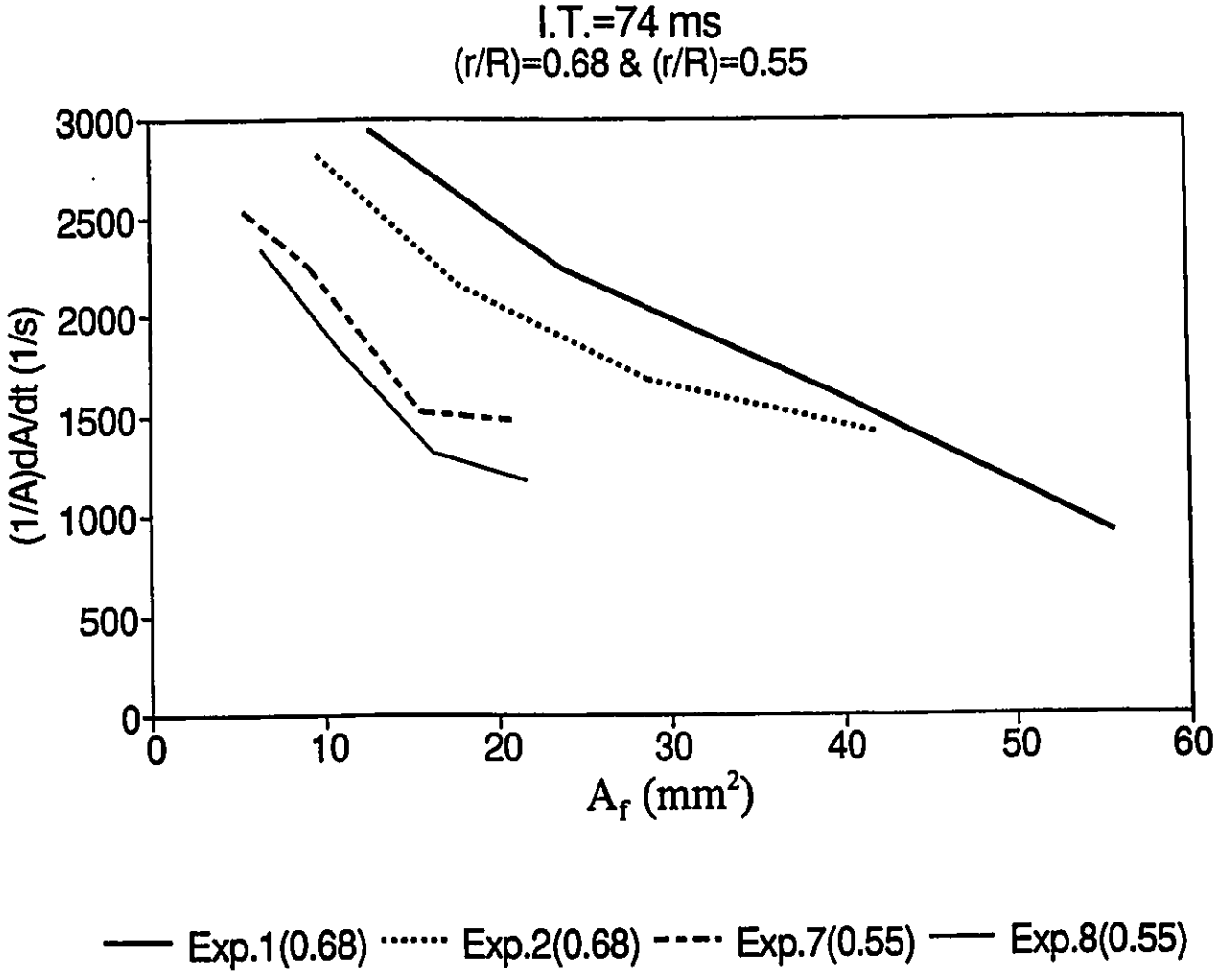

Figure 54 : Comparing the values of the specific rate of growth of flame area at different spark locations for I.T.=74 ms using the 2-D model.

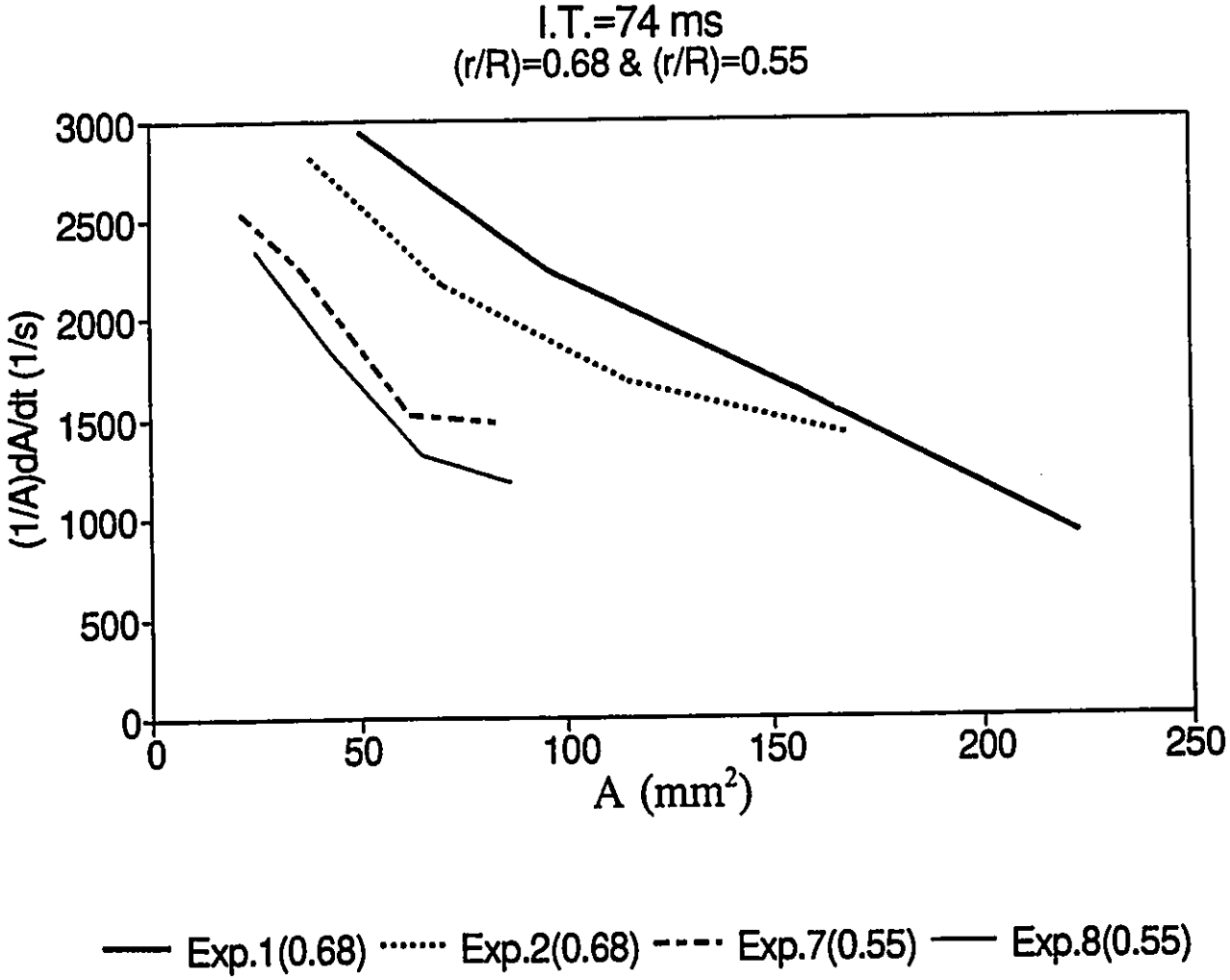

Figure 55 : Comparing the values of the specific rate of growth of flame area at different spark locations for I.T.=74 ms using the spherical model.

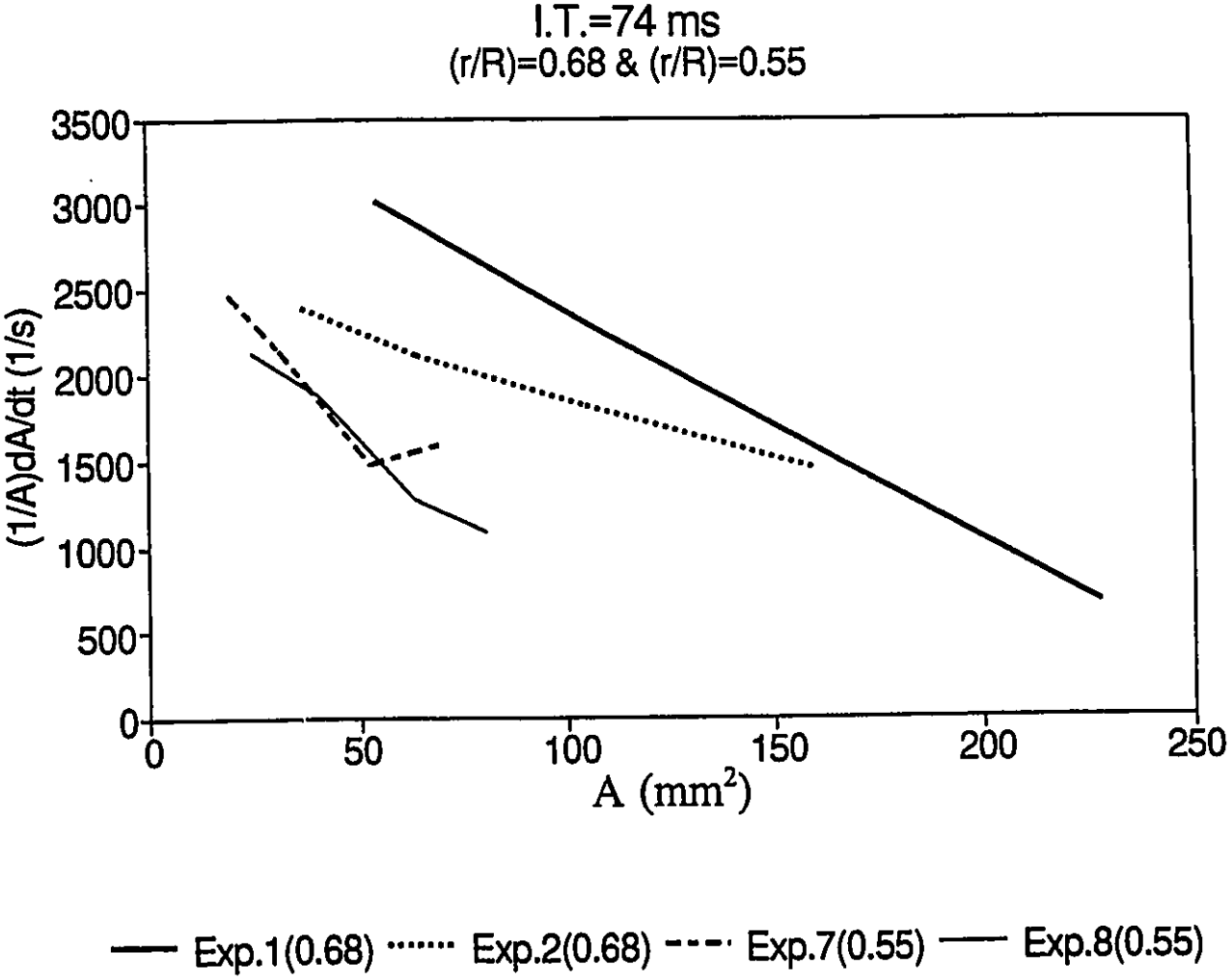

Figure 56 : Comparing the values of the specific rate of growth of flame area at different spark locations for I.T.=74 ms using the elliptical model.

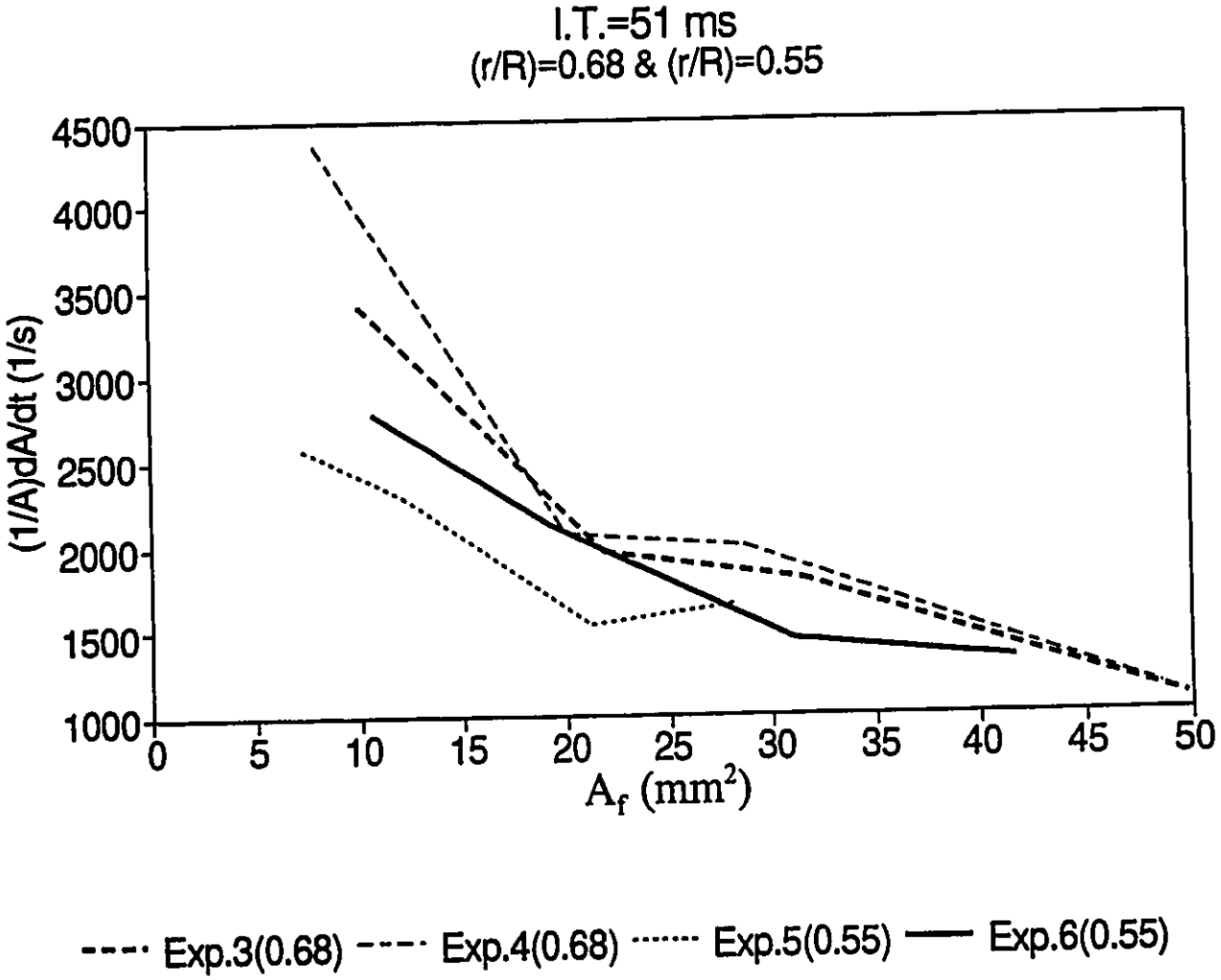

Figure 57 : Comparing the values of the specific rate of growth of flame area at different spark locations for I.T.=51 ms using the 2-D model.

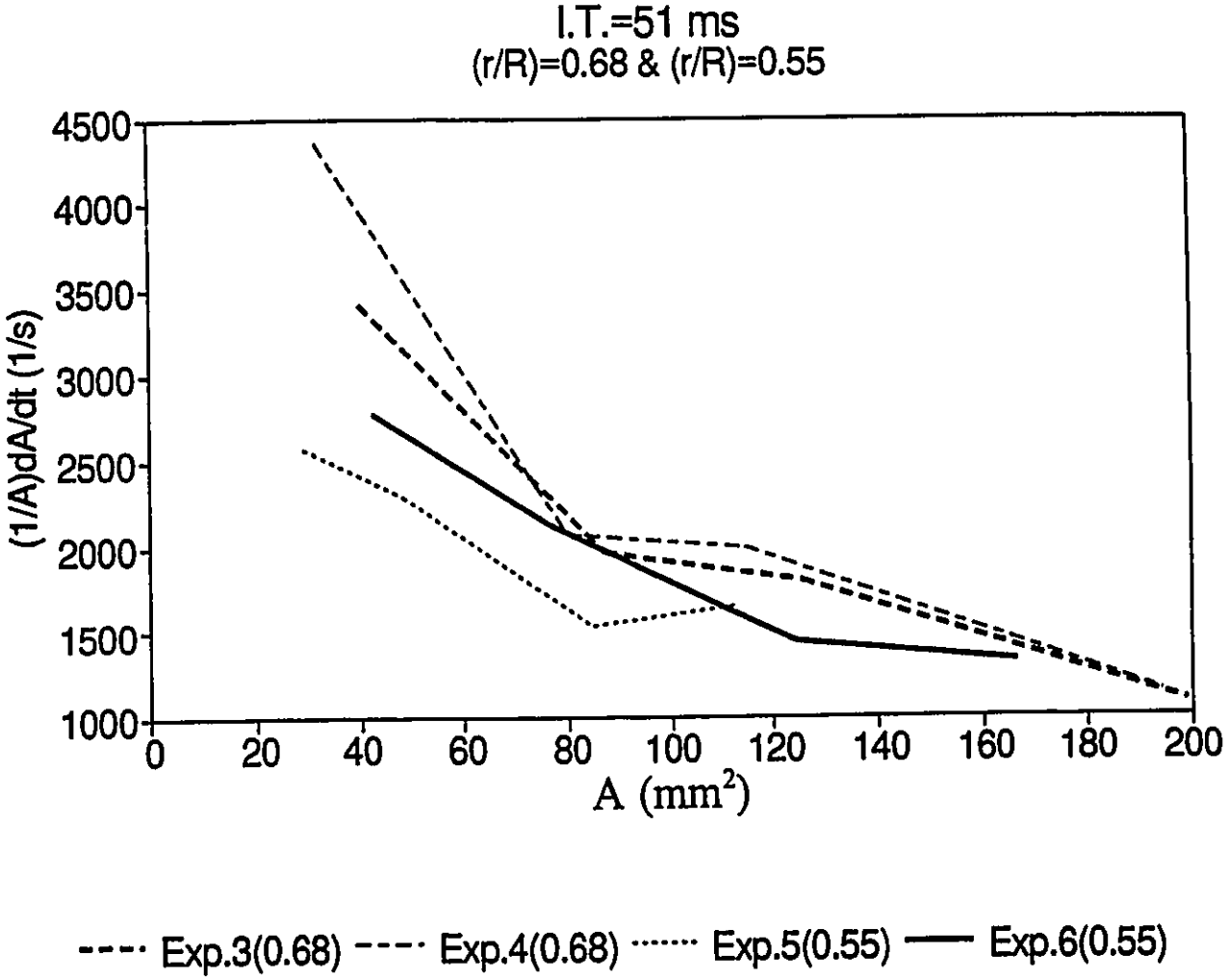

Figure 58 : Comparing the values of the specific rate of growth of flame area at different spark locations for I.T.=51 ms using the spherical model.

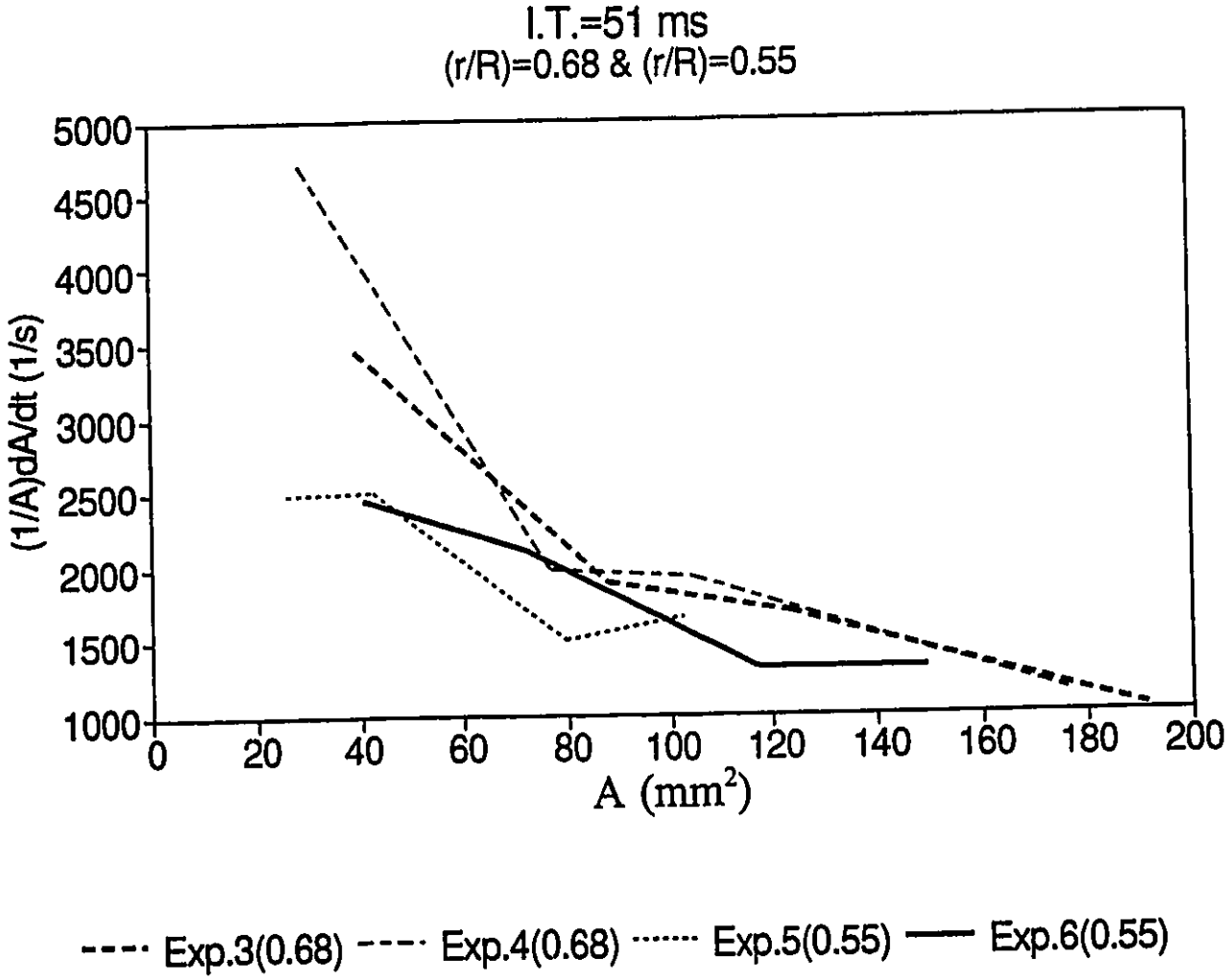

Figure 59 : Comparing the values of the specific rate of growth of flame area at different spark locations for I.T.=51 ms using the elliptical model.

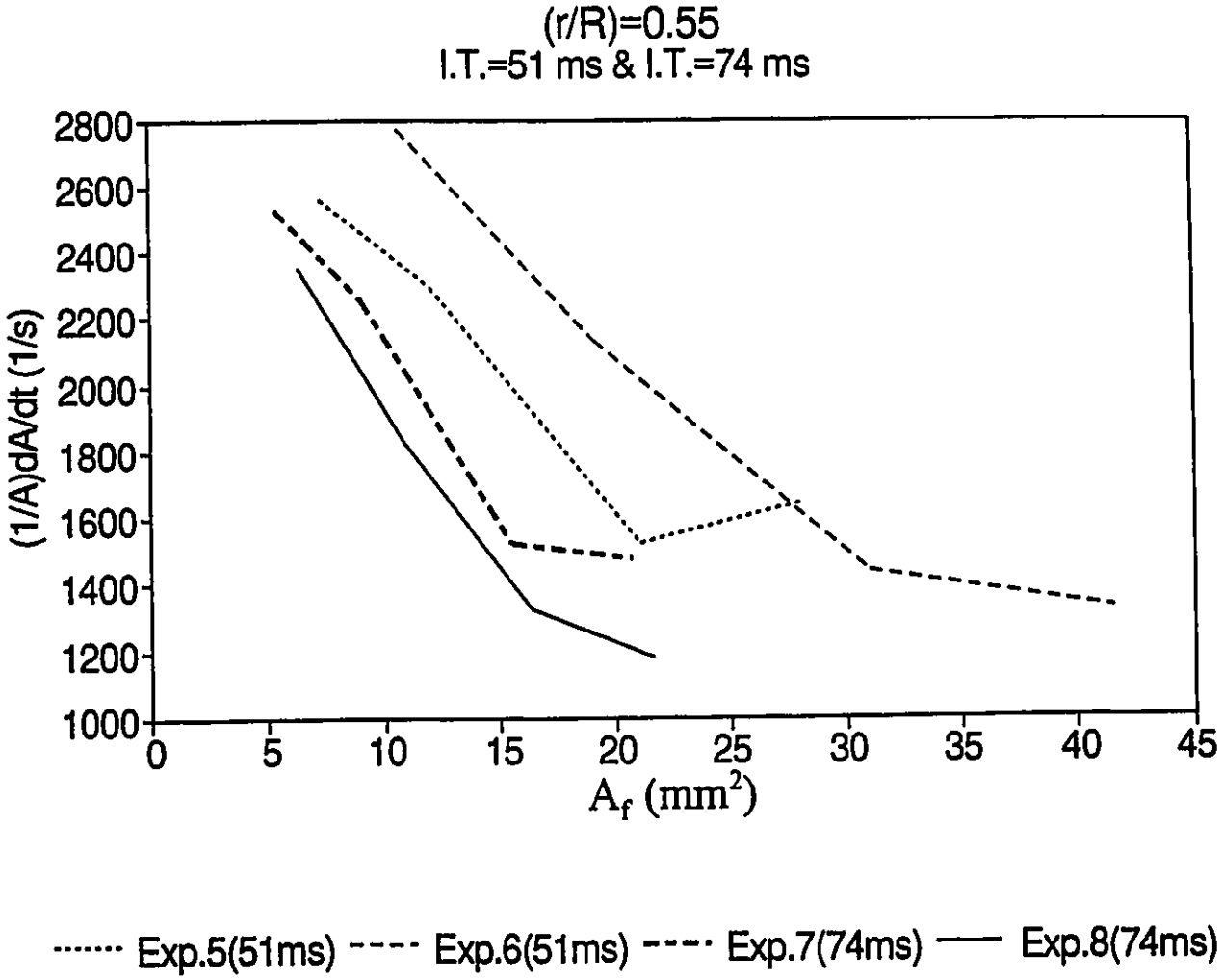

Figure 60 : Comparing the values of the specific rate of growth of flame area at different swirling levels for (r/R)=0.55 using the 2-D model.

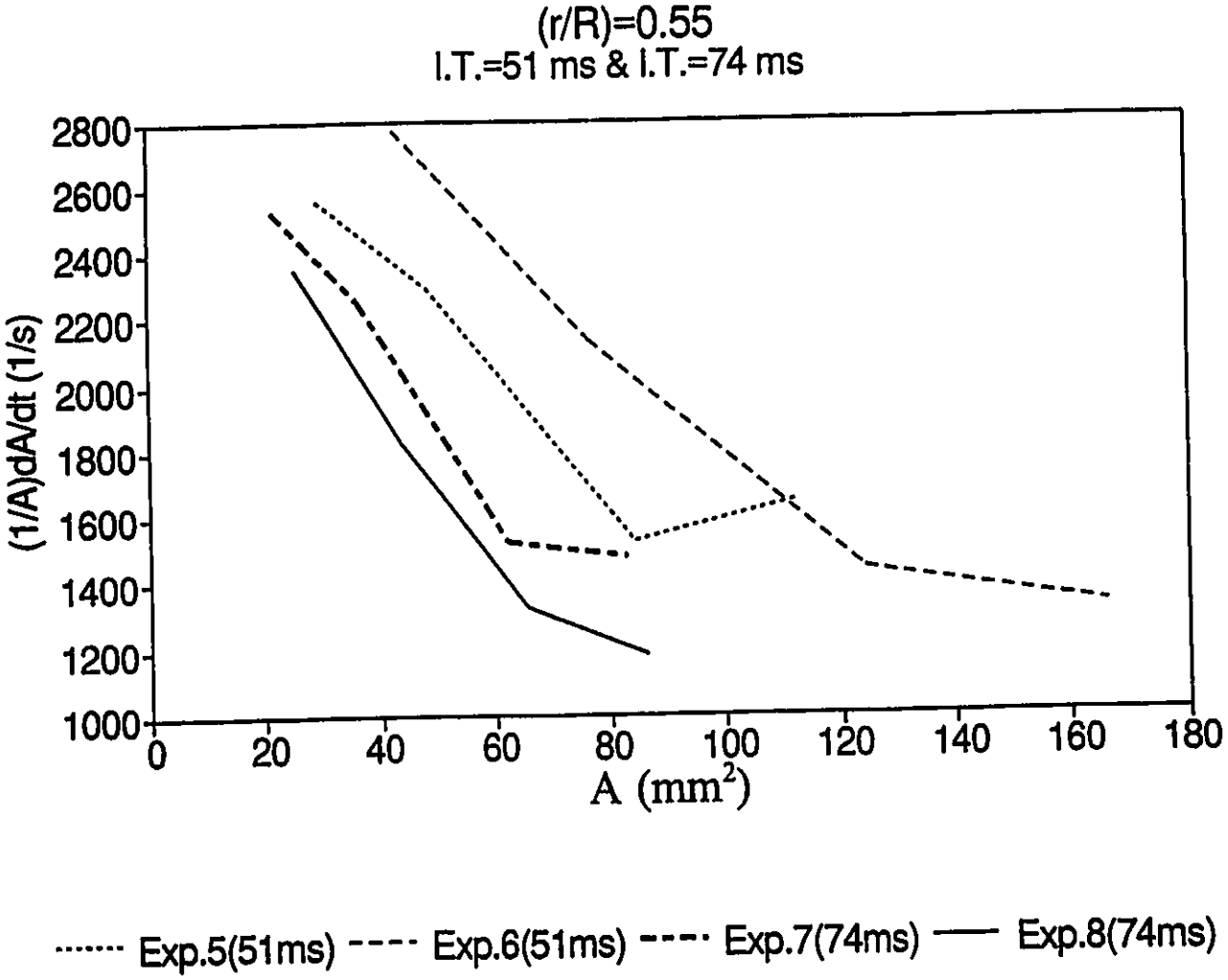

Figure 61 : Comparing the values of the specific rate of growth of flame area at different swirling levels for (r/R)=0.55 using the spherical model.

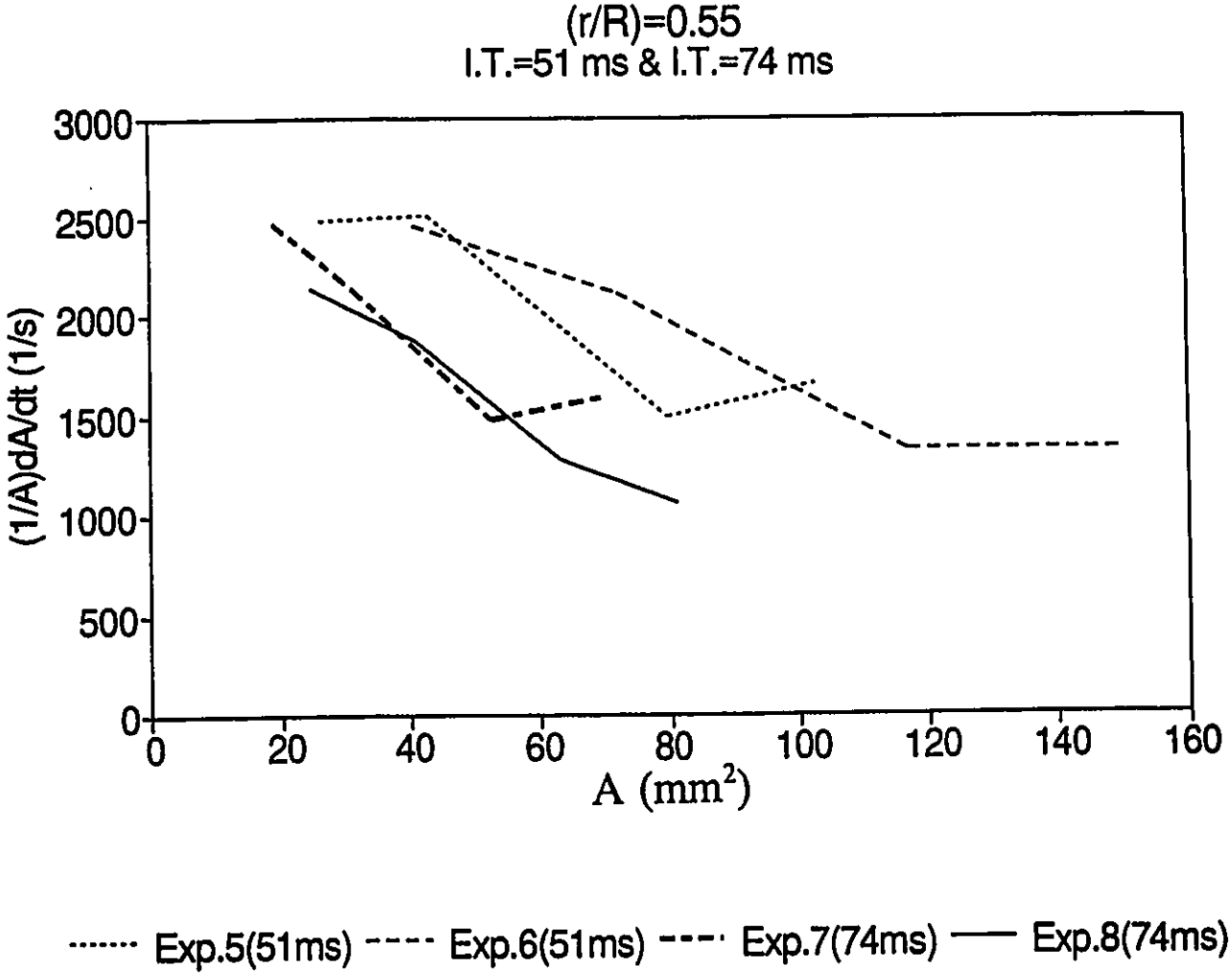

Figure 62 : Comparing the values of the specific rate of growth of flame area at different swirling levels for (r/R)=0.55 using the elliptical model.

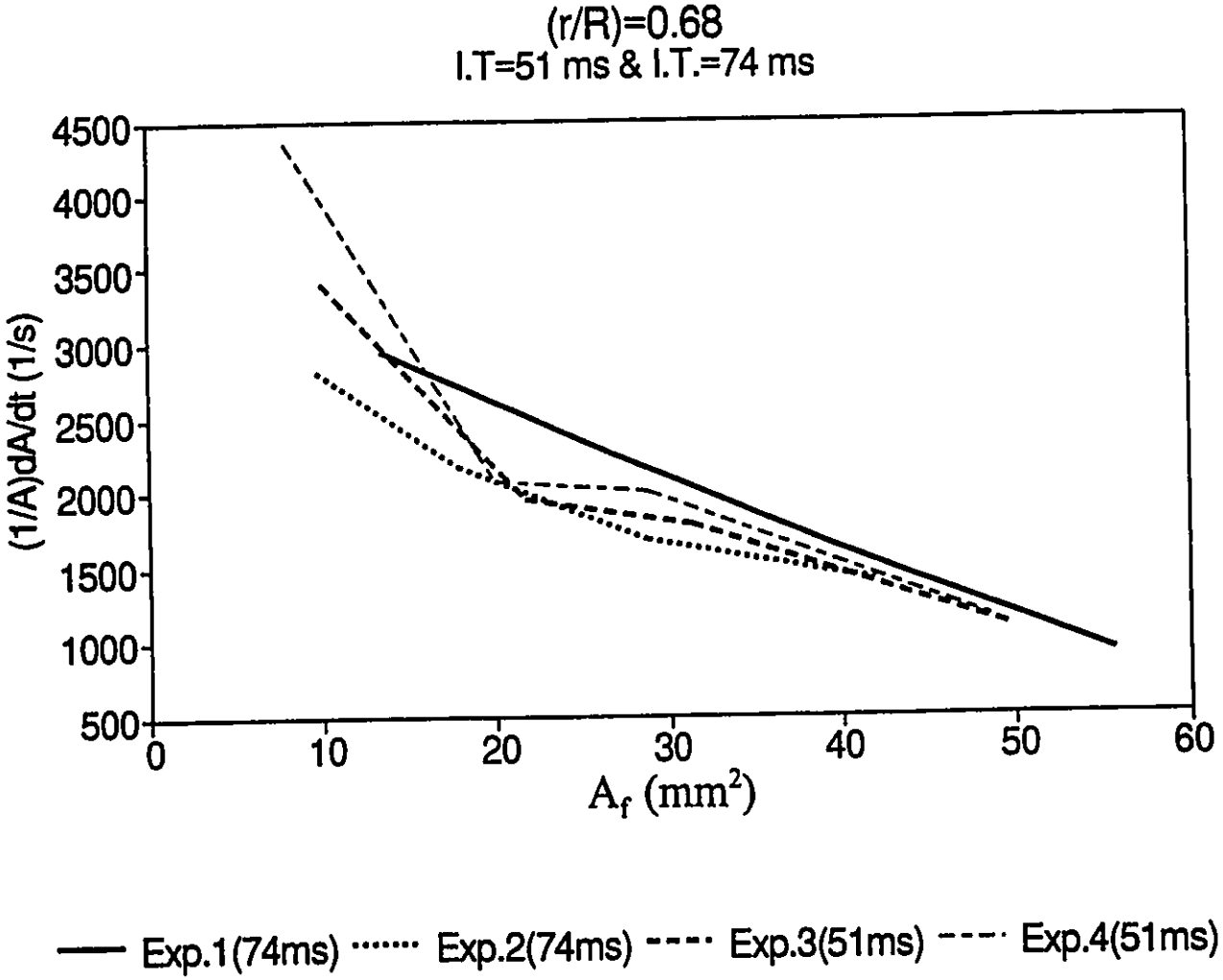

Figure 63 : Comparing the values of the specific rate of growth of flame area at different swirling levels for (r/R)=0.68 using the 2-D model.

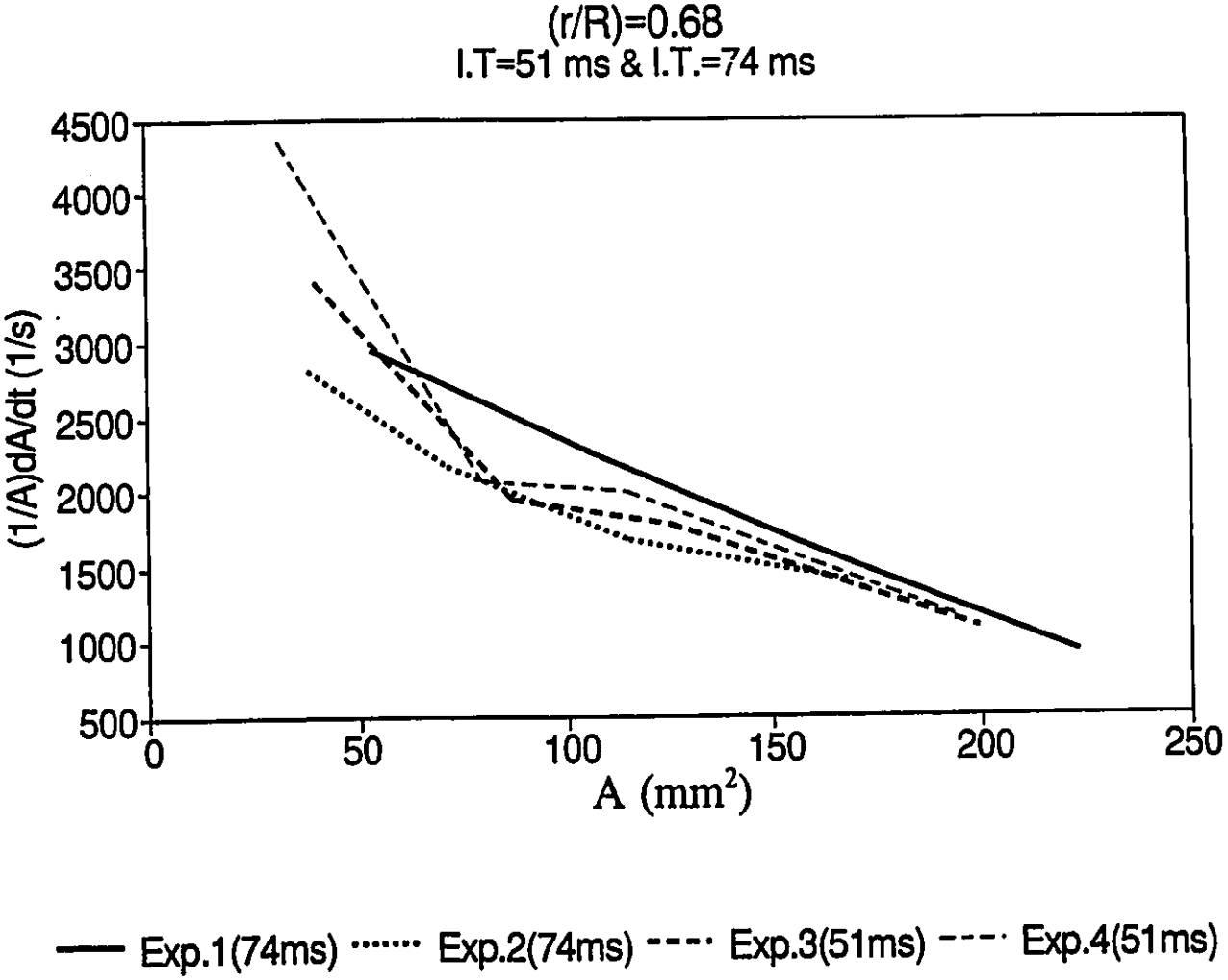

Figure 64 : Comparing the values of the specific rate of growth of flame area at different swirling levels for (r/R)=0.68 using the spherical model.

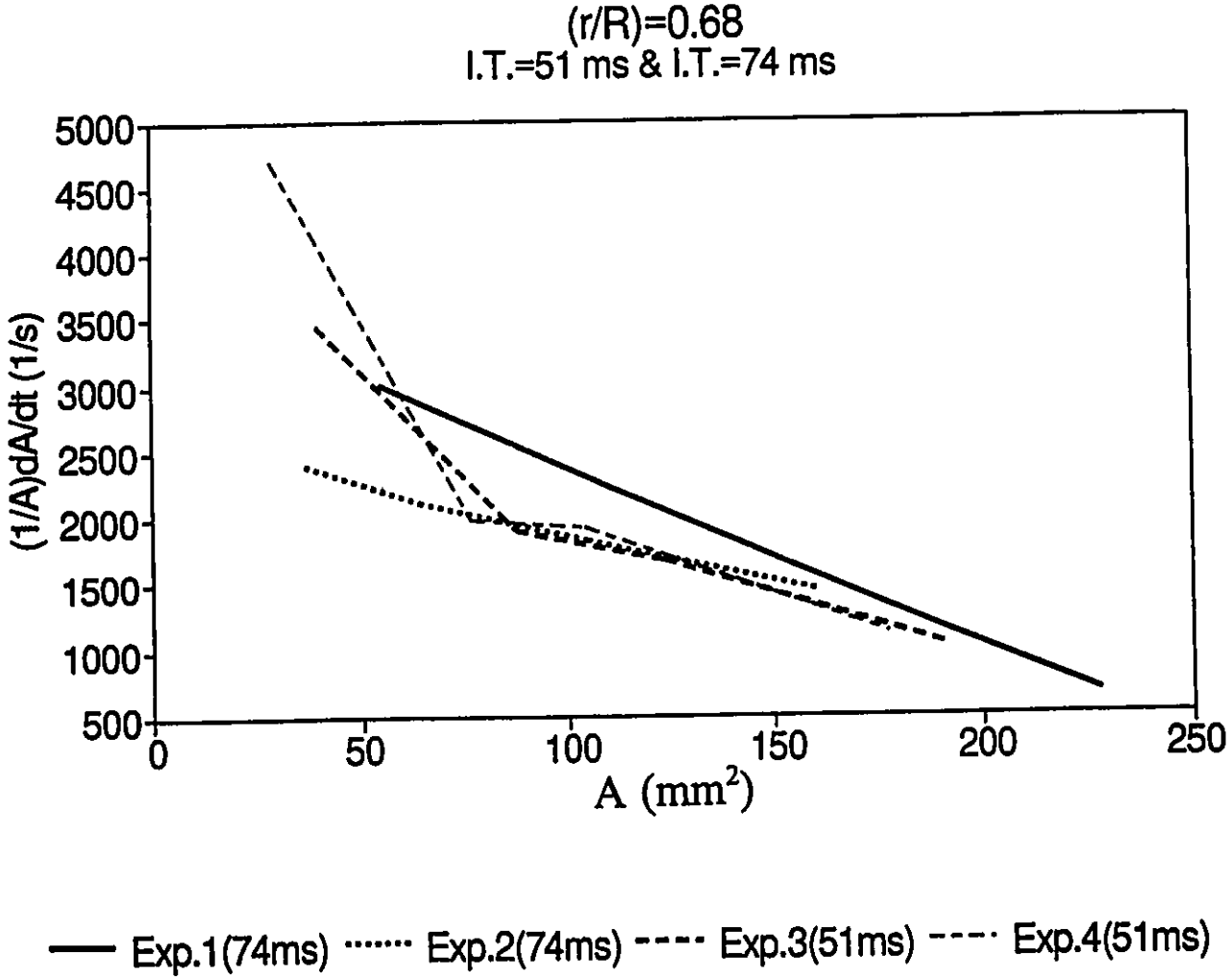

Figure 65 : Comparing the values of the specific rate of growth of flame area at different swirling levels for (r/R)=0.68 using the elliptical model.

Appendix A

Contours & Photographs of Early Flame Propagation

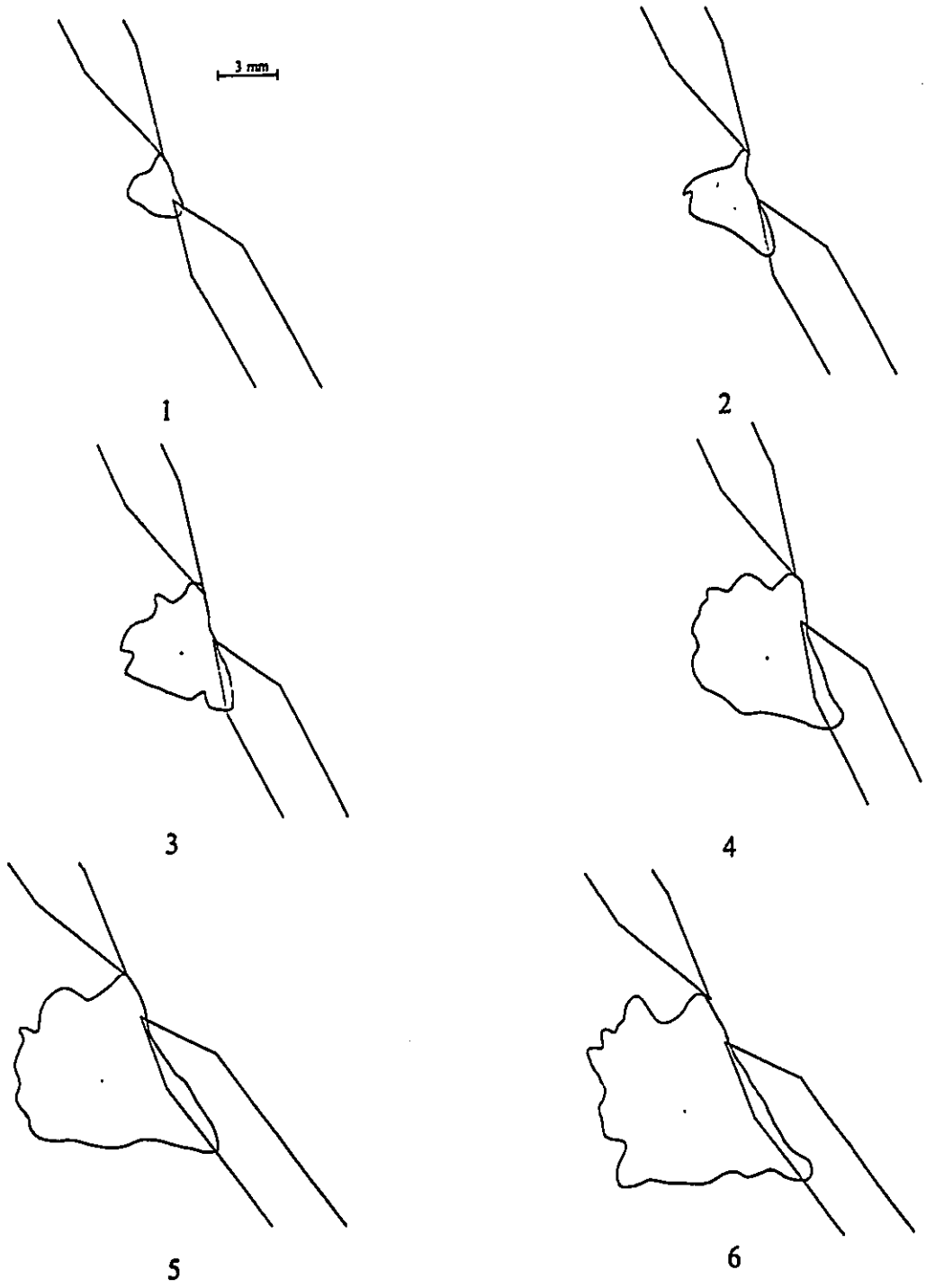

Figure A1: Contours of early flame propagation of experiment 1.

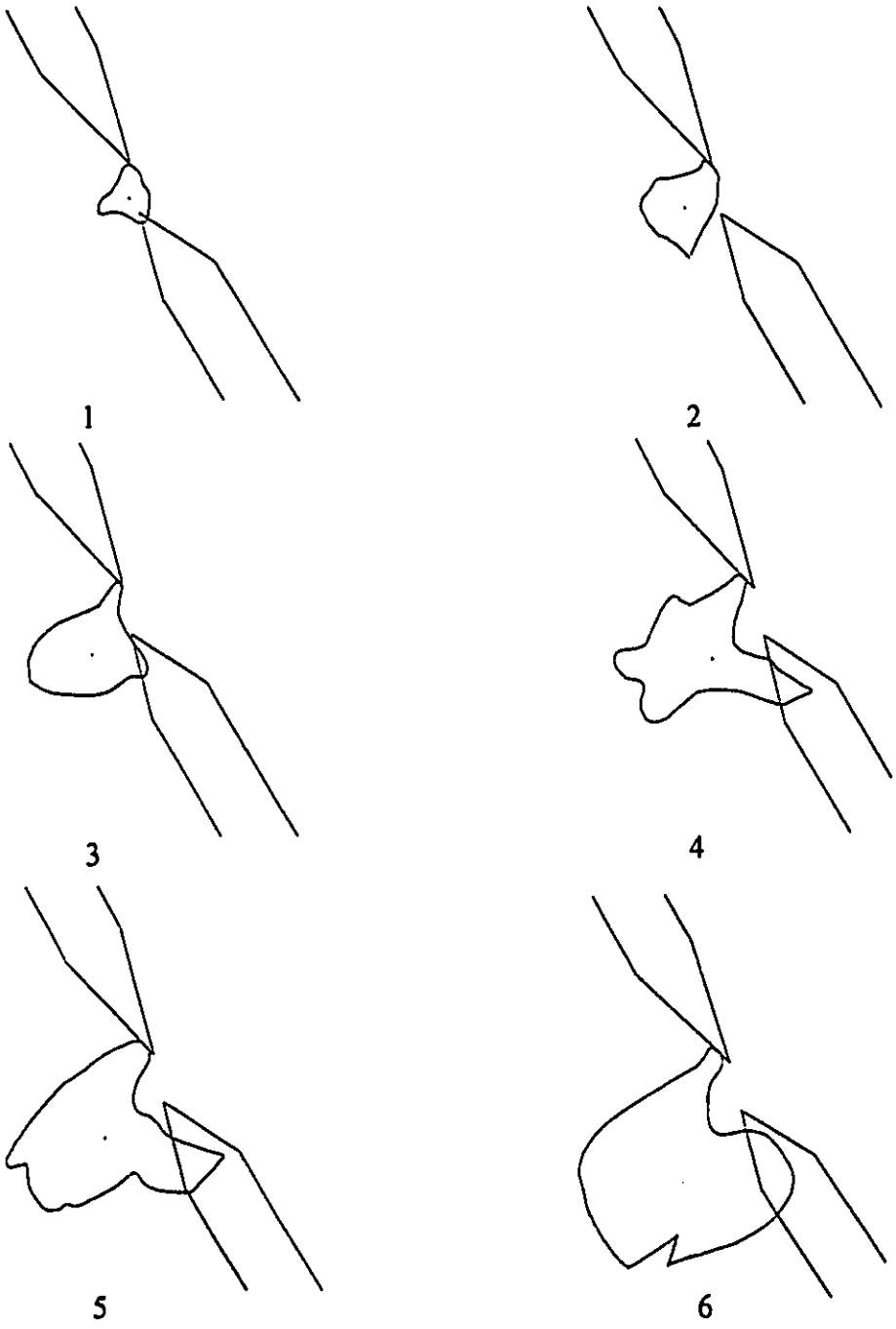

Figure A2: Contours of early flame propagation of experiment 2.

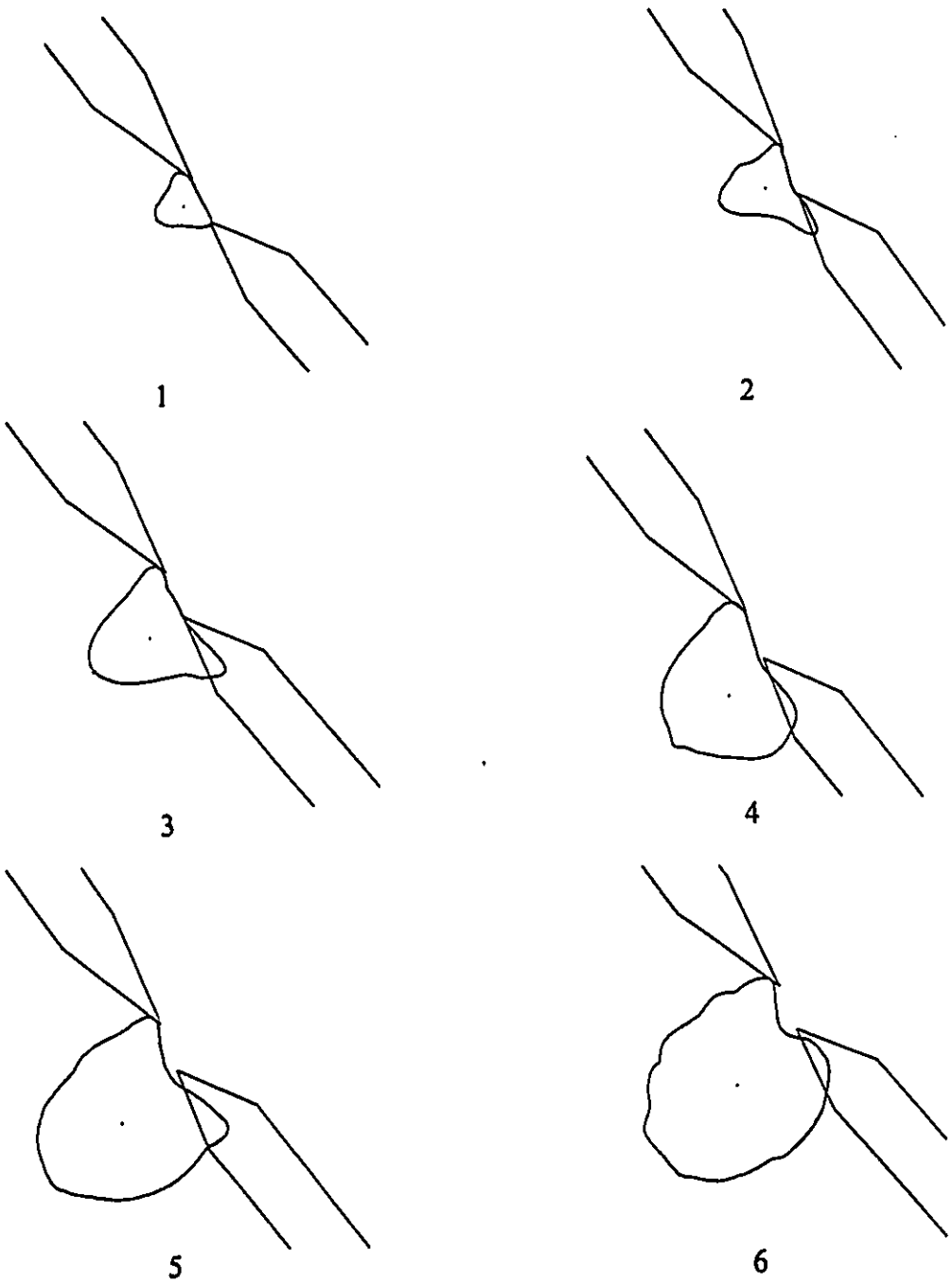

Figure A3: Contours of early flame propagation of experiment 3.

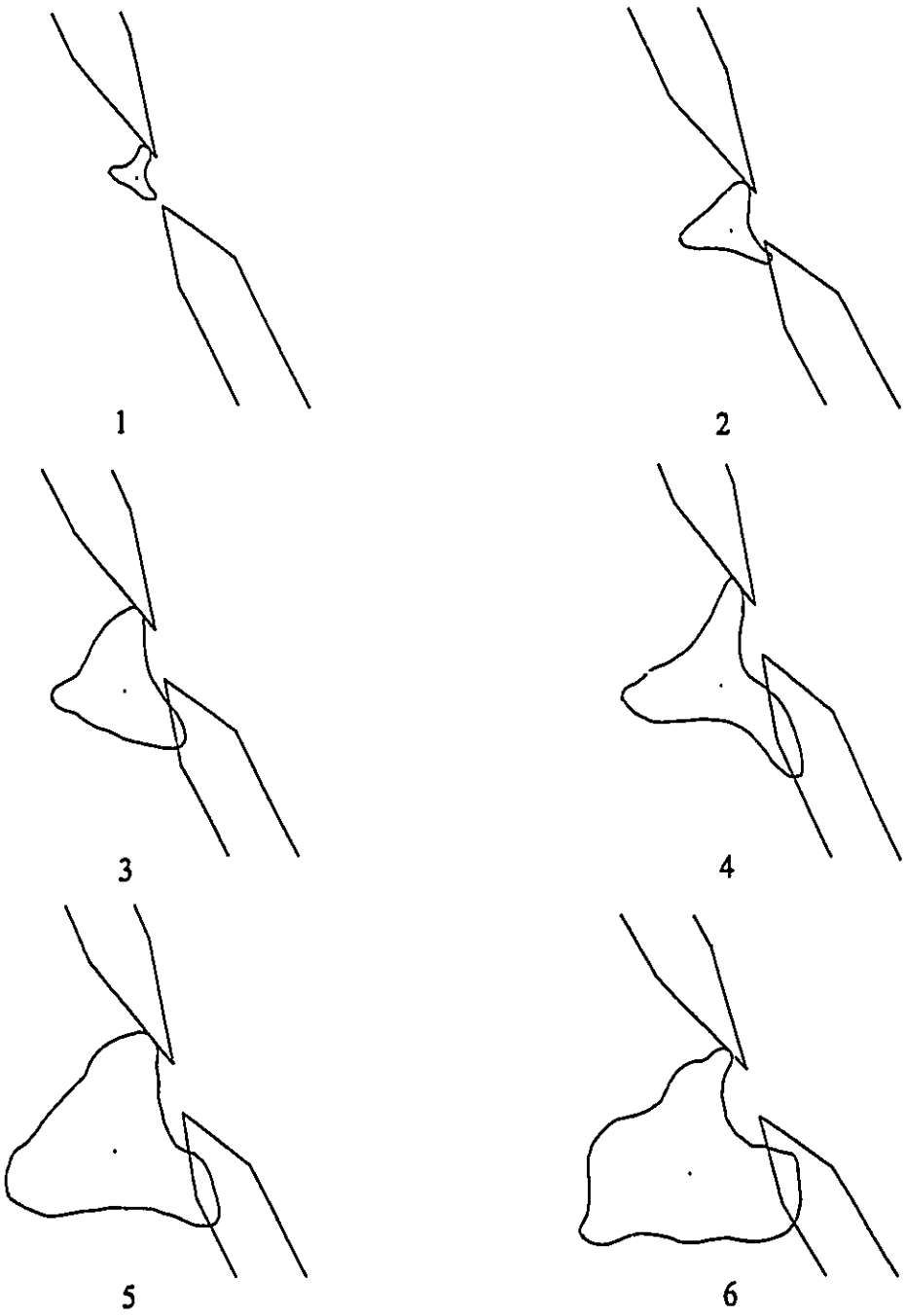

Figure A4: Contours of early flame propagation of experiment 4.

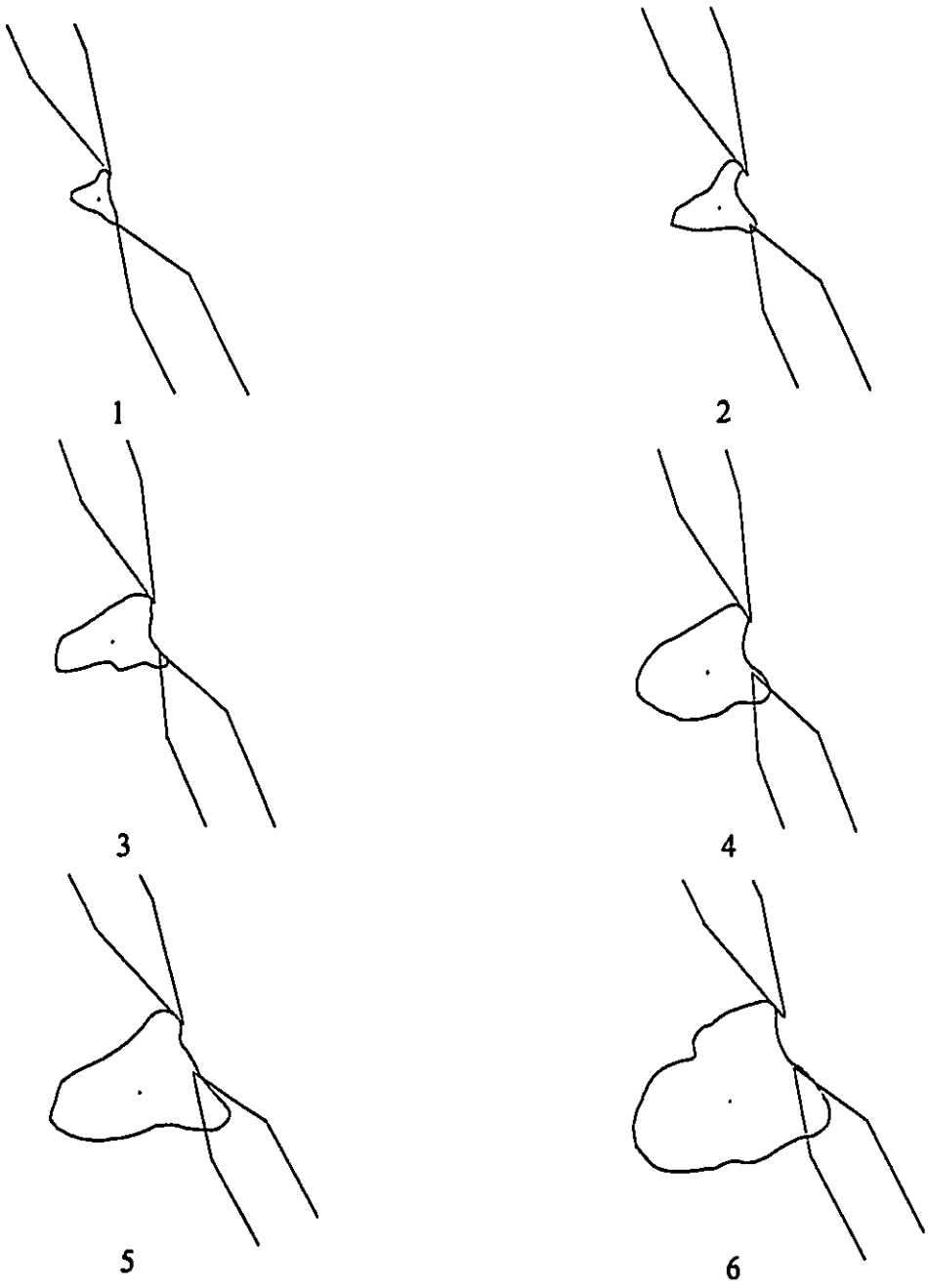

Figure A5: Contours of early flame propagation of experiment 5.

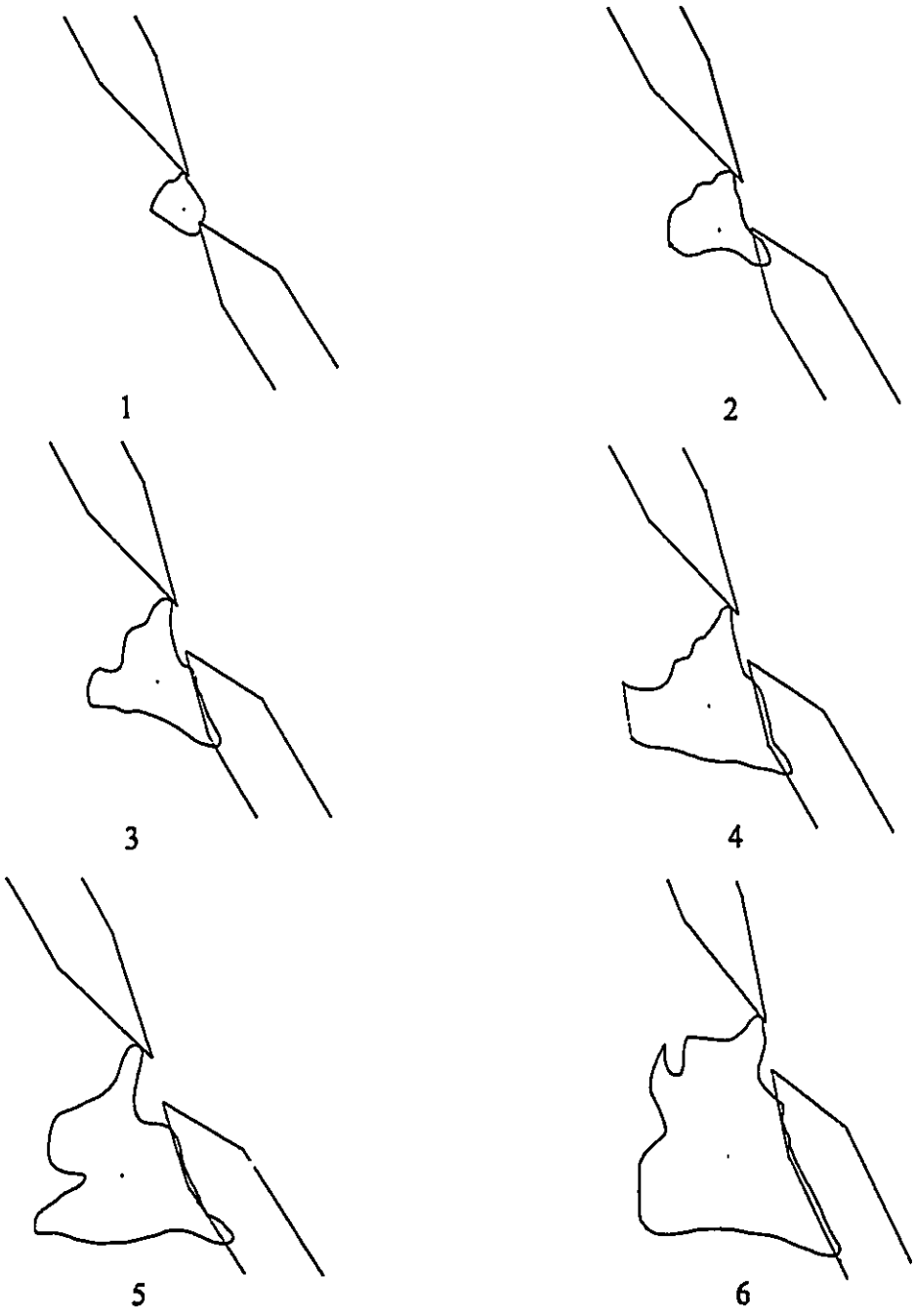

Figure A6: Contours of early flame propagation of experiment 6.

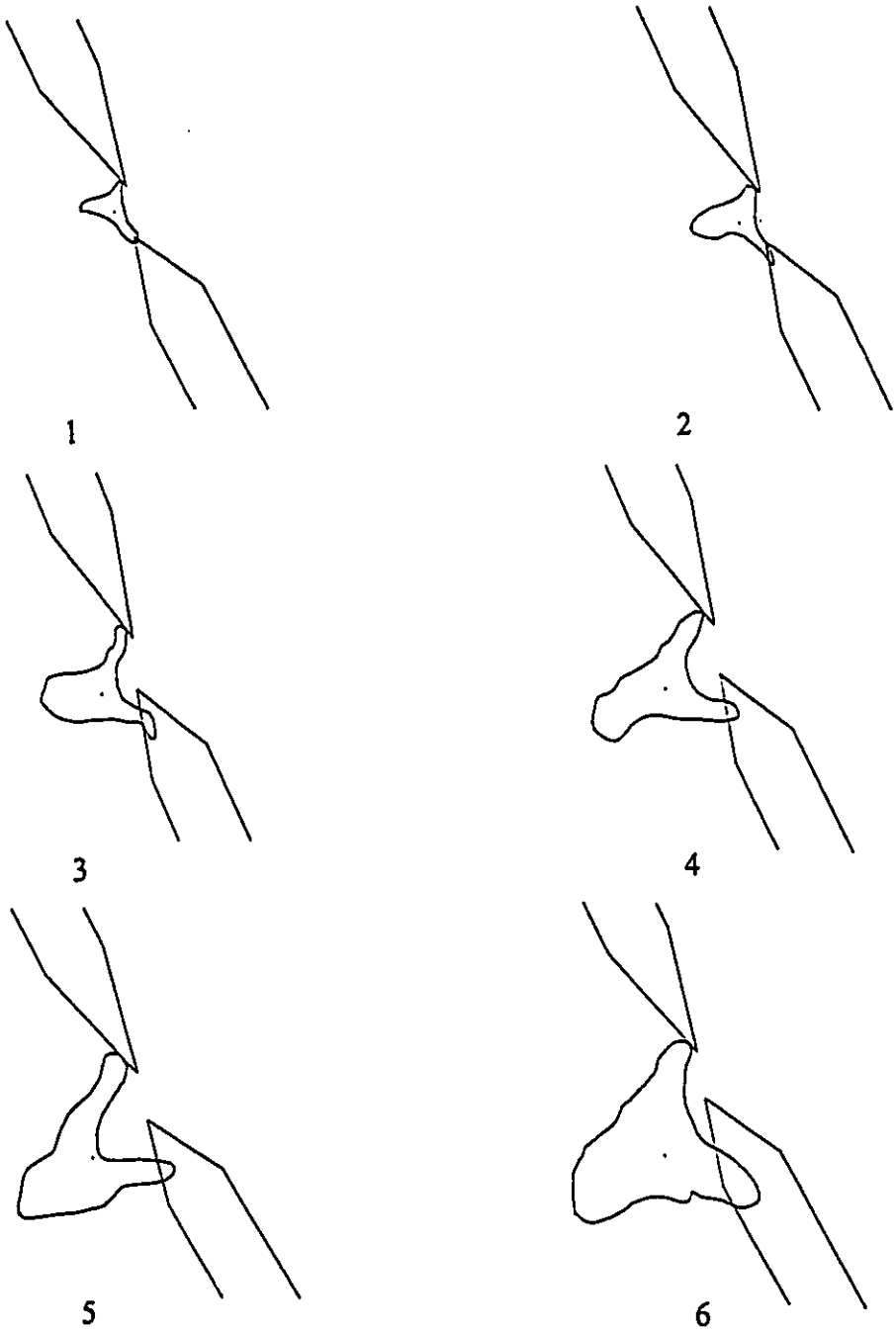

Figure A7: Contours of early flame propagation of experiment 7.

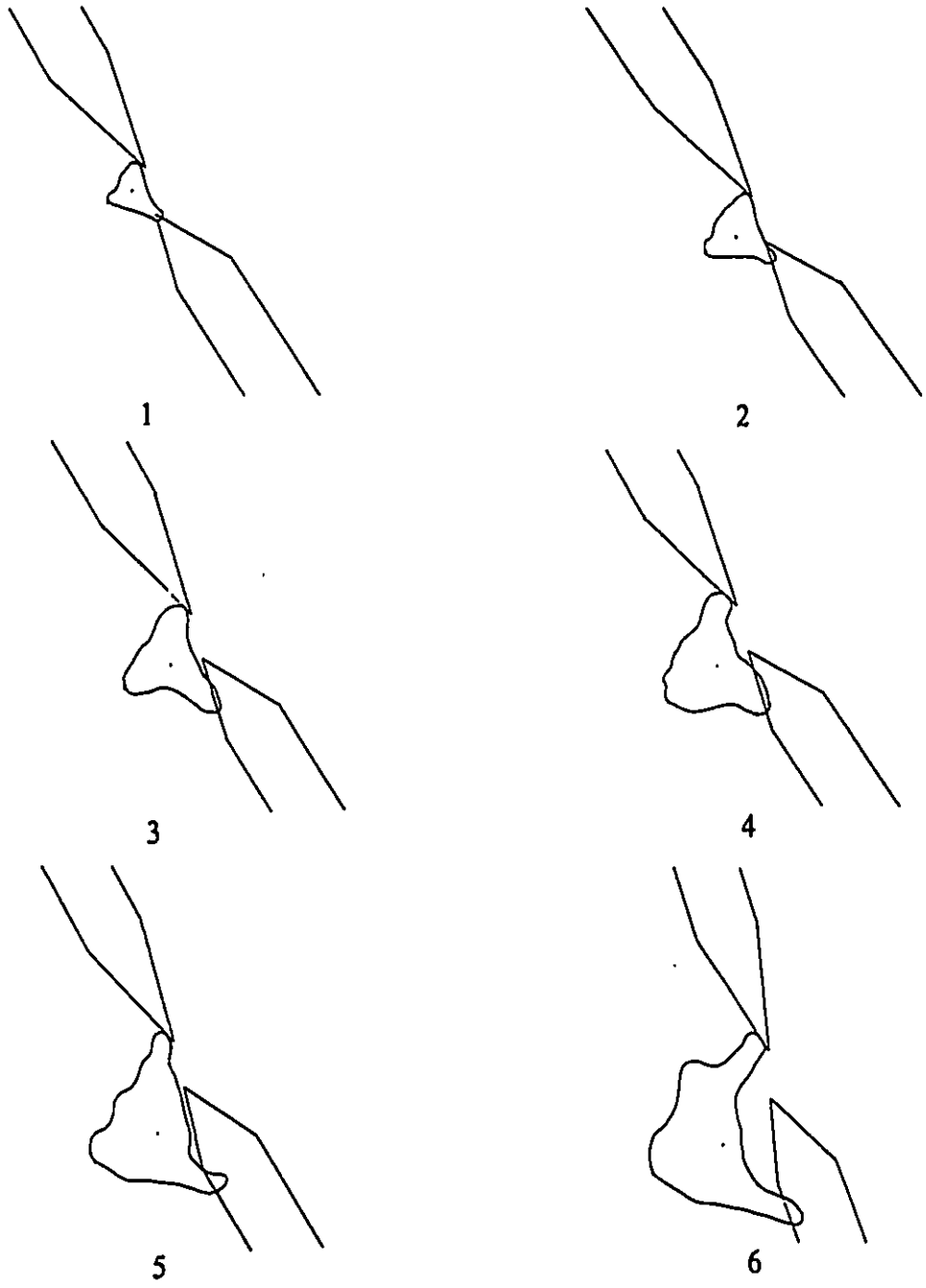

Figure A8: Contours of early flame propagation of experiment 8.

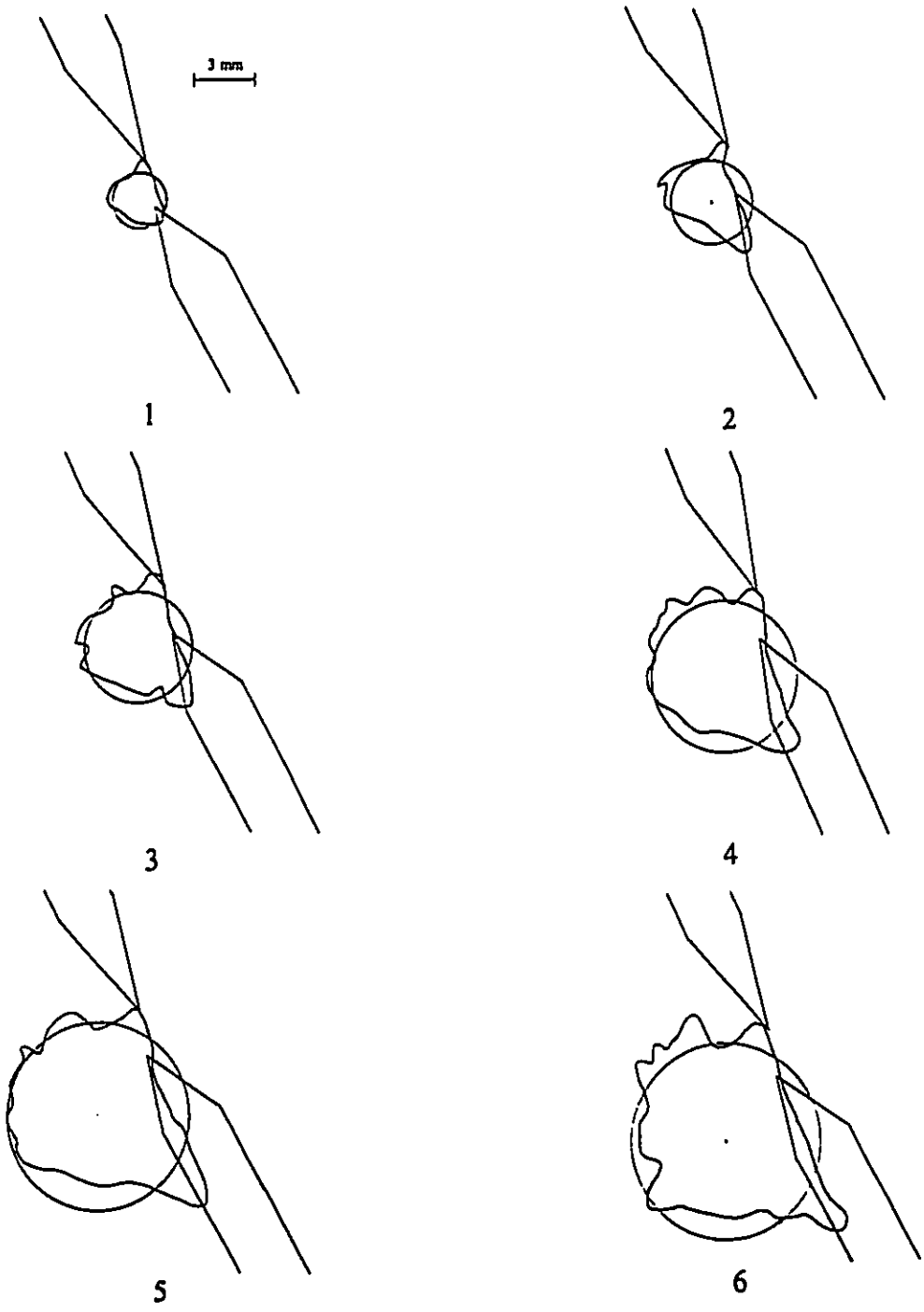

Figure A9: Applying the circular model for the early flame propagation of experiment 1.

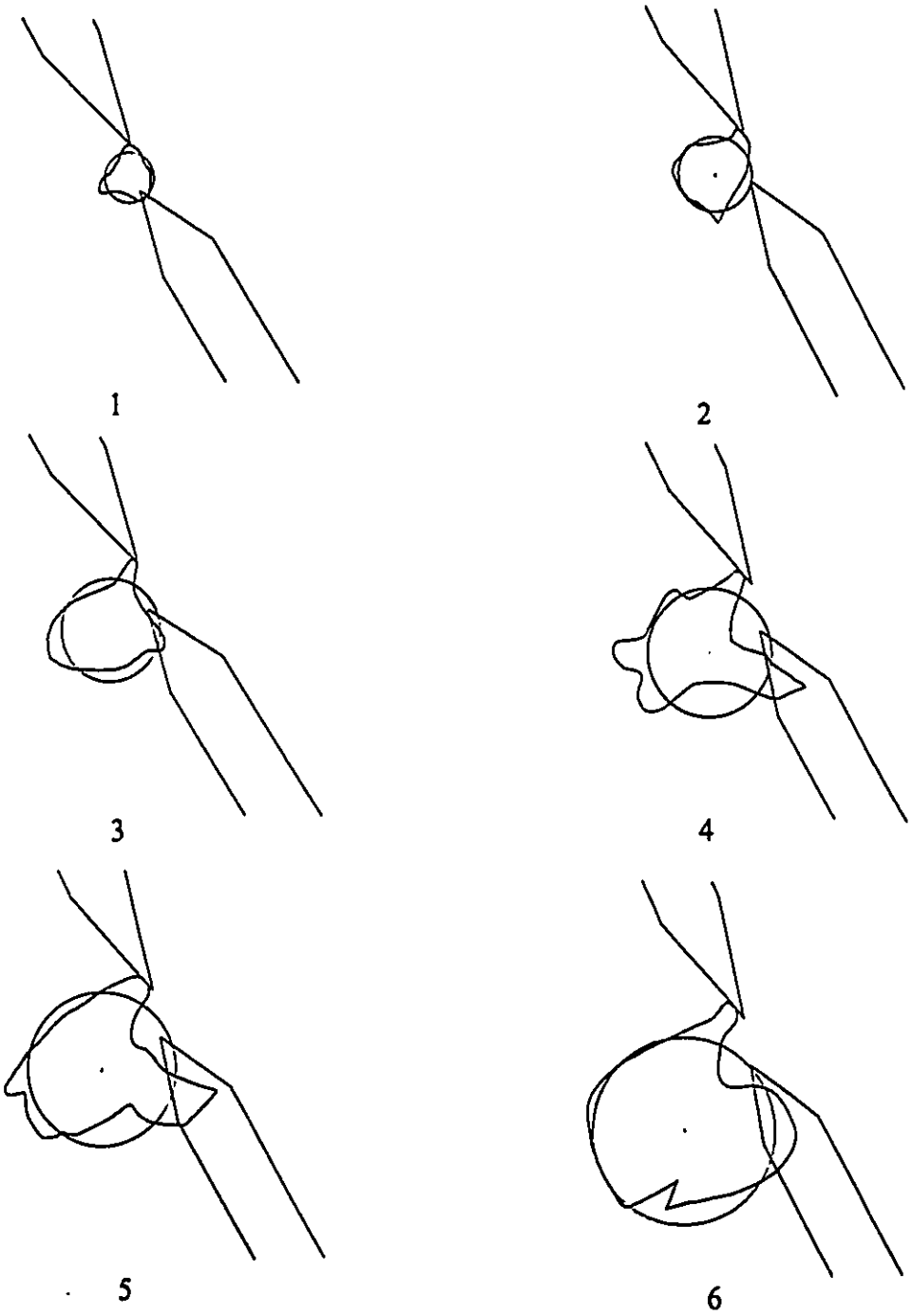

Figure A10: Applying the circular model for the early flame propagation of experiment 2.

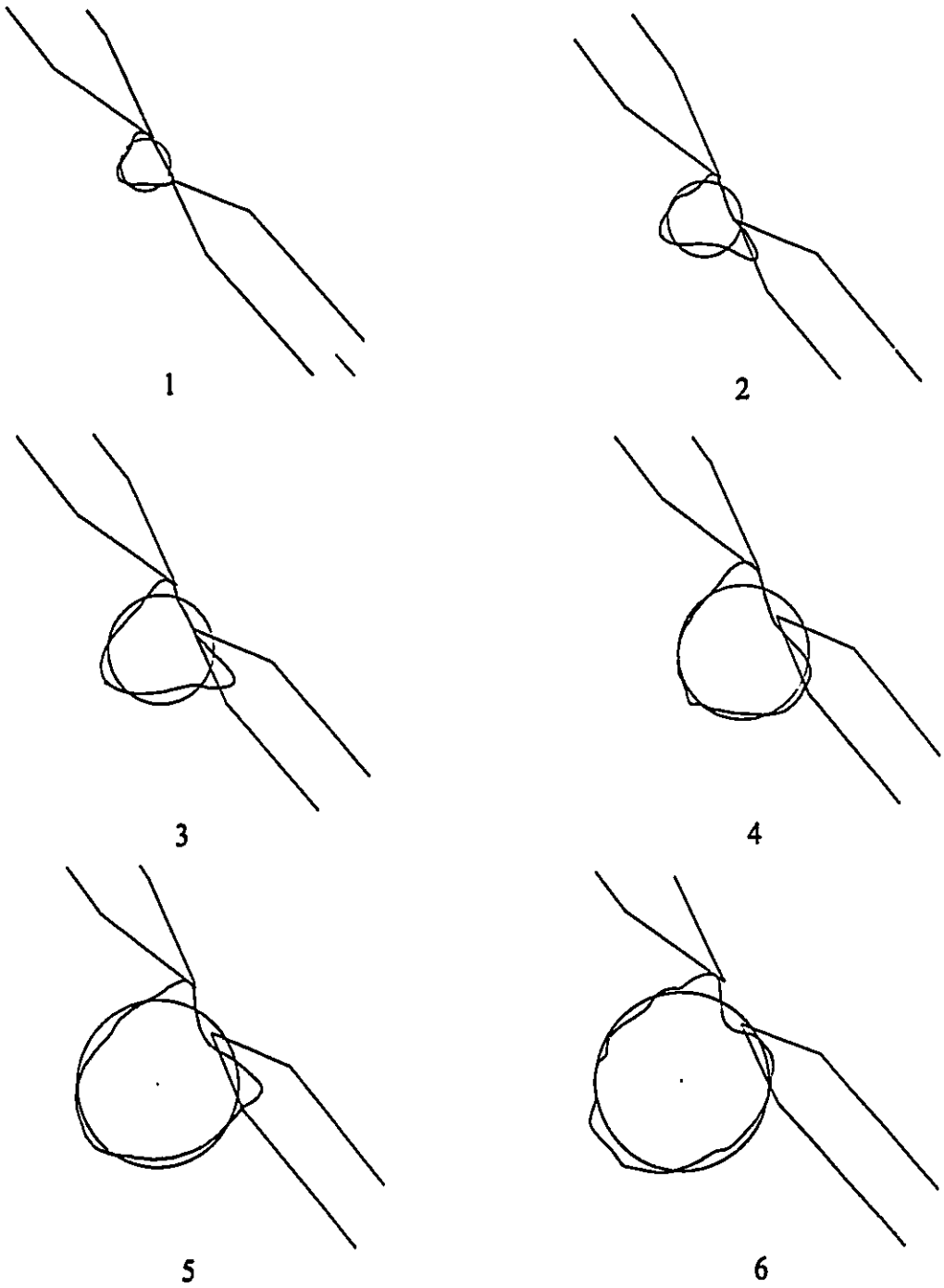

Figure A11: Applying the circular model for the early flame propagation of experiment 3.

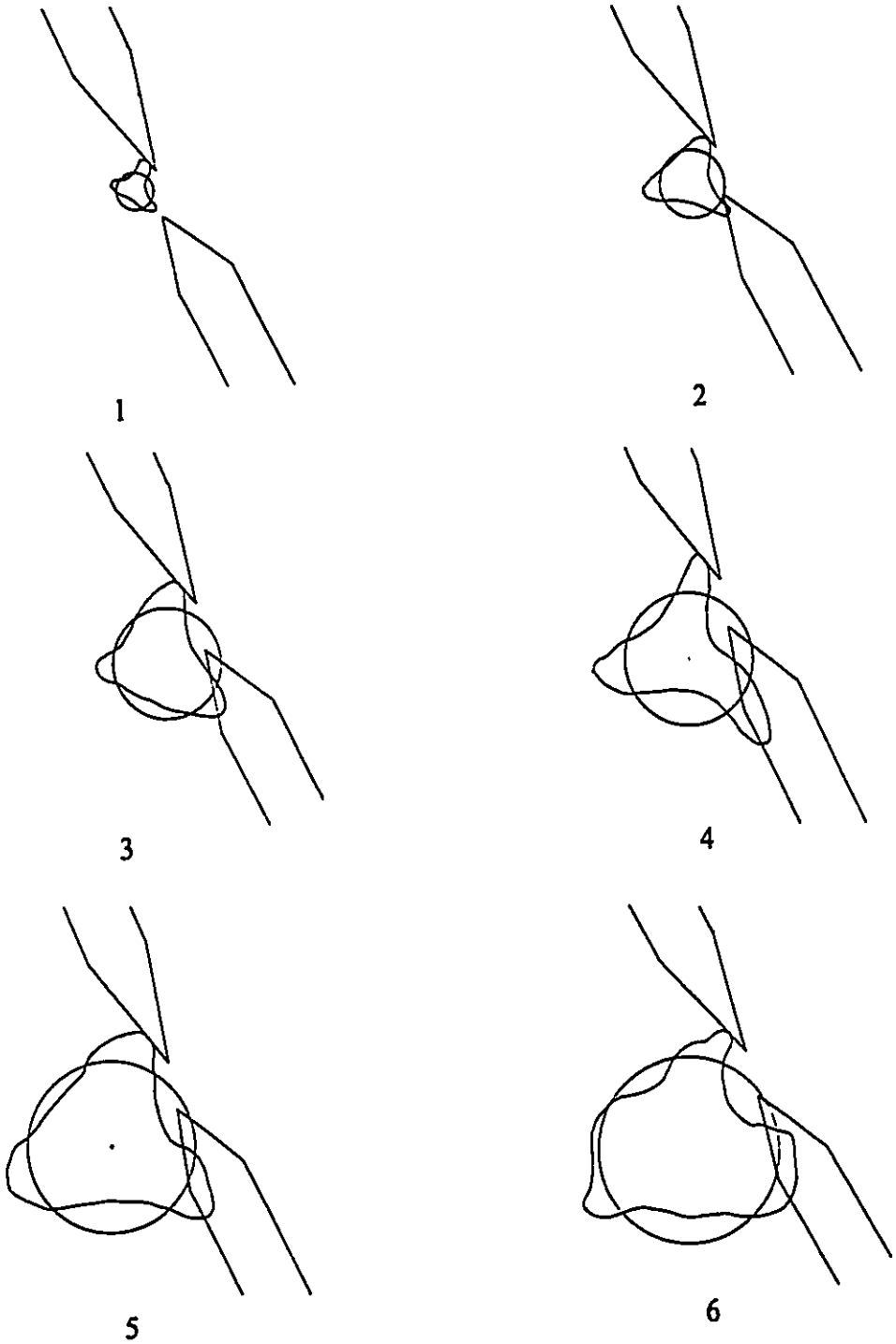

Figure A12: Applying the circular model for the early flame propagation of experiment 4.

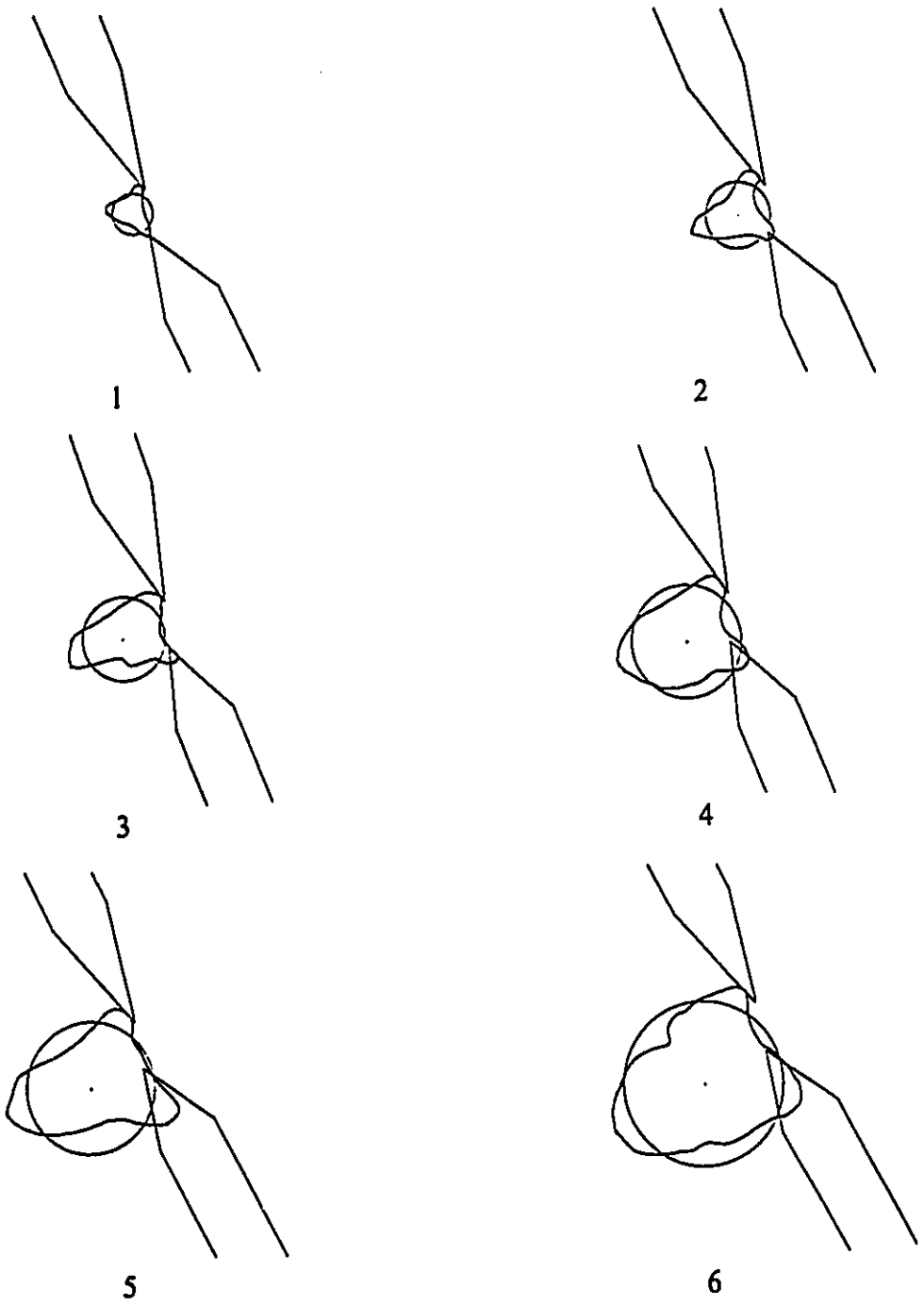

Figure A13: Applying the circular model for the early flame propagation of experiment 5.

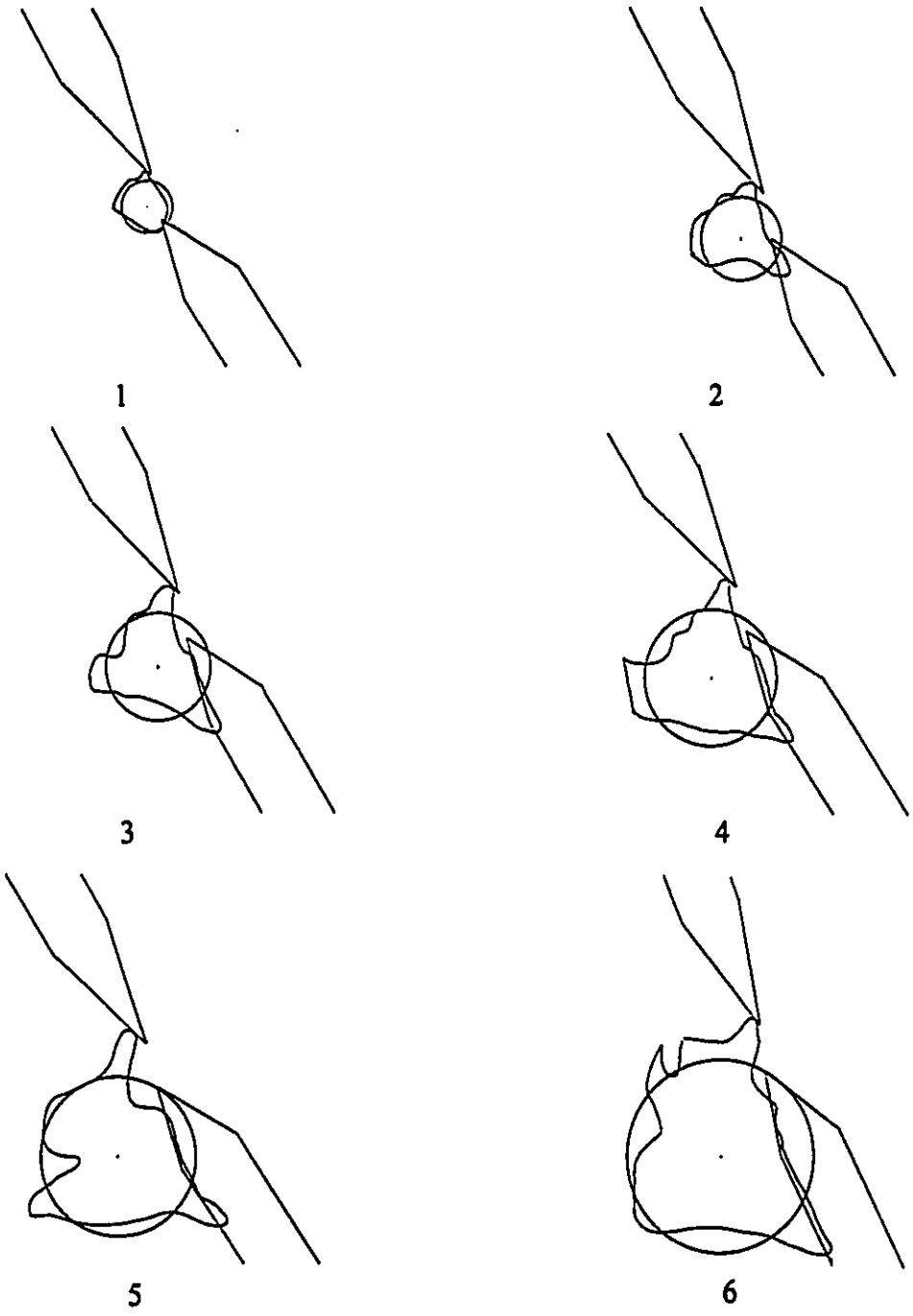

Figure A14: Applying the circular model for the early flame propagation of experiment 6.

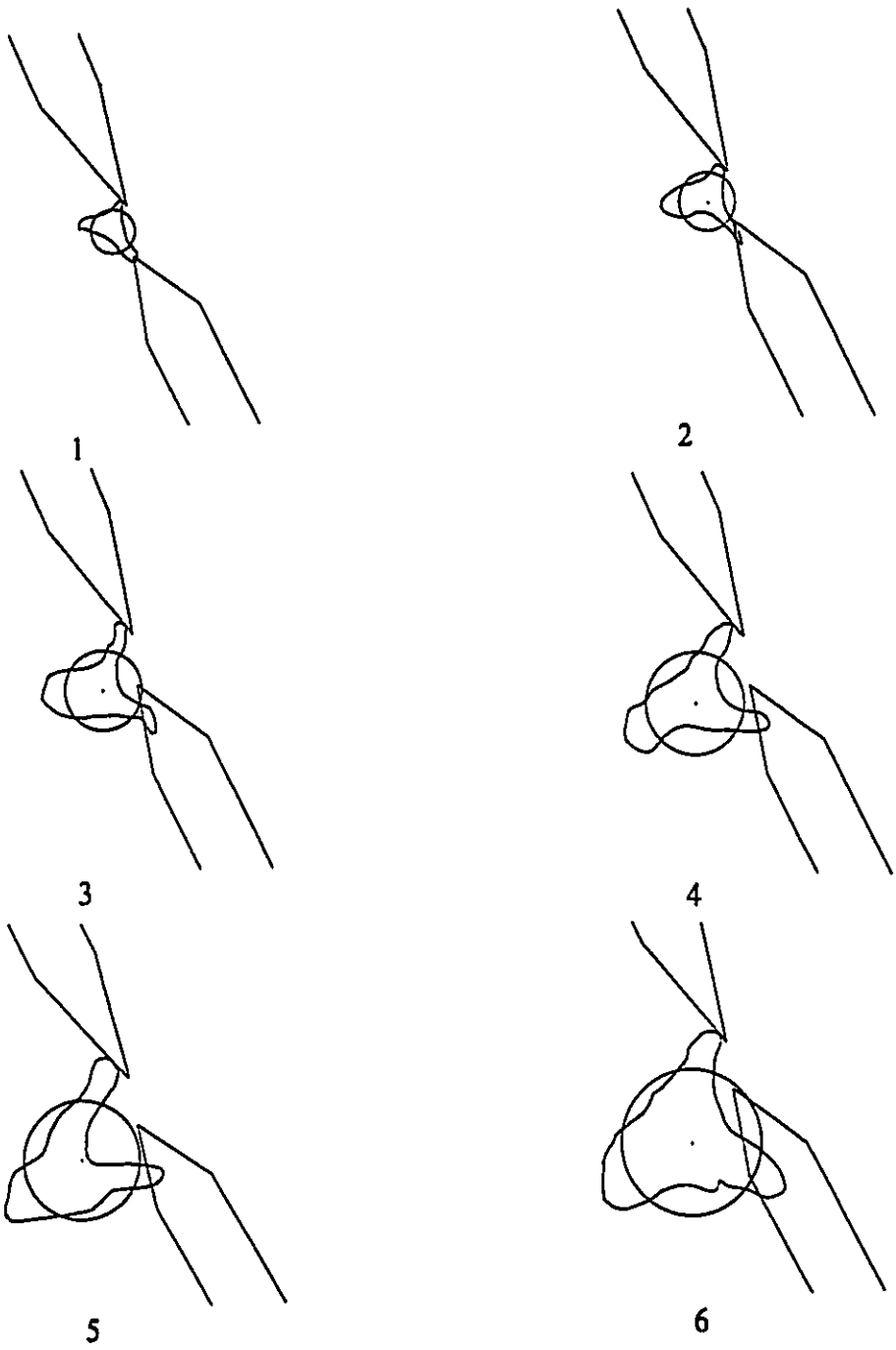

Figure A15: Applying the circular model for the early flame propagation of experiment 7.

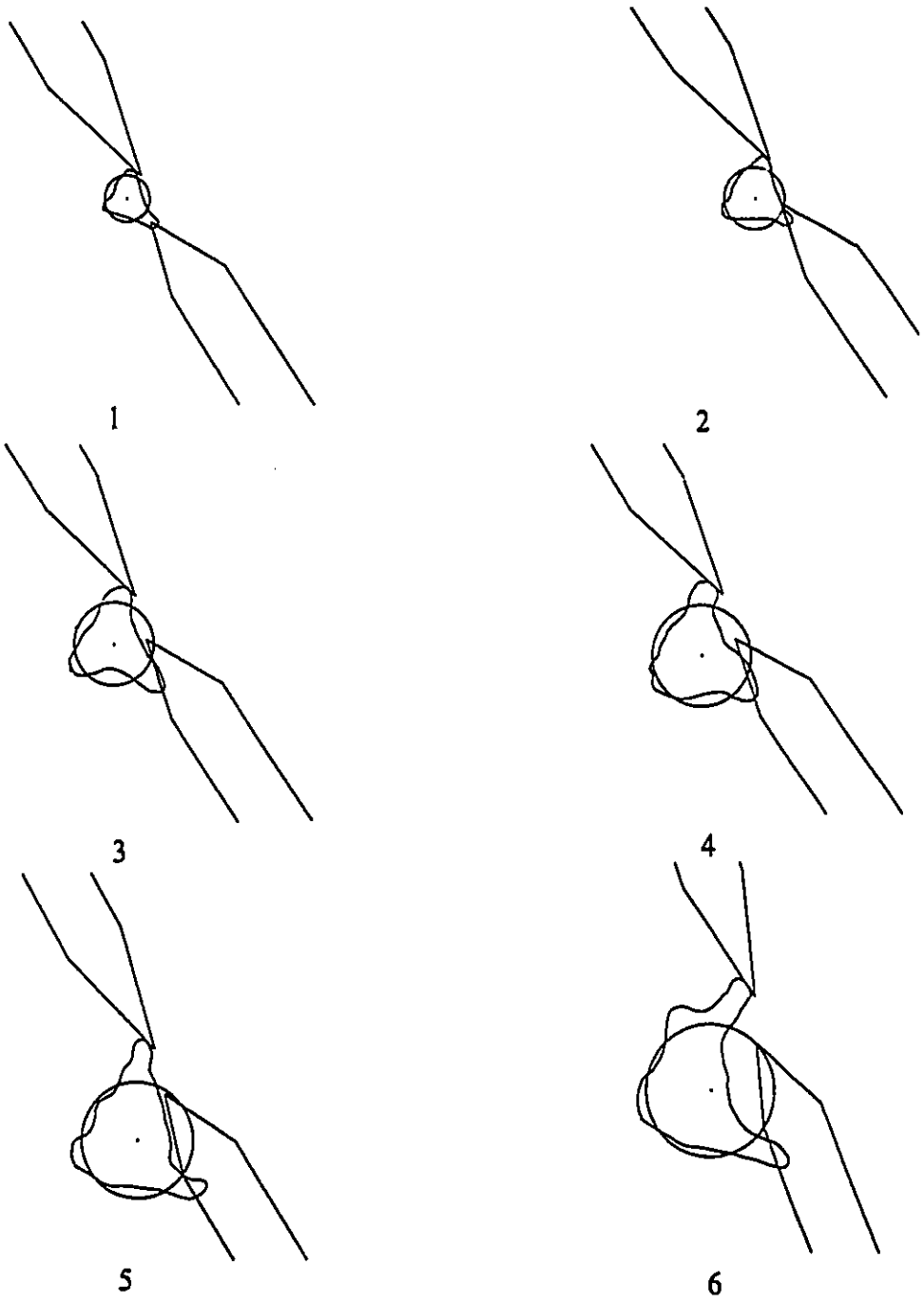

Figure A16: Applying the circular model for the early flame propagation of experiment 8.

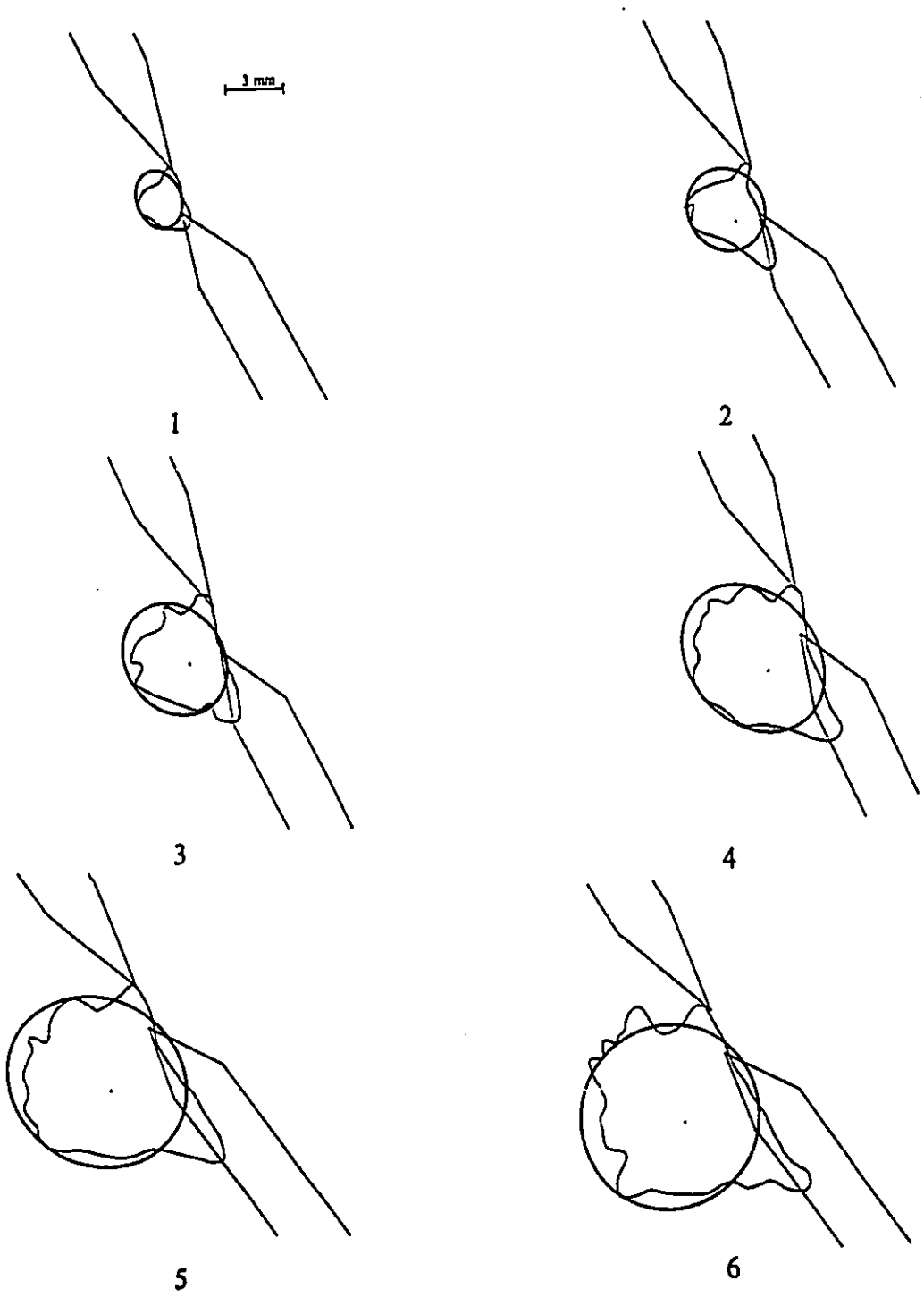

Figure A17: Applying the elliptical model for the early flame propagation of experiment 1. One axis is taken from the spark gap to the farthest point of the flame.

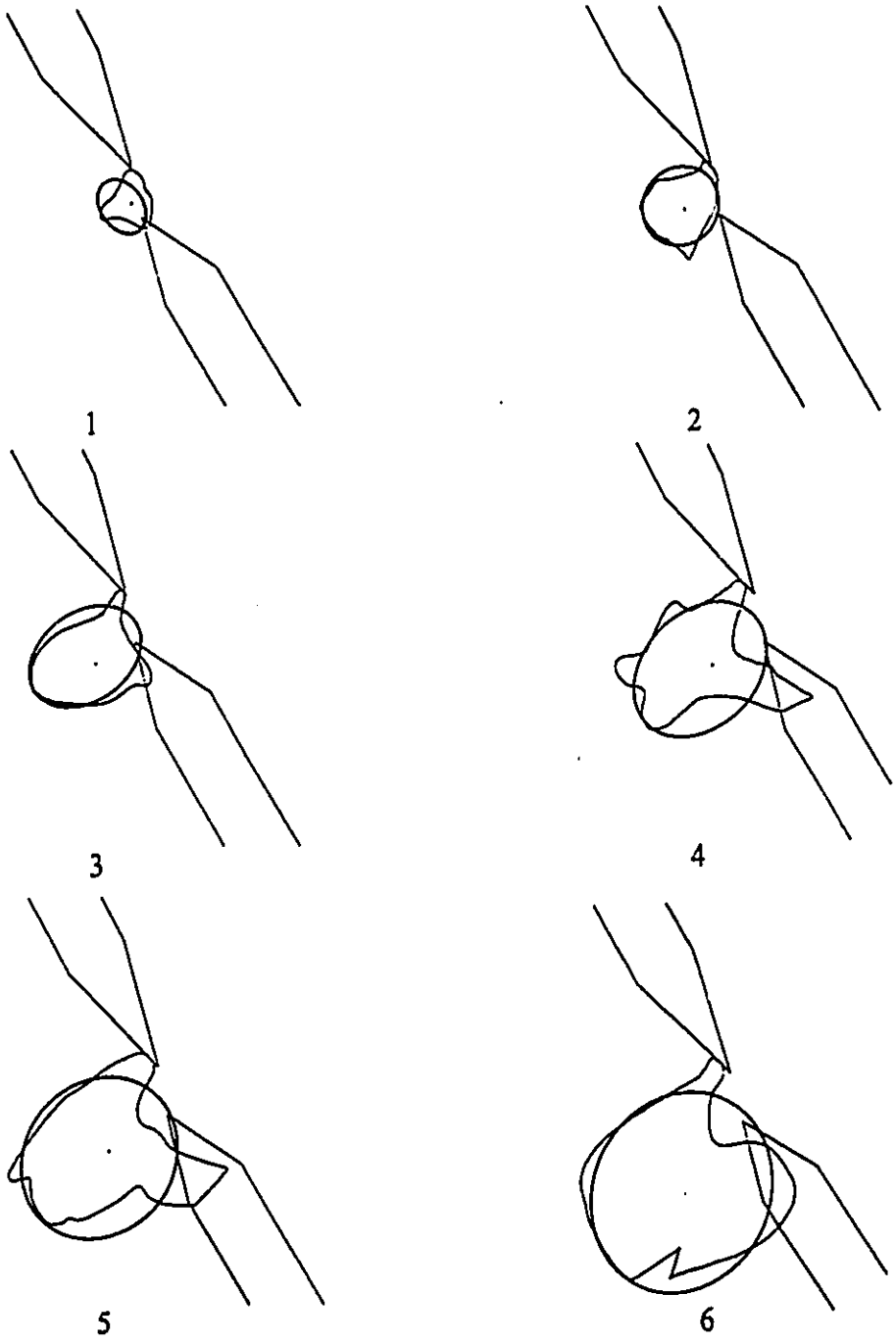

Figure A18: Applying the elliptical model for the early flame propagation of experiment 2. One axis is taken from the spark gap to the farthest point of the flame.

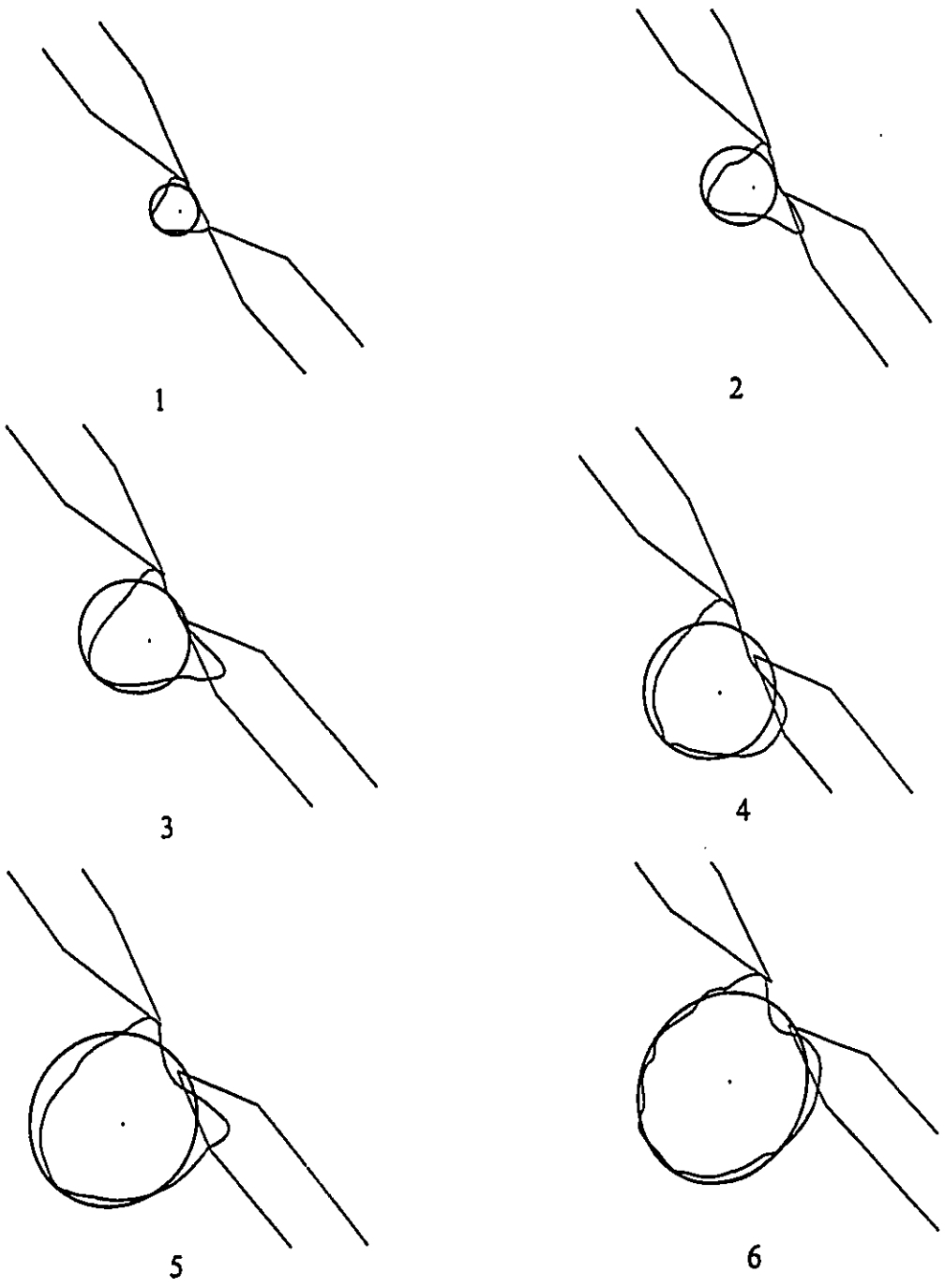

Figure A19: Applying the elliptical model for the early flame propagation of experiment 3. One axis is taken from the spark gap to the farthest point of the flame.

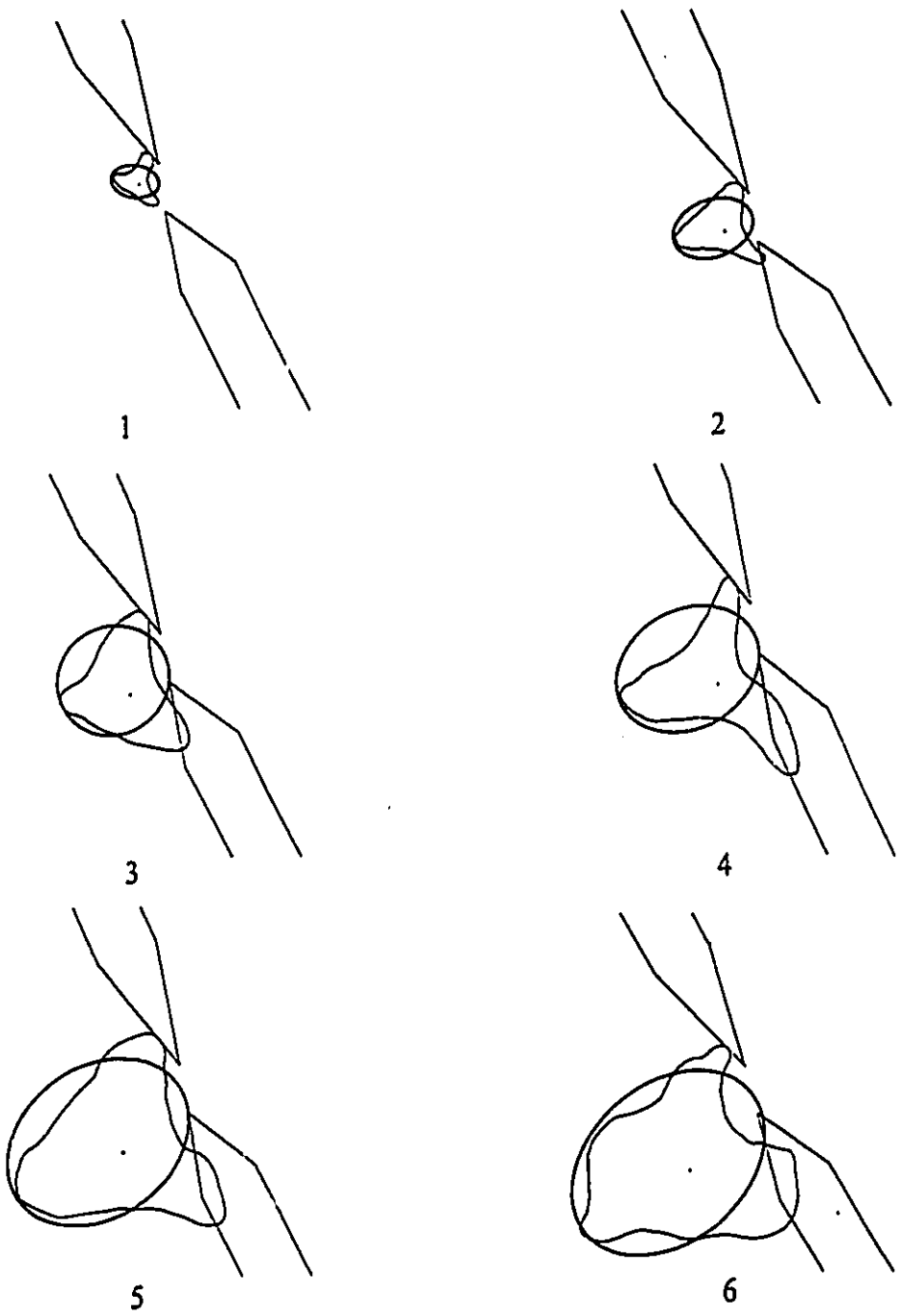

Figure A20: Applying the elliptical model for the early flame propagation of experiment 4. One axis is taken from the spark gap to the farthest point of the flame.

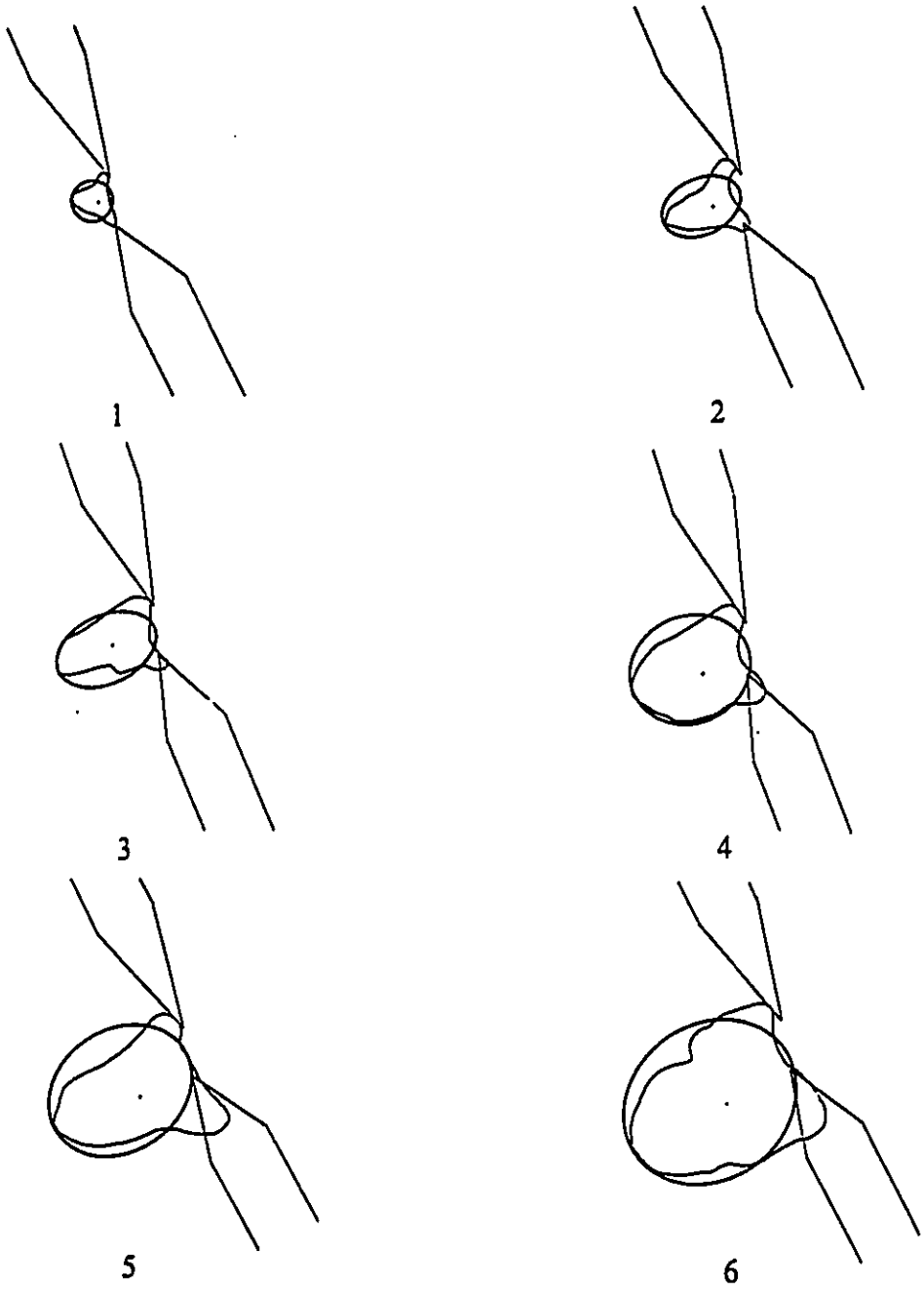

Figure A21: Applying the elliptical model for the early flame propagation of experiment 5. One axis is taken from the spark gap to the farthest point of the flame.

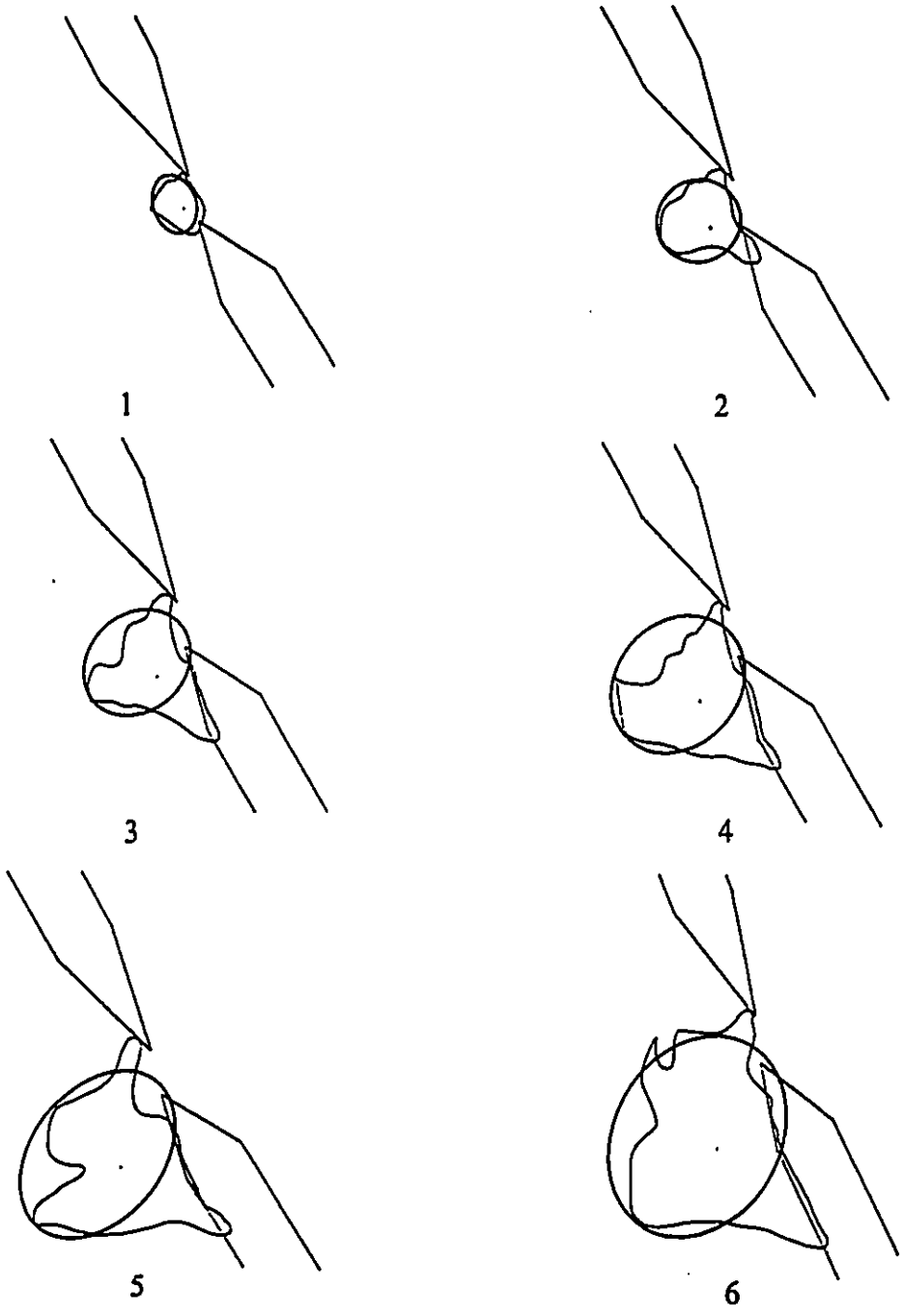

Figure A22: Applying the elliptical model for the early flame propagation of experiment 6. One axis is taken from the spark gap to the farthest point of the flame.

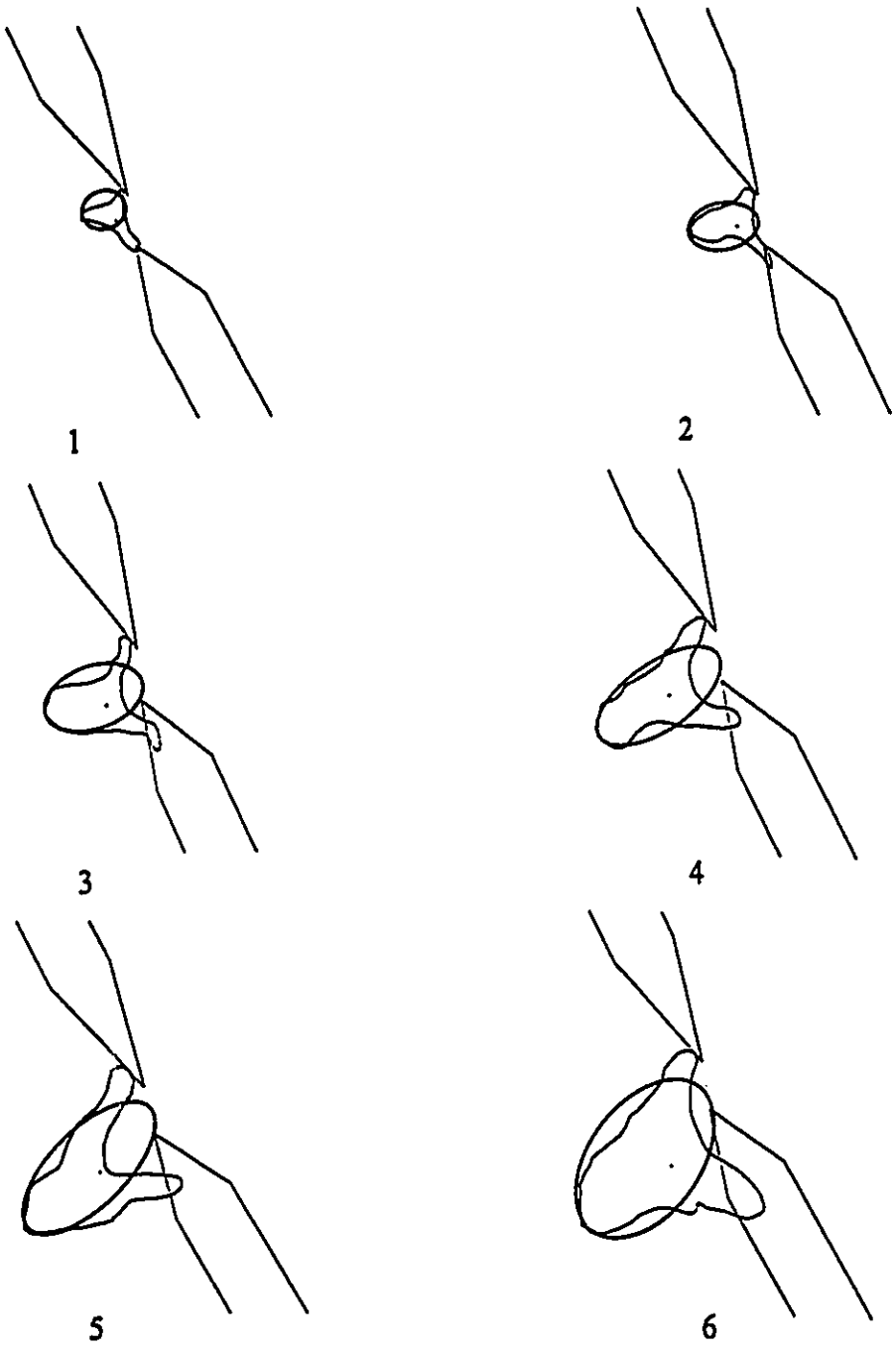

Figure A23: Applying the elliptical model for the early flame propagation of experiment 7. One axis is taken from the spark gap to the farthest point of the flame.

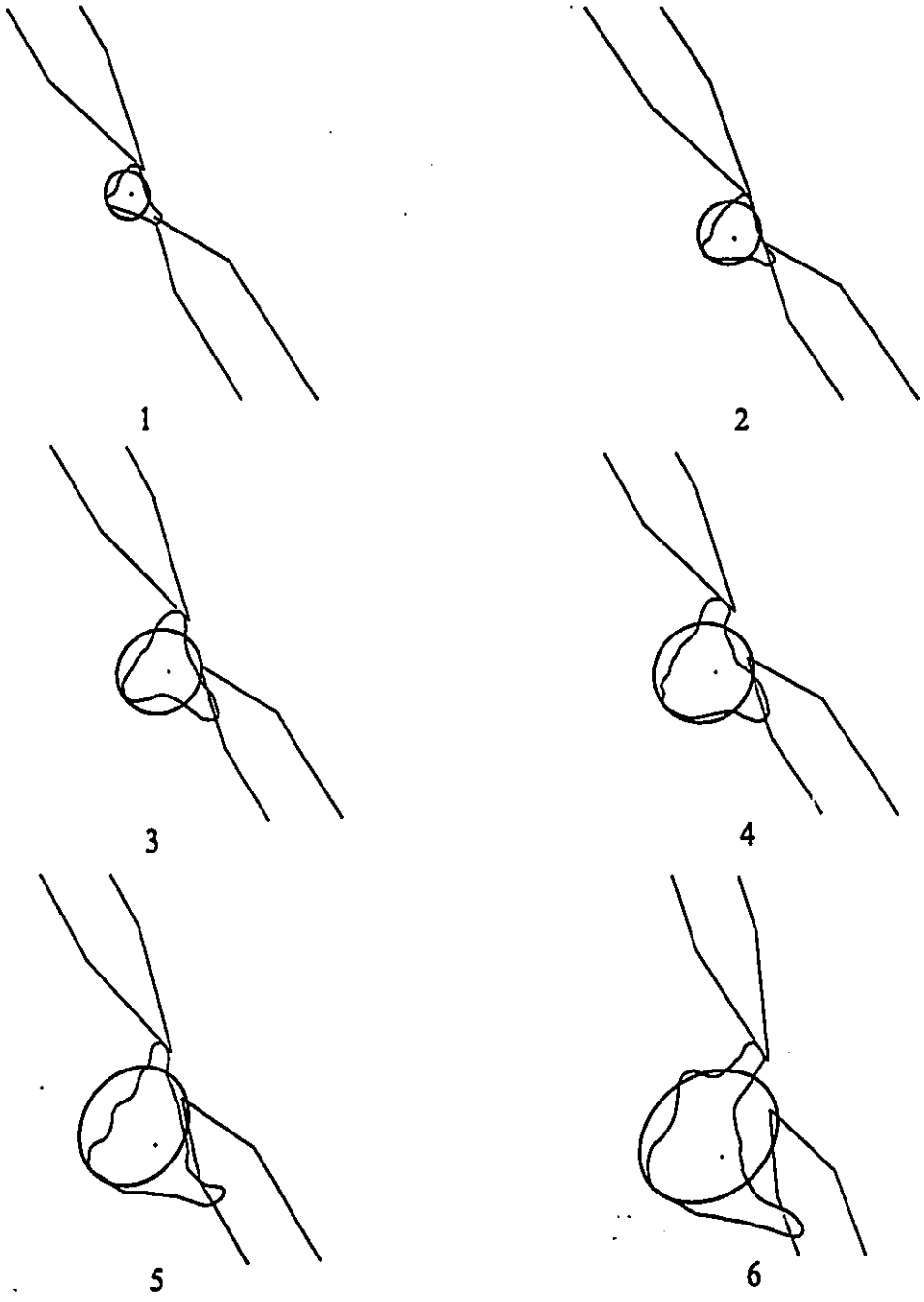

Figure A24: Applying the elliptical model for the early flame propagation of experiment 8. One axis is taken from the spark gap to the farthest point of the flame.

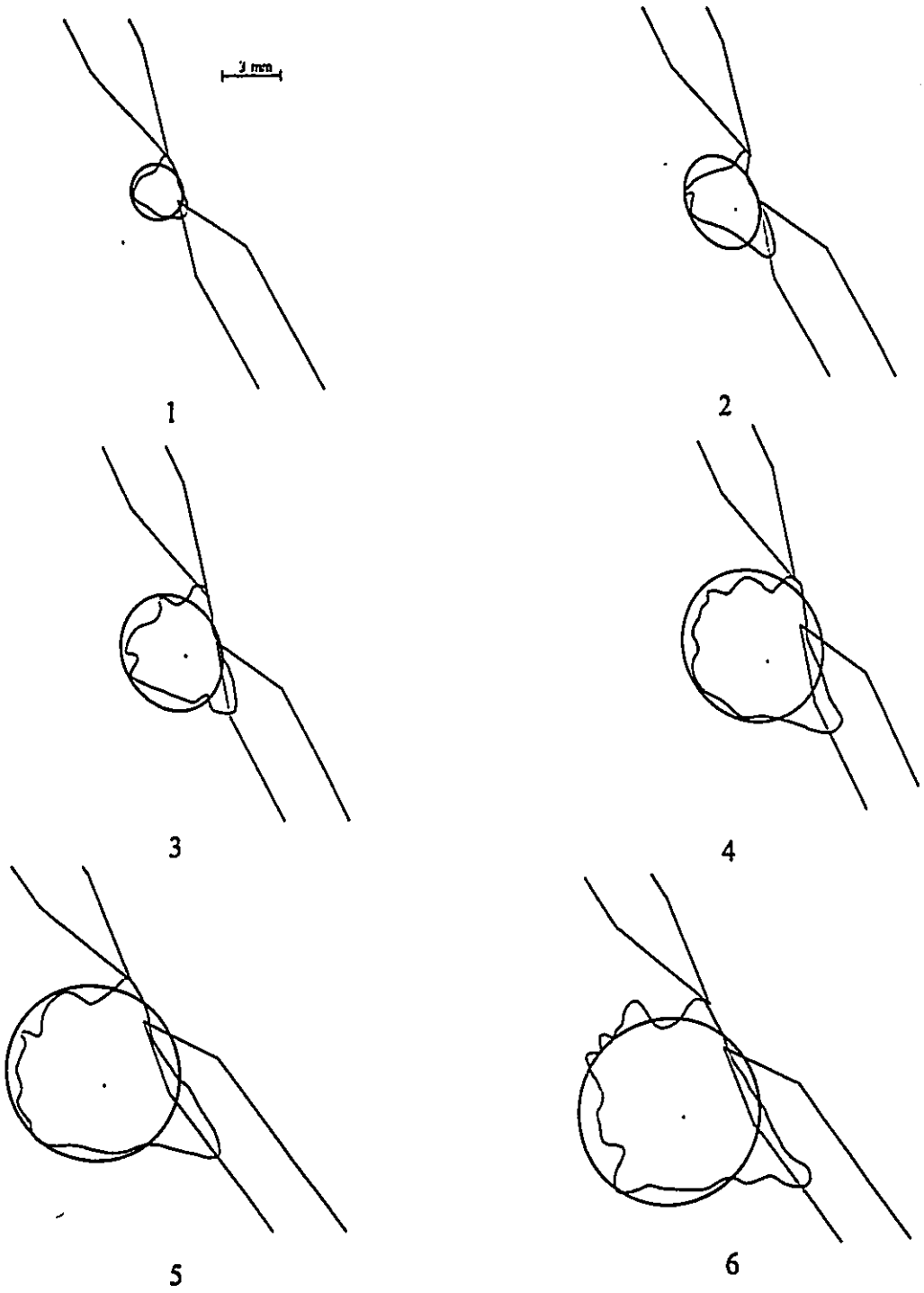

Figure A25: Applying the elliptical model for the early flame propagation of experiment 1. one axis is taken from the flame edge near the spark gap to the farthest point of the flame.

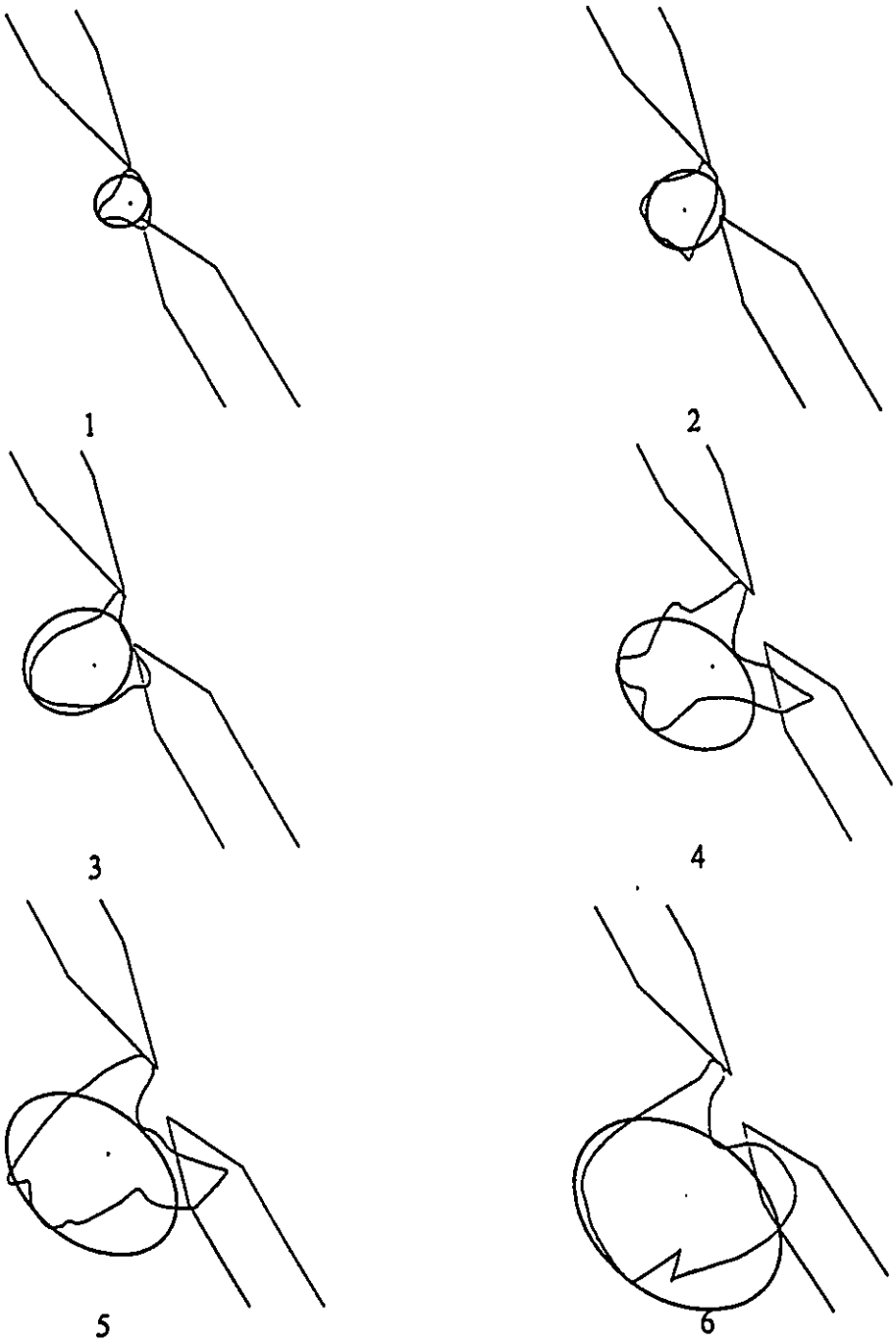

Figure A26: Applying the elliptical model for the early flame propagation of experiment 2. one axis is taken from the flame edge near the spark gap to the farthest point of the flame.

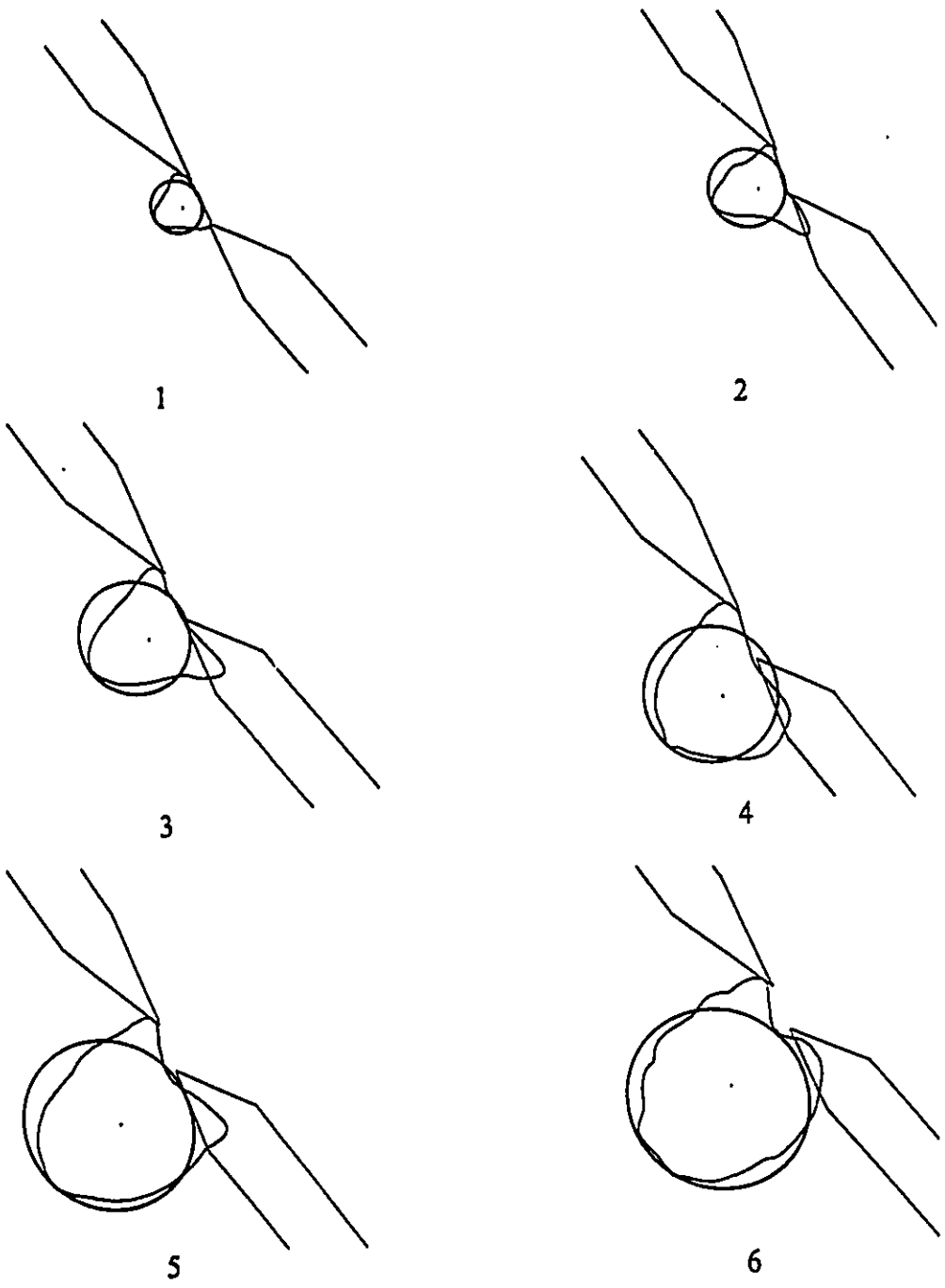

Figure A27: Applying the elliptical model for the early flame propagation of experiment 3. one axis is taken from the flame edge near the spark gap to the farthest point of the flame.

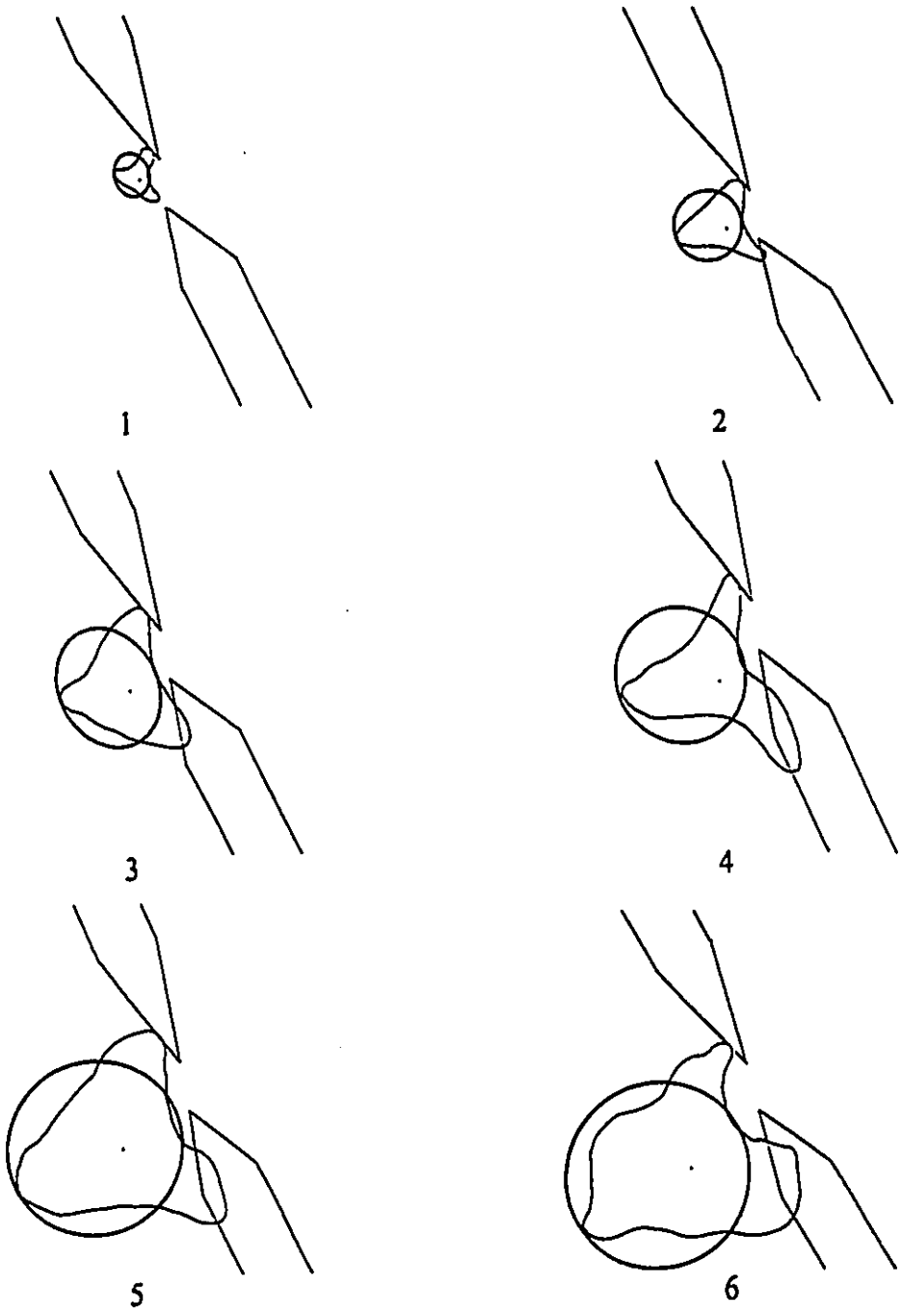

Figure A28: Applying the elliptical model for the early flame propagation of experiment 4. one axis is taken from the flame edge near the spark gap to the farthest point of the flame.

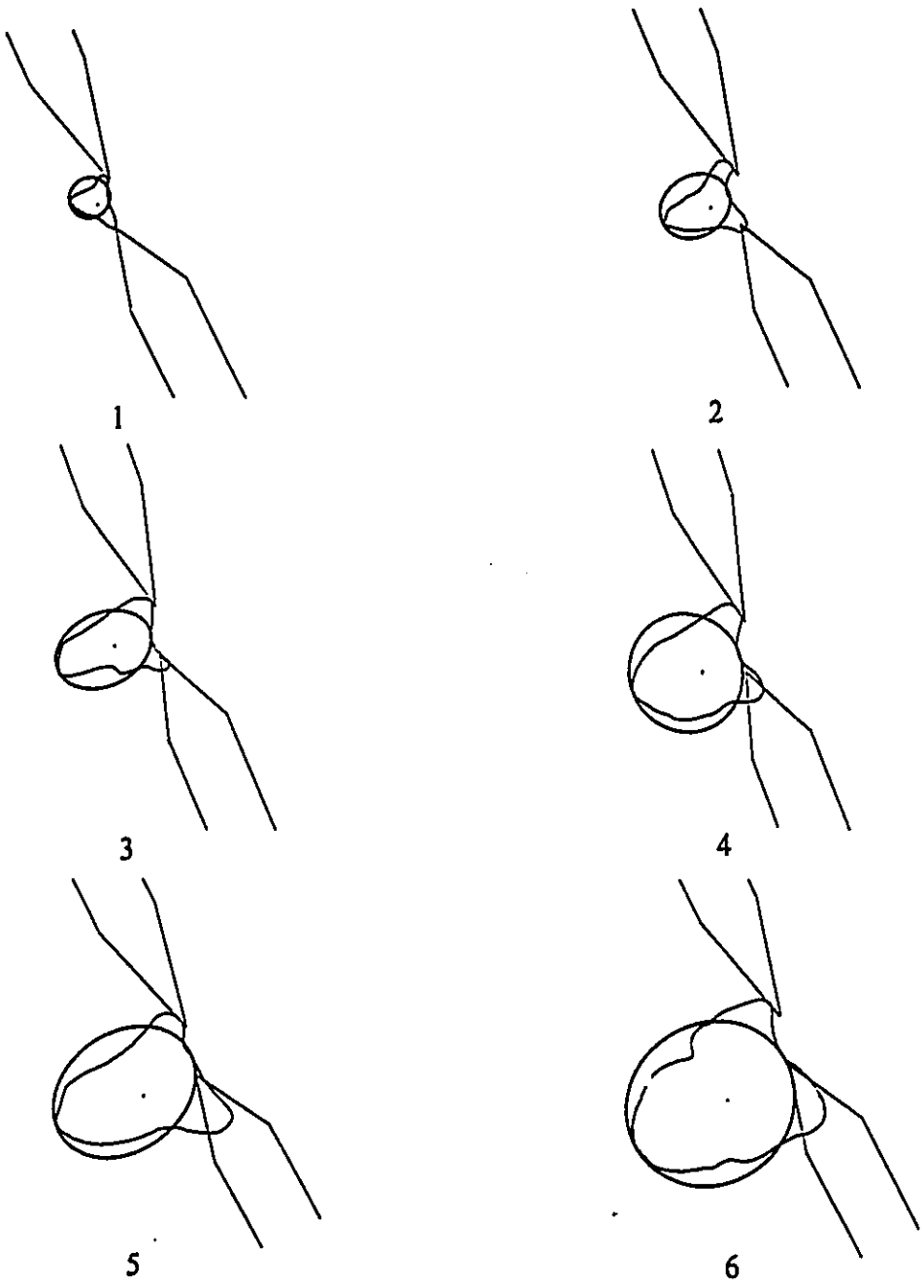

Figure A29: Applying the elliptical model for the early flame propagation of experiment 5. one axis is taken from the flame edge near the spark gap to the farthest point of the flame.

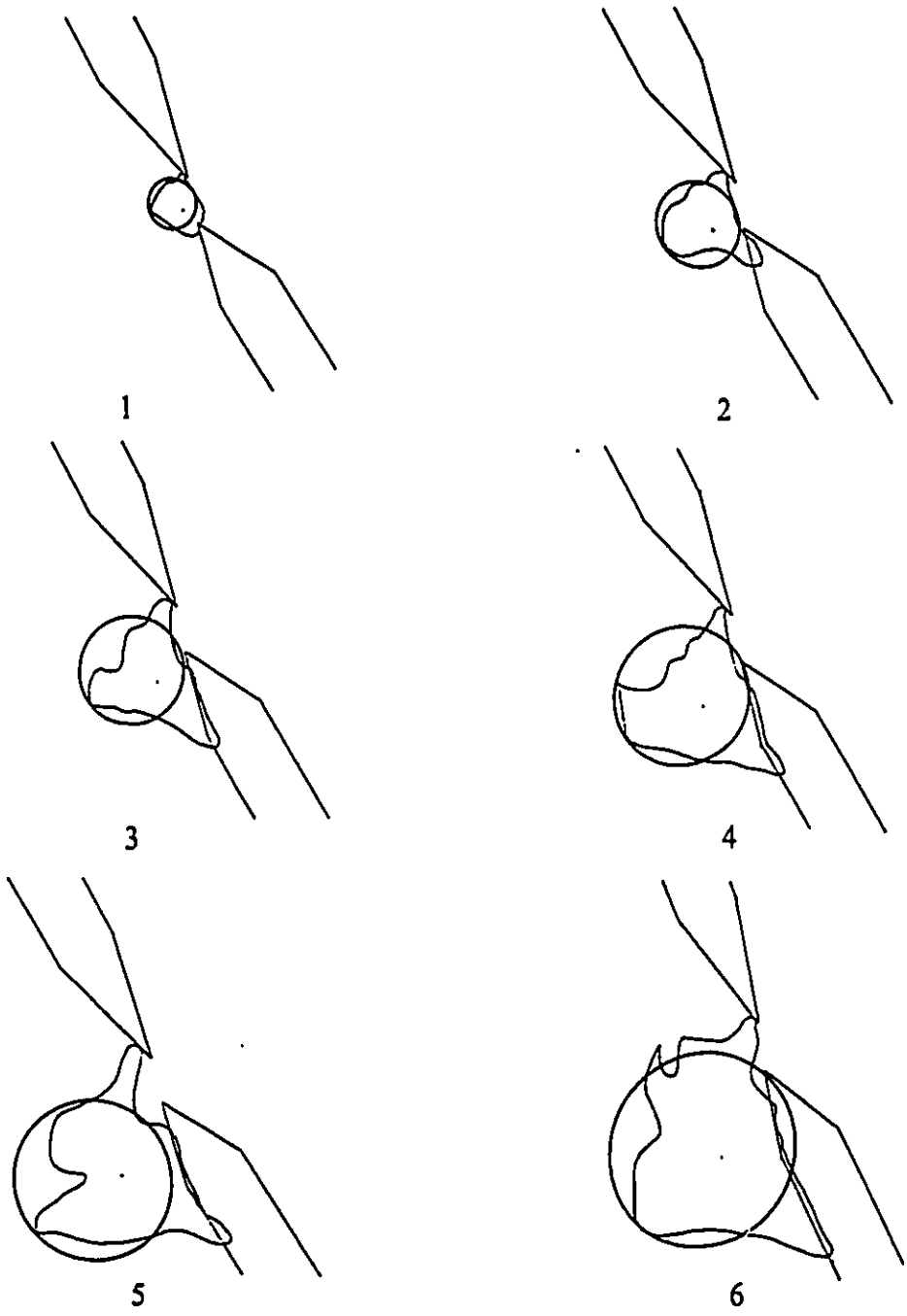

Figure A30: Applying the elliptical model for the early flame propagation of experiment 6. one axis is taken from the flame edge near the spark gap to the farthest point of the flame.

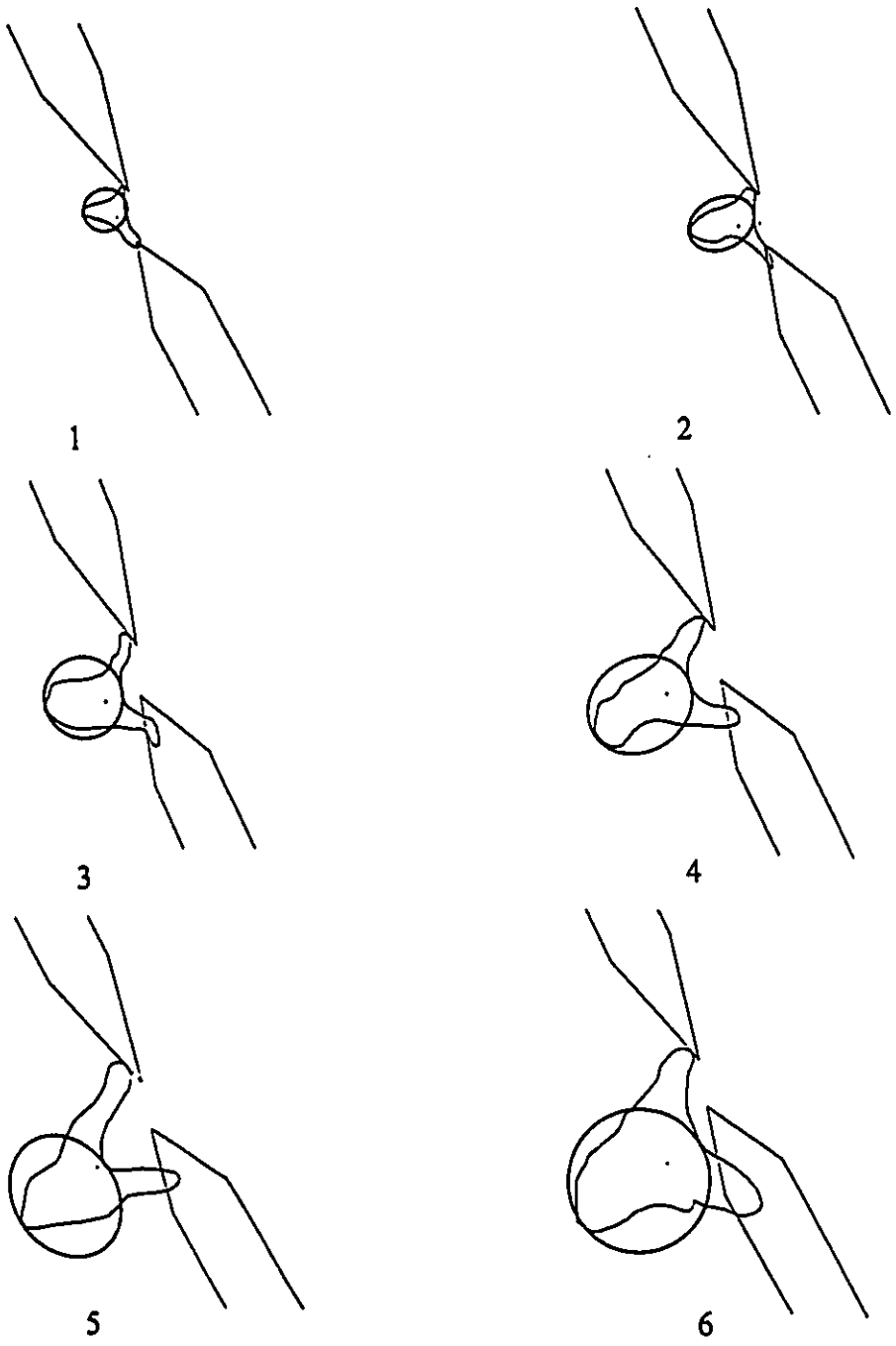

Figure A31: Applying the elliptical model for the early flame propagation of experiment 7. one axis is taken from the flame edge near the spark gap to the farthest point of the flame.

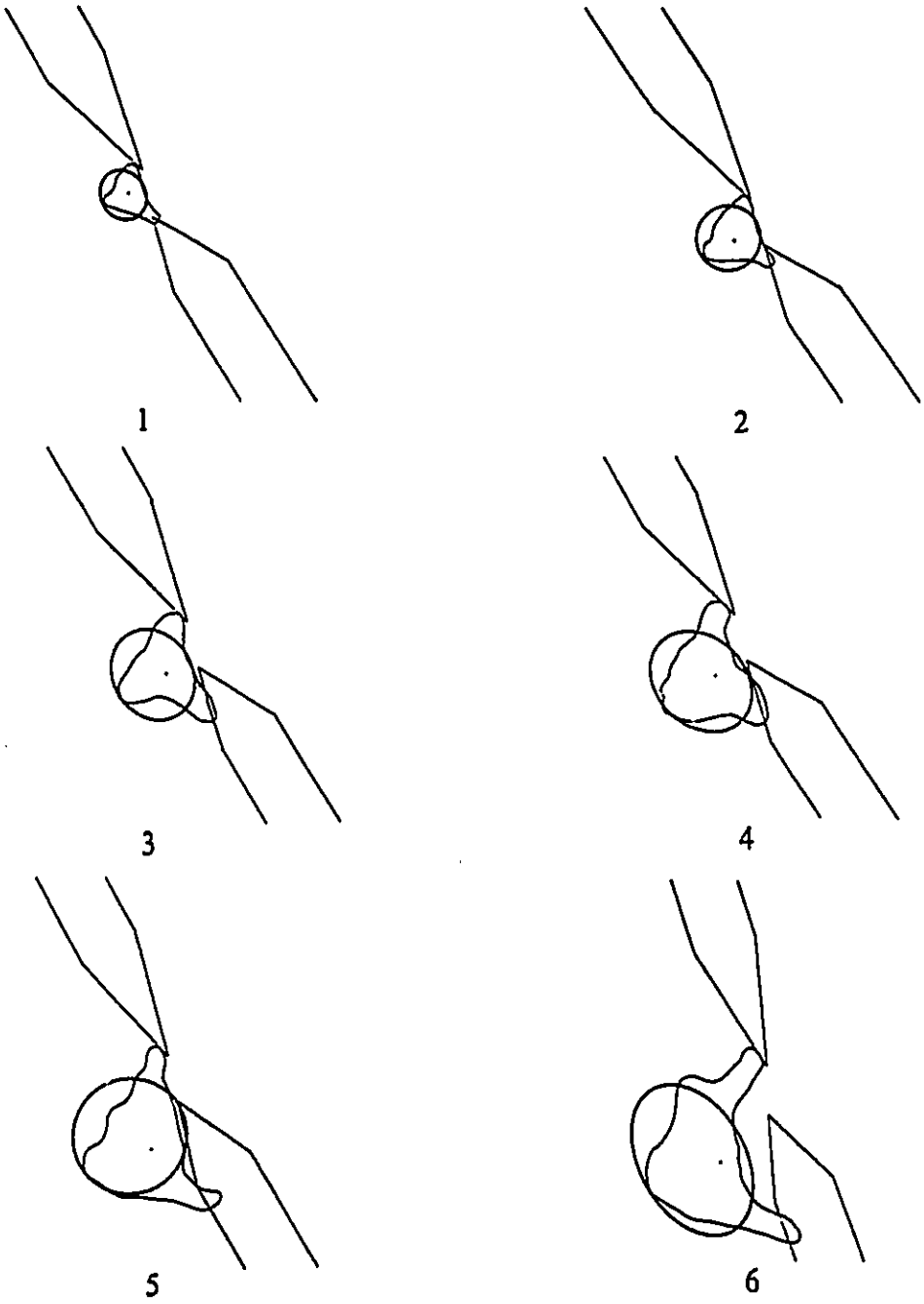

Figure A32: Applying the elliptical model for the early flame propagation of experiment 8. one axis is taken from the flame edge near the spark gap to the farthest point of the flame.

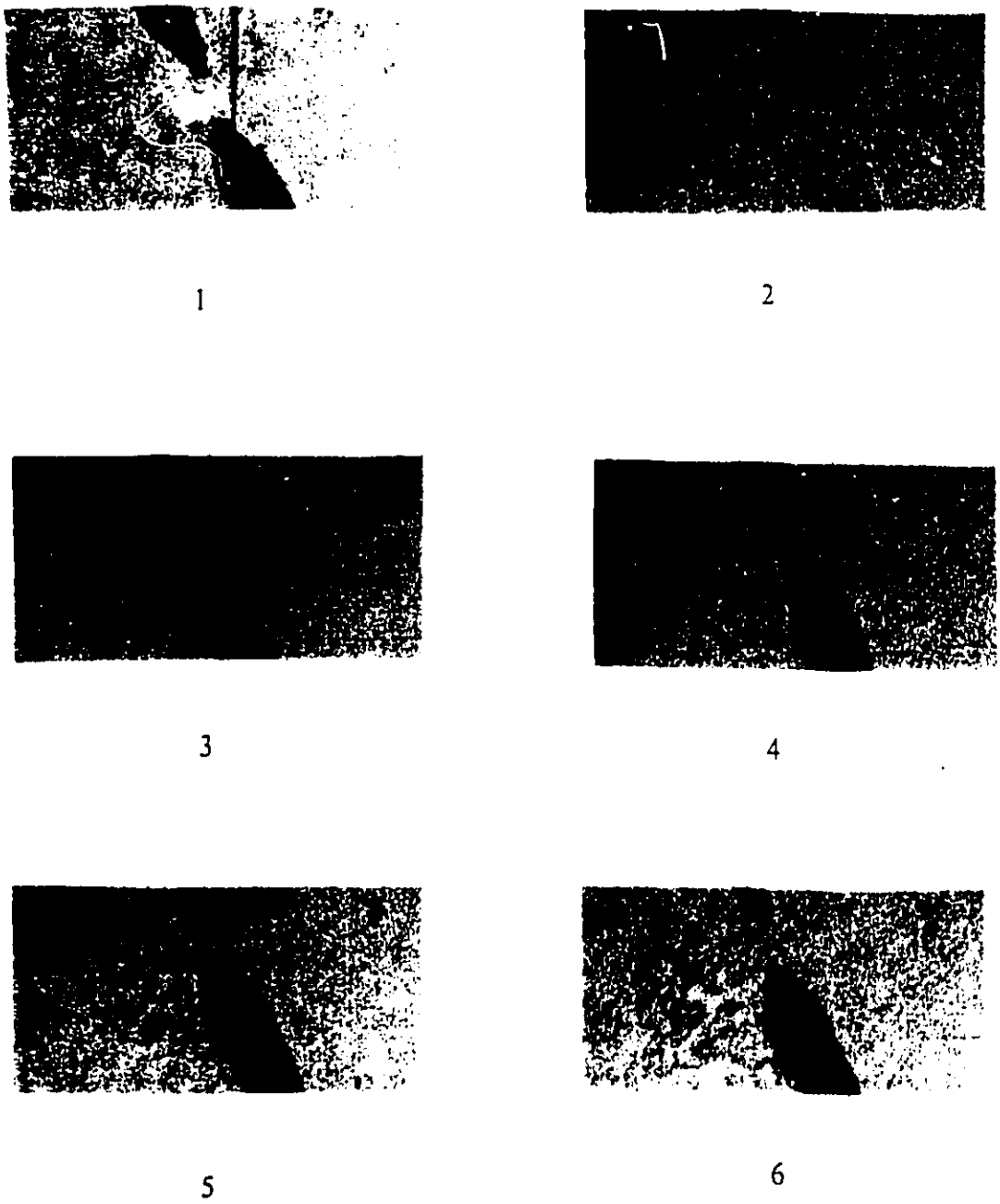

Figure A33: Photographs of early flame propagation of experiment 1 with time interval of 0.25 ms between frames (enlarged by 2.3 times).

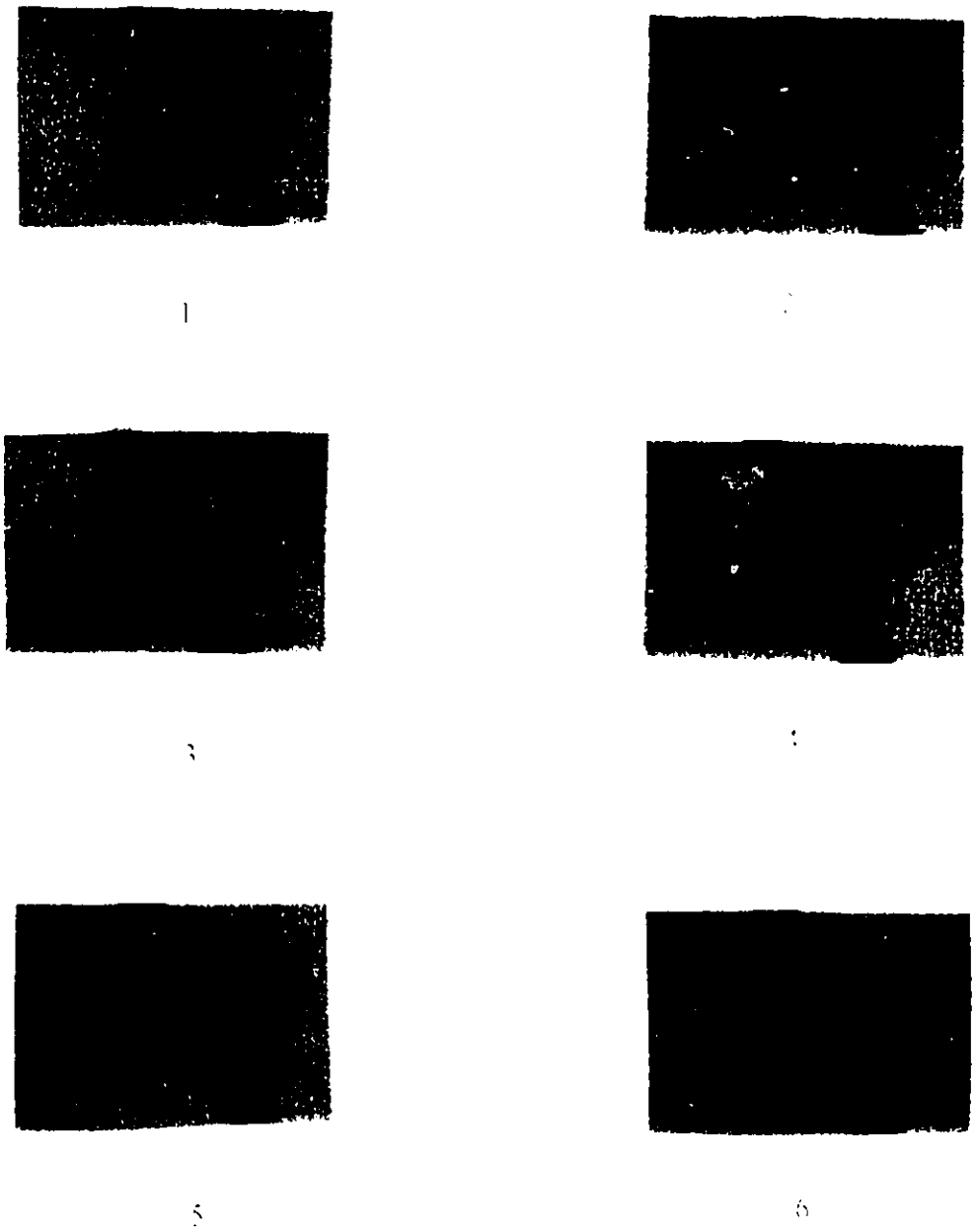

Figure A34: Photographs of early flame propagation of experiment 2 with time interval of 0.25 ms between frames (enlarged by 2.3 times)

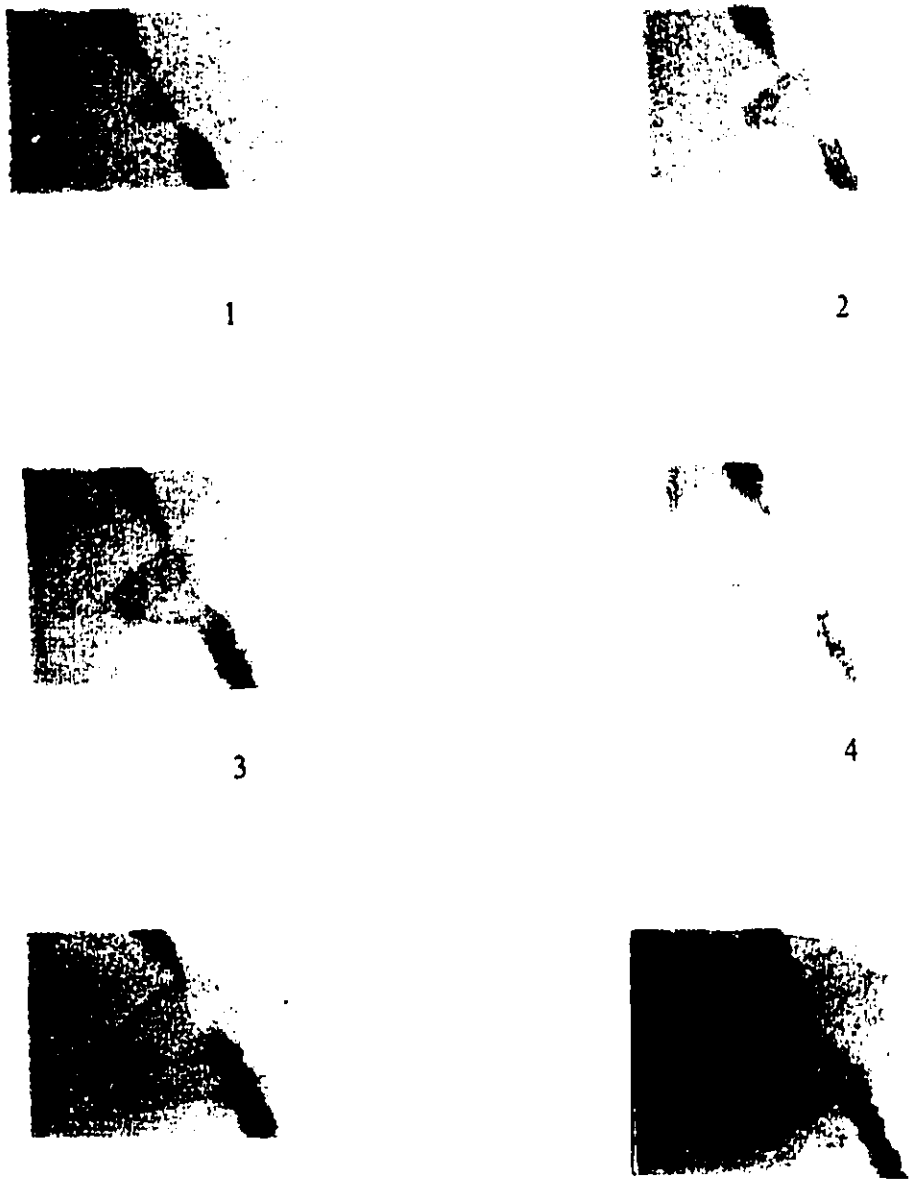

Figure A35: Photographs of early flame propagation of experiment 3 with time interval of 0.25 ms between frames (enlarged by 1.5 times).

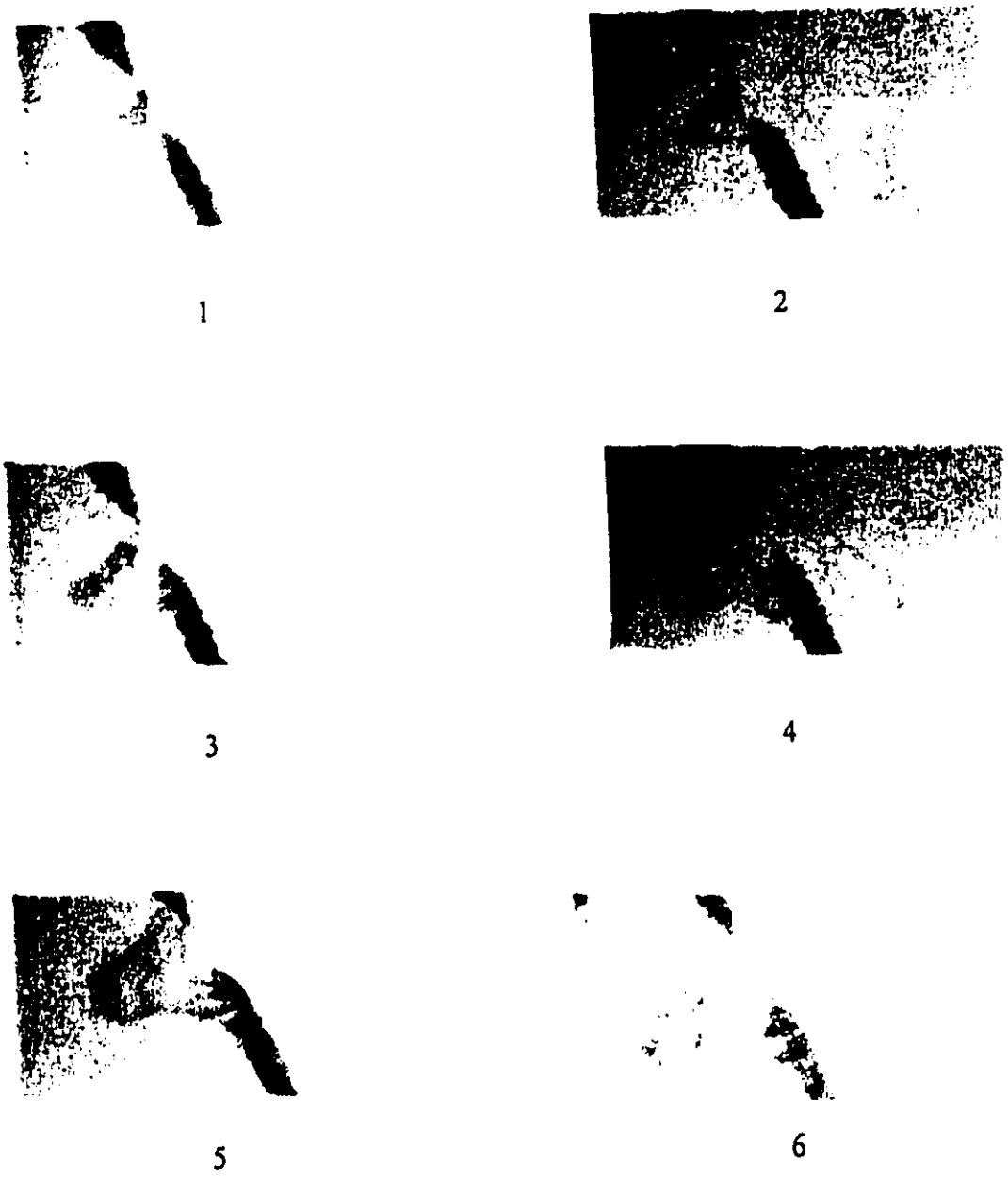

Figure A36: Photographs of early flame propagation of experiment 4 with time interval of 0.25 ms between frames (enlarged by 1.5 times).

Figure A37: Photographs of early flame propagation of experiment 5 with time interval of 0.25 ms between frames (enlarged by 1.5 times).

1

2

3

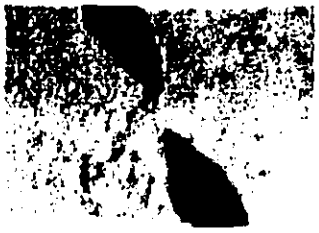

4

5

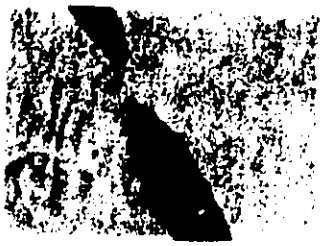

6

Figure A38: Photographs of early flame propagation of experiment 6 with time interval of 0.25 ms between frames (enlarged by 2.3 times)

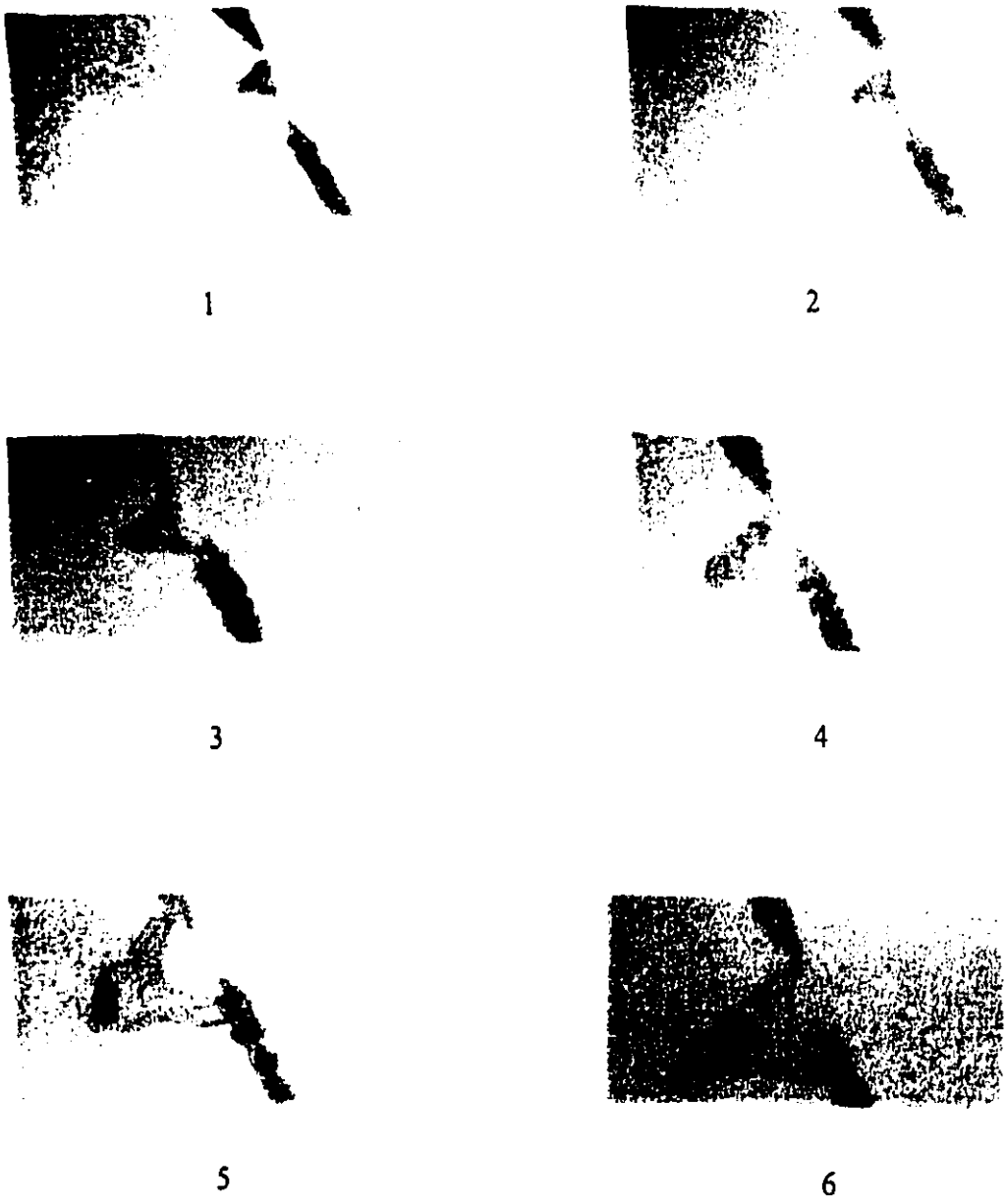

Figure A39: Photographs of early flame propagation of experiment 7 with time interval of 0.25 ms between frames (enlarged by 1.5 times).

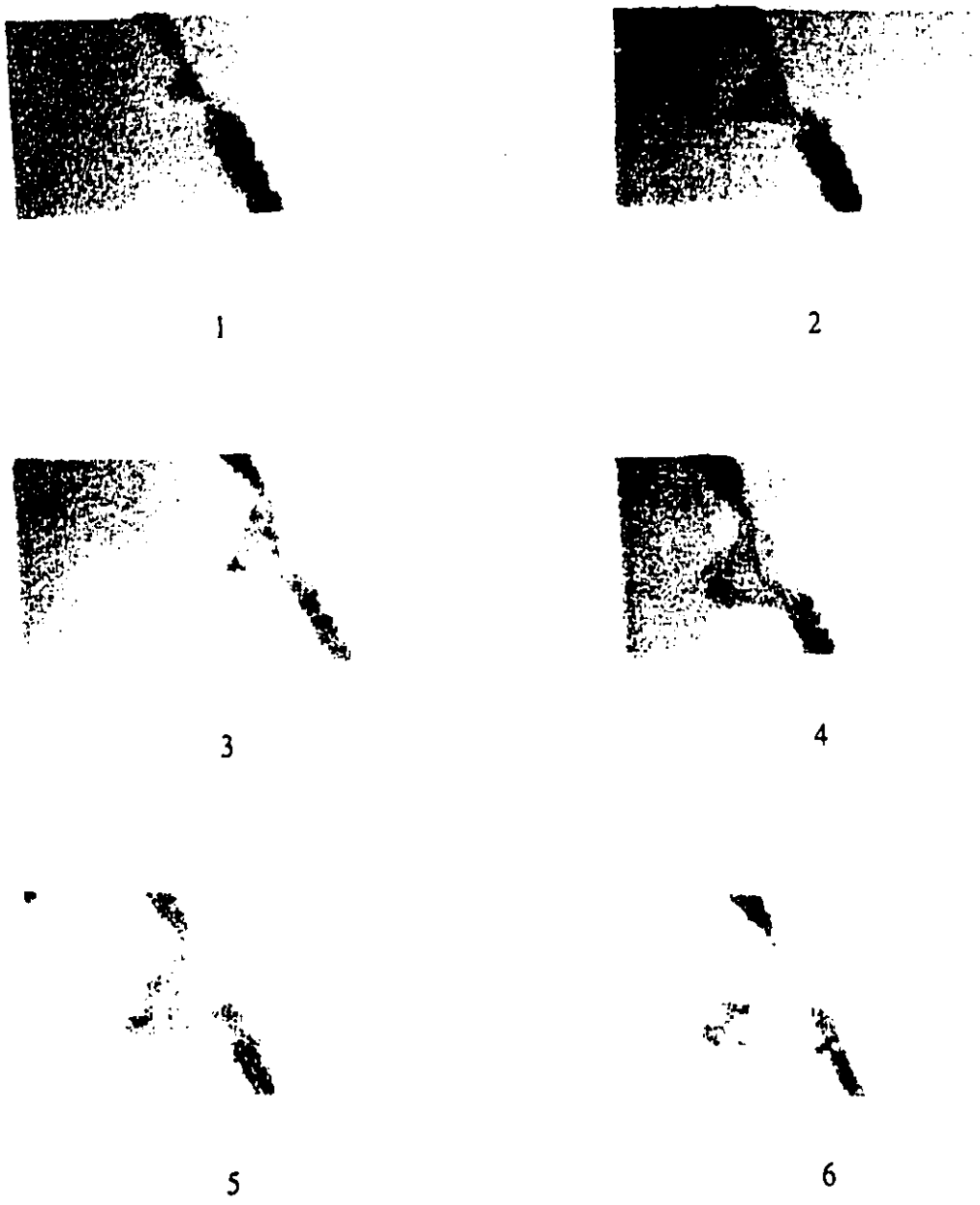

Figure A40: Photographs of early flame propagation of experiment 8 with time interval of 0.25 ms between frames (enlarged by 1.5 times).

APPENDIX : B

Measured and Calculated Data

The measured and calculated data are given in this appendix. The negative and positive signs before each symbol indicate the using of the minimum and maximum value of flame area which is used in calculating that parameter at each time step. The number after each symbol shows the experiment number. The symbols on the parenthesis are defined as below:

(2D).....The parameter is calculated using the two-dimensional model.

(S).....The parameter is calculated using the Spherical model.

(E).....The parameter is calculated using the ellipsoidal model.

(C).....The parameter is calculated using central difference method.

(F).....The parameter is calculated using forward difference method.

(L).....The linearized value of the parameter.

(gf).....The parameter is calculated using the assumption that the major axis of the ellipse is taken from the spark gap to the farthest point of the ellipse.

(ff).....The parameter is calculated using the assumption that the major axis of the ellipse is taken from the flame edge near the spark gap to the farthest point of the ellipse.

(CE)..... .The parameter is calculated using the ellipse center coordinates.

The symbols are defined as below:

A.....Flame area.

a.....Major axis of the ellipse.

b.....Minor axis of the ellipse.

Displace.....Displacement of the flame centroid.

FvolB.....Volume fraction of burned gas.

p.....Perimeter of the ellipse.

R.....Equivalent flame radius.

S_k .....Flame speed using the Keck's analysis.

S_w .....Flame speed using the elliptical model.

S_{ws}.....Flame speed using the smoothed elliptical model.

S.G..... .....Specific rate of growth of flame area.

Teta.....The angle between the major axis of the ellipse and the lower electrode axis.

V_k .....Convection velocity using the Keck's analysis.

V_{rk}.....Radial velocity using the Keck's analysis .

V_w .....Convection velocity using the elliptical model.

V_{ws}.....Convection velocity using the smoothed elliptical model.

X , Y.....Flame centroid coordinates.

XEC , YEC.....Ellipse center coordinates.

time	-A1(2D)	+A1(2D)	-A1(S)	+A1(S)	-S.G.1(S)	+S.G.1(S)
250	5.3	5.38	21.2	21.52		
500	12.56	12.6	50.24	50.4	2936.306	2955.556
750	23.74	24	94.96	96	2219.04	2275
1000	38.9	39.9	155.6	159.6	1600	1644.11
1250	54.86	56.8	219.44	227.2	909.9526	915.493
1500	63.86	65.9	255.44	263.6		
Average:					1916.324	1947.54

time	-A2(2D)	+A2(2D)	-A2(S)	+A2(S)	-S.G.2(S)	+S.G.2(S)
250	4.15	4.23	16.6	16.92		
500	9.05	10.1	36.2	40.4	2848.619	2786.139
750	17.04	18.3	68.16	73.2	2177.23	2153.005
1000	27.6	29.8	110.4	119.2	1713.768	1664.43
1250	40.69	43.1	162.76	172.4	1411.158	1433.875
1500	56.31	60.7	225.24	242.8		
Average:					2037.694	2009.362

time	-A3(2D)	+A3(2D)	-A3(S)	+A3(S)	-S.G.3(S)	+S.G.3(S)
250	4.59	4.64	18.36	18.56		
500	9.95	10.12	39.8	40.48	3342.714	3490.119
750	21.22	22.3	84.88	89.2	1924.599	1989.238
1000	30.37	32.3	121.48	129.2	1795.851	1791.331
1250	48.49	51.23	193.96	204.92	1108.682	1085.302
1500	57.25	60.1	229	240.4		
Average:					2042.962	2088.997

time	-A4(2D)	+A4(2D)	-A4(S)	+A4(S)	-S.G.4(S)	+S.G.4(S)
250	2.51	2.56	10.04	10.24		
500	7.91	8.1	31.64	32.4	4285.714	4429.63
750	19.46	20.5	77.84	82	1976.362	2156.098
1000	27.14	30.2	108.56	120.8	2016.949	1986.755
1250	46.83	50.5	187.32	202	1187.273	1124.752
1500	54.94	58.6	219.76	234.4		
Average:					2366.575	2424.309

time	-A5(2D)	+A5(2D)	-A5(S)	+A5(S)	-S.G.5(S)	+S.G.5(S)
250	2.7	2.75	10.8	11		
500	7.03	7.6	28.12	30.4	2611.664	2513.158
750	11.88	12.3	47.52	49.2	2254.209	2325.203
1000	20.42	21.9	81.68	87.6	1490.695	1564.384
1250	27.1	29.43	108.4	117.72	1666.421	1624.193
1500	43	45.8	172	183.2		
Average:					2005.747	2006.734

time	-A6(2D)	+A6(2D)	-A6(S)	+A6(S)	-S.G.6(S)	+S.G.6(S)
250	4.39	4.46	17.56	17.84		
500	10.17	11.11	40.68	44.44	2843.658	2707.471
750	18.85	19.5	75.4	78	2122.016	2146.667
1000	30.17	32.04	120.68	128.16	1447.796	1441.948
1250	40.69	42.6	162.76	170.4	1331.04	1327.23
1500	57.25	60.31	229	241.24		
Average:					1936.127	1905.829

time	-A7(2D)	+A7(2D)	-A7(S)	+A7(S)	-S.G.7(S)	+S.G.7(S)
250	2.21	2.32	8.84	9.28		
500	5.31	5.4	21.24	21.6	2542.373	2518.519
750	8.96	9.12	35.84	36.48	2205.357	2302.632
1000	15.19	15.9	60.76	63.6	1487.821	1552.201
1250	20.26	21.46	81.04	85.84	1478.776	1491.146
1500	30.17	31.9	120.68	127.6		

time	-A8(2D)	+A8(2D)	-A8(S)	+A8(S)	-S.G.8(S)	+S.G.8(S)
250	3.41	3.47	13.64	13.88		
500	6.24	6.5	24.96	26	2314.103	2384.615
750	10.63	11.22	42.52	44.88	1815.616	1836.007
1000	15.89	16.8	63.56	67.2	1312.775	1332.143
1250	21.06	22.41	84.24	89.64	1174.739	1186.97
1500	28.26	30.1	113.04	120.4		
Average:					1654.308	1684.934

time	X1	Y1	Vk1(C)	Vrk1(C)		Displace
250	1.11	29.89				0.578138
500	1.598	29.58	2.337349	0.497105		0.603593
750	2.18	29.42	3.333182	2.634525		1.163765
1000	2.823	28.45	4.424644	1.236435		1.15317
1250	3.893	28.02	3.040795	1.017993		0.36855
1500	4.22	27.85			gap-F.C1	0.833333
Average:			3.283993	1.346515	Sum:	4.700549

time	X2	Y2	Vk2(C)	Vrk2(C)		Displace
250	0.6	30.06				1.23657
500	1.792	30.389	4.40525	2.427484		1.216601
750	2.766	29.66	2.529083	2.452258		0.137899
1000	2.72	29.53	2.078924	0.217082		1.050202
1250	3.75	29.325	3.891377	3.006969		1.06848
1500	4.318	28.42			gap-F.C1	0.5
Average:			3.226158	2.025949	Sum:	5.209751

time	X3	Y3	Vk3(C)	Vrk3(C)		Displace
250	1.5	30.56				0.466152
500	1.927	30.373	2.319483	1.913604		0.748424
750	2.31	29.73	3.74468	1.759653		1.173456
1000	3.3	29.1	4.922642	4.669419		1.492548
1250	3.61	27.64	3.764306	-3.28889		2.502039
1500	5.1	29.65			gap-F.C1	0.833333
Average:			3.687778	1.263447	Sum:	7.215953

time	X4	Y4	Vk4(C)	Vrk4(C)		Displace
250	1.155	30.775				0.55563
500	1.565	30.4	3.418801	1.866033		1.156125
750	2.5	29.72	4.046097	3.7481		0.974166
1000	2.79	28.79	2.751363	-1.46208		1.140395
1250	3.81	29.3	3.086487	1.582522		0.662193
1500	4.33	28.89			gap-F.C1	1
Average:			3.325687	1.433644	Sum:	5.48851

time	X5	Y5	Vk5(C)	Vrk5(C)		Displace
250	0.78	24.93				0.742428
500	1.52	24.87	2.82	-0.42241		0.672681
750	2.19	24.93	2.112637	1.905458		0.654728
1000	2.42	24.317	2.628289	0.636261		0.792341
1250	3.166	24.05	3.24462	0.76772		0.830106
1500	3.94	23.75			gap-F.C1	0.666667
Average:			2.701386	0.721758	Sum:	4.358952

time	X6	Y6	Vk6(C)	Vrk6(C)		Displace
250	0.82	24.32				0.980008
500	1.8	24.316	4.00125	3.333423		1.326211
750	2.45	23.16	4.306209	1.991306		0.885858
1000	3.188	22.67	3.733631	2.763359		1.01626
1250	3.76	21.83	3.816548	3.39102		0.912428
1500	4.035	20.96			gap-F.C1	0.583333
Average:			3.964409	2.869777	Sum:	5.704098

time	X7	Y7	Vk7(C)	Vrk7(C)		Displace
250	0.69	25				0.638634
500	1.263	24.718	3.417335	2.168519		1.085896
750	2.066	23.987	4.01928	-0.39335		1.074079
1000	3.14	24	3.301569	2.070648		0.719311
1250	3.637	23.48	3.182263	3.095492		1.155798
1500	3.2	22.41			gap-F.C1	0.75
Average:			3.480112	1.735328	Sum:	5.423718

time	X8	Y8	Vk8(C)	Vrk8(C)		Displace
250	0.77	24.914				0.744269
500	1.43	24.57	2.776415	1.324199		0.644906
750	1.978	24.23	2.04841	2.023118		0.501442
1000	2.016	23.73	3.512574	3.136902		1.271643
1250	2.49	22.55	3.387965	0.349668		0.613922
1500	3.09	22.42			gap-F.C1	0.75
Average:			2.931341	1.708472	Sum:	4.526182

time	Xi2	Yi2	Vki2(C)	Vrki2(C)		Displace
250	0.4	30.12				1.441284
500	1.83	30.3	4.557558	3.061891		1.097504
750	2.597	29.515	2.41139	-1.47428		0.324275
1000	2.87	29.69	2.501859	0.598916		1.025031
1250	3.837	29.35	4.671209	3.84661		1.483029
1500	4.513	28.03			gap-F.C1	0.5
Average:			3.535504	1.508285	Sum:	5.871123

time	X1(L)	Y1(L)	Vk1(L)	Vrk1(L)
250	0.988783	30.00083		
500	1.648033	29.54833	3.198417	1.660343
750	2.307283	29.09583	3.198417	1.595877
1000	2.966533	28.64333	3.198417	1.528714
1250	3.625783	28.19083	3.198417	1.458824
1500	4.285033	27.73833		
Average:			3.198417	1.56094

time	X2(L)	Y2(L)	Vk2(L)	Vrk2(L)
250	0.913617	30.3862		
500	1.611367	30.0562	3.087407	1.168691
750	2.309117	29.7262	3.087407	1.099883
1000	3.006867	29.3962	3.087407	1.029145
1250	3.704617	29.0662	3.087407	0.956537
1500	4.402367	28.7362		
Average:			3.087407	1.063564

time	X3(L)	Y3(L)	Vk3(L)	Vrk3(L)
250	1.240683	30.46423		
500	1.927433	30.08173	3.144346	1.35122
750	2.614183	29.69923	3.144346	1.283242
1000	3.300933	29.31673	3.144346	1.213035
1250	3.987683	28.93423	3.144346	1.14063
1500	4.674433	28.55173		
Average:			3.144346	1.247032

time	X4(L)	Y4(L)	Vk4(L)	Vrk4(L)
250	1.055917	30.62133		
500	1.710167	30.23133	3.046685	1.409704
750	2.364417	29.84133	3.046685	1.348421
1000	3.018667	29.45133	3.046685	1.285033
1250	3.672917	29.06133	3.046685	1.219549
1500	4.327167	28.67133		
Average:			3.046685	1.315677

time	X5(L)	Y5(L)	Vk5(L)	Vrk5(L)
250	0.8382	25.1143		
500	1.4372	24.8568	2.60801	0.889979
750	2.0362	24.5993	2.60801	0.828837
1000	2.6352	24.3418	2.60801	0.766137
1250	3.2342	24.0843	2.60801	0.701948
1500	3.8332	23.8268		
Average:			2.60801	0.796725

time	X6(L)	Y6(L)	Vk6(L)	Vrk6(L)
250	1.05445	24.6433		
500	1.7027	23.9358	3.8383	2.638876
750	2.35095	23.2283	3.8383	2.554511
1000	2.9992	22.5208	3.8383	2.462933
1250	3.64745	21.8133	3.8383	2.363603
1500	4.2957	21.1058		
Average:			3.8383	2.504981

time	X7(L)	Y7(L)	Vk7(L)	Vrk7(L)
250	0.850817	25.1226		
500	1.443567	24.6476	3.038362	1.758122
750	2.036317	24.1726	3.038362	1.694264
1000	2.629067	23.6976	3.038362	1.626974
1250	3.221817	23.2226	3.038362	1.556151
1500	3.814567	22.7476		
Average:			3.038362	1.658878

time	X8(L)	Y8(L)	Vk8(L)	Vrk8(L)
250	0.903783	25.09617		
500	1.327033	24.55367	2.752299	2.075471
750	1.750283	24.01117	2.752299	2.041174
1000	2.173533	23.46867	2.752299	2.004625
1250	2.596783	22.92617	2.752299	1.96567
1500	3.020033	22.38367		
Average:			2.752299	2.021735

time	Xi2(L)	Yi2(L)	Vki2(L)	Vrki2(L)
250	0.7561	30.43833		
500	1.5236	30.06333	3.416855	1.34269
750	2.2911	29.68833	3.416855	1.259338
1000	3.0586	29.31333	3.416855	1.173302
1250	3.8261	28.93833	3.416855	1.084659
1500	4.5936	28.56333		
Average:			3.416855	1.214997

time	-R1	+R1	-Sk1(C)	+Sk1(C)
250	1.299191	1.30896		
500	2	2.003182	2.936306	2.960258
750	2.749638	2.764654	3.050778	3.144794
1000	3.519735	3.564689	2.815788	2.930371
1250	4.179873	4.253137	1.901743	1.946858
1500	4.509721	4.581186		
Average:			2.676154	2.74557

time	-R2	+R2	-Sk2(C)	+Sk2(C)
250	1.149633	1.160661		
500	1.697694	1.793477	2.418042	2.498438
750	2.329539	2.41413	2.535971	2.598818
1000	2.964761	3.080657	2.540457	2.563768
1250	3.599805	3.704877	2.539946	2.656165
1500	4.234752	4.396727		
Average:			2.508604	2.579297

time	-R3	+R3	-Sk3(C)	+Sk3(C)
250	1.209042	1.21561		
500	1.780109	1.795252	2.975198	3.132821
750	2.599608	2.664941	2.501602	2.650601
1000	3.10998	3.207277	2.79253	2.872648
1250	3.929717	4.039219	2.178404	2.191885
1500	4.269951	4.374943		
Average:			2.611934	2.711989

time	-R4	+R4	-Sk4(C)	+Sk4(C)
250	0.894071	0.902932		
500	1.58717	1.606119	3.401078	3.557256
750	2.489468	2.555125	2.460045	2.754549
1000	2.939951	3.101263	2.964866	3.080725
1250	3.861866	4.010337	2.292545	2.255318
1500	4.182919	4.320002		
Average:			2.779634	2.911962

time	-R5	+R5	-Sk5(C)	+Sk5(C)
250	0.927293	0.93584		
500	1.49628	1.555758	1.95389	1.954932
750	1.945107	1.979191	2.192338	2.301011
1000	2.550134	2.640932	1.900737	2.065715
1250	2.937784	3.061472	2.447792	2.486211
1500	3.700577	3.819161		
Average:			2.123689	2.201967

time	-R6	+R6	-Sk6(C)	+Sk6(C)
250	1.182408	1.191798		
500	1.799682	1.881015	2.558839	2.546396
750	2.45014	2.492025	2.599618	2.674774
1000	3.099723	3.194342	2.243883	2.303037
1250	3.599805	3.683324	2.395742	2.444309
1500	4.269951	4.38258		
Average:			2.44952	2.492129

time	-R7	+R7	-Sk7(C)	+Sk7(C)
250	0.838941	0.859566		
500	1.300416	1.311391	1.653072	1.651381
750	1.689232	1.704247	1.862679	1.962127
1000	2.19945	2.250265	1.636194	1.746432
1250	2.540124	2.614268	1.878137	1.949128
1500	3.099723	3.187356		
Average:			1.75752	1.827267

time	-R8	+R8	-Sk8(C)	+Sk8(C)
250	1.042107	1.051235		
500	1.409703	1.438772	1.631098	1.715458
750	1.839932	1.890304	1.670305	1.735306
1000	2.249558	2.313076	1.476582	1.540674
1250	2.589789	2.671506	1.521163	1.585499
1500	3	3.096125		
Average:			1.574787	1.644234

time	X1	Y1	Vk1(F)	Vrk1(F)
250	1.11	29.89	2.312554	1.166706
500	1.598	29.58	2.41437	0.513486
750	2.18	29.42	4.65506	3.67933
1000	2.823	28.45	4.612678	1.28898
1250	3.893	28.02	1.474199	0.49353
1500	4.22	27.85		
Average:			3.093772	1.428406

time	X2	Y2	Vk2(F)	Vrk2(F)
250	0.6	30.06	4.946279	-1.41089
500	1.792	30.389	4.866402	2.6816
750	2.766	29.66	0.551594	0.534839
1000	2.72	29.53	4.200809	0.438651
1250	3.75	29.325	4.273919	3.30257
1500	4.318	28.42		
Average:			3.767801	1.109354

time	X3	Y3	Vk3(F)	Vrk3(F)
250	1.5	30.56	1.864609	0.663366
500	1.927	30.373	2.993695	2.469837
750	2.31	29.73	4.693826	2.205663
1000	3.3	29.1	5.970193	5.663084
1250	3.61	27.64	10.00816	-8.74416
1500	5.1	29.65		
Average:			5.106096	0.451559

time	X4	Y4	Vk4(F)	Vrk4(F)
250	1.155	30.775	2.222521	1.437438
500	1.565	30.4	4.6245	2.524121
750	2.5	29.72	3.896665	3.609674
1000	2.79	28.79	4.561579	-2.42403
1250	3.81	29.3	2.648773	1.358095
1500	4.33	28.89		
Average:			3.590808	1.301059

time	X5	Y5	Vk5(F)	Vrk5(F)
250	0.78	24.93	2.969714	0.147317
500	1.52	24.87	2.690725	-0.40304
750	2.19	24.93	2.618913	2.362085
1000	2.42	24.317	3.169366	0.767246
1250	3.166	24.05	3.320424	0.785657
1500	3.94	23.75		
Average:			2.953828	0.731852

time	X6	Y6	Vk6(F)	Vrk6(F)
250	0.82	24.32	3.920033	-0.11611
500	1.8	24.316	5.304845	4.419442
750	2.45	23.16	3.543431	1.638577
1000	3.188	22.67	4.065039	3.008643
1250	3.76	21.83	3.649712	3.242786
1500	4.035	20.96		
Average:			4.096612	2.438669

time	X7	Y7	Vk7(F)	Vrk7(F)
250	0.69	25	2.554535	1.064335
500	1.263	24.718	4.343584	2.756283
750	2.066	23.987	4.296315	-0.42046
1000	3.14	24	2.877246	1.804525
1250	3.637	23.48	4.623192	4.497131
1500	3.2	22.41		
Average:			3.738974	1.940363

time	X8	Y8	Vk8(F)	Vrk8(F)
250	0.77	24.914	2.977075	1.29379
500	1.43	24.57	2.579625	1.230341
750	1.978	24.23	2.005768	1.981002
1000	2.016	23.73	5.086572	4.54256
1250	2.49	22.55	2.455687	0.253448
1500	3.09	22.42		
Average:			3.020945	1.860228

time	Xi2	Yi2	Vki2(F)	Vrki2(F)
250	0.4	30.12	5.765137	-0.79589
500	1.83	30.3	4.390014	2.949331
750	2.597	29.515	1.297098	-0.79302
1000	2.87	29.69	4.100125	0.981523
1250	3.837	29.35	5.932117	4.884932
1500	4.513	28.03		
Average:			4.296898	1.445374

time	-R1(L)	+R1(L)	-Sk1(L)	+Sk1(L)	-FvolB(L)	+FvolB(L)
250	1.37429	1.371448			3.98E-05	3.96E-05
500	2.04179	2.054698			0.000131	0.000133
750	2.70929	2.737948			0.000305	0.000315
1000	3.37679	3.421198			0.000591	0.000614
1250	4.04429	4.104448			0.001015	0.00106
1500	4.71179	4.787698			0.001604	0.001683
Average:			2.67	2.73		

time	-R2(L)	+R2(L)	-Sk2(L)	+Sk2(L)	-FvolB(L)	+FvolB(L)
250	1.107983	1.145566			2.09E-05	2.31E-05
500	1.729983	1.790816			7.94E-05	8.81E-05
750	2.351983	2.436066			0.0002	0.000222
1000	2.973983	3.081316			0.000403	0.000449
1250	3.595983	3.726566			0.000713	0.000794
1500	4.217983	4.371816			0.001151	0.001282
Average:			2.48	2.58		

time	-R3(L)	+R3(L)	-Sk3(L)	+Sk3(L)	-FvolB(L)	+FvolB(L)
250	1.226027	1.235033			2.83E-05	2.89E-05
500	1.862027	1.894283			9.9E-05	0.000104
750	2.498027	2.553533			0.000239	0.000255
1000	3.134027	3.212783			0.000472	0.000509
1250	3.770027	3.872033			0.000822	0.00089
1500	4.406027	4.531283			0.001312	0.001427
Average:			2.54	2.63		

time	-R4(L)	+R4(L)	-Sk4(L)	+Sk4(L)	-FvolB(L)	+FvolB(L)
250	0.96511	0.974632			1.38E-05	1.42E-05
500	1.64286	1.684382			6.8E-05	7.33E-05
750	2.32061	2.394132			0.000192	0.00021
1000	2.99836	3.103882			0.000413	0.000459
1250	3.67611	3.813632			0.000762	0.000851
1500	4.35386	4.523382			0.001266	0.001419
Average:			2.71	2.84		

time	-R5(L)	+R5(L)	-Sk5(L)	+Sk5(L)	-FvolB(L)	+FvolB(L)
250	0.916933	0.93226			1.18E-05	1.24E-05
500	1.453933	1.49201			4.71E-05	5.09E-05
750	1.990933	2.05176			0.000121	0.000132
1000	2.527933	2.61151			0.000248	0.000273
1250	3.064933	3.17126			0.000442	0.000489
1500	3.601933	3.73101			0.000717	0.000797
Average:			2.14	2.24		

time	-R6(L)	+R6(L)	-Sk6(L)	+Sk6(L)	-FvolB(L)	+FvolB(L)
250	1.198851	1.228365			2.64E-05	2.84E-05
500	1.812851	1.858865			9.14E-05	9.85E-05
750	2.426851	2.489365			0.000219	0.000237
1000	3.040851	3.119865			0.000431	0.000466
1250	3.654851	3.750365			0.000749	0.000809
1500	4.268851	4.380865			0.001193	0.00129
Average:			2.45	2.52		

time	-R7(L)	+R7(L)	-Sk7(L)	+Sk7(L)	-FvolB(L)	+FvolB(L)
250	0.835073	0.838239			8.93E-06	9.03E-06
500	1.278823	1.297989			3.21E-05	3.35E-05
750	1.722573	1.757739			7.84E-05	8.33E-05
1000	2.166323	2.217489			0.000156	0.000167
1250	2.610073	2.677239			0.000273	0.000294
1500	3.053823	3.136989			0.000437	0.000473
Average:			1.77	1.84		

time	-R8(L)	+R8(L)	-Sk8(L)	+Sk8(L)	-FvolB(L)	+FvolB(L)
250	1.040413	1.052044			1.73E-05	1.79E-05
500	1.432913	1.461794			4.51E-05	4.79E-05
750	1.825413	1.871544			9.33E-05	0.000101
1000	2.217913	2.281294			0.000167	0.000182
1250	2.610413	2.691044			0.000273	0.000299
1500	3.002913	3.100794			0.000415	0.000457
Average:			1.57	1.64		

time	a(gf)1	-b(gf)1	+b(gf)1	-p(gf)1	+p(gf)1	-Sk(gf)1	+Sk(gf)1
250	1.125	1.500354	1.523001	8.327439	8.408116		
500	1.875	2.133333	2.140127	12.61228	12.63496	2.924134	2.947379
750	2.5	3.024204	3.057325	17.42392	17.53753	3.02343	3.113323
1000	3.25	3.811857	3.909848	22.2443	22.57719	2.79802	2.905587
1250	4.15	4.209961	4.358837	26.25095	26.72579	1.901645	1.945686
1500	4.75	4.281596	4.418371	28.39732	28.80751		
Average:						2.661807	2.727994

time	a(gf)2	-b(gf)2	+b(gf)2	-p(gf)2	+p(gf)2	-Sk(gf)2	+Sk(gf)2
250	1	1.321656	1.347134	7.359633	7.450168		
500	1.875	1.537155	1.715499	10.76656	11.28529	2.394452	2.493512
750	2.83	1.91758	2.059373	15.18021	15.54215	2.443971	2.535041
1000	3.58	2.455254	2.650963	19.27698	19.7815	2.453704	2.507393
1250	3.955	3.27651	3.470573	22.80667	23.36586	2.517685	2.644884
1500	4.79	3.743867	4.035743	26.99693	27.81385		
Average:						2.452453	2.545208

time	a(gf)3	-b(gf)3	+b(gf)3	-p(gf)3	+p(gf)3	-Sk(gf)3	+Sk(gf)3
250	1.165	1.25475	1.268418	7.603239	7.64783		
500	1.83	1.731579	1.761164	11.18763	11.27833	2.972927	3.13167
750	2.625	2.574462	2.70549	16.32708	16.73965	2.501366	2.649996
1000	3.25	2.975992	3.165115	19.56854	20.14522	2.787127	2.872145
1250	4.25	3.633571	3.838891	24.82997	25.4319	2.165125	2.186231
1500	4.75	3.838418	4.029501	27.11911	27.66031		
Average:						2.606636	2.710011

time	a(gf)4	-b(gf)4	+b(gf)4	-p(gf)4	+p(gf)4	-Sk(gf)4	+Sk(gf)4
250	1.165	0.686149	0.699817	6.003931	6.03496		
500	1.955	1.288546	1.319498	10.3975	10.47377	3.260398	3.425701
750	2.705	2.29111	2.413554	15.74152	16.09829	2.44322	2.745633
1000	3.58	2.414333	2.686546	19.17479	19.87594	2.854791	3.018725
1250	4.665	3.197002	3.447546	25.11334	25.75864	2.213962	2.205085
1500	5.165	3.387573	3.613247	27.42889	27.99105		
Average:						2.693093	2.848786

time	a(gf)5	-b(gf)5	+b(gf)5	-p(gf)5	+p(gf)5	-Sk(gf)5	+Sk(gf)5
250	1	0.859873	0.875796	5.856552	5.902898		
500	1.915	1.169114	1.263907	9.963307	10.18898	1.842762	1.874574
750	2.5	1.513376	1.566879	12.97721	13.10182	2.063618	2.182902
1000	2.875	2.261977	2.425921	16.24456	16.70451	1.873858	2.050943
1250	3.58	2.410775	2.618048	19.16596	19.69487	2.356261	2.427028
1500	4.29	3.192137	3.399997	23.74548	24.30777		
Average:						2.034125	2.133861

time	a(gf)6	-b(gf)6	+b(gf)6	-p(gf)6	+p(gf)6	-Sk(gf)6	+Sk(gf)6
250	1	1.398089	1.420382	7.633047	7.71378		
500	2	1.619427	1.769108	11.42765	11.85719	2.530703	2.536858
750	2.75	2.182976	2.258251	15.59154	15.80153	2.565494	2.64911
1000	3.5	2.745223	2.915378	19.7527	20.22776	2.211344	2.28399
1250	4.455	2.908776	3.045315	23.62649	23.96335	2.292342	2.359436
1500	5	3.646497	3.841401	27.48063	27.99935		
Average:						2.399971	2.457349

time	a(gf)7	-b(gf)7	+b(gf)7	-p(gf)7	+p(gf)7	-Sk(gf)7	+Sk(gf)7
250	1.16	0.606743	0.636943	5.813219	5.876577		
500	1.665	1.015665	1.03288	8.660711	8.700765	1.558763	1.563081
750	2.33	1.224679	1.246549	11.68885	11.73435	1.6905	1.789618
1000	3.33	1.452727	1.520629	16.13319	16.25611	1.400839	1.518198
1250	3.915	1.648079	1.745695	18.86269	19.03507	1.58832	1.681108
1500	4.165	2.30691	2.439192	21.14275	21.43352		
Average:						1.559606	1.638001

time	a(gf)8	-b(gf)8	+b(gf)8	-p(gf)8	+p(gf)8	-Sk(gf)8	+Sk(gf)8
250	1	1.085987	1.105096	6.555563	6.618232		
500	1.5	1.324841	1.380042	8.887036	9.051174	1.624839	1.712485
750	2.08	1.627572	1.717908	11.72813	11.97951	1.645616	1.719603
1000	2.415	2.095449	2.215453	14.19831	14.55312	1.469189	1.537815
1250	2.955	2.269715	2.415209	16.54612	16.94743	1.495215	1.56956
1500	3.58	2.513966	2.67765	19.42563	19.85226		
Average:						1.558714	1.634866

time	-A(gf)(E)	+A(gf)(E)	-S.G.(E)1	+S.G.(E)1
250	25.73205	26.38694		
500	54.79291	55.0847	2999.805	3032.188
750	107.9161	109.9005	2194.352	2286.054
1000	173.1958	180.704	1313.415	1383.234
1250	221.655	234.8785	668.9566	655.4264
1500	247.3346	257.6768		
Average:			1794.132	1839.226

time	-A(gf)(E)	+A(gf)(E)	-S.G.(E)2	+S.G.(E)2
250	20.02586	20.67754		
500	34.127	39.29342	2425.462	2357.652
750	61.41274	66.99763	2136.339	2097.096
1000	99.72621	109.5437	1854.241	1800.646
1250	153.8709	165.6223	1429.861	1461.793
1500	209.7332	230.5964		
Average:			1961.476	1929.297

time	-A(gf)(E)	+A(gf)(E)	-S.G.(E)3	+S.G.(E)3
250	19.30176	19.65391		
500	39.11303	39.99542	3327.583	3570.646
750	84.37768	91.05866	1874.172	1936.046
1000	118.1822	128.1423	1702.174	1677.543
1250	184.961	198.5408	1047.617	1013.459
1500	215.0662	228.7487		
Average:			1987.886	2049.423

time	-A(gf)(E)	+A(gf)(E)	-S.G.(E)4	+S.G.(E)4
250	8.8061	9.012875		
500	28.34557	29.16866	4602.427	4809.716
750	74.03531	79.15934	1874	2076.753
1000	97.71665	111.3659	1947.412	1910.642
1250	169.1826	185.5495	1169.931	1091.696
1500	196.6826	212.6477		
Average:			2398.442	2472.202

time	-A(gf)(E)	+A(gf)(E)	-S.G.(E)5	+S.G.(E)5
250	10.31551	10.56158		
500	24.82284	27.24223	2543.46	2428.776
750	41.88346	43.64422	2452.552	2565.708
1000	76.18353	83.2314	1461.186	1543.268
1250	97.5426	107.8684	1682.622	1630.85
1500	158.2472	171.19		
Average:			2034.955	2042.151

time	-A(gf)(E)	+A(gf)(E)	-S.G.(E)6	+S.G.(E)6
250	22.00724	22.6		
500	38.22491	42.79184	2536.495	2382.042
750	70.4859	73.56598	2106.699	2135.421
1000	112.4712	121.339	1334.576	1322.763
1250	145.5366	153.8174	1336.183	1330.585
1500	209.703	223.6726		
Average:			1828.488	1792.703

time	-A(gf)(E)	+A(gf)(E)	-S.G.(E)7	+S.G.(E)7
250	7.607119	8.045251		
500	18.74676	19.12386	2481.145	2452.803
750	30.86384	31.49878	2094.569	2198.155
1000	51.06998	53.74346	1448.41	1519.549
1250	67.84896	72.33169	1582.86	1605.51
1500	104.7677	111.8081		
Average:			1901.746	1944.004

time	-A(gf)(E)	+A(gf)(E)	-S.G.(E)8	+S.G.(E)8
250	14.41922	14.84518		
500	24.02381	25.33049	2096.65	2175.149
750	39.60398	42.39397	1860.445	1890.91
1000	60.86432	65.41207	1265.006	1285.529
1250	78.10085	84.43853	1069.67	1077.64
1500	102.6354	110.9092		
Average:			1572.943	1607.307

time	-b(gf)1	-Sw(gf)1	-Sws(gf)1	+b(gf)1	+Sw(gf)1	+Sws(gf)1
250	1.500354	6.001415		1.523001	6.092003	
500	2.133333	4.266667	3.0477	2.140127	4.280255	3.068648
750	3.024204	4.032272	3.357047	3.057325	4.076433	3.539441
1000	3.811857	3.811857	2.371514	3.909848	3.909848	2.603024
1250	4.209961	3.367969	0.939478	4.358837	3.487069	1.017045
1500	4.281596	2.854397		4.418371	2.945581	
Average:		4.055763	2.428935		4.131865	2.55704

time	-b(gf)2	-Sw(gf)2	-Sws(gf)2	+b(gf)2	+Sw(gf)2	+Sws(gf)2
250	1.321656	5.286624		1.347134	5.388535	
500	1.537155	3.07431	1.191848	1.715499	3.430998	1.424478
750	1.91758	2.556773	1.836198	2.059373	2.745831	1.870927
1000	2.455254	2.455254	2.717861	2.650963	2.650963	2.822399
1250	3.27651	2.621208	2.577225	3.470573	2.776458	2.769561
1500	3.743867	2.495911		4.035743	2.690496	
Average:		3.08168	2.080783		3.280547	2.221842

time	-b(gf)3	-Sw(gf)3	-Sws(gf)3	+b(gf)3	+Sw(gf)3	+Sws(gf)3
250	1.25475	5.018999		1.268418	5.073672	
500	1.731579	3.463158	2.639424	1.761164	3.522328	2.874144
750	2.574462	3.432616	2.488826	2.70549	3.60732	2.807902
1000	2.975992	2.975992	2.118218	3.165115	3.165115	2.266802
1250	3.633571	2.906857	1.724851	3.838891	3.071113	1.728771
1500	3.838418	2.558945		4.029501	2.686334	
Average:		3.392761	2.24283		3.52098	2.419405

time	-b(gf)4	-Sw(gf)4	-Sws(gf)4	+b(gf)4	+Sw(gf)4	+Sws(gf)4
250	0.686149	2.744594		0.699817	2.799267	
500	1.288546	2.577093	3.209923	1.319498	2.638995	3.427473
750	2.29111	3.054813	2.251573	2.413554	3.218071	2.734097
1000	2.414333	2.414333	1.811784	2.686546	2.686546	2.067985
1250	3.197002	2.557601	1.94648	3.447546	2.758037	1.853402
1500	3.387573	2.258382		3.613247	2.408831	
Average:		2.601136	2.30494		2.751625	2.520739

time	-b(gf)5	-Sw(gf)5	-Sws(gf)5	+b(gf)5	+Sw(gf)5	+Sws(gf)5
250	0.859873	3.43949		0.875796	3.503185	
500	1.169114	2.338228	1.307006	1.263907	2.527814	1.382166
750	1.513376	2.017834	2.185726	1.566879	2.089172	2.324027
1000	2.261977	2.261977	1.794798	2.425921	2.425921	2.102338
1250	2.410775	1.92862	1.860319	2.618048	2.094438	1.948152
1500	3.192137	2.128091		3.399997	2.266665	
Average:		2.352374	1.786962		2.484532	1.939171

time	-b(gf)6	-Sw(gf)6	-Sws(gf)6	+b(gf)6	+Sw(gf)6	+Sws(gf)6
250	1.398089	5.592357		1.420382	5.681529	
500	1.619427	3.238854	1.569774	1.769108	3.538217	1.675738
750	2.182976	2.910635	2.251592	2.258251	3.011002	2.292539
1000	2.745223	2.745223	1.4516	2.915378	2.915378	1.574128
1250	2.908776	2.327021	1.802548	3.045315	2.436252	1.852047
1500	3.646497	2.430998		3.841401	2.560934	
Average:		3.207515	1.768879		3.357218	1.848613

time	-b(gf)7	-Sw(gf)7	-Sws(gf)7	+b(gf)7	+Sw(gf)7	+Sws(gf)7
250	0.606743	2.426971		0.636943	2.547771	
500	1.015665	2.031331	1.235873	1.03288	2.06576	1.219212
750	1.224679	1.632906	0.874123	1.246549	1.662065	0.975498
1000	1.452727	1.452727	0.846799	1.520629	1.520629	0.998292
1250	1.648079	1.318463	1.708367	1.745695	1.396556	1.837127
1500	2.30691	1.53794		2.439192	1.626128	
Average:		1.73339	1.16629		1.803151	1.257532

time	-b(gf)8	-Sw(gf)8	-Sws(gf)8	+b(gf)8	+Sw(gf)8	+Sws(gf)8
250	1.085987	4.343949		1.105096	4.420382	
500	1.324841	2.649682	1.08317	1.380042	2.760085	1.225625
750	1.627572	2.170096	1.541217	1.717908	2.290544	1.670821
1000	2.095449	2.095449	1.284284	2.215453	2.215453	1.394602
1250	2.269715	1.815772	0.837035	2.415209	1.932167	0.924395
1500	2.513966	1.675978		2.67765	1.7851	
Average:		2.458488	1.186426		2.567288	1.303861

time	-Vw(gf)1	-Vws(gf)1	+Vw(gf)1	+Vws(gf)1	Teta1
250	2.998585		2.907997		103
500	3.233333	2.4523	3.219745	2.431352	91
750	2.634395	2.142953	2.590234	1.960559	83
1000	2.688143	4.228486	2.590152	3.996976	74
1250	3.272031	5.060522	3.152931	4.982955	71
1500	3.478936		3.387753		68
Average:	3.050904	3.471065	2.974802	3.34296	

time	-Vw(gf)2	-Vws(gf)2	+Vw(gf)2	+Vws(gf)2	Teta2
250	2.713376		2.611465		89
500	4.42569	6.128152	4.069002	5.895522	83
750	4.989893	4.983802	4.800836	4.949073	85
1000	4.704746	1.782139	4.509037	1.677601	78
1250	3.706792	2.262775	3.551542	2.070439	73
1500	3.890756		3.696171		65
Average:	4.071875	3.789217	3.873009	3.648158	

time	-Vw(gf)3	-Vws(gf)3	+Vw(gf)3	+Vws(gf)3	Teta3
250	4.301001		4.246328		110
500	3.856842	3.200576	3.797672	2.965856	102
750	3.567384	3.191174	3.39268	2.872098	88
1000	3.524008	4.381782	3.334885	4.233198	75
1250	3.893143	4.275149	3.728887	4.271229	77
1500	3.774388		3.647		75
Average:	3.819461	3.76217	3.691242	3.585595	

time	-Vw(gf)4	-Vws(gf)4	+Vw(gf)4	+Vws(gf)4	Teta4
250	6.575406		6.520733		127
500	5.242907	2.950077	5.181005	2.732527	103
750	4.15852	4.248427	3.995262	3.765903	95
1000	4.745667	6.028216	4.473454	5.772015	89
1250	4.906399	4.39352	4.705963	4.486598	86
1500	4.628285		4.477835		82
Average:	5.042864	4.40506	4.892375	4.189261	

time	-Vw(gf)5	-Vws(gf)5	+Vw(gf)5	+Vws(gf)5	Teta5
250	4.56051		4.496815		116
500	5.321772	4.692994	5.132186	4.617834	98
750	4.648832	1.654274	4.577495	1.515973	90
1000	3.488023	2.525202	3.324079	2.217662	89
1250	3.79938	3.799681	3.633562	3.711848	90
1500	3.591909		3.453335		85
Average:	4.235071	3.168038	4.102912	3.015829	

time	-Vw(gf)6	-Vws(gf)6	+Vw(gf)6	+Vws(gf)6	Teta6
250	2.407643		2.318471		107
500	4.761146	5.430226	4.461783	5.324262	94
750	4.422698	3.748408	4.322332	3.707461	82
1000	4.254777	5.3684	4.084622	5.245872	80
1250	4.800979	4.197452	4.691748	4.147953	73
1500	4.235669		4.105732		62
Average:	4.147152	4.686121	3.997448	4.606387	

time	-Vw(gf)7	-Vws(gf)7	+Vw(gf)7	+Vws(gf)7	Teta7
250	6.853029		6.732229		121
500	4.628669	3.444127	4.59424	3.460788	110
750	4.580427	5.785877	4.551268	5.684502	95
1000	5.207273	5.493201	5.139371	5.341708	85
1250	4.945537	1.631633	4.867444	1.502873	79
1500	4.015393		3.927205		73
Average:	5.038388	4.08871	4.968626	3.997468	

time	-Vw(gf)8	-Vws(gf)8	+Vw(gf)8	+Vws(gf)8	Teta8
250	3.656051		3.579618		109
500	3.350318	3.23683	3.239915	3.094375	96
750	3.37657	2.118783	3.256123	1.989179	88
1000	2.734551	2.215716	2.614547	2.105398	81
1250	2.912228	3.822965	2.795833	3.735605	73
1500	3.097356		2.988233		71
Average:	3.187846	2.848574	3.079045	2.731139	

time	XEC(gf)1	YEC(gf)1	Vk(CE)(F)	Vrk(CE)F
250	1.166	30.416	2.678184	0.242004
500	1.83	30.33	3.572786	1.117651
750	2.66	30	3.34401	2.492887
1000	3.16	29.33	3.609986	0.952483
1250	4	29	2.828427	1.707967
1500	4.5	28.5		
Average:			3.206679	1.302598

time	XEC(gf)2	YEC(gf)2	Vk(CE)(F)	Vrk(CE)F
250	1	30.16	2.716468	0.552163
500	1.66	30	4.36	-0.24088
750	2.75	30	3.541073	2.109157
1000	3.41	29.41	2.347765	1.435592
1250	3.83	29	3.605551	2.71231
1500	4.33	28.25		
Average:			3.314172	1.313667

time	XEC(gf)3	YEC(gf)3	Vk(CE)(F)	Vrk(CE)F
250	1.08	30.5	3.68	-0.13023
500	2	30.5	2.969714	1.184342
750	2.66	30.16	4.022735	2.752948
1000	3.33	29.41	3.335386	-0.05556
1250	4.16	29.33	2.112439	0.392404
1500	4.66	29.16		
Average:			3.224055	0.828782

time	XEC(gf)4	YEC(gf)4	Vk(CE)(F)	Vrk(CE)F
250	1	31	3.587757	1.252252
500	1.83	30.66	3.381124	0.441055
750	2.66	30.5	4.224879	1.007324
1000	3.66	30.16	4.123106	0.510841
1250	4.66	29.91	1.895257	1.094902
1500	5	29.58		
Average:			3.442425	0.861275

time	XEC(gf)5	YEC(gf)5	Vk(CE)(F)	Vrk(CE)F
250	1	24.83	3.32	-0.1336
500	1.83	24.83	2.417602	0.507636
750	2.41	24.66	1.797776	0.473559
1000	2.83	24.5	2.755358	-0.9433
1250	3.5	24.66	3.875874	1.513622
1500	4.33	24.16		
Average:			2.833322	0.283584

time	XEC(gf)6	YEC(gf)6	Vk(CE)(F)	Vrk(CE)F
250	1	24.83	4.057388	0.518484
500	2	24.66	3.875874	1.725074
750	2.83	24.16	2.860489	0.681417
1000	3.5	23.91	4.47464	2.487501
1250	4.33	23.16	4.373191	4.121455
1500	4.5	22.08		
Average:			3.928317	1.906786

time	XEC(gf)7	YEC(gf)7	Vk(CE)(F)	Vrk(CE)F
250	0.66	25.08	3.375204	-0.40828
500	1.5	25.16	3.27756	1.139122
750	2.25	24.83	5.187678	1.89179
1000	3.41	24.25	2.375879	1.429695
1250	3.83	23.83	2.302694	2.064218
1500	4	23.28		
Average:			3.303803	1.223309

time	XEC(gf)8	YEC(gf)8	Vk(CE)(F)	Vrk(CE)F
250	1	24.91	2.236068	0.918971
500	1.5	24.66	2.526341	0.857296
750	2.08	24.41	2.136539	1.172596
1000	2.5	24.08	1.955096	1.567753
1250	2.75	23.66	3.067507	0.289362
1500	3.5	23.5		
Average:			2.38431	0.961196

time	a(ff)1	-b(ff)1	+b(ff)1	-p(ff)1	+p(ff)1	-Sk(ff)1	+Sk(ff)1
250	1.23	1.372275	1.392988	8.183346	8.252069		
500	1.68	2.380952	2.388535	12.93995	12.96748	2.850088	2.8718
750	2.5	3.024204	3.057325	17.42392	17.53753	3.02343	3.113323
1000	3.415	3.627682	3.720939	22.1241	22.42743	2.813221	2.924989
1250	4.33	4.034951	4.177638	26.28228	26.71827	1.899379	1.946234
1500	4.75	4.281596	4.418371	28.39732	28.80751		
Average:						2.646529	2.714087

time	a(ff)2	-b(ff)2	+b(ff)2	-p(ff)2	+p(ff)2	-Sk(ff)2	+Sk(ff)2
250	1.25	1.057325	1.077707	7.270217	7.328995		
500	1.875	1.537155	1.715499	10.76656	11.28529	2.394452	2.493512
750	2.58	2.103392	2.258925	14.7818	15.22763	2.509843	2.587401
1000	2.665	3.29824	3.561143	18.82985	19.75156	2.511969	2.511195
1250	3.08	4.207337	4.456531	23.15442	24.0562	2.479872	2.568984
1500	3.705	4.840249	5.217601	27.06783	28.4167		
Average:						2.474034	2.540273

time	a(ff)3	-b(ff)3	+b(ff)3	-p(ff)3	+p(ff)3	-Sk(ff)3	+Sk(ff)3
250	1.165	1.25475	1.268418	7.603239	7.64783		
500	1.83	1.731579	1.761164	11.18763	11.27833	2.972927	3.13167
750	2.625	2.574462	2.70549	16.32708	16.73965	2.501366	2.649996
1000	3.25	2.975992	3.165115	19.56854	20.14522	2.787127	2.872145
1250	3.915	3.944489	4.167378	24.67897	25.39104	2.178373	2.189749
1500	4.25	4.289996	4.503559	26.81588	27.49771		
Average:						2.609948	2.71089

time	a(ff)4	-b(ff)4	+b(ff)4	-p(ff)4	+p(ff)4	-Sk(ff)4	+Sk(ff)4
250	0.83	0.963088	0.982273	5.645784	5.710589		
500	1.625	1.55022	1.587457	9.972957	10.0878	3.399192	3.55677
750	2.33	2.659851	2.802001	15.70233	16.18249	2.449318	2.731346
1000	3.08	2.80627	3.122674	18.50286	19.47686	2.958461	3.080579
1250	4.165	3.580795	3.861417	24.39088	25.22097	2.279541	2.252094
1500	4.33	4.040835	4.310028	26.3001	27.12976		
Average:						2.771628	2.905197

time	a(ff)5	-b(ff)5	+b(ff)5	-p(ff)5	+p(ff)5	-Sk(ff)5	+Sk(ff)5
250	1	0.859873	0.875796	5.856552	5.902898		
500	1.705	1.313111	1.419579	9.556423	9.852027	1.921221	1.938687
750	2.33	1.623794	1.681201	12.6114	12.75866	2.123476	2.241579
1000	2.665	2.440219	2.617082	16.04592	16.58642	1.897055	2.065545
1250	3.58	2.410775	2.618048	19.16596	19.69487	2.356261	2.427028
1500	4.08	3.356438	3.574997	23.46069	24.08894		
Average:						2.074503	2.16821

time	a(ff)6	-b(ff)6	+b(ff)6	-p(ff)6	+p(ff)6	-Sk(ff)6	+Sk(ff)6
250	1.165	1.200077	1.219212	7.427157	7.488361		
500	1.875	1.727389	1.887049	11.32099	11.81289	2.554546	2.54637
750	2.5	2.401274	2.484076	15.39312	15.65008	2.598563	2.674747
1000	3.25	2.956394	3.139637	19.50987	20.06645	2.238867	2.30235
1250	3.58	3.61972	3.789631	22.60747	23.15	2.395669	2.442332
1500	4.58	3.980892	4.19367	26.94694	27.57602		
Average:						2.446911	2.49145

time	a(ff)7	-b(ff)7	+b(ff)7	-p(ff)7	+p(ff)7	-Sk(ff)7	+Sk(ff)7
250	1	0.703822	0.738854	5.43023	5.521232		
500	1.5	1.127389	1.146497	8.332551	8.383806	1.620152	1.622175
750	1.83	1.559291	1.587136	10.67627	10.75687	1.850834	1.95224
1000	2.5	1.935032	2.025478	14.03854	14.2879	1.609854	1.727335
1250	2.5	2.580892	2.733758	15.95602	16.45038	1.877661	1.945243
1500	3.58	2.683877	2.837775	19.86883	20.28613		
Average:						1.739625	1.811749

time	a(ff)8	-b(ff)8	+b(ff)8	-p(ff)8	+p(ff)8	-Sk(ff)8	+Sk(ff)8
250	1	1.085987	1.105096	6.555563	6.618232		
500	1.5	1.324841	1.380042	8.887036	9.051174	1.624839	1.712485
750	1.83	1.849918	1.952595	11.55511	11.88358	1.670256	1.733484
1000	2.08	2.432937	2.572268	14.21389	14.68967	1.467578	1.523519
1250	2.705	2.479485	2.638426	16.29468	16.77966	1.518287	1.585253
1500	2.5	3.6	3.834395	19.46293	20.32654		
Average:						1.57024	1.638685

time	-A(ff)(E)1	+A(ff)(E)1	-S.G.(E)1	+S.G.(E)1
250	22.81923	23.39733		
500	63.54881	63.88929	2678.156	2707.909
750	107.9161	109.9005	1826.065	1914.497
1000	162.0797	169.0914	1316.786	1357.383
1250	214.6282	224.6614	794.4428	788.6122
1500	247.3346	257.6768		
Average:			1653.863	1692.1

time	-A(ff)(E)2	+A(ff)(E)2	-S.G.(E)2	+S.G.(E)2
250	15.78279	16.17312		
500	34.127	39.29342	2835.244	2753.833
750	64.16198	70.27687	2907.594	3004.709
1000	127.4055	144.8742	2144.799	2083.1
1250	200.7915	221.1706	1416.341	1455.17
1500	269.6001	305.7946		
Average:			2325.994	2324.203

time	-A(ff)(E)3	+A(ff)(E)3	-S.G.(E)3	+S.G.(E)3
250	19.30176	19.65391		
500	39.11303	39.99542	3327.583	3570.646
750	84.37768	91.05866	1874.172	1936.046
1000	118.1822	128.1423	1872.505	1914.875
1250	195.026	213.7469	1152.284	1140.192
1500	230.5448	249.9985		
Average:			2056.636	2140.44

time	-A(ff)(E)4	+A(ff)(E)4	-S.G.(E)4	+S.G.(E)4
250	11.09506	11.46694		
500	31.1741	32.16701	4746.791	5058.125
750	85.08354	92.81931	1746.04	1935.044
1000	105.4538	121.9717	1779.456	1712.542
1250	178.9087	197.2602	1225.029	1137.381
1500	215.038	234.1517		
Average:			2374.329	2460.773

time	-A(ff)(E)5	+A(ff)(E)5	-S.G.(E)5	+S.G.(E)5
250	10.31551	10.56158		
500	26.08793	28.77859	2511.415	2389.429
750	43.07432	44.94378	2478.217	2596.127
1000	79.46169	87.11846	1370.932	1444.576
1250	97.5426	107.8684	1698.509	1646.536
1500	162.3002	175.9231		
Average:			2014.768	2019.167

time	-A(ff)(E)6	+A(ff)(E)6	-S.G.(E)6	+S.G.(E)6
250	17.91946	18.39847		
500	39.6488	44.65152	2851.614	2663.888
750	74.451	77.87179	2082.48	2109.322
1000	117.1702	126.7799	1529.216	1565.049
1250	164.0402	177.0801	1246.356	1218.747
1500	219.3964	234.6878		
Average:			1927.416	1889.251

time	-A(ff)(E)7	+A(ff)(E)7	-S.G.(E)7	+S.G.(E)7
250	8.030353	8.523792		
500	19.58846	20.00174	2666.318	2640.223
750	34.14489	34.92831	2158.486	2277.189
1000	56.4391	59.77092	1724.849	1881.689
1250	82.81935	91.16345	1323.113	1304.672
1500	111.2288	119.2401		
Average:			1968.192	2025.943

time	-A(ff)(E)8	+A(ff)(E)8	-S.G.(E)8	+S.G.(E)8
250	14.41922	14.84518		
500	24.02381	25.33049	2366.758	2529.937
750	42.84849	46.88744	2174.836	2225.788
1000	70.61803	77.51123	1108.219	1085.347
1250	81.9786	88.95074	1803.561	1871.256
1500	144.5447	160.736		
Average:			1863.344	1928.082

time	-b(ff)1	-Sw(ff)1	-Sws(ff)1	+b(ff)1	+Sw(ff)1	+Sws(ff)1
250	1.372275	5.489099		1.392988	5.571954	
500	2.380952	4.761905	3.303858	2.388535	4.77707	3.328673
750	3.024204	4.032272	2.49346	3.057325	4.076433	2.664808
1000	3.627682	3.627682	2.021494	3.720939	3.720939	2.240626
1250	4.034951	3.227961	1.307827	4.177638	3.34211	1.394864
1500	4.281596	2.854397		4.418371	2.945581	
Average:		3.998886	2.28166		4.072348	2.407243

time	-b(ff)2	-Sw(ff)2	-Sws(ff)2	+b(ff)2	+Sw(ff)2	+Sws(ff)2
250	1.057325	4.229299		1.077707	4.310828	
500	1.537155	3.07431	2.092134	1.715499	3.430998	2.362435
750	2.103392	2.804523	3.52217	2.258925	3.011899	3.691288
1000	3.29824	3.29824	4.20789	3.561143	3.561143	4.395212
1250	4.207337	3.36587	3.084018	4.456531	3.565225	3.312915
1500	4.840249	3.226832		5.217601	3.4784	
Average:		3.333179	3.226553		3.559749	3.440463

time	-b(ff)3	-Sw(ff)3	-Sws(ff)3	+b(ff)3	+Sw(ff)3	+Sws(ff)3
250	1.25475	5.018999		1.268418	5.073672	
500	1.731579	3.463158	2.639424	1.761164	3.522328	2.874144
750	2.574462	3.432616	2.488826	2.70549	3.60732	2.807902
1000	2.975992	2.975992	2.740055	3.165115	3.165115	2.923777
1250	3.944489	3.155591	2.628008	4.167378	3.333903	2.676888
1500	4.289996	2.859998		4.503559	3.002373	
Average:		3.484392	2.624078		3.617452	2.820678

time	-b(ff)4	-Sw(ff)4	-Sws(ff)4	+b(ff)4	+Sw(ff)4	+Sws(ff)4
250	0.963088	3.852352		0.982273	3.929092	
500	1.55022	3.100441	3.393525	1.587457	3.174914	3.639456
750	2.659851	3.546468	2.512099	2.802001	3.736001	3.070433
1000	2.80627	2.80627	1.841889	3.122674	3.122674	2.118832
1250	3.580795	2.864636	2.46913	3.861417	3.089134	2.374709
1500	4.040835	2.69389		4.310028	2.873352	
Average:		3.14401	2.554161		3.320861	2.800857

time	-b(ff)5	-Sw(ff)5	-Sws(ff)5	+b(ff)5	+Sw(ff)5	+Sws(ff)5
250	0.859873	3.43949		0.875796	3.503185	
500	1.313111	2.626221	1.527842	1.419579	2.839158	1.610809
750	1.623794	2.165058	2.254218	1.681201	2.241601	2.395005
1000	2.440219	2.440219	1.573962	2.617082	2.617082	1.873695
1250	2.410775	1.92862	1.832437	2.618048	2.094438	1.915831
1500	3.356438	2.237625		3.574997	2.383331	
Average:		2.472872	1.797115		2.613132	1.948835

time	-b(ff)6	-Sw(ff)6	-Sws(ff)6	+b(ff)6	+Sw(ff)6	+Sws(ff)6
250	1.200077	4.800306		1.219212	4.876849	
500	1.727389	3.454777	2.402395	1.887049	3.774098	2.529729
750	2.401274	3.201699	2.458011	2.484076	3.312102	2.505177
1000	2.956394	2.956394	2.436893	3.139637	3.139637	2.611109
1250	3.61972	2.895776	2.048996	3.789631	3.031705	2.108064
1500	3.980892	2.653928		4.19367	2.79578	
Average:		3.327147	2.336573		3.488362	2.43852

time	-b(ff)7	-Sw(ff)7	-Sws(ff)7	+b(ff)7	+Sw(ff)7	+Sws(ff)7
250	0.703822	2.815287		0.738854	2.955414	
500	1.127389	2.254777	1.710939	1.146497	2.292994	1.696565
750	1.559291	2.079055	1.615287	1.587136	2.116181	1.757962
1000	1.935032	1.935032	2.043201	2.025478	2.025478	2.293244
1250	2.580892	2.064713	1.497691	2.733758	2.187006	1.624595
1500	2.683877	1.789251		2.837775	1.89185	
Average:		2.156353	1.716779		2.244821	1.843091

time	-b(ff)8	-Sw(ff)8	-Sws(ff)8	+b(ff)8	+Sw(ff)8	+Sws(ff)8
250	1.085987	4.343949		1.105096	4.420382	
500	1.324841	2.649682	1.527862	1.380042	2.760085	1.694998
750	1.849918	2.466558	2.216193	1.952595	2.60346	2.384452
1000	2.432937	2.432937	1.259133	2.572268	2.572268	1.371663
1250	2.479485	1.983588	2.334125	2.638426	2.110741	2.524253
1500	3.6	2.4		3.834395	2.556263	
Average:		2.712786	1.834328		2.8372	1.993842

time	-Vw(ff)1	-Vws(ff)1	+Vw(ff)1	+Vws(ff)1
250	4.350901		4.268046	
500	1.958095	1.776142	1.94293	1.751327
750	2.634395	4.44654	2.590234	4.275192
1000	3.202318	5.298506	3.109061	5.079374
1250	3.700039	4.032173	3.58589	3.945136
1500	3.478936		3.387753	
Average:	3.220781	3.88834	3.147319	3.762757

time	-Vw(ff)2	-Vws(ff)2	+Vw(ff)2	+Vws(ff)2
250	5.770701		5.689172	
500	4.42569	3.227866	4.069002	2.957565
750	4.075477	-0.36217	3.868101	-0.53129
1000	2.03176	-2.20789	1.768857	-2.39521
1250	1.56213	1.075982	1.362775	0.847085
1500	1.713168		1.4616	
Average:	3.263154	0.433447	3.036584	0.219537

time	-Vw(ff)3	-Vws(ff)3	+Vw(ff)3	+Vws(ff)3
250	4.301001		4.246328	
500	3.856842	3.200576	3.797672	2.965856
750	3.567384	3.191174	3.39268	2.872098
1000	3.524008	2.419945	3.334885	2.236223
1250	3.108409	1.371992	2.930097	1.323112
1500	2.806669		2.664294	
Average:	3.527385	2.545922	3.394326	2.349322

time	-Vw(ff)4	-Vws(ff)4	+Vw(ff)4	+Vws(ff)4
250	2.787648		2.710908	
500	3.399559	2.606475	3.325086	2.360544
750	2.666866	3.307901	2.477332	2.749567
1000	3.35373	5.498111	3.037326	5.221168
1250	3.799364	2.53087	3.574866	2.625291
1500	3.079443		2.899981	
Average:	3.181102	3.485839	3.00425	3.239143

time	-Vw(ff)5	-Vws(ff)5	+Vw(ff)5	+Vws(ff)5
250	4.56051		4.496815	
500	4.193779	3.792158	3.980842	3.709191
750	4.048275	1.585782	3.971733	1.444995
1000	2.889781	3.426038	2.712918	3.126305
1250	3.79938	3.827563	3.633562	3.744169
1500	3.202375		3.056669	
Average:	3.78235	3.157885	3.64209	3.006165

time	-Vw(ff)6	-Vws(ff)6	+Vw(ff)6	+Vws(ff)6
250	4.519694		4.443151	
500	4.045223	2.937605	3.725902	2.810271
750	3.464968	3.041989	3.354565	2.994823
1000	3.543606	1.883107	3.360363	1.708891
1250	2.832224	3.271004	2.696295	3.211936
1500	3.452739		3.310887	
Average:	3.643076	2.783427	3.481861	2.68148

time	-Vw(ff)7	-Vws(ff)7	+Vw(ff)7	+Vws(ff)7
250	5.184713		5.044586	
500	3.745223	1.609061	3.707006	1.623435
750	2.800945	2.384713	2.763819	2.242038
1000	3.064968	0.636799	2.974522	0.386756
1250	1.935287	2.822309	1.812994	2.695405
1500	2.984082		2.881483	
Average:	3.28587	1.863221	3.197402	1.736909

time	-Vw(ff)8	-Vws(ff)8	+Vw(ff)8	+Vws(ff)8
250	3.656051		3.579618	
500	3.350318	1.792138	3.239915	1.625002
750	2.413442	0.103807	2.27654	-0.06445
1000	1.727063	2.240867	1.587732	2.128337
1250	2.344412	-0.65413	2.217259	-0.84425
1500	0.933333		0.77707	
Average:	2.404103	0.870672	2.279689	0.711158

time	XEC(ff)1	YEC(ff)1	Vk(CE)(F)	Vrk(CE)F
250	1.083	30.416	3.684096	0.213261
500	2	30.33	2.95161	1.143432
750	2.66	30	2.723821	2.230662
1000	3	29.41	4.212173	0.907268
1250	4	29.08	3.06307	2.025822
1500	4.5	28.5		
Average:			3.326954	1.304089

time	XEC(ff)2	YEC(ff)2	Vk(CE)(F)	Vrk(CE)F
250	0.66	30.16	4.050876	0.552335
500	1.66	30	6	-0.33149
750	3.16	30	6.156493	3.487745
1000	4.33	29	1.484857	0.477616
1250	4.66	28.83	4.472136	3.629617
1500	5.16	27.83		
Average:			4.432872	1.563164

time	XEC(ff)3	YEC(ff)3	Vk(CE)(F)	Vrk(CE)F
250	1.08	30.5	3.68	-0.13023
500	2	30.5	2.969714	1.184342
750	2.66	30.16	4.022735	2.752948
1000	3.33	29.41	4.812151	0.586352
1250	4.5	29.13	2.260619	0.178032
1500	5.05	29		
Average:			3.549044	0.914289

time	XEC(ff)4	YEC(ff)4	Vk(CE)(F)	Vrk(CE)F
250	1.16	31.16	4.323147	1.490059
500	2.16	30.75	4.123106	0.717257
750	3.16	30.5	4.224879	0.940539
1000	4.16	30.16	3.909578	0.804794
1250	5.08	29.83	3.345206	0.955351
1500	5.83	29.46		
Average:			3.985183	0.9816

time	XEC(ff)5	YEC(ff)5	Vk(CE)(F)	Vrk(CE)F
250	1	24.83	4	-0.16096
500	2	24.83	2.726169	0.465845
750	2.66	24.66	2.099905	0.421819
1000	3.16	24.5	1.503064	-0.80871
1250	3.5	24.66	4.90355	1.689925
1500	4.58	24.08		
Average:			3.046538	0.321582

time	XEC(ff)6	YEC(ff)6	Vk(CE)(F)	Vrk(CE)F
250	0.91	24.75	5.012943	0.176043
500	2.16	24.66	4.624111	1.962122
750	3.16	24.08	4.123106	0.471044
1000	4.16	23.83	5.198307	2.582663
1250	5.16	23	4.555436	4.543208
1500	4.83	21.91		
Average:			4.702781	1.947016

time	XEC(ff)7	YEC(ff)7	Vk(CE)(F)	Vrk(CE)F
250	1	25.25	3.021523	0.240999
500	1.75	25.16	4.060542	1.050372
750	2.71	24.83	6.389241	2.034891
1000	4.16	24.16	4.624111	1.607601
1250	5.16	23.58	2.864402	2.137114
1500	4.58	23.16		
Average:			4.191964	1.414195

time	XEC(ff)8	YEC(ff)8	Vk(CE)(F)	Vrk(CE)F
250	1	24.91	2.236068	0.918971
500	1.5	24.66	3.798012	0.775695
750	2.416	24.41	2.330651	1.468919
1000	2.83	24	1.738505	1.50936
1250	3	23.6	5.712162	1.392523
1500	4.33	23.08		
Average:			3.16308	1.213093